

**THE ROLE OF CDC42, IRSP53 AND ITS BINDING  
PARTNERS IN FILOPODIA FORMATION**

**LIM KIM BUAY**  
**(B.Sc.(Hons.), Univ. of Edinburgh, Scotland)**

**A THESIS SUBMITTED  
FOR THE DEGREE OF DOCTOR OF PHILOSOPHY**

**DEPARTMENT OF PHYSIOLOGY**

**INSITITUTE OF MOLECULAR AND CELL BIOLOGY  
NATIONAL UNIVERSITY OF SINGAPORE**

**2007**

## **Acknowledgement**

I wish to extend my gratitude to Prof. Sohail Ahmed for giving me the opportunity to study in his lab and for all support and patience throughout the duration of my studies. For his guidance, encouragement and enthusiasm during my studentship. Thank you to Dr. Sudhaharan Thankiah for his help and advice in the FRET experiments. I am also indebted to Helen Pu and Dr. Esther Koh for their advice and stimulating discussion sessions. I would like to extend my sincerest thanks to members of my committee, Dr. Ed Manser and Dr. Uttam Surana for their support and guidance.

I would like to acknowledge members of the lab who have offered me invaluable practical instructions. A special mention to Sem Kai Ping, Bu Wenyu and Dr. Yu Feng Gang. With lots of appreciation towards Wah Ing, for proof reading the thesis twice. I also thank all my colleagues past and present, for providing an enjoyable working environment and motivating me especially during the period I have spent writing my thesis.

Finally, many thanks to my family and all my friends, who have continually been a source of inspiration and offered their genuine support and encouragement, for which, I am sincerely grateful.

## Table of Contents

<b>Acknowledgements</b>	<b>ii</b>
<b>Contents</b>	<b>iii</b>
<b>Summary</b>	<b>xi</b>
<b>List of Tables</b>	<b>xii</b>
<b>List of Figures</b>	<b>xiii</b>
<b>List of Abbreviations</b>	<b>xvi</b>

### **Chapter 1 Introduction**

<b>1.1 The cell as a fundamental unit of life</b>	<b>1</b>
1.1.1 Cell migration	2
1.1.2 Lamellipodia and membrane ruffling	2
1.1.3 Filopodia	4
<b>1.2 The Cytoskeleton</b>	<b>7</b>
1.2.1 Components of the cytoskeleton	7
1.2.2 Actin microfilaments	8
1.2.3 Microtubules	9
1.2.4 Intermediate filaments	10
<b>1.3 Microfilaments assembly and disassembly: Actin dynamics</b>	<b>11</b>
1.3.1 Arp 2/3 complex	12
1.3.2 Myosin	13
1.3.3 Actin binding proteins	14
<b>1.4 The Ras Superfamily</b>	<b>18</b>
1.4.1 Ras superfamily members	19
1.4.2 Ras as a molecular switch	21
1.4.3 Mutations and oncogenic Ras	23
1.4.4 Ras GTPase regulatory proteins	25
1.4.4.1 Ras guanine nucleotide exchange factors (RasGEFs)	25
1.4.4.2 Ras GTPase activating proteins (RasGAPs)	26
1.4.5 Ras effectors	28

<b>1.5 Rho Family</b>	29
1.5.1 Regulators of Rho GTPases	30
1.5.2 Rho GEFs	30
1.5.3 Rho GAPs	33
1.5.4 Rho GDIs	35
<b>1.6 Rho Family Functions</b>	37
1.6.1 Cdc42	37
1.6.2 Rac1	39
1.6.3 Rho	40
<b>1.7 Rho Family Effector Proteins</b>	41
1.7.1 The CRIB motif	41
1.7.2 PAK family kinases	41
1.7.3 MRCK	43
1.7.4 ACK	45
1.7.5 ROK	45
1.7.6 PKN	46
1.7.7 Rho GTPase effectors – adaptor proteins	46
<b>1.8 The WASP and VASP family of actin polymerization regulators</b>	47
1.8.1 WASP family domain structure	48
1.8.2 WASP	51
1.8.3 N-WASP	52
1.8.4 WAVE family proteins	55
1.8.5 Ena/VASP family of proteins	56
1.8.6 Ena/VASP and Mena	56
1.8.7 EVL	60
1.8.8 Abi proteins	62
<b>1.9 IRSp53</b>	63
1.9.1 Introduction	63
1.9.2 Domain families and structure	64
1.9.3 IRSp53 function	64



<b>1.10 Functional roles of filopodia</b>	67
1.10.1 Components of filopodia	67
1.10.2 Rho family signalling, lamellipodia and filopodia	68
1.10.3 Axonal guidance	69
1.10.4 Metastasis	70
1.10.5 Cell motility and immunity	73
1.10.6 Wound healing	75
1.10.7 Aims of thesis	77
<b>Chapter 2 Materials and methods</b>	
<b>2.1 Materials</b>	78
2.1.1 General laboratory reagents	78
2.1.2 DNA manipulation reagents	78
2.1.3 Protein manipulation reagents	78
2.1.4 Tissue culture reagents	79
2.1.5 Reagents for immunodetection and immunofluorescence	79
2.1.5.1 Phalloidin	79
2.1.5.2 Primary antibodies	80
2.1.5.3 Secondary antibodies	80
2.1.6 cDNA constructs	80
2.1.7 Oligomers synthesis and DNA sequencing service	81
<b>2.2 Methods</b>	81
<b>2.2.1 Plasmid DNA preparation</b>	81
2.2.1.1 Transformation of <i>E.coli</i> (XL1-Blue competent cells)	81
2.2.1.2 Qiagen Mini preps	81
2.2.1.3 Qiagen Maxi preps	82
2.2.1.4 Quantification of DNA in solution	84
2.2.1.5 Qiagen “Magic DNA clean-up system”	84
2.2.1.6 Gel electrophoresis of DNA	84
2.2.1.7 Visualization of DNA with ethidium bromide	85
2.2.1.8 Isolation of DNA fragments from agarose gels	85

2.2.1.9	Enzymatic modifications of DNA	86
2.2.1.9.1	Digestion of DNA with restriction enzymes	86
2.2.1.9.2	Stratagene Klenow fill-in kit	86
2.2.1.10	DNA ligation	87
2.2.1.11	Inactivation and removal of enzymes	87
2.2.1.12	Polymerase chain reaction (PCR)	87
2.2.1.13	SiRNA	89
2.2.1.14	Cloning of WAVE1/2 RNAi fragment into pSUPER vector	90
<b>2.2.2</b>	<b>Protein expression and purification</b>	<b>91</b>
2.2.2.1	Expression of recombinant GST-fusion proteins	91
2.2.2.2	Purification of recombinant GST-fusion proteins	92
2.2.2.3	Dialysis and concentration of GST-fusion proteins	93
2.2.2.4	Quantification of Protein Concentration	93
2.2.2.5	Preparation of SDS-Polyacrylamide Gels	93
2.2.2.6	Separation of proteins by SDS-PAGE	95
2.2.2.7	Visualization of separated proteins	95
2.2.2.8	Gel drying	96
2.2.2.9	Western transfer of proteins onto nitrocellulose filters (Semi-dry blotting)	96
2.2.2.10	Immunoanalysis of nitrocellulose immobilized proteins	96
2.2.2.11	<i>In vitro</i> transcription-translation and binding assay	97
<b>2.2.3</b>	<b>Cell culture</b>	<b>98</b>
2.2.3.1	Cell culture of N1E115 cells	98
2.2.3.2	Cell culture of N-WASP WT and KO cells	98
2.2.3.3	Cell culture of Mena WT and KO cells	99
2.2.3.4	Cell maintenance	99
2.2.3.5	-70°C storage of cells	100
2.2.3.6	Cell plating from stocks in liquid nitrogen storage	100
2.2.3.7	Preparation of coverslips	101
2.2.3.7.1	Preparation of laminin-coated coverslips	101
2.2.3.7.2	Preparation of fibronectin-coated coverslips	101

2.2.3.8	Transient transfection of N1E115 neuroblastoma cells	101
2.2.3.9	Transient transfection of N-WASP WT/KO cells	102
2.2.3.10	Delivery of RNAi into N1E115 cells	102
2.2.3.11	Microinjection of N-WASP WT/KO cells	103
2.2.3.12	Microinjection of Mena WT/KO cells	103
2.2.3.13	Fluorescence microscopy	104
2.2.3.14	Live cell imaging studies	105
2.2.3.14.1	Actin dynamics of N1E115 cells	105
2.2.3.14.2	Actin dynamics of N-WASP WT/KO cells	105
2.2.3.14.3	Actin dynamics of Mena WT/KO Cells	106
<b>2.2.4</b>	<b><i>S.cerevisiae</i> (Yeast) two hybrid</b>	106
2.2.4.1	Preparation of competent cells	106
2.2.4.2	<i>S.cerevisiae</i> transformation	107
2.2.4.3	Isolation of plasmid DNA from <i>S.cerevisiae</i>	107
2.2.4.4	Recovery of target protein cDNA by electroporation	108
2.2.4.5	Filter assay for $\beta$ -galactosidase activity	109
2.2.4.6	Generation of mating pairs	110
<b>2.2.5</b>	<b>Mass spectrometry analysis</b>	111
<b>2.2.6</b>	<b>Statistical analysis of morphology</b>	112
<b>2.2.7</b>	<b>Forster Resonance Energy Transfer (FRET) analysis</b>	112
2.2.7.1	Tissue culture	112
2.2.7.2	Conditions for FRET	113
2.2.7.3	Acceptor Photo-bleaching (AP)-FRET measurement	114
 <b>Chapter 3</b>		
<b>3</b>	<b>The IRSp53 phenotype</b>	117
3.1	Introduction	117
3.2	Study of cytoskeletal dynamics using GFP-actin in N1E115 cells	117
3.3	Phenotype of IRSp53 overexpression in N1E115 cells	118
3.4	Role of the IRSp53 SH3 domain in filopodia and lamellipodia formation	123

## **Chapter 4**

<b>4</b>	<b>IRSp53 SH3 domain binding partners</b>	125
4.1	Introduction	125
4.2	IRSp53 SH3 domain associates with both N-WASP and WAVE 1/2 in complexes	125
4.3	IRSp53 interacts with N-WASP directly	127
4.4	FRET analysis of IRSp53-N-WASP interaction	130

## **Chapter 5**

<b>5</b>	<b>N-WASP knock out</b>	134
5.1	Introduction	134
5.2	IRSp53 requires N-WASP for filopodia formation	134
5.3	The effect of Rac1N17 on IRSp53 phenotype in N-WASP KO cells	136
5.4	IRSp53 expression is comparable in both N-WASP WT and KO cells	138
5.5	Effect of N-WASP reconstitution in KO fibroblasts of IRSp53 phenotype	138
5.6	Characterization of filopodia induced by N-WASP reconstitution experiment	141
5.7	WAVE1(SCAR) and WAVE1 $\Delta$ WA can reconstitute N-WASP function in N-WASP KO Cells	141
5.8	The SH3 domain is required for IRSp53 induced filopodia formation	144
5.9	FRET analysis of the IRSp53-N-WASP interaction in the KO cells	144

## **Chapter 6**

<b>6</b>	<b>The IRSp53 IMD</b>	148
6.1	Introduction	148
6.2	IRSp53 IMD domain produces protrusions	148
6.3	The IMD-4K is important for IRSp53 filopodia formation	152
6.4	IRSp53 interacts directly with F-actin but IMD does not	153

## **Chapter 7**

<b>7</b>	<b>The role of G-Proteins</b>	156
7.1	Introduction	156
7.2	The Cdc42 phenotype	156
7.3	The effect of Rac1N17 on the Cdc42 phenotype in N-WASP KO cells	157
7.4	Cdc42 requires N-WASP for filopodia formation	160

## **Chapter 8**

<b>8</b>	<b>Role of WAVE1, WAVE2 and Mena in IRSp53 induced filopodia formation</b>	162
8.1	Introduction	162
8.2	Phenotype of WAVE1, WAVE2 and Mena overexpression in N1E115 cells	163
8.3	Localization of WAVE1 and WAVE2 with IRSp53 overexpression in N1E115 cells	163
8.4	Effect of WAVE1 and WAVE2 knockdown on IRSp53 phenotype in N1E115 cells	165
8.5	IRSp53 phenotype in Mena knock out cells	169

## **Chapter 9**

<b>9</b>	<b>Discussion</b>	171
9.1	Are all protrusive structures filopodia?	171
9.2	Cdc42 effectors in filopodia formation and Rac1 activation	171
9.3	IRSp53 phenotype in N1E115 cells	172
9.4	IRSp53 SH3 domain function	172
9.5	IRSp53 phenotypes in N-WASP KO cells	174
9.6	The role of IRSp53 IMD in filopodia formation	175
9.7	Cdc42 does not induce filopodia in N-WASP KO cells	177
9.8	Relationship between IRSp53 and WAVE1, WAVE2 and Mena	178
9.9	Relationship between IRSp53 and Mena	179
9.10	Is IRSp53 a Cdc42 or Rac effector?	179

9.11	The relation between IMD and BAR domains	180
9.12	Conclusion	183
	<b>References</b>	186
	<b>Appendices</b>	253
	<b>CD-Rom: CD of live imaging movies</b> (see inside of back cover).	

## Summary

The Cdc42 effector IRSp53 is an adaptor protein consisting of a SH3 domain, a potential WW binding motif, a partial CRIB motif, an IMD domain, as well as a PDZ domain binding motif in some isoforms. Previous work has shown that IRSp53 can induce the formation of filopodia and neurites in N1E115 neuroblastoma cells in a Cdc42-dependent manner (Govind et al., 2001). In this study I show that the SH3 domain of IRSp53 is essential for its induction of complex neurites (with multiple filopodia and lamellipodia). The SH3 domain of IRSp53 has been reported to bind a number of proteins known to be involved in remodeling of the actin cytoskeleton, including, Mena, WAVE1/2, mDia2/p140 and Espin. I show here that the SH3 domain of IRSp53 interacts directly with N-WASP. I also show that N-WASP is a key component for IRSp53-induced filopodia formation as overexpression of IRSp53 in N-WASP knock out (KO) fibroblasts was unable to induce filopodia formation. IRSp53-induced filopodia formation can be reconstituted in N-WASP KO fibroblasts by full length N-WASP and by N-WASP $\Delta$ WA (a mutant unable to activate the Arp2/3 complex). Interestingly, the filopodia reconstituted with N-WASP have a shorter half-life than those reconstituted with N-WASP $\Delta$ WA. I show that IMD domain induces “partial filopodia”, dynamic protrusions that lack F-actin. Full length IRSp53 requires cooperation between the IMD, CRIB and SH3 domains for its filopodia formation activity. Taken together, these results suggested that Cdc42, IRSp53 and N-WASP protein-protein interactions are important for filopodia formation and turnover.

## List of Tables

### Chapter 4

Table 4.1	AP-FRET assay of mRFP-IRSp53 and GFP-N-WASP	133
-----------	---	-----

### Chapter 6

Table 6.1	Characterization of IMD/IMD-4KD induced protrusions	151
Table 6.2	AP-FRET assay of mRFP-IRSp53, mRFP-IMD and GFP-actin	155



## List of Figures

### Chapter 1

Figure 1.1	A model of cell migration	3
Figure 1.2	Morphological characteristics of a migrating cell	5
Figure 1.3	Functions of ABPs	15
Figure 1.4	Ras as molecular switch	22
Figure 1.5	The Rho family GTPases as molecular switches	31
Figure 1.6	WAVE2 and N-WASP protein complexes	49
Figure 1.7	Schematic of WASP/WAVE family	50
Figure 1.8	Schematic of VASP/Mena family	58
Figure 1.9	Schematic of IRSp53 and Missing in Metastasis (MIM)	65

### Chapter 2

Figure 2.1	FRET analysis by acceptor photobleaching (AP-FRET)	116
------------	--	-----

### Chapter 3

Figure 3.1	Time-lapse imaging of N1E115 cells transfected with GFP-actin	119
Figure 3.2	Time-lapse imaging of N1E115 cells transfected with GFP-actin and HA-IRSp53	121
Figure 3.3	Time-lapse imaging of GFP-actin and tdRed-IRSp53 in N1E115 cells	122
Figure 3.4	Effect of mutations of SH3 domains (W/R and FP/AA) on IRSp53 phenotype in N1E115 cells	124

## Chapter 4

Figure 4.1	Mass Spectrometry analysis of brain proteins binding to the IRSp53 SH3 domain affinity column	126
Figure 4.2	IRSp53 SH3 domain interaction with <sup>35</sup> S-labelled N-WASP <i>in vitro</i>	128
Figure 4.3	IRSp53 SH3 domain interaction with N-WASP using Yeast Two Hybrid	129
Figure 4.4	AP-FRET assay of mRFP-IRSp53 and GFP-N-WASP	132

## Chapter 5

Figure 5.1	IRSp53 phenotypes in N-WASP WT and KO cells	135
Figure 5.2	Effect of Rac1N17 on IRSp53 induced phenotype	137
Figure 5.3	IRSp53 expression in N-WASP WT and KO cells	139
Figure 5.4	Reconstitution of N-WASP KO cells with N-WASP or N-WASP $\Delta$ WA	140
Figure 5.5	IRSp53 induced filopodia dynamics in N-WASP KO cells reconstituted with either N-WASP or N-WASP $\Delta$ WA	142
Figure 5.6	IRSp53 induced filopodia dynamics in N-WASP KO cells transfected with either WAVE1(SCAR) or WAVE1 $\Delta$ WA (SCAR mutant)	143
Figure 5.7	Morphological activity of the SH3 domain mutant IRSp53-FP/AA	146
Figure 5.8	IRSp53-FP/AA induced morphological effects in N-WASP KO cells reconstituted with N-WASP	147

## Chapter 6

Figure 6.1	Characterization of IMD domain driven protrusive structures	150
Figure 6.2	Phenotype of the IRSp53-4K in N-WASP WT and N-WASP KO cells	154

## **Chapter 7**

Figure 7.1	Phenotype of Cdc42V12 in N1E115 cells	158
Figure 7.2	Phenotype of Cdc42V12 in N-WASP WT and KO cells	159
Figure 7.3	Cdc42V12/Rac1N17 phenotype in N-WASP KO cells with N-WASP reconstitution	161

## **Chapter 8**

Figure 8.1	Phenotype of WAVE1, WAVE2 and Mena overexpression in N1E115 cells	164
Figure 8.2	Localization of WAVE1 and WAVE2 in IRSp53 overexpression in N1E115 cells	166
Figure 8.3	Effect of WAVE1 and WAVE2 RNAi treatment on IRSp53 induced morphology	167
Figure 8.4	Effect of WAVE1 and WAVE2 knockdown on IRSp53 phenotype	168
Figure 8.5	IRSp53 phenotypes in Mena WT and KO cells	170

## **Chapter 9**

Figure 9.1	Comparison of the IMD with known structures of different BAR domains	182
Figure 9.2	Proposed model of filopodia formation through IRSp53	185

## List of Abbreviations

aa	amino acid residues
ARF	ADP-ribosylation factor
Arp2/3	Actin-related protein 2/3
ATP	Adenosine triphosphate
Bp	base pairs
<i>C.elegans</i>	<i>Caenorhabditis elegans</i>
CIP4	Cdc42 interacting protein
Cdc42	Cell Division Cycle 42
CRIB	Cdc42/Rac interacting binding region
DAG	Diacylglycerol
DH	Dbl homology domain
DMEM	Dulbecco's modified eagle medium
cDNA	complementary DNA
CRIK	Citron Kinase
ECL	Enhanced Chemiluminescence
<i>E.coli</i>	<i>Escherichia coli</i>
EDTA	Ethylenediamine tetra acetic acid
ERK	Extracellular signal-regulated protein kinase
F-actin	Filamentous actin
FBS	Fetal Bovine Serum
FCS	Fetal Calf Serum
FITC	Fluorescein isothiocyanate
G-actin	globular monomeric actin
$\beta$ -gal	$\beta$ -galactosidase
GAL4BD	GAL4 DNA binding domain
GAL4AD	GAL4 activation domain
GAP	GTPase activating protein
GDI	Guanine nucleotide inhibitor protein
GDP	Guanosine-5 -diphosphate
GEF	Guanine nucleotide exchange factor
GFP	Green fluorescence protein
GRB2	Growth factor receptor-bound protein
GST	Glutathione-S-transferase
GTP	Guanosine-5 -triphosphate
HA	Heamagglutinin
HRP	Horseradish peroxidase
"his"	Histidine deficient media
IMD	IRSp53-MIM homology domain
IPTG	Isopropyl-thio- $\beta$ -D-galactoside
IQGAP	GAP containing Ile-Glu motif
IGF-1	Insulin-like growth factor
IP <sub>3</sub>	Inositol-1,4,5-triphosphate
IR	Insulin receptor
IRS-1	Insulin receptor substrate-1

IRSp53	Insulin receptor substrate 53 kDa
JNK	c-Jun amino-terminal kinase
kDa	Kilo dalton
Klenow	<i>E.coli</i> DNA polymeraseI (large fragment)
lacZ	gene encoding $\beta$ -galactosidase
LB	Luria Bertani medium
“leu <sup>-</sup> ”	leucine deficient media
LPA	Lysophosphatidic acid
MCS	Multiple cloning site
MAPK	Mitogen-activated kinase
MENA	Mammalian Enabled
MIM	Missing in metastasis protein
MKK	MAPK kinase
MKKK	MAPK kinase kinase
MLC	myosin light chain
MLCK	Myosin light chain kinase
MRCK	Myotonic Dystrophy kinase-related Cdc42-binding kinase
mRFP	monomeric Red Fluorescence protein
MTOC	Microtubule organizing center
NADPH	Reduced nicotinamide adenine dinucleotide
NGF	Nerve growth factor
dNTP	deoxynucleotide 5'-triphosphate
ddNTP	2',3'-dideoxynucleotide triphosphate
N-WASP	Neuronal-Wiskott Aldrich Syndrome Protein
OD	Optical density
p21	Member of the Ras superfamily of low molecular weight GTPases
p38	Hog1-related MAPK
PAK	p21 –activated kinase
PAGE	Polyacrylamide gel eletrophoresis
PBD	p21 binding domain
PBS	Phosphate buffered saline
PDGF	Platelet-derived growth factor
PH	Plestrin homology domain
PIP2	Phosphotidylinositol 4,5,-biphosphate
PI3-K	Phosphotidylinositol 3-kinase
PIX	PAK-interacting nucleotide exchange factor
PKC	Protein kinase C
PLC $\gamma$	Phospholipase C $\gamma$
PMSF	Phenylmethyl-sulfonyl fluoride
POR-1	Partner of Rac
PTB	Phosphotyrosine binding domain
mRNA	messenger RNA
RNaseA	Ribonuclease A
RNAi	RNA interference
ROK	Rho kinase
RTK	Receptor tyrosine kinase

SD	Synthetic Drop-out media
SDS	Sodium dodecyl sulphate
SH2	Src homology domain
SH3	Src homology domain
<i>S.cerevisiae</i>	<i>Saccharomyces cerevisiae</i>
<i>S.pombe</i>	<i>Schizosaccharomyces pombe</i>
sos	Son-of-sevenless
TEMED	N, N, N', N'-tetramethylethylenediamine
Tm	Melting temperature
Tris	2-amino-2(hydroxymethyl)-1,3-propanediol
TRITC	tetramethylrhodamine isothiocyanate
Triton-X	Octylphenoxypolyethoxyethanol
“trp <sup>-</sup> ”	tryptophan deficient media
Tween-20	Polyoxyethylenesorbitan monolaurate
v/v	volume by volume
w/v	weight by volume
WASP	Wiskott Aldrich Syndrome Protein
WAVE	WASP family Verprolin-homologous protein
WIP	WASP-interacting protein
X-gal	5-bromo-4-chloro-3-indolyl b-D-galactopyranoside

# **INTRODUCTION**

## **Chapter 1. Introduction**

### **1. 1. The cell as a fundamental unit of life.**

The advent of light microscopy initiated a major paradigm shift in thinking about the nature of life. In 1665 Robert Hooke made thin slices of cork and likened the structures he saw to the cells in a monastery. However, he did not make the link between the structures he saw and life. At about the same time Antony van Leeuwenhoek invented a simple (one-lens) microscope that was able to magnify specimens around 200 times and achieved higher resolutions than the best compound microscopes of his day, mainly because he crafted better lenses. Antony van Leeuwenhoek made observations of, for the first time, single-cell organisms, or "little animalcules" as he called them. These likely included microorganisms, red blood cells and sperm cells. About 100 hundred years later Henri Dutrochet made the connection between plant cells and animal cells explicit. He put forward the idea that the cell constitutes the basic unit of life. From these initial observations and subsequent work by other people (e.g. Raspail, Schleiden and Schwann) the three main parts of the cell theory emerged: (i) all living matter is composed of one or more cells, (ii) cells are the simplest independent units of all organisms and (iii) all cells are generated from pre-existing cells. Further improvements in microscopy, in particular the advent of Electron Microscopy, revealed subcellular structures such as the endoplasmic reticulum, mitochondria and the cytoskeleton.

The application of genetics, biochemistry and molecular biology, to simple single cell organisms, helped elucidate the mechanism by which cells grow and divide. In particular, the demonstration that the human Cdc2 kinase can fulfill the function of the



*Schizosaccharomyces pombe* homolog in control of the cell cycle confirms the fundamental nature of the cell (Nurse et. al., 2002).

### **1.1.1. Cell migration.**

Like cell growth and division, cell migration, is a fundamental cell process. Cell migration underlies the development of all organisms and the function of different tissue systems. Cell migration over a substrate has been described as the succession of protrusion, attachment and retraction (Abercrombie et. al., 1980). The first step in the sequence, protrusion is driven by actin polymerization at the leading edge of the cell (Pollard et. al., 2003). Two morphological structures, lamellipodia and filopodia, which are comprised of different F-actin networks and dynamics are the basic units of cell migration (for review, Svitkina et. al., 1996). Protrusion is followed by retraction of the trailing edge and finally the cell translocates to a new position (Figure 1.1).

### **1.1.2. Lamellipodia and membrane ruffling.**

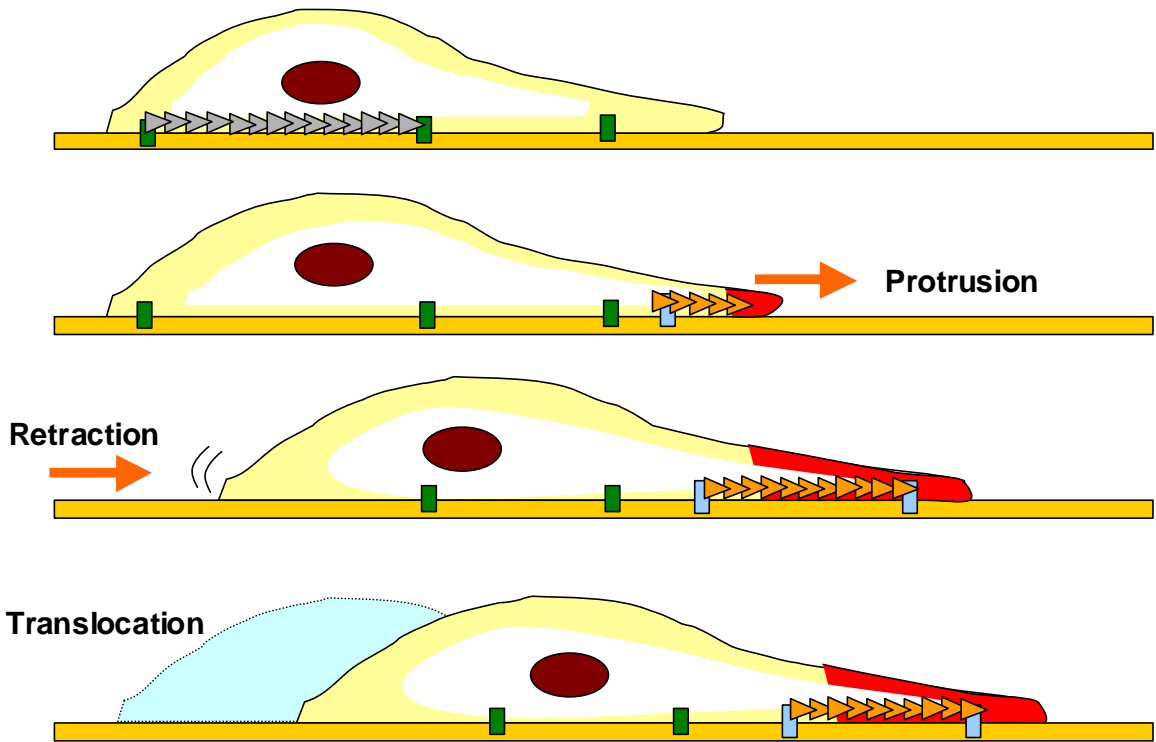
Lamellipodia are broad, flat protrusions, in which actin filaments form a branched network (Svitkina et. al., 1997, Svitkina and Borisy, 1999). The current model for lamellipodial dynamics (Borisy and Svitkina, 2000, Pollard et. al., 2000) suggests that treadmilling of the branched actin filament array consists of repeated cycles of dendritic nucleation, elongation, capping and depolymerization of filaments. During the elongation after nucleation, the filament pushes the membrane. When a filament elongates beyond the efficient length for pushing, its growth is thought to be terminated by capping protein

**Figure 1.1 A model of cell migration.**




Cell migration consists of the following successive steps.

1. **Protrusion.** Extracellular stimuli induce de novo actin polymerization at the leading edge leading to the formation of F-actin-based membrane protrusions such as filopodia and lamellipodia.
2. **Retraction.** Adhesive structures and stress fibres at the trailing edge are broken down.
3. **Translocation.** The net result of 1 and 2 is that the cell has moved to a new position.

Figure 1.1



**Key**

-  nucleus
-  Focal adhesions (stress fibers)
-  Focal adhesions (Lamellipodia/Filopodia)
-  Actin
-  monomers

(Copper and Schafer, 2000). Depolymerization is assisted by proteins of the ADF/cofilin family (Bamburg, 1999). There are other proteins playing supporting roles in this process. Profilin targets filament elongation to barbed ends (Carlier and Pantaloni, 1997), enabled/vasodilator-stimulated phosphoprotein (Ena/VASP) family proteins protect elongating barbed ends from capping (Bear et. al., 2002), contactin stabilizes branches (Weaver et. al., 2001), and filamin A (Flangan et. al., 2001) and  $\alpha$ -actinin stabilize and consolidate the whole network. If the actin treadmilling rate exceeds that at which the cell can migrate, the plasma membrane is seen to move vertically and then back over the cell in the form of a wave. This phenomenon is known as membrane ruffling and is linked with high levels of F-actin (Figure 1.2).

### **1.1.3. Filopodia.**

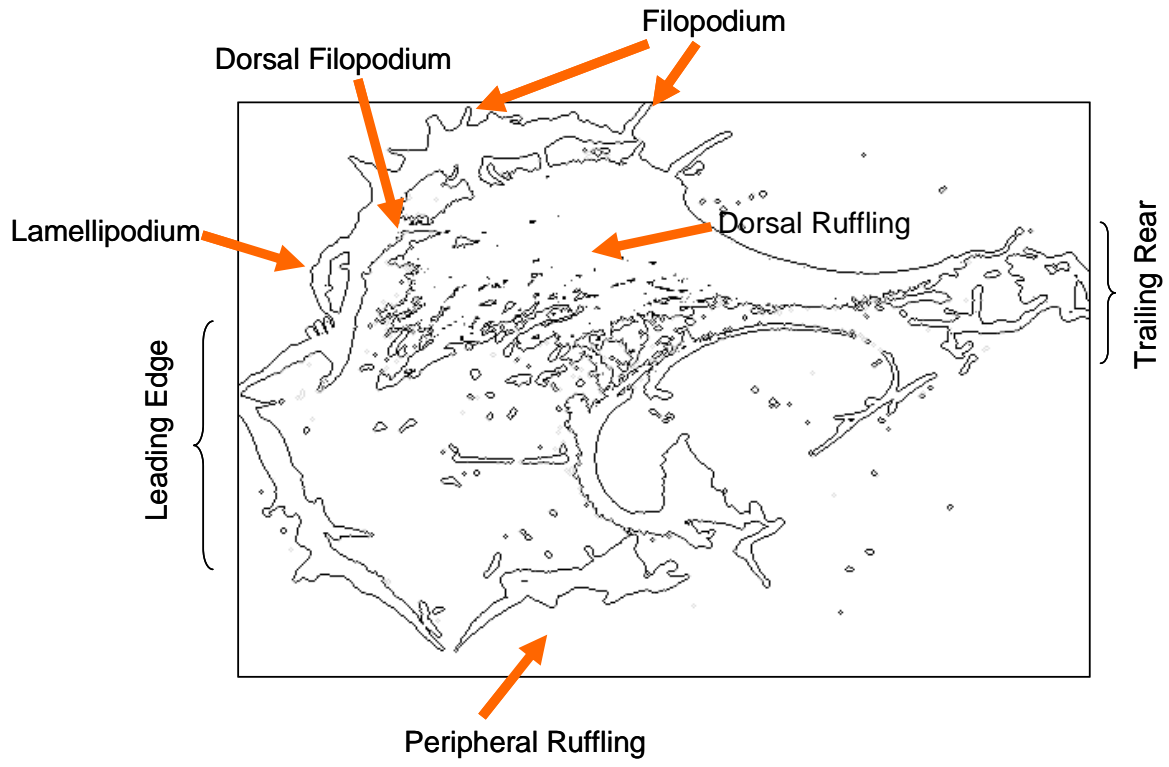
Filopodia are thin cellular processes, in which actin filaments are long, parallel, and organized into tight bundles (Small et. al., 1998, Lewis and Bridgman, 1992; Small et. al., 2002). There are other cellular structures, such as microspikes and retraction fibres that bear similarities to filopodia and may be related to them. Microspikes are parallel actin bundles within the lamellipodium. Retraction fibres are long, thin cellular processes that remain attached to the substratum after cell withdrawal. They also contain parallel bundles of F-actin filaments (Small et. al., 1998, Lewis and Bridgman, 1992).

Filopodia first came to prominence in the 1960s, when they were shown to be involved in sea urchin gastrulation. During the invagination of the sea urchin endoderm, mesenchymal cells extend filopodia to ectodermal cells across the blastocoel cavity and

**Figure 1.2 Morphological characteristics of a migrating cell.**

The image shows an electron micrograph of a fully spread fibroblast. The cell has a broad flattened area at its leading edge and an elongated tail at its rear. Lamellipodia and filopodia decorate the peripheral regions of the cell. Dorsal membrane ruffling and filopodia are also visible.

Figure 1.2



these filopodia are responsible for the directed migration of the mesenchyme. Many types of motile cells have and use filopodia.

Filopodia are often found associated with the lamellipodia and when the two merge, ribs are seen to form. In neurons, filopodia are clearly seen in growth cones, and dendritic spines are essentially short filopodia. At times, the visualization of filopodia is difficult due to their size and dynamic nature and the fact that they can be damaged by the process of fixation. However, with improvements in image processing, CCD cameras and microscopy, filopodia can be detected and followed in real time.

Filopodia appear to explore the extracellular matrix (ECM) and surfaces of other cells. They are likely to play a role in; identification of appropriate targets for adhesion, axonal guidance and chemotaxis. These functions are essential in cell migration and many morphogenetic events, including axonal path finding, epithelial cell adhesion, gastrulation, dorsal closure in *Drosophila*, ventral enclosure in *Caenorhabditis elegans*, and wound healing.

Filopodia can have different sizes and tensile strength. Classical sea urchin filopodia are long, thin and straight with a diameter range of 0.2 to 0.4  $\mu\text{m}$ . These filopodia normally extend between 5 to 35  $\mu\text{m}$ , but occasionally they can extend to more than 70  $\mu\text{m}$  in length. They have a growth rate of 10  $\mu\text{m}/\text{min}$ , with a burst of maximum activity at up to 25  $\mu\text{m}/\text{min}$ . The filopodia retraction rate is of similar magnitude and kinking is sometimes observed during the process. Filopodia can be robust and maintain structural

integrity even when they exceed over 70  $\mu\text{m}$  in length. Specialized filopodia such cytonemes are found in the *Drosophila* wing imaginal disc and can grow up to a length of 800  $\mu\text{m}$ .

Filopodia protrusion is thought to occur by a filament treadmilling mechanism, which was originally proposed for both filopodia and lamellipodia (Small et. al., 1994). According to this model, all actin filaments within a bundle elongate at their barbed ends and release subunits from their pointed ends. Existing experimental data support this model of filopodia elongation. Structurally, actin filaments in filopodia are long and unbranched (Svitkina and Borisy, 1999), suggesting that assembly occurs by elongation, not by branched nucleation. Dynamic observations (Mallavarapu and Mitchison, 1999) revealed that labeled actin incorporated at the filopodial tips, moved backward and dissipated at the rear (as predicted by the treadmilling mechanism), and that actin turnover in filopodia was slow; consistent with the idea of long filaments adding or losing subunits only at their ends.

## **1.2. The cytoskeleton.**

### **1.2.1. Components of the cytoskeleton.**

The ability of eukaryotic cells to adapt to a variety of shapes and to carry out coordinated movements depends on a complex network of protein filaments that extend throughout the cytoplasm. This network is called the cytoskeleton. It is a highly dynamic structure that reorganizes continuously as the cell changes shape and responds to its environment. The diverse activity of the cytoskeleton is dependent on three type of protein filaments;



actin microfilaments, microtubules and intermediate filaments (IFs). Each type of filament is formed from different protein subunits: actin for actin microfilaments, tubulin for microtubules and a family of related fibrous proteins such as lamin for IFs.

### **1.2.2. Actin microfilaments.**

Actin genes are highly conserved and are present in all eukaryotic species. Actin is the most abundant protein in many cells and is distributed throughout the cytoplasm. There are six types of actin in mammalian cells and they can be divided into 3 classes according to their isoelectric point.  $\alpha$ -Actins are found mainly in muscle while  $\beta$ -actin and  $\gamma$ -actin are found in non-muscle cells. Actin exists in two forms, the globular monomeric form known as G-actin and the filamentous form, F-actin. G-actin is non-covalently associated with a molecule of ATP. Polymerization of actin results in the hydrolysis of the terminal phosphate of ATP, resulting in actin filaments that consist of tight helix of uniformly orientated actin molecules. The actin monomer has polarities and contains a “plus” end and a “minus” end (as defined with decoration of filaments by myosin heads). The general belief is that a dynamic equilibrium exists between the monomeric (G)-actin and filamentous (F)-actin. While there are no control factors, a process known as treadmilling occurs. G-actin is added to the barbed or plus end and this is matched by dissociation from the pointed or minus end (Wenger, 1976).

Actin networks can be organized into three general arrays. In parallel bundles of actin filaments, filaments orientated with polarity give rise to structures such as filopodia and microspikes. In contractile bundles, commonly found in the contractile ring in mitosis as

well as in stress fibres, the bundles are arranged with opposite polarities and they are associated with the motor protein myosin. The third and last class of array is a dendritic arrangement. F-actin is in an open organization, forming a meshwork of many interconnecting filaments, resulting in a gel-like network found in lamellipodia (Matsudaria, 1991).

### **1.2.3. Microtubules.**

Microtubules are made up of the protein tubulin. Tubulin exists as a heterodimer consisting of  $\alpha$ - and  $\beta$ -tubulin subunits that form a tightly linked globular protein. Tubulin heterodimers contain 13 linear protofilaments, each composed of alternating  $\alpha$ - and  $\beta$ -tubulin subunits, bundled into parallel to form a cylinder. The protofilaments are aligned in parallel with the same polarity to form a polar microtubule. Microtubules, like actin, have a fast growing plus end and a slower growing minus end. The  $\beta$ -tubulin monomer is arranged such that it faces the plus end, whereas  $\alpha$ -tubulin monomer is exposed at the minus end. The polarity set up of the microtubule structure is important for the function of the motor protein families; kinesin (Vale and Fletterick, 1997) and dynein. These proteins utilize the energy release from ATP hydrolysis to move unidirectionally along microtubules (Desai and Mitchison, 1997). The minus end of the microtubule is unstable, but it is stabilized by attachment to a microtubule organizing centre (MTOC) of the centrosome. Biochemical studies have shown that microtubules undergo continual depolymerization and repolymerization, a process known as dynamic instability (Erickson et. al., 1992). This dynamic instability requires an input of energy from GTP hydrolysis to achieve a balance between polymerization and depolymerization. GTP

binds  $\beta$ -tubulin of the heterodimeric tubulin molecules to the end of a microtubule, and this leads to the hydrolysis of GTP to GDP. GTP hydrolysis provides a mechanism for microtubules to depolymerize by weakening the bonds between tubulin subunits in the microtubule.

Microtubules play an important role in non-dividing as well as dividing eukaryotic cells. In non-dividing cells, they are important for organizing the cytoplasm, nucleus and organelle position and forming structures such as flagella and cilia (Desai and Mitchison, 1997). They also play an important role in axon formation and axonal transport (Stevens et. al., 1998; Hirokawa et. al., 1996). Microtubules are stabilized by the MAPs (microtubule associated proteins). In neuronal cells, MAPs have been shown to increase polymerization of tubulin, depress catastrophe and promote rescue. (Drechsel et. al., 1992; Trinczek et al., 1995), thus increasing the amount of polymerized, stable tubulin in the cell.

#### **1.2.4. Intermediate filaments.**

Expression of IFs is cell-type specific and they are highly diverse and can account for up to 85% of total protein in differentiated cells such as keratinocytes and neuronal cells (Fuchs and Cleavland, 1998). IFs play a structural or tension bearing role in the cell. They are found as dimers composed of two  $\alpha$ -helical chains that are parallel and intertwined in a coiled-coil rod. The end rods are highly conserved and associate from head to tail. The dimers form linear arrays, of which four of these will be in an antiparallel, half-staggered manner forming photofibrils. When three or four photofibrils

intertwined, an apolar intermediate filament of 10 nm in diameter is formed. In the neuronal system, IFs are made up of three type of proteins; neurofilaments NF-L (67kD), NF-M (150kD) and NF-H (200kD). NF-L forms the backbone on which NF-M and NF-H integrate to form peripheral dimer arrays. In this formation, NF-M and NF-H tails are turned, protruding away from the backbone, leaving them open to associate with other neurofilaments and microtubules in the axoplasm. The nonpolarised structure of IFs distinguishes them from actin microfilaments and microtubules that are polarized and whose functions are dependent on this polarity (Stewart, 1993).

### **1.3. Microfilament assembly and disassembly: Actin dynamics.**

Actin polymerization is required in many processes such as cell motility, neurite extension, nerve growth cone movement and cell spreading. Actin rapidly cycles between G-actin and F-actin forms. The rate of cycling is determined by actin binding proteins (ABPs) which includes the sequestering proteins and the capping proteins. Sequestering proteins inhibit polymerization by binding to monomeric G-actin, sequestering them away from the working pool. Capping proteins bind to the barbed or plus end of the actin filament, thus preventing its growth (Barkalow et. al., 1996). New actin filaments are produced by either elongation of existing filaments or *de novo* nucleation of monomeric G-actin with elongation. Actin microfilaments can also be formed by severing of barbed ends to create new ones or uncapping of existing of barbed ends (Higgs and Pollard, 1999).

The Rho GTPases play important roles in actin polymerization. Activated Rac1 induces uncapping of filaments that result in further actin polymerization (Hartwig et. al., 1995). Other effectors like WASP and N-WASP have also been shown to play an active role in actin polymerization. These proteins will be covered in more detail in section 1.8.

Depolymerization of actin filaments occurs through severing of existing actin filaments. The plus ends of these severed filaments are prevented from renewed actin polymerization as ADP-bound G-actin is less efficiently polymerized into the ends of severed filaments. Severed filaments are also capped by capping proteins such as CapG and CapZ (Carlier et. al., 1997).

### **1.3.1. Arp2/3 complex.**

The identification of the Arp2/3 complex was an important event that contributed to the understanding of the actin polymerization process. The Arp2/3 complex consists of seven polypeptides, of which two major components are actin related proteins: Arp2 and Arp3 (Machesky et. al., 1999). The Arp2/3 complex was first identified in *Acanthamoeba castellanii* extracts on a profilin affinity column (Machesky et. al., 1994). The Arp2/3 complex is regulated by members of the WASP/SCAR family *via* a C-terminal region consisting of one or two WASP homology 2 (WH2) motif, a central linking region and an acidic region (Higgs et. al., 2001), to which actin monomers are recruited and added to existing filaments (Rohatigi et. al., 1999). The Arp2/3 complex nucleates actin at a 70° angle and this phenomena leads to the branching of actin filaments (Blanchoin et al, 2000). The lone Arp2/3 complex is intrinsically inactive *in vivo*, and its activation

requires actin filaments, ATP and activating proteins such as N-WASP (neural-WASP). Upon binding of ATP, a conformational change occurs. The two Arp proteins come into close proximity to form a structure that is favorable for actin polymerization (Robinson et. al., 2001). There are currently two models for actin polymerization by Arp2/3 complex. The dendritic actin-nucleation model (Mullins et. al., 1998; Pollard et. al., 2000) and the barbed-end nucleation model (Pantaloni et. al., 2000). The exact mechanism and actions of the Arp2/3 complex is still unclear.

### **1.3.2. Myosin.**

Myosins are characterized by three domains, a N-terminal motor or “head” that binds actin and ATP, a neck domain consisting of one or more light chain binding IQ motifs and a C-terminal tail. By sequence analysis of the motor domains, ~20 distinct classes have been identified (Berg et al., 2001) and the best studied ones are Myosin I and V which have been implicated to be involved in vesicle transport (Depina et. al., 1999). All myosin proteins possess a conserved head region of approximately 80 kDa, followed by a neck or regulatory region. The neck region is of variable length and binds between one and six light chains of calmodulin/EF-hand family proteins. The head and neck region comprise the motor domain which is responsible for ATP hydrolysis and provides energy to power a unidirectional force along the actin filament (Bahler, 1996). This ATPase activity is regulated by the phosphorylation and dephosphorylation of myosin light chain (MLC). The phosphorylation of MLC is catalyzed by MLC kinase (MLCK) and dephosphorylation is regulated by myosin phosphatase (Citi, 1987). While the myosin head is conserved across all myosins, the tail is highly variable. Myosin can possess a

membrane binding site and/or a site that allows binding to a second actin filament. The myosin tail region also determines the function of the protein; vesicle trafficking, attachment to plasma membrane or alignment of actin filaments relative to each other (Alberts et. al., 1994).

### **1.3.3. Actin binding proteins.**

Regulation of polymerization and depolymerization of actin is carried out by a group of proteins that are responsible for the crosslinking, severing, sequestering of monomeric actin subunits and capping of existing actin filaments. This group of proteins is collectively known as actin binding proteins (see figure 1.3).

**$\beta$ -thymosin** is the most abundant of these actin-monomer binding proteins and is widely expressed. It is an unusually small protein with a molecular weight of about 5 kDa.  $\beta$ -thymosin sequesters G-actin thereby inhibiting filament growth (Cassineris et. al., 1992).

**Profilin**, another actin-monomer binding protein which is widely expressed, is thought to play a part in controlling actin polymerization in response to external stimuli. It is associated predominantly with the plasma membrane and the binding of profilin to G-actin accelerates the ADP/ATP nucleotide exchange (Goldschmit-clermont et. al., 1991). Profilin is thought to play a role in stimulating actin polymerization as a mutant yeast that is deficient in profilin lacks actin filaments.

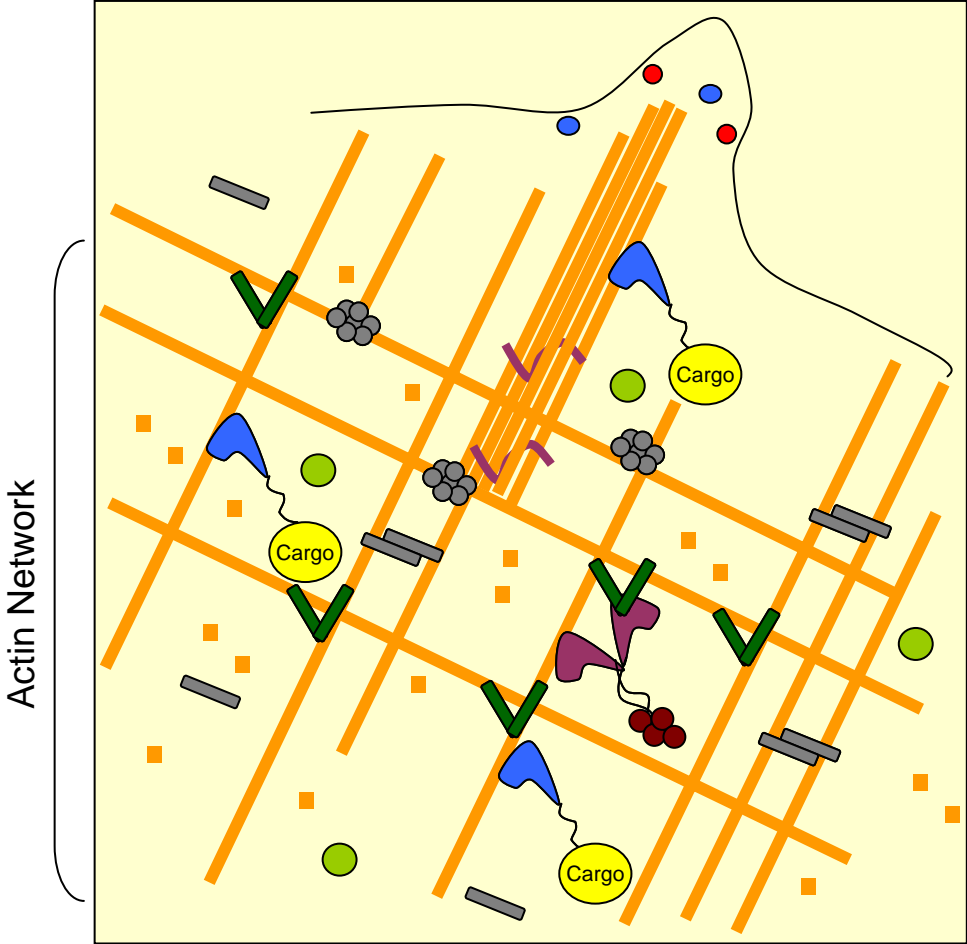
### **Figure 1.3 Functions of ABPs.**

A schematic of ABPs is shown illustrating their function in the modification of the actin network.

The ABPs have the following activities; Profilin and ADF cofilin bind G- and F-actin and they are mostly concentrated at the leading edge of the cell. They promote the disassembly of actin filament. Gelsolin is responsible for F-actin severing and capping. Filamin, actinin and fimbrin crosslink F-actin. Myosins are involved in vesicle trafficking, attachment to plasma membrane and transport of cargo. The Arp2/3 complex facilitates branching of F-actin with angle of  $70^\circ$ .



Figure 1.3



- Key:
- F-actin
  - Profilin
  - ADF Cofilin
  - Gelsolin
  - Filamin
  - α-Actinin
  - Fimbrin
  - Myosin X
  - Arp2/3
  - Myosin I
  - Adhesion receptors

**Fimbrin and  $\alpha$ -actinin** are widely distributed actin cross-linking (bundling) proteins. They are enriched in parallel bundles at the leading edge and in microspikes or filopodia, together with fimbrin, while  $\alpha$ -actinin is accountable for the loose cross-linking of actin filaments in stress fibres (Albert et. al., 1994).

**Tropomyosin** is comprised of two alpha-helical chains in a coiled coil conformation, forming a chain of subunits, polymerized end to end. It is ubiquitously expressed and is widely distributed in the cell. It is found to associate with actin along the two grooves of the F-actin filament, giving rise to both structural stability and function modulation (Perry, 2001).

**Filamin** plays a role in the organization of F-actin into networks and stress fibres. They form dimers in a tail-to-tail manner and anchor transmembrane proteins to the actin cytoskeleton, providing a scaffold for cytoplasmic Signaling proteins (Van der Flier et. al., 2001).

**Cofilin** is a ubiquitous actin-binding protein that enhances turnover of actin filaments by increasing the polymerization rate from the pointed end (Carlier et. al., 1997) and severing the actin filaments directly (Du et. al., 1998). **Actin depolymerizing factor (ADF)** is homologous to cofilin. Both cofilin and ADF bind monomeric and filamentous actin and promote the disassembly of actin filaments. They inhibit polymerization and nucleotide exchange of ATP-actin for ADP-actin. Their binding activities are inhibited by

protein phosphorylation and competitive binding of phosphoinositides (Theriot et. al., 1997).

**Gelsolin** is an actin filament severing and capping protein, and is regulated by calcium and PIP<sub>2</sub> (Kwiatkowski et. al., 1999; Robinson et. al., 1999). Gelsolin binds to actin filaments and causes a conformational change in the actin filament. Gelsolin remains attached to the severed filament as a capping protein, preventing short filament re-annealing or elongation at the barbed ends. The severing process results in an increased number of actin filaments and the uncapping of gelsolin exposes many barbed ends where actin monomers can be added. This allows the cell to rebuild its actin cytoskeleton network in response to external cues.

**Spectrin and ankyrin** were first discovered as prominent components of the membrane-associated cytoskeleton of mammalian red blood cells. They form heterodimers or heterotetramers via interchain binding at the 'head' end between  $\alpha$  and  $\beta$  chains. The 'tail' end contains sites that associate spectrin with other proteins such as actin. Spectrins are connected at their ends by very short actin filaments. Spectrins are also link to an abundant transmembrane protein (band 3) through ankyrin bridges. They provide mechanical support to the plasma membrane of erythrocytes.

The **formins** family of proteins is another group of proteins that constitute a second mechanism for inducing actin polymerization in eukaryotic cells. Rho stimulates actin polymerization in mammalian cells through the diaphanous-related formin (DRF),

mDia1/mDia2, and in *S. cerevisiae* through Bnr1 and Bni1, the only two formins in this organism. Binding of Rho GTPases to mDia1 relieves an auto-inhibitory interaction, exposing an FH2 domain that then binds to the barbed end of an actin filament (Zigmond et. al., 2004). mDia1 also contains an essential FH1 domain which interacts with a profilin/actin complex and delivers it to the filament end. mDia1 remains bound to the barbed end after adding an actin monomer, ready to add another one, and this has been described as a leaky cap. Exactly how monomer assembly occurs at the barbed end with formin bound is still unclear.

#### **1.4. The Ras superfamily.**

The Ras superfamily of small guanosine triphosphatases (GTPases) comprise over 150 members in humans, with evolutionarily conserved orthologs found in *Drosophila*, *C. elegans*, *S. cerevisiae*, *S. pombe*, *Dictyostelium* and plants (Colicelli, 2004). The Ras oncogene proteins are the founding members of this family, which is divided into five major branches on the basis of sequence and functional similarities: Ras, Rho, Rab, Ran and Arf. Small GTPases share a common biochemical mechanism and act as binary molecular switches. Despite being similar to the heterotrimeric G protein  $\alpha$  subunits in biochemistry and function, Ras family proteins function as monomeric G proteins. Variations in structure (Biou and Cherfils, 2004), post-translational modifications that dictate specific subcellular locations and the proteins that serve as their regulators and effectors allow these small GTPases to function as sophisticated modulators of a complex and diverse range of cellular processes.

#### **1.4.1. Ras superfamily members.**

The Ras sub-families control diverse cellular functions. Ras sarcoma (Ras) oncoproteins are the founding members of the Ras family (36 members) and have been subject of intense research, in large part because of their critical roles in human oncogenesis (Repasky et. al., 2004). Ras proteins serve as signaling nodes activated in response to diverse extracellular stimuli. Activated Ras interacts with multiple, catalytically distinct downstream effectors, which are responsible for regulating cytoplasmic Signaling networks that control gene expression and regulation of cell proliferation, differentiation, and survival.

Like Ras, Ras homologous (Rho) proteins also serve as key regulators of extracellular-stimulus-mediated Signaling networks that regulate actin organization, cell cycle progression and gene expression (Etienne-Manneville and Hall, 2002). Twenty members have been identified to date. The 3 best studied members are RhoA (ras homolog gene family, member A), Rac1 (ras-related C3 botulinum toxin substrate 1) and Cdc42 (Cell division cycle 42).

First described as Ras-like proteins in brain (Rab), Rab proteins comprise the largest branch of the superfamily, with 61 members identified (Pereira-Leal and Seabra, 2001). Rab GTPases are regulators of intracellular vesicular transport and the trafficking of proteins between different organelles of the endocytic and secretory pathways (Zerial and McBride, 2001).

The Ras-like nuclear (Ran) protein is the most abundant small GTPase in the cell and is best known for its function in nucleocytoplasmic transport of both RNA and proteins (Weis, 2003). Unlike other small GTPases, Ran function is dependent on a spatial gradient of the GTP-bound form of Ran. There is a single human Ran protein that is regulated by a Ran-specific nuclear GEF and cytoplasmic GAP activities. Thus, there is a high concentration of Ran-GTP in the nucleus, which facilitates the directionality of nuclear import and export. Nuclear Ran-GTP interacts with importin to promote cargo release, and with exportin-complexed cargo to facilitate nuclear import and export of cargo. By a similar mechanism, Ran GDP/GTP cycling also regulates mitotic spindle assembly, DNA replication and nuclear envelope assembly (Li et. al., 2003).

The ADP-ribosylation factor (Arf) family of proteins is involved in regulation of vesicular transport like the Rab proteins, and Arf 1 is the best characterized member (Memon, 2004). Arf GDP/GTP cycling is regulated by distinct GEFs and GAPs (Nie et. al., 2003). The active form, Arf-GTP interacts with effectors including vesicle coat proteins. Conformational differences between the two nucleotide-bound forms are not restricted to the switch I and II regions but also changes in the N-terminal region that facilitate interaction with membranes in their GTP-bound state (Pasqualato et. al., 2002). Arf1 regulates the formation of vesicle coats at different steps in the exocytic and endocytic pathways (Nie et. al., 2003; Memon, 2004). GTP- and donor-membrane-bound Arf associates with and activates coat proteins. The Arf-coat-protein complex then facilitates cargo sorting and vesicle formation and release. GAP-mediated formation of

Arf-GDP is required for dissociation of the Arf-coat-protein complex and subsequent vesicle fusion with acceptor membranes.

#### **1.4.2. Ras as a molecular switch.**

Ras superfamily GTPases function as guanosine-5 –diphosphate (GDP)/GTP-regulated molecular switches (Vetter and Wittinghofer, 2001; Figure 1.4). They share a set of conserved G box GDP/GTP-binding motif elements from the N-terminal end, which together make up ~20kDa G domain (Ras residues 5-166). It has a conserved structure and biochemistry shared by all Ras superfamily proteins, as well as G $\alpha$  and other GTPases.

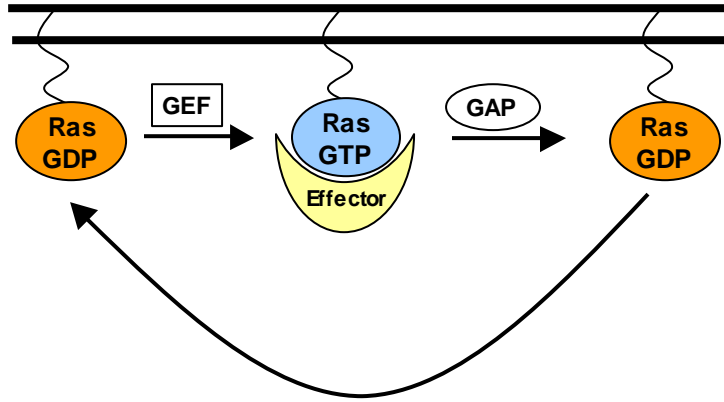
The GTPase proteins are able to bind and hydrolyze magnesium complexes of nucleotide GTP and exchanging GDP for GTP in a cyclic fashion. In their GTP-bound stage, these proteins are able to transduce signals to a downstream effector to elicit their biological effects. The cycling between the GTP-bound and GDP-bound conformations is dependent on the relative rates of reactions, the exchange of GDP for GTP and the hydrolysis of bound GTP. These reactions occur spontaneously at a slow rate. But the rates of these reactions can be accelerated by regulatory proteins, guanine nucleotide exchange factors (GEFs) and GTPase activating proteins (GAPs) (Bourne et. al., 1990).

#### **Figure 1.4 Ras as molecular switch.**

Ras GTPase is a monomeric protein of 21 kDa that shuttles between a GTP-bound form and GDP-bound form. It acts as a molecular switch. In its resting (or "off") state it is found complexed with GDP. In its active (or "on") state it has a molecule of GTP bound to it. Ras is turned "on" by removing the GDP and replacing it with a GTP. This nucleotide exchange reaction is controlled and catalyzed by proteins called "exchange factors" - RasGEFs. Ras possesses a GTPase activity that converts GTP to GDP by hydrolyzing the  $\gamma$ -phosphate off the GTP. Thus the Ras protein has the ability to return to "off" state through phosphate hydrolysis. This reaction is also regulated by other proteins, called GTPase activating proteins - RasGAPs.



Figure 1.4



### **1.4.3. Mutations and oncogenic Ras.**

The ras genes were first identified as the agents responsible for conferring transforming ability to the Harvey and Kirsten strains of murine sarcoma retrovirus (Ellis et. al., 1981). Mutations in the RAS family of proto-oncogenes (comprising H-ras1, H-ras2, N-ras and K-ras) are very common, being found in 20% to 30% of all human tumours (Bos et. al., 1989).

Oncogenic Ras disrupts the usual cycling between active and inactive states by having a lower intrinsic GTPase activity, and it is also insensitive to GAP stimulation, resulting in a highly active protein. The mutant of Ras is generated by the changes of residues 12, 13 and 61 (Barbacid, et al., 1987). A second class of mutations is located at residues 28, 116-119, 144 and 146. These latter mutants display a lower affinity for GDP guanine nucleotide, leading to a rapid exchange of GDP and GTP. All these mutations give Ras the ability to continue signaling to downstream effectors even in the absence of extracellular stimuli, and have been used extensively (in particular G12V mutant) in the study of Ras function.

A different approach to understanding the function of a protein is to generate a dominant inhibitory protein that interferes with the function of the endogenous protein. A mutation that has been very useful in this aspect in the study of Ras function is a serine to asparagine substitution at amino acid residue 17 in H-ras. This mutation yields a protein that has higher affinity for binding to GDP than GTP. The S17N mutated Ras is thought to interfere with endogenous Ras function by titrating RasGEFs so that they are no longer

available (Feig and Cooper, 1988). The serine residue is involved in binding  $Mg^{2+}$  and the mutation is thought to result in defective  $Mg^{2+}$  complexing. Proper binding of  $Mg^{2+}$  by serine 17 may be necessary so that Ras can reach an active conformation, because the 'effector' domain also binds this tethered  $Mg^{2+}$  (through threonine 35) when Ras switches to the active state. (Feig et. al., 1999).

Important mutations that affect the biological activity of Ras without interfering with nucleotide binding or intrinsic GTPase activity reside within the effector loop. Certain mutations in this region abrogate Ras's ability to modulate particular downstream pathways (White et. al., 1995).

The residues that are required for Ras function are those between residues 26 and 48, with the most critical residues for biological function being E31, P43, T35, D38, Y40, V45 and G48. The importance of these residues within the effector domain has been shown through the generation of a chimeric Ras/Rho protein. Rho does not induce a malignant phenotype when substituted with amino acid residues 23-46 of Ras but does induce transformed foci in NIH3T3 cells in a manner similar to RasV12 (Self et. al., 1993). Many studies have utilized these mutations in the effector domain of Ras to investigate pathways downstream of Ras, to assume or exclude a role for candidate effectors of Ras-mediated pathways. These approaches provided a paradigm for the investigation of the Rho family of GTPases.

#### **1.4.4. Ras GTPase regulatory proteins.**

##### **1.4.4.1. Ras guanine nucleotide exchange factors (RasGEFs).**

RasGEFs have a common ~250 amino acid CDC25 homology catalytic domain (also known as the RasGEF domain) and an adjacent ~50 amino acid amino-terminal Ras exchange motif (REM; also known as the RasGEFN domain). There are three main classes of RasGEFs, namely Son-of-sevenless (Sos), Ras guanine nucleotide releasing factor (RasGRF) and Ras guanyl releasing protein (RasGRP), and they are distinguished by additional flanking domains and motifs that facilitate their activation by distinct upstream signaling mechanisms or possess additional catalytic functions. RasGRF (also known as Cdc25Mn) is brain specific (Shou et. al., 1992), SosGEFs are closely related to the *Drosophila* Sos gene product, and RasGRP constitute a group of RasGEFs activated by diacylglycerol (DAG) and phorbol ester (Wennerberg et. al., 2004).

The ability of the CDC25 homology domains to concurrently activate other Ras family proteins and the presence of separate Rho-specific GEF catalytic domains in Sos and RasGRF proteins provide the links between Ras activation and the function of Ras and Rho family of proteins. The two main RasGFF families, Sos and RasGRF also serve as GEFs for the Rac1 small GTPase, a member of the Rho branch of the Ras superfamily (Wennerberg et. al., 2004). Sos1 and Sos2 contain a CDC25 homology domain which acts as a GEF for Ras as well as R-Ras2 and R-Ras3 proteins. In addition to the CDC25 homology domain, the amino termini of Sos proteins contain Dbl homology (DH; also called RhoGEF) and pleckstrin homology (PH) domains. The tandem DH-PH domain cluster is a signature motif of Dbl family proteins, which comprise the majority of GEFs

for Rho family GTPases (Rossman et. al., 2005). The catalytic DH domain mediates the GDP/GTP exchange of Rho GTPases, while the PH domain modulates the activity of the DH domain by a variety of mechanisms, by promoting membrane association, facilitating GTPase substrate binding, or by controlling intramolecular interactions. Therefore, Sos proteins are endowed with a dual GEF catalytic activity for Ras and Rac1 GTPases.

#### **1.4.4.2. Ras GTPase activating factors (RasGAPs).**

RasGAPs have a common ~250 amino acid residue RasGAP catalytic domain, but otherwise do not share any sequence similarity or domain architecture in the sequences that flank this RasGAP domain. GAPs accelerate the very slow intrinsic GTP hydrolysis activity of Ras by several orders of magnitude.

p120 RasGAP was the first GAP to be discovered and provided an important biochemical explanation for why missense mutations at Ras residues G12 and Q61 result in constitutively activated, highly transforming proteins (Bernards et. al., 2004). These tumor-associated mutant Ras proteins, found in 30% of all human cancers are insensitive to the action of GAPs and therefore are persistently GTP-bound.

Neurofibromin is the gene product of NF1, a tumor suppressor gene lost in autosomal dominantly inherited disorder neurofibromatosis type 1 (NF1; Dasgupta et. al., 2003). Affected individuals are prone to development of benign and malignant tumors. Loss of neurofibromin expression in NF1 associated tumors or NF1-deficient mouse cells is associated with elevated Ras activity and Signaling as well as increased cell proliferation.

Tumor-associated Ras mutant proteins are also insensitive to neurofibromin-mediated inhibition. Similar to p120 RasGAP, evidence for regulation of neurofibromin-mediated inhibition of normal Ras function is limited.

Other additional RasGAPs have been identified and mechanisms for their regulation has been described. GAP<sup>IP4BP</sup> and GAP<sup>1m</sup> are founding members of a family of four RasGAPs having common domain architecture yet displaying distinct mechanism of regulation. The RasGAP domains are flanked by amino-terminal tandem Ca<sup>2+</sup>-dependent lipid-binding C2 domains and a carboxy-terminal PH domain which contains a Bruton's tyrosine kinase (Btk) motif. Despite their similar domain architecture, RasGAP family members exhibit different modes of regulation and associate differently with membrane. GAP<sup>IP4BP</sup> has a constitutive PH-domain-dependent plasma membrane association (Lockyer et. al., 1997), that could be mediated by phosphatidylinositol 4,5 bi-phosphate (PIP<sub>2</sub>) binding (Cozier et. al., 2000), and its Ras GAP activity may be regulated by inositol 1,3,4,5-tetrakisphosphate (Cullen et. al., 1995). Interestingly, GAP<sup>1m</sup> was not found at the plasma membrane, but showed a distinct, perinuclear and cytoplasmic localization. It is however translocated to the plasma membrane upon EGF activation of phosphoinositide 3-phosphohate lipid kinase (PI3K) and production of phosphatidylinositol 3,4,5-phosphate (PIP<sub>3</sub>) through a PH-domain dependent translocation. CAPRI, is the third member of the family, and is normally cytosolic and inactive. A G-linked receptor-stimulated increase of Ca<sup>2+</sup> levels causes CAPRI to undergo rapid, C2-domain-dependent association with plasma membrane that activates the RasGAP activity of CAPRI, leading to reduced Ras activity (Lockyer et. al., 2001). A fourth member, RASAL, also

undergoes  $\text{Ca}^{2+}$  -stimulated plasma membrane association but it also oscillates in synchrony with simultaneously measured repetitive  $\text{Ca}^{2+}$  spikes between the plasma membrane and cytosol. Therefore,  $\text{Ca}^{2+}$  regulation controls the activities of RasGAPs as well as RasGEFs.

#### **1.4.5. Ras effectors.**

One of the most studied Ras effectors are the Raf serine/threonine kinases (A-Raf, B-Raf and C-Raf1). Raf is activated by interaction with the GTP-bound form of Ras at its core effector binding region, and this lead to the activation of the mitogen activated kinase kinases (MEK1/2). This in turn leads to activation of downstream extracellular-signal-regulated kinase (ERK) mitogen-activated protein kinases (Erk MAPKs) cascade (Bargi et. al., 2000; Pruitt et. al., 2001).

PI3K is another extensively studied effector of Ras (Downward, 1998). PI3K is activated by binding to Ras and this facilitates the conversion of  $\text{PIP}_2$  to  $\text{PIP}_3$ . This in turn leads to the activation of the Akt/PKB serine/theorinine kinase (Franke at. el, 1995). Activation of Rac1-GEFs has also been linked with an increase of  $\text{PIP}_3$  levels, and this is thought to provide a link between Ras and Rho GTPases (Hawkins, 1995).

Ral-GEFs family has also been identified as targets of Ras. Ral-GDS, Rlf, RGL1 and RGL2 have been reported to bind to Ras, and this interaction only occurs with GTP-bound form (Katz and McCormick, 1997). Interaction is abolished by mutations in the

effector binding region. The Ral-GEFs/Ral-GDS competes with Raf for interaction with active Ras (Hermann et. al., 1996).

### **1.5. Rho family.**

The Rho GTPases form a subgroup of the Ras superfamily of small GTP-binding proteins and are highly conserved throughout eukaryotes. 20 genes encoding different members of the Rho family have been identified in the human genome to date. The mammalian Rho-like GTPases comprise at least 10 distinct proteins: RhoA, B, C, D and E; Rac1, Rac2 and Rac 3; Cdc42Hs, and TC10. A comparison of the amino acid sequences of the Rho proteins from various species revealed that they are conserved in primary structure and are 50%-55% homologous to each other. Like all members of the Ras superfamily, the Rho GTPases function as molecular switches, cycling between an inactive GDP-bound state and an active GTP-bound state. Their interconversion is tightly controlled by GEFs that increase GDP/GTP exchange rates. It is well established that members of the Rho subfamily are involved primarily in the regulation of cytoskeletal organization in response to extracellular growth factors. Further studies have also revealed that Rho GTPases play crucial roles in diverse cellular events such as membrane trafficking, transcriptional regulation, cell growth control and development. Many targets of the Rho GTPases have now been identified and characterization of some of them has provided major insights toward the understanding of Rho GTPase function at the molecular level (see section 1.8).



### **1.5.1. Regulators of Rho GTPases.**

As with all members of the Ras superfamily, the activity of the Rho GTPases is determined by the ratio of their GTP/GDP-bound forms in the cell (Boguski and McCormick, 1993). The ratio of the two forms are regulated by the opposing effects of the GEFs, which enhance the exchange of bound GDP for GTP, and the GAPs, which increase the intrinsic rate of hydrolysis of bound GTP. In addition, Rho-like GTPases are further regulated by guanine nucleotide dissociation inhibitors (GDIs), which can inhibit both the exchange of GTP and the hydrolysis of bound GTP (Figure 1.5).

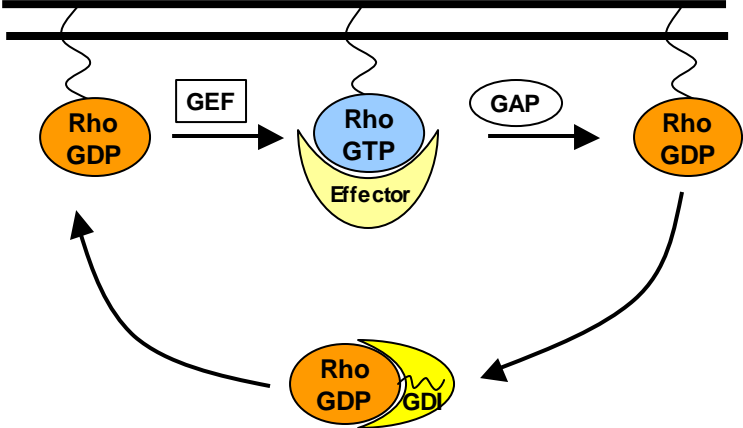
### **1.5.2. RhoGEFs.**

GEFs for Rho-like GTPases were originally identified as oncogenes after transfection of immortalized fibroblast cell lines with cDNA expression libraries. They share a common feature: a Dbl homology (DH) domain adjacent to a PH domain. The Dbl oncogene was originally discovered by its ability to induce focus formation in NIH3T3 cells (Eva and Aaronson, 1985). Dbl was observed to have a 29% sequence identity with the cell division cycle protein Cdc24, which is a GEF for Cdc42 in *S. cerevisiae* (Ron et. al., 1991). Biochemical analysis show that Dbl is indeed able to release GDP from the human homolog of Cdc42 in vitro. It was also demonstrated through deletion studies that the DH domain was essential and sufficient for the GEF activity. The PH domain of the GEF is always positioned adjacent to the DH domain, suggesting a functional interdependence between the two domains (Musacchio et. al., 1993).

**Figure 1.5 The Rho family GTPases as molecular switches.**

Rho GTPases act as molecular switches that regulate diverse pathways that control the cytoskeleton, gene transcription and cell growth. They are GTP-binding proteins of about 21 kDa that cycle between GDP-bound inactive and GTP-bound active states. The GTPase cycle is regulated by three classes of proteins. GDIs sequester the GDP-bound GTPases, masking the isoprenyl modification on the CAAX motif, and thereby keeping them from interacting with membranes. GAPs stimulate the intrinsic GTP hydrolysis activity of the GTPases, resulting in a more rapid conversion back to the inactive GDP state. GEFs catalyze the release of bound GDP which results in formation of the GTP-bound active protein. In contrast to the Ras GTPase cycle, the Rho GTPase cycle not only changes the activation state of the proteins but also their location – cytosol vs. membrane-bound.

Figure 1.5



This assumption is supported by studies on the Rac1GEF, vav where it was suggested that the PH domain fulfils an autoinhibitory role on vav's GEF activity. The deletion of the PH domain results in a constitutively active protein (Ma et. al., 1998).

It was generally assumed that all proteins that contain a DH and PH domains in tandem will be GEFs for Rho subtype proteins. This appears to be true for some but not all DH/PH-containing proteins. RhoGEFs also differs in their specificity, in which some exhibit exchange activity *in vitro* for a wide range of Rho-like GTPases whereas others appear to be more specific. Lbc, Lfc and Lsc are specific for Rho whereas Fgd1 is specific for Cdc42 (Glaven et. al., 1996; Zheng et. al., 1996). Vav, which has been previously reported to be an activator of Ras was shown to function as a GEF for members of the Rho family (Crespo et. al., 1997; Han et. al., 1997). Therefore it is not clear what determines the selectivity of GEFs for specific Rho family members. Work has also been done to determine whether the proteins that serve as Rho GEF *in vitro* can perform similar functions *in vivo*. Lbc has been reported to induce stress fibre formation in Swiss 3T3 cells (Zheng et. al., 1995, Olsen et. al., 1997). Fgd1, the faciogenital dysplasia gene product implicated in normal skeletal development also functions as a GEF (Pasteris et. al., 1994). FDG1 was shown to display GFF activity specific for Cdc42 and induces Cdc42-type morphological phenotype in Swiss 3T3 cells and also activates Jun-kinase and p70<sup>s6</sup> kinase downstream of Cdc42 (Zheng et. al., 1996; Olsen et. al., 1997; Nagata et. al., 1998). Both Dbl and Vav were observed to trigger the formation of filopodia, lamellipodia and stress fibres mediated by Cdc42, Rac1 and Rho, respectively. Both Dbl and Vav also stimulated the SAPK/JNK activity (Olson et. al., 1996). Tiam was

first identified as an invasion and metastasis inducing gene in T-lymphoma cells (Habets et al., 1995). T-cell lymphoma invasion and metastasis 1 (Tiam1) activates Rac1 and Cdc42 *in vitro*, but *in vivo* it activates Rac1 exclusively, inducing Rac1-dependent membrane ruffles (Michiels et al., 1995). Michiels et al. (1997) further demonstrated that an intact amino-terminal PH domain was essential for these activities.  $\alpha$ PIX and  $\beta$ PIX are Rac1 GEFs that were identified through their ability to interact with PAK. The two PIX isoforms contain the conserved DH and PH domains common to RhoGEFs. PIX exhibits GEF activity on both Cdc42 and Rac1 *in vitro* but act exclusively to Rac1 *in vivo* (Manser et al., 1998).

Other than DH and PH domains, many of the exchange factors have other domains that are commonly found in Signaling molecules, such as the Src homology (SH3) domain and a diacylglycerol-binding zinc butterfly motif, suggesting that they may have additional functions (Cerione and Zheng 1996).

### **1.5.3. RhoGAPs.**

About 80 GTPase-activating proteins (GAPs) which increase the intrinsic rate of GTP hydrolysis of Rho GTPases have been identified to date. The GAP domain of RhoGAP is highly conserved and through sequence similarity of this domain with n-chimaerin and bcr-encoded protein, it led to identification of other Rho family GAPs (Diekmann et al., 1991). The first GAP protein described for Rho GTPases was identified by biochemical analysis of cell extracts with recombinant Rho (Garrett et al., 1989). The protein designated p50RhoGAP, was shown to have GAP activity toward Rho, Cdc42 and Rac1

*in vitro* (Hall 1990; Lancaster et. al., 1994) but *in vivo*, its activity is restricted to Rho only (Ridley et. al., 1993). Therefore, similar to their GEFs counterpart, GAPs also differ in their specificity for members of the Rho GTPases.

The p190GAP was first identified as a tyrosine-phosphorylated Ras GAP-associated protein in Src-transformed cells and in growth factor treated cells. However it was later shown to possess GAP activity for Rho GTPases (Ellis et. al., 1981; Settleman et al, 1992). *In vitro* studies show inhibition of Rho-mediated stress fibre formation (Ridley et. al., 1993). p190GAP interaction with RasGAP was proposed to provide a link between Ras and Rho Signaling pathways (Hu and Settlement, 1997). Indeed recent work has provided proof for this assumption. Tiam1/Rac1 signaling is shown to antagonize Rho activity directly at the GTPase level in COS-7 cells. p190-RhoGap plays a central regulatory role in this Signaling pathway. Interfering with its activation by Src-kinase-dependent tyrosine phosphorylation or its recruitment to the membrane through interaction with the SH2 domain of p120-RasGAP blocked the Tiam1-mediated rapid downregulation of Rho. This process is mediated by Rac1, but not Rac2 or Rac3 isoforms. These data provide evidence for a biochemical pathway of the reciprocal regulation of two related small GTPases (Herbrand et. al., 2006).

Other than accelerating the hydrolysis of GTP, RhoGAPs may mediate other downstream functions of the Rho proteins in mammalian system. A role for p190 in regulating Rho function in cells undergoing cytoskeletal rearrangements has been suggested (Chang et. al., 1995). Some GAP proteins also display effector function as well as GAP activity,

such as n-chimaerin and GRAP (Kozma et. al., 1996; Taylor et. al., 1999). n-Chimaerin is a brain specific GAP that display GAP activity preferentially for Rac1 and minimal activity for Cdc42 *in vitro*. The activity is regulated by phospholipids and phorbol esters through its protein kinase C-like domain (Hall et. al., 1990; Manser et. al., 1992, Ahmed et. al., 1993). Injection of the GAP domain of n-chimaerin downregulates Rac1 activity in Swiss 3T3, inhibiting Rac1-induced lamellipodia formation (Kozma et. al., 1996). In contrast, full-length n-chimaerin expression induced both lamellipodia and filopodia formation independent of the GAP activity, suggesting both effector function as well as GAP activity for n-chimaerin. It is also able to induce neurite outgrowth in N1E115 neuroblastoma cells (Kozma et. al., 1996).

#### **1.5.4. RhoGDIs.**

GDIs form the third class of Rho family regulatory proteins. RhoGDIs are ubiquitously expressed and was first identified as an inhibitor of RhoGDP dissociation and GTP binding protein (Fukumoto et. al., 1990). Association of Rho proteins with membranes is mediated by an iso-prenyl lipid (20-carbon geranylgerany or 15-carbon farnesyl) attached to their C-terminal cysteine. RhoGDIs, which were initially named after their ability to inhibit the spontaneous dissociation of GDP, form cytosolic complexes with geranylgeranylated Rho GTPases, thus maintaining a GDP-bound soluble fraction in resting cells (Olofsson et. al. 1999). They are therefore regarded as housekeeping regulators whose major function is to act as chaperones to provide the cell with a reservoir of inactive Rho proteins that can be distributed to any membrane with little or no specificity. Compared with the large number of RhoGEFs and RhoGAPs, there are

only three RhoGDI in mammals and plants, and only one has been found in several other eukaryotic genomes. In mammals, RhoGDI is the most abundant and ubiquitous representative, and it is able to form cytosolic complexes with most members of the Rho family (Fukumoto et. al., 1990; Leonard et. al., 1992). On the other hand, RhoGDI2 (also known as KyGDI or D4GDI) is found predominantly in hematopoietic cells where it appears to have a more narrow specificity for the Rac1 subfamily (Lelias et. al., 1993). The third member, RhoGDI3 (also known as RhoGDI $\gamma$ ) (Zalcman et. al., 1996; Adra et. al., 1998) is a low abundance member that interacts *in vitro* with several Rho GTPases as other RhoGDIs do but seems to be specific for RhoG in the cell (Brunet et. al., 2002). It also differs from other RhoGDIs by an N-terminal extension responsible for its unique localization to the Golgi apparatus.

Other than the classical function of RhoGDIs as universal chaperones for GDP-bound proteins, more evidence indicating of extra roles played by this family of proteins is accumulating. Recent *in vitro* studies provided insight into the mechanism by which RhoGDIs act in isolation, delivering and extracting Rho proteins from membranes. This reveals how their modularity allows them to function both in the cytoplasm and at the membrane interfaces (Nomanbhoy et. al., 1999; Hoffman et. al., 2000; Golovanov et al., 2001; Dransart et. al., 2005).

Potential new functions of RhoGDIs may include the modulation of this basic mechanism by RhoGDI-binding proteins by phosphorylation or by the lipid composition of membranes to achieve the specificity in the delivery of Rho proteins to subcellular



membranes. In addition, RhoGDI may uncouple from the GEF-regulated GDP/GTP cycle, by regulating GTP-bound populations of Rho or by the ability of certain Rho proteins to undergo GDP/GTP cycles without leaving the membrane.

## **1.6. Rho family functions.**

### **1.6.1. Cdc42.**

The Rho GTPase Cdc42 is implicated in a wide variety of cellular functions such as receptor-mediated signal transduction leading to initiation of transcription, cell cycle progression, actin cytoskeleton rearrangement and apoptosis. All Cdc42 proteins share a common C-terminal membrane targeting consensus sequence C-X-X-L with the exception of two brain-specific members, Cdc42Mmb and G25K, which have a phenylalanine in place of the leucine residue. Cdc42 contain many domains, four of them located at the N-terminus are responsible for the binding and hydrolysis of GTP to GDP. The Switch I domain or effector binding region (resides 26-50) has the potential to bind to multiple effectors simultaneously and might also possess regions that are specific for certain effectors to bind. Rho GTPases have an insert domain of ~13 residues and this is a unique feature not found in other Ras superfamily members. GEF interaction is believed to primarily be at a central region comprised of the  $\beta$ 4- $\alpha$ 3 strand region (residues 82-100; Johnson, 1999).

**Transcriptional activation.** Cdc42 couples cell surface receptors to the MAP kinases, providing a passage for relaying extracellular cues to intracellular events that include mitogenesis, cell growth, stress response and immune gene expression. During stress

response, stress-activated protein kinase (SAPKs) and c-Jun kinases (JNKs) are activated. Activation of JINK and p38 by Cdc42 results in an elevation of the c-Jun AP-1 transcriptional activity (Minden et. al., 1995). Activation of JNK/SPAK and p38 kinases causes them to translocate to the nucleus where various transcriptional activators are phosphorylated and gene expression is initiated (Johnson, 1999).

**Actin cytoskeleton organization.** In response to extracellular cues, Cdc42 interacts with a number of downstream effectors, which results in the rearrangement of the actin cytoskeleton. Microinjection of constitutively active Cdc42 into Swiss 3T3 fibroblast cells causes the formation of peripheral actin microspikes. It also induces vinculin containing focal complexes and a reduction in Rho induced stress fibres (Kozma et al, 1995; Nobes et. al., 1995). Cdc42 is also required for the assembly of functional cell-cell contacts (Kuroda et. al., 1998). Integrin-dependent adhesion and cell spreading in NIH-3T3 fibroblasts are mediated by Cdc42 (Clark et. al., 1998). During the differentiation of cultured cortical rat neurons, Cdc42 also plays a role in the generation of filopodia, that serve to sense guidance cues in the surrounding environment.

**Cell polarity.** Cdc42 is involved in the regulation of cell polarity. Studies carried out on Bac-1 macrophages to CSF-1 suggested that Cdc42 is required for cell polarity. Wound healing assays have also provided evidence for role of Cdc42 in cell polarity. Making a wound in the monolayer of REF cells will result in a margin of cells that develop to a morphological polarity. These cells are observed to process protrusive activity at the site of injury and nowhere else.

### **1.6.2. Rac1**

The Rho GTPase Rac1 regulates various aspects of the actin cytoskeleton. It also possesses other functions such oxidative destruction of bacterial invaders during phagocytosis, and provides means to interact with and regulate inositol lipid kinases.

**NADPH oxidase.** The nicotinamide adenine dinucleotide phosphate-oxidase (NADPH oxidase) enzyme generates superoxide, and eventually forms hydrogen peroxide which leads to the production of hydroxyl free radicals and hypochlorous acid. These are effective destructive agents utilized by leukocytes for phagocytosis. It has been shown that Rac1 and its effector p67<sup>phox</sup> are components of the NADPH oxidase complex (Diekmann et. al., 1994) and Rac1 is an essential component (Knaus et. al., 1991). NADPH oxidase is active when Rac1 is in a GTP-bound state and inactive when Rac1 is GDP-bound (Heyworth et. al., 1993).

**Inositol lipid kinases.** Phosphatidylinositol lipids have been shown to play a role in the regulation of the actin cytoskeleton. Rac1 was shown to regulate the activity of type-I phosphatidylinositol 4-phosphate 5-kinase (PIP5K). PIP5K generates the enzymatic product PIP2, which is involved in the regulation of profilin,  $\alpha$ -actinin, vinculin, talin and actin-capping proteins. Rac1 has also been implicated in the activation of PI3K in a GTP-dependent manner (Bokoch et. al., 1996), which in turns mediates the interleukin-2 activation of protein kinase C (Gomez et. al., 1997).

**Actin cytoskeleton organization.** Rac1 induces formation of membrane ruffles when overexpressed. Treatment of fibroblast with PDGF results in a phenotype of membrane ruffling that is due to the upregulation of Rac1 activity (Ridley et. al., 1992). Rac1 is also involved in the migration of border cells in the developing embryo of *Drosophila*. Inhibition of Rac1 blocks the migration of these cells during oogenesis (Murphy et. al., 1996).

### **1.6.3. Rho.**

Rho plays a role in the reorganization of the actin cytoskeleton as with other members of the Rho GTPase family. It is also implicated in the process of oncogenic transformation.

**Oncogenic transformation.** The progression to malignancy is a multi-stage process which results in the uncontrolled ability of cells to leave their normal environment and invade surrounding tissues. Overexpression of RhoC results in metastasis while its inhibition diminishes the ability of cells to invade and metastatise (Clark et. al., 2000). RhoA and its downstream effector Rho kinase (ROK) have also been implicated in tumour-cell invasion. Invasive abilities of lysophosphatidic acid (LPA) induced tumour cells are suppressed when ROK is inhibited (Itoh et. al., 1999).

**Actin cytoskeleton organization.** Overexpression of RhoA has been shown to induce stress fibre formation in fibroblast cells (Paterson et. al., 1990). LPA activation of the Rho pathway induces both stress fibre and focal adhesion formation in fibroblast cells (Ridley et. al., 1992). Interaction of Rho and its downstream effectors ROK and mDia

accounts for the formation of bundled actin stress fibres and alignment with microtubules (Watanabe et. al., 1997; Tominaga et. al., 2000; Ishizaki et. al., 2001).

## **1.7. Rho family effector proteins.**

### **1.7.1. The CRIB motif.**

All Cdc42 and Rac1 effector proteins share a common feature known as the Cdc42/Rac1 interactive binding (CRIB) motif (Burbelo et. al., 1995). This was first reported by Manser et al, (1994) as a conserved sequence present in rat p65 p21 Activated Kinase (p65PAK), Activated Cdc42 associated kinase (ACK) and Sterile 20 (Ste20), the yeast PAK homologue. The binding sequence is reported to span over 40 amino acid residues. Burbelo *et al* later redefined the motif as a minimal consensus binding sequence of 16 amino acids. CRIB has been identified in over 25 proteins, including CIP4, IRSp53 and N-WASP.

### **1.7.2. PAK family kinases.**

PAKs were the first GTPase-regulated kinases to be identified, through a screen for Rho GTPase binding partners in rat brain cytosol (Manser et. al., 1994). GTP bound forms of Rac1 and Cdc42 were shown to interact in overlay assays with proteins of 68, 65 and 62 kDa. These protein targets turned out to be the three major PAK isoforms. The human forms are termed PAK1 (rat  $\alpha$ PAK), PAK3 (rat  $\beta$ PAK) and PAK2 (rat  $\gamma$ PAK) respectively (Manser et. al., 1995; Bagrodia et. al., 1995). PAKs have an ancient origin and serve as important regulators of cytoskeletal dynamics and cell motility. They are also implicated in transcription through MAPK cascades, death and survival signaling

and cell-cycle progression (Bokoch et. al., 2003). Consequently, PAKs are implicated in a number of pathological conditions and in cell transformation.

PAK1 binds to and is activated by Rac1, Rac2, Rac3 (Manser et. al., 1994; Knaus et. al., 1998; Mira et. al., 2000) and Cdc42 (Manser et. al., 1994). Conserved residues within the N-terminal PDB (p21-binding domain) are involved primarily in binding and activation by GTPases. Other features include two conserved canonical PXXP SH3 (Src homology 3) binding motifs, and a conserved non-classical SH3 binding site for PIX (PAK-interacting exchange factor, also known as Rac1/Cdc42 GEF6) (Manser et. al., 1998). Nck binds to the first conserved SH3 binding site (Bokoch et. al., 1996) while Grb2 binds to the second SH3 site, suggesting that all three PAKs can be recruited in a similar manner to a variety of signal transduction pathways.

PAK1 exist as a homodimer in solution and in cells, and is probably in a trans-inhibited conformation, where the KI region of one PAK molecule packs against the C-terminal catalytic domain of the other (Parrini et. al., 2002). Binding of Rac1 or Cdc42 to the CRIB motif results in a conformational change causing the C-terminal kinase domain to become exposed. The protein is then autophosphorylated in seven sites (S21, S57, S144, S149, S199, S204 and T42) (Manser et. al., 1997) and becomes active. It is then able to interact with other substrates such as NADPH oxidase component p67<sup>phox</sup> (Benna et. al., 1994; Knaus et. al., 1995).

PAK1-PAK3 complex with the focal adhesion-associated protein PIX, which is a Cdc42/Rac1 GFP. Both  $\alpha$ PIX and  $\beta$ PIX bind PAK via their SH3 domains (Manser et. al., 1995; Bagrodia et. al., 1998). Analysis of  $\alpha$ PIX deficient cells suggested a key role for the PIX-PAX complex in Cdc42 mediated direction sensing of chemotactic leucocytes (Li et. al., 2003). PIX is tightly associated with GIT1, a 90 kDa protein that targets focal adhesions by binding paxillin (Turner et. al., 1999). Overexpression of GIT1 leads to disassembly of focal adhesions together with loss of paxillin. This could be an indirect consequence of PAK activation by GIT1 (Loo et. al., 2004). Therefore, GIT1 and PIX are critical partners that both localize and activate PAK at focal adhesions, at the leading edge of motile cells and also at cell-cell junctions (Zegers et. al., 2003; Zhao et. al., 2000; Manabe et. al., 2002).

Two closely related human protein phosphatases that efficiently dephosphorylate PAK1 have been identified. POPX1 and POPX2 bind to various forms of PIX and form multimeric complexes containing PAK (Koh et. al., 2002). Overexpression of either of these PP2C-related phosphatases antagonizes the cellular effects of active PAK (Koh et. al., 2002). Other protein kinases that might downregulate PAK function include Akt that phosphorylates PAK1 at Ser-21. This modification decreases binding of Nck to the PAK1 N-terminus while increasing kinase activity (Zhao et. al., 2000; Tang et. al., 2000).

### **1.7.3. MRCK.**

The myotonic dystrophy kinase-related Cdc42-binding kinase (MRCK) family is Cdc42/Rac1 effectors that are related to PAK in the GTPase-binding domain but to the

Rho effectors ROK/ CRIK (Citron Kinase) in the kinase domain (Madaule et. al., 1998), and thus act on related substrates (Tan et. al., 2001). MRCK $\alpha$  was isolated through its interaction with Cdc42 and the human gene for MRCK $\alpha$  extends over approximately 250-300 kb (Moncrieff et. al., 1999). The new described MRCK $\gamma$  is a lot more compact but its product contains all the features of the  $\alpha$ - and  $\beta$ - isoforms (Pirone et. al., 2001). MRCK expression is ubiquitous in mammals, with the highest level in the brain. The MRCK proteins encode the conserved p21-binding domain. MRCKs contain a kinase domain, coiled-coil  $\alpha$ -helix region, a cysteine rich region and PH domain.

MRCK as an effector for Cdc42 induces cytoskeletal changes. Cotransfection of MRCK and Cdc42V12 result in a Cdc42 phenotype in HeLa cells where MRCK colocalizes with Cdc42 at cell-cell junctions and Cdc42-induced surface protrusions. Cdc42V12-mediated microspikes and focal complex formation were blocked when kinase dead MRCK was used instead.

MRCK $\alpha$  can contain two CRIB domains, and CRIB1 binds preferentially to Cdc42-GTP, while the addition of CRIB2 increases the interaction of MRCK with Rac1-GTP (Leung et. al., 1998). MRCK $\alpha$  exons 21-24 is region of alternative splicing with at least 13 isoforms detected (Moncrieff et. al., 1999). The conserved stretch of about 70 amino acid residues N-terminal to the Myotonic Dystrophy Protein Kinase domain (DMPK) is essential for kinase activity. Together, the kinase activity and the C-terminal cysteine-rich/PH domain and a citron homology region in MRCK $\alpha$  were shown to be required for neurite outgrowth (Chen et. al., 1999).



#### **1.7.4. ACK.**

ACK (Activated Cdc42 associated Kinase) is a non-receptor tyrosine kinase that binds specifically to Cdc42 in its activated form (Manser et. al., 1993). ACK is thought to be involved in regulating cell adhesion (Yang and Cerione, 1997)

#### **1.7.5. ROK.**

ROK was the first kinase effector of RhoA to be discovered (Leung et. al., 1995, 1996; Nakagawa et. al., 1996; Matsui et. al., 1996; Fujisawa et. al., 1996). ROK interacts with GTP-bound RhoA as well as with other Rho members B and C but does not interact with Cdc42 nor Rac1 (Leung et. al., 1996). Both ROK  $\alpha$  and ROK  $\beta$  mRNAs are expressed in most mammalian tissues (Leung et. al., 1996; Nakagawa et. al., 1996), with the ROK  $\alpha$  transcript being most abundant in muscle and brain. Both isoforms are 160 kD proteins with a N-terminal serine/threonine kinase domain, coiled-coil region, a Rho-binding domain and a C-terminal cysteine/histidine-rich/pleckstrin homology domain. The N-terminal kinase domain contains a highly conserved 30 amino acid sequence found in both isoforms, of which 20 are identical and these are essential for binding of RhoA.

The catalytic activity of ROK is dependent on the intramolecular interaction of the C-terminus with the kinase domain and formation of multimeric complexes that leads to trans-autophosphorylation of the kinase domain. Binding of activated Rho to the Rho binding domain disrupts the autoinhibitory interaction between the C-terminus and the kinase domain, activating the protein (Amano et. al., 1999). The ROK kinase domain displays high homology to the myotonic dystrophy kinase (Brook et. al., 1992). ROK is

translocated to the plasma membrane upon association with Rho, resulting in stress fibre and focal adhesion complex formation. The cytoskeletal rearrangement is dependent on the N-terminal kinase domain, and mutation or removal of this domain leads to disassembly of stress fibres and focal complexes (Leung et. al., 1996).

#### **1.7.6. PKN.**

PKN is a Rho specific target protein. Its serine/threonine kinase is activated upon binding of Rho in its GTP bound form (Watanabe et. al., 1996). It was proposed that PKN is involved in Rho mediated actin cytoskeleton reorganization events such as stress fibre formation (Amano et. al., 1996).

#### **1.7.7. Rho GTPase effectors – adaptor proteins.**

Many Rho GTPases effectors/interactors have been identified to date, some of which are specific to Cdc42, Rac1 or Rho and a small proportion are able to interact with more than one effector or even all three.

**p67<sup>phox</sup>** is a Rac1 specific effector (Diekman et. al., 1994) and is phosphorylated in a Pak dependent manner (Ahmed et. al., 1998). It was proposed that this interaction between p67<sup>phox</sup> and Pak is one means of NADPH oxidase regulation.

**n-Chimaerin**, which was first identified as a Rac1 GAP (Hall et. al., 1990; Manser et. al., 1992, Ahmed et. al., 1993) was shown to have effector functions for both Rac1 and Cdc42 (Kozma et. al., 1996).

**POR1** (Partner Of Rac1) is a Rac1 specific interactor as its name implies and is believed to synergise with Ras V12 in inducing membrane ruffles (Van-Aelst et. al., 1996).

**p35** is a specific interactor of Rac1 and upon binding, it regulates Cdk5 activity. It is neuron specific and is therefore often used as a neuronal marker (Nikolic et. al., 1998). The p35/Cdk5 pair is often involved in neuronal cell migration, neurite outgrowth and regulation of adhesion. It also played an important role in neuronal development (Paglini and Caceres, 2001).

**p140sra-1** (Specifically Rac1 associated protein) is a Rac1 specific interactor and colocalizes with Rac1V12 and the cortical actin of membranes ruffles (Kobayashi et. al., 1998).

**Borgs** (Binders Of Rho GTTPases) is a family of proteins that consist of five family members. They interact with Cdc42 and TC10 GTPase. Borgs-1 and 3 was proposed as to be involved in cell spreading (Joberty et. al., 1999). Borg-5 has been shown to be involved in Cdc42 mediated actin cytoskeleton reorganization events

### **1.8. The WASP and VASP family of actin polymerization regulators.**

A major mechanism for Rho GTPases to modulate the actin cytoskeleton is through the WASP family of proteins. WASP family of proteins are key regulators of Arp2/3 nucleated actin polymerization at the membrane proximal site (Higgs and Pollard, 2001). The family consists of Wiskott-Aldrich Syndrome Protein (WASP), the protein mutated

in patients with Wiskott-Aldrich syndrome, it's ubiquitously expressed homologue N-WASP, as well as the more distantly related WAVE proteins (also known as SCAR). At least one family member has been found in all eukaryotes examined so far. They are multidomain proteins that interact with signaling molecules, actin monomers and the Arp2/3 complex (Figure 1.6). Ena/VASP family consists of *Drosophila* Enabled (Ena), its mammalian homolog Mena (mammalian Ena), VASP (vasodilator-stimulated phosphoprotein), and Evl (Ena-VASP-like) proteins. They are associated with microfilaments, adherens-type cell-matrix, cell-cell junctions, and highly dynamic membrane regions as well as in tip complexes.

### **1.8.1 WASP family domain structure.**

The two subgroups of the WASP family (WASP, N-WASP and WAVE1, WAVE2, WAVE3) retain functionally conserved binding sites for the Arp2/3 complex and actin, the VCA domain (V, verprolin-homology; C, cofilin-homology or central domain; A, acidic region; N-WASP contains two verprolin-homology domain), also called the WA region. The VVCA/VCA will be referred to as the WA domain throughout the rest of the thesis (Figure 1.7). The WA is sufficient to activate the Arp2/3 complex (Machevsky and Insall, 1998, Egile et. al., 1999, Machesky et. al., 1999, Rhoatagi et. al., 1999, Winter et. al., 1999, Yamaguchi et. al., 2000). For maximal activation, WA must bind both the Arp2/3 complex and an actin monomer (Machesky and Insall, 1998, Miki and Takenawa, 1998).

**Figure 1.6 WAVE2 and N-WASP protein complexes.**

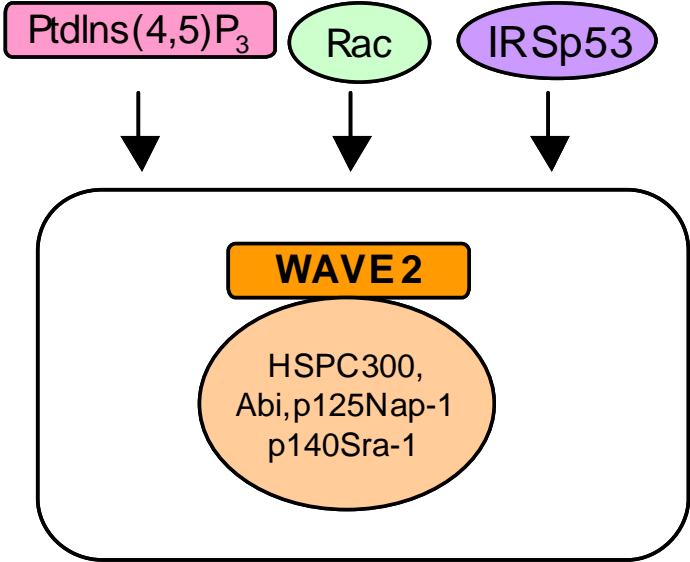
N-WASP and WAVE2 are ubiquitous isoforms of the WASP and WAVE families, respectively. Both contain multiple domains and motifs which can bind to other interacting proteins allowing protein complex formation.

(A) The WAVE2 complex exists as a pentameric heterocomplex that consists of WAVE2, Abi (Abelson-interacting protein), p125Nap-1, p140Sra-1 (or the closely related PIR121) and HSPC300. Regulators of the WAVE2 complex include PIP<sub>2</sub>, Rac1 and IRSp53.

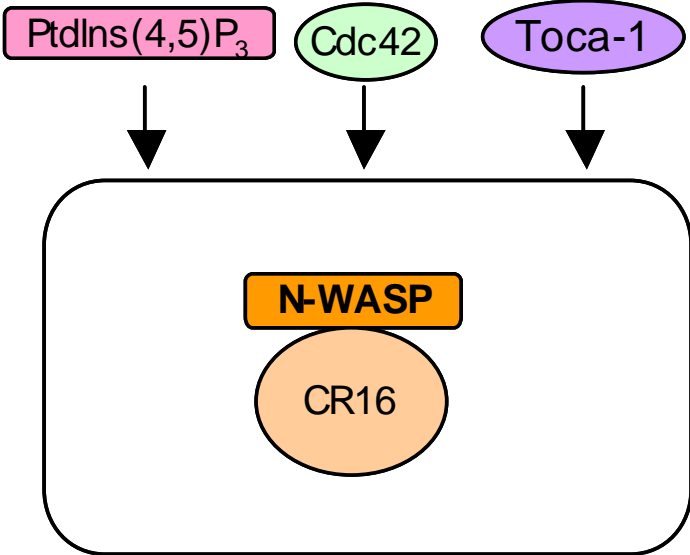
(B) The N-terminal region of N-WASP contains a WH1 domain that binds to a specific proline-rich sequence of the WASP-interacting protein (WIP) and regional expression-16 (CR-16) as well as CR-16 homologous protein, WICH (WIP-related, WIRE). WIP, CR-16 and WICH/WIRE form heterocomplexes with N-WASP. Regulators of the N-WASP complex include PIP<sub>2</sub>, Rac1 and IRSp53.

Figure 1.6

**A**



**B**



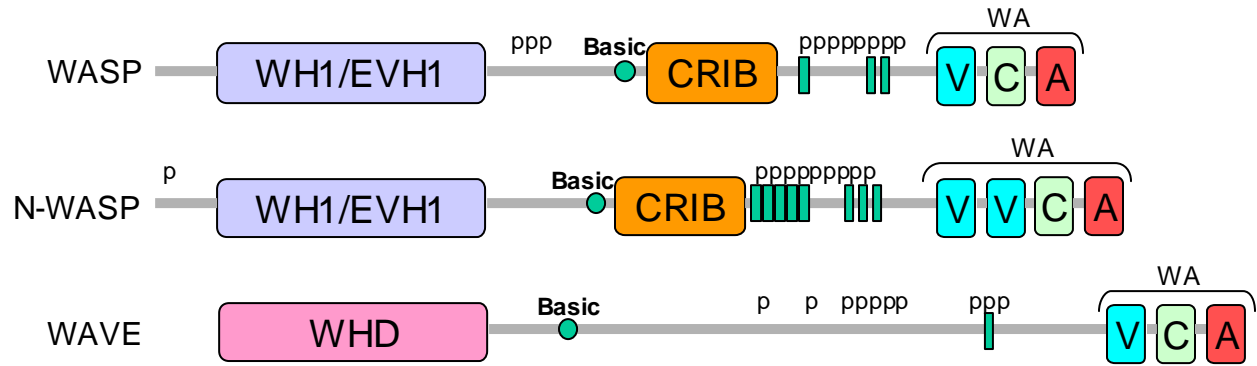
**Figure 1.7 Schematic of WASP/WAVE family.**

The Wiskott-Aldrich syndrome protein (WASP) family of proteins consist of multiple functional domains. WASP and N-WASP are activated by direct binding to Cdc42 via the CRIB domain, whereas WAVE (WASP-family verprolin-homologous proteins) link to Rac1 via intermediates. The C-terminal verprolin-homology, cofilin-like and acidic (VCA) or WA domains are important for induction of actin polymerization. The V and CA domains bind actin monomer (G-actin) and the Arp2/3 complex, respectively.

Regions of WASP and WAVE family proteins.

- WA - CA cofilin-like and acidic and, V, verprolin homology
- CRIB - Cdc42 and Rac1 interactive binding.
- IQ - IQ motif.
- P - Proline-rich.
- WH1 - WASP homology 1.
- WHD - WAVE homology domain.

**Figure 1.7**





Both N-WASP and WAVE family also contain a conserved polyproline region which is important for interaction with SH3 containing proteins such as IRSp53 and Toca-1, respectively.

### **1.8.2. WASP.**

Wiskott Aldrich Syndrome Protein (WASP), the gene product that is mutated in patients with Wiskott-Aldrich Syndrome (Derry et. al., 1994), is expressed exclusively in all cells of hematopoietic stem cell-derived lineages, i.e. the lymphocytic and megakaryocytic cell lineages. Wiskott-Aldrich Syndrome is a human X chromosome-linked recessive hereditary disorder characterized by immunodeficiency, thrombocytopenia with small platelets and eczema (Ochs, 1998; Snapper and Rosen, 1999). WASP phenotypes can range from mild to severe, with affected cells showing a reduced cell and cytoskeletal abnormalities like aberrant cell surface microvilli, suggesting a role of WASP in the regulation of the cytoskeleton (Molina et. al., 1992).

T cells of WASP patients have both signaling and cytoskeletal abnormalities (Remold-O'Donnell et al, 1996). In these T cells, the response to antigen receptor stimulation is severely depressed or absent (Molina et. al., 1993). In contrast, responses to non-specific mitogens are often normal, suggesting a role of WASP in T cell receptor proximal signaling events (Molina et. al., 1993; Sullivan et. al., 1994). Peripheral blood lymphocytes also show a paucity of cell surface microvilli (Kenney et. al., 1986). Defective regulation of the actin cytoskeleton may be responsible for the abnormal expression of cell surface glycoproteins (Remold-O'Donnell et. al., 1992). WASP has

also been reported to be predominantly cytoplasmic with some of the protein found in membrane (16%) and nuclear (>3%) fractions (Stewart et. al., 1996).

The carboxy-terminal WA domain of WASP were found to activate Arp2/3 nucleation of actin assembly (Machesky and Insall, 1998). Full length WASP is a less potent activator due to an intramolecular interaction resulting in autoinhibition (Kim et. al., 2000), which is released upon regulatory interactions of the amino-terminal part of WASP with signaling proteins such as Cdc42 in its GTP-bound form (Higgs and Pollard, 2000; Kim et. al., 2000).

### **1.8.3. N-WASP.**

N-WASP was first identified as a 65 kDa protein from bovine brain that binds to the adaptor protein Ash (abundant Src homology)/Grb2 (growth factor receptor-bound protein 2) (Miki et. al., 1996; Miura et. al., 1996). The predicted amino acid sequence revealed 50% overall sequence identity to WASP (Wiskott-Aldrich-Syndrome protein) (Miki et. al., 1996), as well as a similar multi-domain organization as shown in Figure 1.7.

N-WASP was first found to be expressed at nerve terminals in the brain with weaker expression levels in other organs (Miura et. al., 1996; Fukuoka et. al., 1997). It was later recognized to be expressed ubiquitously (Miki et. al., 1998). This is further confirmed in the mouse, where N-WASP expression was detected in Northern blot analysis in all tissue analyzed, which included brain, colon, lung, heart, muscle, kidney, testis, liver embryonic stem cells and lymphocytes (Snapper and Rosen, 1999).

At the amino-terminal, N-WASP contains a WH1 (WASP homology 1) domain which shares similarity to polyproline binding EVH1 domains (Ena/VASP homology domain 1) (Fedorov et. al., 1999; Prehoda et. al., 1999). Indeed, the WH1 domain of N-WASP has been shown to bind to the proline-rich actin-binding protein WIP (WASP interacting protein) (Ramesh et. al., 1997; Moreau et. al., 2000). The N-WASP-WIP complex is thought to act as a functional unit in integrating signaling cascades that lead to actin polymerization (Moreau et. al., 2000; Martinez-Quiles et. al., 2001), such as in the formation of filopodia protrusions and the mobility of intracellular pathogens (Frischknecht and Way, 2001). Other than binding to WIP, the WH1 domain has also been shown to bind to a similar proline-rich actin containing protein predominantly expressed in the brain, CR16 (Ho et. al., 2001). The amino-terminal sequences have also been shown to bind to F-actin (Egile et. al., 1999).

It has been proposed that a PH domain is located at the amino-terminus of N-WASP at overlapping sequences with the WH1 domain, which allows interaction with phosphatidylinositol 4,5-biphosphate (PIP<sub>2</sub>) coated surfaces, and was important for the localization of N-WASP to membranes (Miki et. al., 1996). However, there is some controversy as to whether or not the amino-terminal sequences of N-WASP really constitute a PH-domain because of the low sequence identity (6 amino acids out of 94 (Insall and Machesky, 1999). Subsequently, the basic region was identified as the binding site for PIP<sub>2</sub> (Prehoda et. al., 2000; Rohatgi et. al., 2000). Binding of PIP<sub>2</sub> is thought to be important for the synergistic stimulation of full Arp2/3 activating ability of N-WASP together with other activating proteins such as activated Cdc42 (Rohatgi et. al., 1999) or

Nck (Rohatgi et. al., 2001) at membrane proximal sites. N-WASP is also the only member of the WASP/WAVE family that contains an IQ motif, which may be a site for  $\text{Ca}^{2+}$ -dependent binding of calmodulin (Miki et. al., 1996), raising the possibility that N-WASP is regulated by  $\text{Ca}^{2+}$ -signaling.

Unlike other members in the same family, N-WASP interacts directly with the Rho family GTPase Cdc42 through their CRIB domain (Burbelo et. al., 1995). The proline-rich region binds to various SH3 domain containing proteins, including the signaling adaptor molecules Ash/Grb2 (Miki et el., 1996) and Nck, as well as the WASP interacting SH3 protein (WISH) (Fukuoka et. al., 2001), and profilin (Suetsugu et. al., 1998). N-WASP was also shown to interact with the SH3 domains of Intersectin-1, the neuronal isoform of dynamin-associated endocytic scaffolding protein Intersectin (Hussain et. al., 2001), as well as with the SH3 domain of Syndapin I (synaptic, dynamin-associated protein I), which is also highly enriched in the brain (Qualmann et. al., 1999; Qualmann and Kelly, 2000).

The WA region of N-WASP is more potent activator of the Arp2/3 complex than other members of the family (Egile et al., 1999; Rohatgi et. al., 1999). This has been attributed to the presence of the two Verprolin-homology domains instead of one (Yamaguchi et. al., 2000) within the WA region. The WA region of N-WASP alone is sufficient to activate Arp2/3 complex *in vitro* (Egile et. al., 1999; Rohatgi et. al., 1999). In fact, full length N-WASP protein is less potent in activating Arp2/3 than the WA domain alone. This is due to the intramolecular autoinhibitory interaction whereby sequences of the cofilin-

homology domain are bound to the CRIB, which prevents the activation of the Arp2/3 complex by WA in full length N-WASP (Orehoda et. al., 2000).

#### **1.8.4. WAVE family proteins.**

WAVE is a homologue of WASP that was identified as a novel protein that possesses a V domain (Miki et. al., 1998; Suetsugu et. al., 1999). Around the same time, a *Dictyostelium* homologue of WAVE was identified and named SCAR (Bear et. al., 1998). Two other homologues of WAVE have been identified to date and they are termed, WAVE2 and WAVE3 (the original WAVE was then termed WAVE1; Suetsugu et. al., 1999). WAVES do not interact with Rho GTPases directly and therefore must be regulated differently from N-WASP and WASP. The amino-terminal of WAVES proteins share sequence homology of an unknown function within their subgroup. This domain is termed the SH domain for SCAR homology domain (reviewed in Higgs and Pollard, 2001). WAVE1 localizes to lamellipodial tips (Hahne et. al., 2001, Nakagawa et. al., 2001) and has been implicated in activating Arp2/3 in lamellipodia formation (Machesky and Insall, 1998; Miki et. al., 1998). WAVE1 was also implicated in dorsal ruffling while WAVE2 was implicated in peripheral ruffling (Suetsugu et. al., 2003). WAVE1-depleted cells revealed a strong inhibition of lamellipodia formation and cell spreading, and filopodia formation was also strongly inhibited (Biyasheva et. al., 2004). WAVE1 and WAVE2 exist as protein complexes composed of the proteins Abi1, p125Nap-1, p140sra-1 and HSPC300. These proteins serve to regulate WAVE family proteins by controlling its stability and localization (Kunda et. al., 2003; Innocenti et. al., 2004).

### **1.8.5. Ena/VASP family of proteins.**

Ena/VASP family proteins consists of the *Drosophila* Ena (Enabled), mena (**m**ammalian Ena), VASP (vasodilator-stimulated phosphoprotein), and EVL (Ena/VASP-like protein) (Gertler et. al., 1996). Ena was identified through genetic interactions with the *Drosophila* Abl (Abelson murine leukemia viral oncogene) homologue (Gertler et. al., 1990; 1995), whereas VASP was identified as a prominent target for cAMP (PKA) and cGMP-dependent protein kinases in platelets (Halbrugge et. al., 1990). Mena and EVL were identified by similarity to Ena (Gertler et. al., 1996). Ena, Mena and VASP are important in processes that require highly dynamic actin reorganization, including axon guidance (Lanier et. al., 1999), platelet aggregation (Hauser et. al., 1999; Aszodi et. al., 1999), and fibroblast motility (Bear et. al., 2000). These proteins are concentrated in regions of the cell associated with movement and adhesion, including the leading edge of lamellipodia, focal adhesions, adherens junctions and tips of filopodia (Gertler et. al., 1996; Reinhard et. al., 1992; Vasioukhin et. al., 2000).

### **1.8.6. Ena/VASP and Mena.**

The Ena/VASP proteins share a common domain structure that consist of an amino-terminal Ena/VASP homology (EVH) 1 domain, a carboxyl-terminal EVH2 domain, and a central proline-rich domain. The EVH1 domain is highly conserved and binds to target sequences that have the consensus (E/D)/FPPPPXDE (Fedorov et. al., 1999; Niebuhr et. al., 1997). Functional EVH1-binding motifs are present in the *Listeria monocytogenes* surface protein ActA (Niebuhr et. al., 1997); in focal adhesion proteins vinculin and Zyxin (Reinhard et. al., 1995) in Fyb/SLAP (Fyn-binding protein/SLP76-associated

protein), a component of the T-cell receptor pathway (Krause et. al., 2000); and in the axon guidance proteins ROBO (Kidd et. al., 1998) and Semaphorin-6A-1. In fibroblasts, the EVH1 domain mediates focal adhesion (Gretler et. al., 1996; Niebuhr et. al., 1997; Carl et. al., 1999) and leading edge targeting (Bear et. al., 2000) and a functional EVH1 domain is required for Ena function in *Drosophila* (Ahern-Djamali et. al., 1998). The EVH2 domain contains conserved motifs implicated in actin binding (Reinhard et. al., 1992; Bachmann et. al., 1999; Laurent et. al., 1999) and formation of both homo- and heteromultimers of the Ena/VASP proteins (Carl et. al., 1999; Ahern-Djamali et. al., 1998; Figure 1.8).

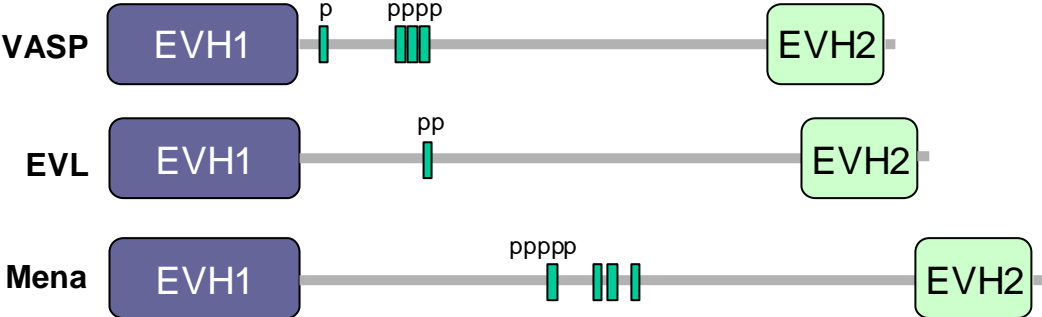
In contrast to the highly conserved EVH1 and EVH2 domains, the central proline-rich domain of the different proteins contains variable lengths of consecutive polyproline clusters. Three types of ligands have been shown to bind to this region in Ena/VASP proteins. They are the SH3, WW domains as well as the actin-binding protein profilin (Gertler et. al., 1996; 1995; Bachmann et. al., 1999; Reinhard et. al., 1995; Ermekova et. al., 1997). There is evidence that suggests that the interactions between profilin and Ena/VASP proteins are important *in vivo*.

**Figure 1.8 Schematic of VASP/Mena family.**

The Ena/VASP family includes three highly related proteins; Mena (mammalian Enabled), VASP (vasodilator-stimulated phosphoprotein), and EVL (Ena-VASP-like). The family members share a conserved domain structure: a proline-rich core (PRO), flanked by two distinct regions called the Enable-VASP-homology domains (EVH1 and EVH2, respectively).



Figure 1.8



In mice, there is potent dosage-sensitive genetic interaction between Mena and Profilin I (Lanier et. al., 1999). Although Mena mutants are viable, they display defects in several nerve fibre tracts in the brain and a reduction of profilin levels by 50% causes Mena mutants to exhibit a severe defect in closure of the cephalic portion of the neural tube. In *Drosophila*, mutations in Ena and profilin have been shown to exhibit dosage-sensitive genetic interactions with Abl (Gretler et. al., 1990; Wills et. al., 1999). Despite all the genetic evidence, the mechanism that regulates the interaction and function of Ena/VASP-profilin complexes remains poorly understood (Lanier et. al., 2000). Barzik et. al., however did show that recombinant His-tagged VASP increased the rate of actin polymerization in the presence of the barbed end cappers, heterodimeric capping protein (CP), CapG, and gelsolin-actin complex. Profilin enhanced the ability of VASP to protect barbed ends from capping by CP, and this required the interactions of profilin with G-actin and VASP. The VASP EVH2 domain was sufficient to protect barbed ends from capping, and the F-actin and G-actin binding motifs within EVH2 were required. Phosphorylation by protein kinase A at sites within the VASP EVH2 domain regulates anti-capping. Therefore, it was proposed that Ena/VASP protein associate at or near actin filament barbed ends, promoting actin assembly and restricting the access of barbed end capping proteins (Barzik et. al., 2005).

Another study documented a 74 kDa novel protein termed PREL1 (Proline Rich EVH1 Ligand) that shares homology with the Grb7-family of signaling adaptors. It was shown that PREL1 binds directly to Ena/VASP proteins and colocalizes with them at lamellipodia tips and at focal adhesions in response to Ras activation. PREL1 also

directly binds to activated Ras in a phosphoinositide-dependent manner. This is the first direct link between Ras signaling and cytoskeletal remodeling *via* Ena/VASP proteins during cell migration and spreading (Jenzora et. al., 2006). Further work on VASP revealed a novel mechanism of action, namely the regulation of tensile strength, contractility and rigidity of the actin cytoskeleton. Fibroblasts derived from VASP-deficient mice were observed to have thicker and more stable actin stress fibres compared to wild-type cells. Furthermore, in the VASP-deficient cells, focal adhesions are enlarged, myosin light chain phosphorylation is increased, and the rigidity of the filament-supported plasma membrane is elevated about three- to four-fold (evident from atomic force microscopy). Fibronectin-coated beads also adhere more strongly to the surface of VASP-deficient cells. The resistance of these beads to mechanical displacement by laser tweezers is dramatically increased in an F-actin-dependent manner. Cytoskeletal stabilization coincides with slower cell adhesion and detachment, while overall adhesion is increased. Interestingly, many of these effects observed in VASP(-/-) cells are seen in VASP-overexpressing cells, suggesting that a balanced stoichiometry necessary for appropriate VASP function (Galler et. al. 2006).

### **1.8.7. EVL.**

The third member of the Ena/VASP family, EVL, partially restores *Listeria* movement in cell-free extracts depleted of VASP and Mena (Laurent et. al., 1999) and shares many structural features with the other family members. The EVH1 domain and distinct parts of EVH2 domain are homologous, but the central portion differs in both length and proline content. The number of conserved cyclic nucleotide-dependent kinase

phosphorylation sites also differs; whereas VASP and Mena has three and two, respectively, EVL has only one site (Gertler et. al., 1996).

Two isoforms, EVL and EVL-I, were highly expressed in hematopoietic cells of thymus and spleen. In CD3-activated T-cells, EVL was found in F-actin rich patches and at the distal tips of the microspikes that formed on the activated side of the T-cells. Like the other family members, EVL localized to focal adhesions and the leading edge of lamellipodia when expressed in fibroblasts. EVL was a substrate for the cAMP-dependent protein kinase, and this phosphorylation regulated several of the interactions between EVL and its ligands. Unlike VASP, EVL nucleated actin polymerization under physiological conditions, whereas phosphorylation of both EVL and VASP decreased their nucleating activity. EVL bound directly to Abl, Lyn and nSrc SH3 domain, as well as to the FE65 WW domain and profilin, most likely through its proline-rich core. Binding of Abl and nSrc SH3 domains but not profilin or other SH3 domains, was abolished by cAMP-dependent protein kinase phosphorylation of EVL. Strong cooperative binding of two profilin dimers on the polyproline sequence of EVL was also observed. These data suggest that the function of EVL could be modulated through interactions with multiple ligands and phosphorylation by cyclic nucleotide dependent kinases (Lambrechts et. al., 2000). EVL has also been shown to interact and colocalized with spectrin.

### **1.8.8. Abi proteins.**

The Abi proteins were originally identified as substrates and binding partners for the Abl tyrosine kinases (Dai et. al., 1995; Shi et. al., 1995; Wang et. al., 1996), a family of proteins that bind actin and regulate actin dynamics (Pendgergast et. al., 2002). Abi1 and Abi2 are the products of different genes, while Abi2a and Abi2b are splice variants that differ primarily in their N termini (Biesova et. al., 1997; Blagg et. al., 2003; Chen et. al., 2001). This family of proteins contains several major domains, including; a coiled-coil region, a homeobox homology region (HR), a polyproline stretch (PRO) and a SH3 domain.

Abi proteins have been linked to Rac1-dependent cytoskeletal reorganization (Biesova et. al., 1997; Blagg et. al., 2003; Bogerd et. al., 1996; Chapman et. al., 1994). Abi1 associates with Sos-1 and EGF-receptor substrate Eps8 in a complex that exhibits Rac1-GEF activity. The depletion of Abi1 by microinjection of antibodies into fibroblast inhibits membrane ruffling in response to PDGF (Chapman et. al., 1994). It is also a scaffolding protein that permits the assembly of different multi-molecular complexes (Stradal et. al., 2004; Innocenti et. al., 2003; Disanza et. al., 2004) including the WAVE-Abi1-p125Nap-1- p140sra-1(PIR121) complex, which is essential for the formation of membrane protrusions where it specifically localizes (Innocenti et. al., 2004; Steffen et. al., 2004). Abi1 interacts directly with WAVE2 WHD domain, thereby increases WAVE2 actin polymerization activity (Innocenti et. al., 2005a). Abi1 also binds to N-WASP, and cooperating with Cdc42, potently induces N-WASP activity *in vitro* (Innocenti et. al., 2005b).

## **1.9. IRSp53.**

### **1.9.1 Introduction.**

IRSp53, also known as brain-specific angiogenesis inhibitor 1-associated protein 2 (BAI-AP2) is a multifunctional adaptor protein enriched in the central nervous system (Abbot et. al., 1999; Oda et. al., 1999; Yeh et. al., 1996). IRSp53 was originally identified as IRSp53/p58, a hamster insulin receptor tyrosine kinase substrate of 53 and 58 kDa (Yeh et al., 1996). Subsequently, IRSp53 was identified as a binding partner for WAVE1 polyproline sequence (Miki et. al., 2000), Cdc42 (Govind et. al., 2001), Rac1 (Krugmann et. al., 2001), DRPLA protein: a product of the gene responsible for a neurodegenerative disorder, dentatorubral pallidolusian atrophy (Okamura et. al., 1999) and the cytoplasmic domain of the Fas ligand (GenBank/EMBL/DDBJ accession number U70669). Previous studies identified at least four isoforms (L-, M-, S- and T-forms) in human, where the first 511 amino acid residues were identical, followed by unique sequences of 9–41 amino acid residues (Okamura et al., 2001, Alvarez et al., 2002), generated by alternative splicing of the 3'-terminal exon. The functional significance of these splice variants has not been resolved.

### **1.9.2. Domain families and structure.**

IRSp53 is composed a half-CRIB motif, a proline-rich domain, a Src homology 3 (SH3) domain and a WW domain-binding motif (WW). The SH3 domain is important for binding with a variety of proteins, such as proteins containing proline-rich motifs (WAVE1/2) whereas the half-CRIB motif allows for direct interaction with Cdc42. At the N-terminus, IRSp53 has high sequence identity to a domain of Missing in Metastasis (MIM) protein, which has been termed the IMD (IRSp53 MIM Homology Domain; Yamagishi et. al., 2004). MIM contains a WASP homology 2 (WH2) domain in the C-terminus, and identified in human and mouse (Figure 1.9).

### **1.9.3. IRSp53 function.**

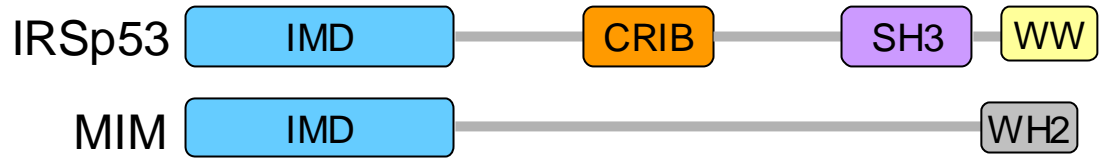
IRSp53 when overexpressed induces filopodia formation and neurite outgrowth (Govind et. al., 2001; Krugmann et. al., 2001). IRSp53 has been shown to be a Cdc42 effector as the IRSp53<sup>1267N</sup> mutant is unable to bind Cdc42 and fails to localize with F-actin, induce filopodia formation or neurite outgrowth (Govind et. al., 2001). Furthermore, binding of activated Cdc42 to the CRIB motif of IRSp53 enhances its ability to promote filopodia formation (Govind et. al., 2001, Krugmann et. al., 2001, Yamagishi et. al., 2004). Taken together, these results suggested that the Cdc42 facilitates filopodia formation and neurite outgrowth by localizing protein complexes via adaptor proteins such as IRSp53 to F-actin. Rac1 is suggested to bind to the IMD/BAR domain IRSp53 (Miki et. al., 2000; Miki and Takenawa. 2002). The Rac1 interaction has not been observed by a number of groups and its role in IRSp53 function is unclear. IRSp53 has been shown to bind to proline-rich regions of a range of known actin regulators through its SH3 domain.

**Figure 1.9 Schematic of IRSp53 and Missing in Metastasis (MIM).**

Schematic representation of IRSp53 and MIM proteins. IRSp53 contains a half-CRIB motif, an SH3 domain, and a 250 amino acid residue stretch, termed the IRSp53 MIM Homology Domain -IMD.



**Figure 1.9**



This includes SCAR2/WAVE2 (Miki et. al., 2000, Miki and Takenawa, 2002), Mena (Krugmann et. al., 2001), mDia1 (Fujiwara et. al., 2000), ProSAP/shank (Bockmann et. al., 2002, Soltau et. al., 2002), espin (Sekerko et. al., 2003) and Eps8 (Funato et. al., 2004). IRSp53 has also emerged as a binding partner of PDZ-domain-containing proteins such as PSD-95 in the post synaptic density and MALS at cell-cell contacts (Hori et al., 2003, Sltau et. al., 2004). Thus IRSp53 is likely to play a promiscuous role in a range of biology's connected actin dynamics.

## **1.10. Functional roles of filopodia.**

### **1.10.1. Components of filopodia.**

The molecular structure of a filopodium can be broken down into 4 components: tip complexes, adhesion complexes, actin filaments and the membrane component. Filopodia extension is driven by polymerization of actin filaments at their tips (Mallavarapu and Mitchison, 1999), although the regulating mechanism of this process is unclear. From electron microscopic studies, it has been revealed that a filopodial tip complex exists at the interface between growing ends of actin filaments and the plasma membrane (Lewis and Bridgman, 1992; Svitkina et. al., 2003). Several components of this tip complex have been identified, including Ena/vasodilator-stimulated phosphoprotein actin-binding proteins (Lanier et. al., 1999; Svitkina et. al., 2003), the motor proteins myosin X and IIIa (Berg et. al., 2002; Les Erickson et. al., 2003) and  $\beta$ 1-integrins (Wu et. al., 1999). The tip complex proteins, such as Ena/VASPs, were proposed to promote growth of long, unbranched filaments by inhibiting the capping process (Bear et al., 2002). Ena/VASPs might also be required to recruit other proteins to further stabilize and organize the actin filaments into bundles as the filopodium grows. In addition, a robust enrichment of tyrosine-phosphorylated proteins at the tips of the growth cone filopodia has been reported.

Studies have shown that different types of adhesions exist on individual filopodia. Adhesions were detected in individual filopodium of sensory growth cones through optical recordings, adhesion markers and electron microscopy. Adhesions on filopodial shafts were able to control veil (lamellar) advance and be modulated by guidance cues.

When a filopodium is lacking in shaft adhesions, veils can readily advance along the filopodium but they rarely advance when shaft adhesions are present. When a cellular cue was contacted by the filopodial tip, veil extension and shaft adhesions were altered in concert. These results suggested that the veil extension was under control of shaft adhesions and that guidance signal cascades can be altered by altering these adhesions (Stekette et. al., 2002).

Mammalian filopodia are made up of actin filaments that are up to 15  $\mu\text{m}$  long and arranged into a tight bundle (Small et. al., 1988, Lewis and Bridgman et. al., 1992). Filopodia arise from the process of actin polymerization, whereby G-actin subunits are polymerized into F-actin containing actin filaments. A typical filopodium may contain from 10 to 30 actin filaments, arranged into a tight bundle (Sheetz et. al., 1992).

#### **1.10.2. Rho family Signaling, lamellipodia and filopodia.**

The protrusion of lamellipodia and filopodia is regulated by two members of the Rho family of GTPases, Rac1, and Cdc42, respectively (Machesky and Hall, 1997; Nobes and Hall, 1995; Ridley, 2001). Insight into the effectors involved downstream of Rac1 and Cdc42 involved in mediating protrusion is now beginning to emerge from information collected on protein complexes affecting actin polymerization *in vitro* (Higgs and Pollard, 2001). The work on the molecular determinants of actin-based pathogen mobility, as well as localization of proteins in lamellipodia and filopodia in living cells are also contributing to the better understanding of the downstream events from Rac1 and Cdc42.

The WASP family of proteins clearly plays important roles downstream of Cdc42 and Rac1 in integrating signaling and actin dynamics.

### **1.10.3. Axonal Guidance.**

Growth cones are specialized motile structures at the ends of developing axons. The activity of growth cones is the main determinant of axon guidance and elongation. In the process of an axon extending through the complex extracellular environment *in vivo*, its growth cone samples the local environment and responds to a variety of molecular guidance cues. These cues can be either attractive or repulsive and they operate at short-range, by a contacted-mediated mechanism involving cell surface ECM molecules, and at longer range, whereby target cells secrete diffusible factors, which either attract or repel the growing axon. Many of these cues have been identified; netrins are diffusible proteins that can attract some axons and repel other. Another group of proteins, the semaphorins, is a large family of cell surface and secreted proteins that can act as long or short-range inhibitors of axon growth. There are also the ephrins that operate bi-directionally, allowing a growth cone to signal to a target cell and vice versa. Many cell adhesion molecules and their receptors play an important role in axonal guidance.

Growth cones sample their environment by extending slender fingerlike projections called filopodia and veil-like structures termed lamellipodia. Both lamellipodia and filopodia are strictly dependent on the polymerization and organization of actin filaments. A migrating axon must read these guidance signals *via* its filopodia in order to be drawn

towards (by attractive cues) or forced away from (repulsive cues) various locations during the journey toward its target destination.

Past studies have shown that single filopodial contacts with environment cues can change the behavior of the growth cone (Bandtlow et. al., 1993; O'connor et. al., 1990). Growth cone behavior is also drastically changed by single filopodial contact with defined molecules. Filopodia have been shown to carry receptors for certain cell adhesion molecules (Letourneau et. al., 1989). Chick dorsal root ganglion (DRG) growth cones behave differently at the border between two substrate molecules, laminin and fibronectin. This illustrates that these ECM molecules provide instructive cues that are picked up and read by individual filopodium (Gomze et. al., 1994). Further evidence for filopodium-dependent steering comes from studies on retinotectal axons in *Xenopus*. These axons grow past their normal turning point into the tectum when stripped of their filopodia by cytochalasin B treatment (Chien et. al., 1993).

#### **1.10.4. Metastasis.**

Metastasis is the dissemination of cancer cells from the primary tumor to a distant site and this is the most frequent cause of death in patients with cancer. Despite this, the molecular mechanisms of metastasis are poorly understood due to its complexity. Cancer cell migration and invasion into adjacent tissues and intravasation into blood and lymphatic vessels are required for metastasis (Chambers et. al., 2002; Friedl et. al., 2003). Invasive carcinoma cells acquire a migratory phenotype associated with elevated expression of several genes involved in cell motility (Wang et. al., 2004; 2005). This

allows for the carcinoma cells to respond to cues from the environment that trigger tumor invasion.

The initial step in cell migration is the protrusion of the cell membrane. This is mediated by localized actin polymerization (Pollard et. al., 1994) which can occur in response to chemotactic signals (DesMarais et. al., 2005). It was reported that carcinoma cells crawling on ECM fibres in primary tumors extend pseudopods that attach to fibres at the migration front (Condeelis et. al., 2003). These pseudopods appears to be functionally equivalent to lamellipodia although the shapes of the former are more three dimensional *in vivo* (Wang et. al., 2002).

The leading protrusions attach to collagen containing fibres, a process that may involve the participation of dynamic adhesion structures i.e. focal complexes. Therefore, increased expression of adhesion molecules such as laminins and integrins (Wang et. al., 2004; 2002) is consistent with the importance of integrins in Rac1 stimulation, adhesion formation and cell migration in invasive tumors cells (Yu et. al., 2005).

Genes responsible for EGF-stimulated protrusions such as cofilin, capping proteins and Arp2/3 complexes are also upregulated. The cofilin pathway is directly involved in directional sensing during chemotaxis of carcinoma cells to EGF (Mouneimne et al, 2004) and it is sufficient to set the direction of cell movement (Ghosh et. al., 2004). The directional sensing of EGF requires a pool of free actin filament barbed ends that is generated by cofilin-mediated severing, which results in localized actin polymerization

(Mouneimne et al, 2004). Studies have also shown that the cofilin-dependent actin polymerization acts in synergy with Arp2/3 complex to generate protrusions in response to EGF that are responsible for cell migration (DesMarais et. al., 2005).

In order to migrate through a physical barrier of dense ECM, cancer cells need to extend protrusions that can remodel and degrade ECM. These protrusions are very important for the invasion of cancer cells through the basement membrane covering blood vessels. Two types of structures account for this function. The first type is the filopodia-like, actin-rich membrane protrusions that extend vertically from the ventral cell membrane on invasive cancer cells cultured on physiological substrates. These are termed invadopodia due to their matrix degradation activity. Invadopodia are enriched with actin regulatory proteins, adhesion molecules, signaling/adaptor proteins, membrane remodeling proteins and matrix degrading proteases (Baldassarre et. al., 2003; Buccione et. al., 2004; McHugh et. al., 2004; Yamaguchi et. al., 2005). Invadopodia are form only in highly invasive cancer cells and only are implicated in tumor cell metastasis.

The second type of structure is the podosomes. Podosomes are dynamic actin-rich adhesion structures very similar to invadopodia in molecular composition. They are formed by monocyte-derived cells, such as macrophages, as well as by some non-hematopoietic cells and by transformed fibroblasts (Linder et. al., 2003). The formation of podosomes and invadopodia are dependent on two key proteins, namely WASP and N-WASP. WASP was shown to regulate podosome formation in macrophages, dendritic cells and osteoclasts (Linder et a., 2003; Calle et. al., 2004). N-WASP on the other hand



is a component of podosomes and invadopodia in non-hematopoietic and cancer cells (Yamaguchi et. al., 2005; Linder et. al., 2003; Moreau et. al., 2003; Spinardi et al; Park et. al., 2005). Upstream activators of N-WASP/WASP, including Cdc42, Nck1 and WIP as well as a downstream effector, the Arp/23 complex have been shown to function in invadopodia/podosome formation (Buccione et. al., 2004; Yamaguchi et. al., 2005; Moreau et al, 2003; Nakahara et. al., 2003; Kaverina et. al., 2003). The WASP/N-WASP signaling pathway most likely plays a role in the ECM remodeling via the formation of podosomes and invadopodia, and hence in tumor invasion and metastasis. Evidence that supports this hypothesis hails from the reduced ability of mammary tumors of rat derived from carcinoma cells with dominant-negative N-WASP to intravasate and spontaneously metastasize (Yamaguchi., Unpublished).

#### **1.10.5. Cell motility and immunity.**

Cell migration is a key aspect of many biological processes, including defense against infections. When tissues become locally infected or suffers an injury, an inflammatory reaction ensues. The inflammatory response is made up of three components; (a) increased blood flow, (b) increased capillary permeability, and (c) increased migration of leukocytes into the affected area. It is characterized by the orderly recruitment and deployment of leukocytes at the focus of tissue necrosis. The cell types seen in different inflammatory foci vary widely and depend on the nature of the stimulus. Movement of cells into sites of inflammation depends initially upon interactions between leukocytes and endothelia (Dustin et. al., 1989; Teddler et. al., 1995). The process is then largely directed by the process of chemotaxis (Downey, 1994). Leukocytes will migrate within

an ECM towards a high point of a concentrate gradient of chemoattractant, and this is mediated by coordinated activation of the cytoskeleton and associated adhesive integrins (Howard and Watts, 1994; Bokoch et. al., 1996; Laudanna et. al., 1996). The actin cytoskeleton is believed to provide both the protrusive and contractile forces required for cell migration. This is achieved via a combination of actin polymerization, depolymerization, actin filament cross-linking, and the interaction of myosin-based motors with actin filaments (Condeelis, 1993; Stossel, 1993; Howard and Watts, 1994; Lauffen-burger and Horwitz, 1996; Mitchison and Cramer, 1996). Three members of the Rho family of GTPases, Cdc42, Rac1 and Rho, are known to regulate the organization of actin-based cytoskeletal structures. Studies on Bac1.2F5 macrophages have shown that Rho regulates cell contraction, while Rac1 and Cdc42 regulate the formation of lamellipodia and filopodia, respectively. Studies using the colony stimulating factor-1 (CSF-1) induced macrophage migration and chemotaxis system, have further elucidated the roles of the three proteins in cell migration. Microinjection of constitutively activated RhoA, Rac1, or Cdc42 inhibited cell migration and this was thought to be due to the cells being unable to polarize significantly in response to CSF-1. Both Rho and Rac1 were required for CSF-1-induced migration. Migration speed was reduced to background levels in cells injected with C3 transferase, an inhibitor of Rho, or with dominant-negative Rac1 mutant, Rac1N17.

In contrast to the effects of inhibiting Rho and Rac1, a dominant-negative Cdc42 mutant, Cdc42N17 does not inhibit cell migration. Cdc42N17 injected cells were observed to migrate in a CSF-1 gradient at almost twice the speed of control Rac1V12A35-injected

cells. The loss of filopodia in these cells were observed, as well as a marked reduction in the degree of cell polarity. These cells retain the ability to migrate but completely lose the ability to move towards a source of CSF-1, suggesting that filopodia have a significant role to play in gradient perception (Allen et. al., 1998).

#### **1.10.6. Wound healing.**

The response to tissue injury requires the harmonious interaction of immune cells, keratinocytes, fibroblasts, and endothelial cells, which unite to regenerate the damaged epithelium. This complex process requires integrin-mediated activation of Rho-GTPases. The subsequent influx of fibroblasts and endothelial cells results in the production of tissue stroma and formation of new blood vessels, which lead to the generation of functional tissue. Initially studies on wound healing utilized an *in vitro* wound healing assay. Wounding of a monolayer of cells induce cells at or close to the leading edge to crawl forward to close the gap and cells were observed to move cooperatively as a sheet, retaining close contacts with their neighbors. Wounding induces an array of immediate dynamic responses, including formation of lamellipodial and filopodial protrusions as well as membrane ruffling at the leading edge of the cell. Microinjection of wound edge cells with Rac1 inhibitor prevents lamellipodia formation and membrane ruffling without affecting filopodia formation, and injected cells were observed to have defective cell migration as no cell movement was observed over the time course of the experiment (Nobes et. al., 1999).

The other protrusive structures seen after wounding are the filopodia, and from work done on Swiss 3T3 cells, these can be blocked by inhibition of Cdc42 in wound edge cells. Interestingly, this results in only a partial block (~50%) of wound closure, suggesting that Cdc42 activity is required for efficient cell movement in the assay but is not absolutely essential. In normal circumstances, cells at the wound margin develop a morphological polarity showing a clear leading edge (with membrane ruffles and filopodia), but have no protrusion activity at their sides or rear, where they are in contact with neighboring cells. Therefore, inhibition of Cdc42 in wound edge cells caused a complete loss of polarity. Cells lose the ability to protrude filopodia and instead, protrude lamellipodia all around their periphery, irrespective of whether there are cell-cell contacts. This establishes a role for filopodia in wound healing.

### **1.10.7. Aims of this thesis.**

In this study I used rapid sequential DIC/fluorescence time-lapse microscopy to follow lamellipodia/membrane ruffles, filopodia formation and GFP-actin in live cells. This combination allowed me to determine with certainty the morphological activity being affected. Another important aspect of the work was the use of cells that either had overexpressed protein or engineered to lack expression. The use of N-WASP and Mena KO cells provided a clean background to understand the function of these proteins. Lastly, the use of FRET (Forster resonance energy transfer), which enabled me to demonstrate protein-protein interactions *in vivo*, was instrumental in investigating the role of proteins in filopodia formation.

The aim of this thesis was to elucidate the mechanism of filopodia formation through studies on Cdc42, IRSp53 and its binding partners. Filopodia inhibitors generated through such a study would then facilitate addressing the wider question of the physiological function of these structures. For example, do filopodia play a role in axonal guidance or wound healing? The answer to this question will not only lead us to understand fundamental aspects of cell biology but may also identify ways of intervening in disease states.

# **MATERIALS AND METHODS**

## **MATERIALS AND METHODS**

### **2.1. Materials.**

#### **2.1.1. General laboratory reagents.**

General laboratory chemicals were obtained from Sigma or BDH. Ethanol, methanol, isopropanol, glycerol, HCl, sodium hydroxide, Tris-HCl, Tween 20, Triton-x-100, bromophenol blue, glycine and glacial-acetic acid were obtained from BDH, Merck and Sigma. Purified water and phosphate buffered saline (PBS) were prepared by central facilities (Biopolis) according to standard protocols. Bovine serum albumin (BSA) and sodium dodecyl sulphate (SDS) were from Sigma.

#### **2.1.2. DNA manipulation reagents.**

DNA restriction enzymes were obtained from NEB, Gibco-BRL and Roche. DNA purification mini-prep system, Maxi-prep system and PCR purification kits were from Qiagen. Agarose and ethidium bromide were obtained from Bio-Rad. DNA markers were from New England Bio-labs. *Escherichia Coli* XL1-Blue competent cells were from Stratagene. DNA modifying enzymes were from New England Bio-labs.

#### **2.1.3. Protein manipulation reagents.**

Pre-stained molecular markers were from Bio-Rad. Sodium vanadate and PMSF were from Sigma. Complete general protease inhibitor tablets were from Roche Diagnostics. PVDF transfer membrane were from NEN. Acrylamide/Bis-acrylamide (30%/0.8% and 40%/10.5%) were from Bio-Rad. DTT, Temed  $\beta$ -Mercaptoethanol were from Sigma and BDH. [<sup>32</sup>P]-dCTP (3000Ci/mmol, 10mCi/ml) from NEN. Hybond-N filters, Hyperfilm-

ECL and ECL (enhanced chemiluminescent) reagents were from Amersham. Autoradiography X- mat film was from Kodak. G-50 Sephadex was from Pharmacia biotech.

#### **2.1.4. Tissue culture reagents.**

Dulbecco's Modified Eagle Medium (DMEM) with 4500 mg/L glucose or 1000 mg/L glucose and 0.25% trypsin were obtained from centralized media preparation facilities (Biopolis). Fetal bovine serum was from Sigma. Anti-microbial /antibiotic cocktails and lipofectAMINE 2000 were obtained from Gibco-BRL. Mouse laminin solution was from Invitrogen. Mouse interferon  $\gamma$  is from ROCHE. N-WASP WT/KO and Mena WT/KO cells were from Dr. Klemens Rottner.

#### **2.1.5. Reagents for immunodetection and immunofluorescence.**

##### **2.1.5.1. Phalloidin.**

Phalloidin, a component from the mushroom *Amanita phalloides*, binds to actin filaments and stabilizes them against depolymerization (Cooper, 1987). The following fluorescent derivatives were used to stain actin filaments in permeabilized cells;

1. FITC-phalloidin (Sigma), diluted 1:1000 (in 1 % BSA in PBS).
2. TRITC-phalloidin (Sigma), diluted 1:1000 (in 1 % BSA in PBS).
3. Alexa647-phalloidin (Molecular Probes), diluted 1:8000 (in 1 % BSA in PBS).



#### **2.1.5.2. Primary antibodies.**

Anti-IRSp53 mouse monoclonal antibody, 1:100. Anti-HA mouse monoclonal antibody (SC-7392, Santa-Cruz), 1:200. Anti-N-WASP rabbit polyclonal antibody (SC-20770, Santa-Cruz), 1:200. Anti-WAVE1 goat polyclonal (SC-10388, Santa-Cruz), 1:200. Anti-WAVE2 goat polyclonal antibody (SC-10394, Santa Cruz), 1:200.

#### **2.1.5.3. Secondary antibodies.**

Goat anti-Rabbit IgG-Alexa Fluor<sup>TM</sup> 350, (1:500, A11046, Molecular Probes). Goat anti-Rabbit IgG-Alexa Fluor<sup>TM</sup> 488, (1:400, A11008, Molecular Probes). Goat anti-Rabbit IgG-Alexa Fluor<sup>TM</sup> 594 (1:400, A11012, Molecular Probes). Goat anti-Rabbit IgG-Cy5 (1:400, 81-6116, Molecular Probes).

#### **2.1.6. cDNA constructs.**

cDNA constructs using the mammalian expression vector pXJ40. HA-IRSp53 as described in Govind et. al., (2001). HA-N-WASP, HA-Cdc42, HA-Cdc42V12, HA-Cdc42-N17, HA-Rac1, HA-Rac1V12, HA-Rac1N17, HA-RhoA, HA-RhoAV14 and HA-Rho1N19 were from Dr. Thomas Leung (Glaxo-IMCB, Singapore). GFP-actin was from Dr. Dong Jing Ming (Glaxo-IMCB, Singapore). GFP-SCAR and GFP-WAVE2 were from Dr. Giorgio Scita (IFOM-IEO, Italy). GFP-IRSp53, GFP-IRSp53 (1-250), GFP-IRSp53 (251-521), GFP-IRSp53 (1-363), GFP-IRSp53-W/R, GFP-IRSp53- FP/AA, pNF-IRSp53 (1-25), pNF-IRSp53 (1-250) and pNF-IRSp53 (251-521) were from Dr. Akiko Yamagishi (NCCRI, Japan). GFP-N-WASP, GFP-N-WASP $\Delta$ WA were from Dr. Silvia Lommel (IZB, Germany). GFP-Mena was from Dr. Klemens Rottner (HCIR, Germany).

### **2.1.7. Oligomer Synthesis and cDNA sequencing Service.**

Oligos were synthesized by Pro-oligo,inc (Singapore). DNA Sequencing provided by Sequencing Core facilities in IMCB.

## **2.2. Methods.**

### **2.2.1. Plasmid DNA preparation.**

#### **2.2.1.1. Transformation of *E.coli* (XL1-Blue competent cells).**

Competent *E.coli* XL1-Blue cells were transformed according to manufacturer protocol. Briefly, cells were thawed on ice and then transferred to pre-chilled eppendorf tubes in 50-100  $\mu$ l aliquots. 1  $\mu$ l (1-50 ng) of plasmid DNA or 10  $\mu$ l of a ligation mix were then added to the cells and left to stand on ice for 30 mins. Cells were then heat shocked at 42°C for 45 secs and were then returned to the ice for a further two mins. 0.9ml of pre-warmed Luria-Bertani broth (L-Broth) media was added to the cells and incubated with agitation (225-250 rpm) at 37°C for 60 mins. If a re-transformation was performed, 50  $\mu$ l of competent cells were used, and the 60 mins amplification step was omitted (for ampicillin selection). Cells were then pelleted briefly in a microcentrifuge at room temperature (RT) and resuspended in 100  $\mu$ l of media and spread directly onto pre-warmed L-Broth ampicillin (80  $\mu$ g/ml) or L-Broth kanamycin (50  $\mu$ g/ml) agar plates and incubated overnight at 37°C.

#### **2.2.1.2. Qiagen Mini-preps.**

A single colony of transformed *E.coli* XL1-Blue competent cells containing the required plasmid DNA was picked using a sterile toothpick. The toothpick was placed into 5 ml of

pre-warmed L-Broth containing 80 µg/ml of ampicillin or 50 mg/ml of kanamycin in a 14 ml falcon tube. The culture was incubated then at 37°C in a shaker for 16 hours. 500 µl of culture was mixed with 500 µl of glycerol and stored at -70°C. The remaining culture was centrifuged at 3,000 rpm in a bench top centrifuge for 10 mins at 4°C. The supernatant was decanted and the pellet was resuspended in 250 µl of cell resuspension buffer (50 mM Tris-Cl, pH 8; 10 mM EDTA, 100 µg/ml RNaseA). Samples were vortexed to ensure full resuspension of the cell pellet. To each preparation 250 µl of cell lysis buffer (200 mM NaOH, 1%SDS) was added and mixed by inverting the tube a few times. Preparations were then incubated at RT for 5 mins. 350 µl of neutralizing buffer (3 M potassium acetate, pH 5.5) was added and mixed immediately by inverting the tube. Preparations were centrifuged at 14,000 rpm for 10 mins to remove bacterial cell debris. The lysates were transferred to mini-prep columns which were placed into 2 ml collection tubes. Columns were centrifuged at 14,000 rpm for 1 min. Flow through was discarded. Columns were washed by the application of 250 µl of column wash solution (1M NaCl, 50 mM MOPS, pH 7, 15% isopropanol) followed by centrifugation at 14,000 rpm for 2 mins at RT. Columns were transferred to a clean eppendorf tubes. Plasmid DNA was eluted by the addition of 50 µl of TE buffer onto the mini-prep columns followed by centrifugation at 14,000 rpm for 1 min.

#### **2.2.1.3. Qiagen Maxi-preps.**

DNA constructs required for transfection and microinjection purposes were prepared using a Qiagen Maxi-prep protocol. Briefly, a 5 ml starter culture was prepared by inoculating L-Broth ampicillin or kanamycin with a single colony. The culture was

allowed to grow for 8 hours at 37°C with shaking at 220rpm. This culture was diluted 1/100 into selective L-Broth ampicillin or L-Broth kanamycin and grown at 37°C overnight with shaking. Cells were harvested by centrifugation at 4000 rpm for 15 mins at 4°C in a Sorvall RC-5C centrifuge. The bacterial pellet is resuspended in 4 ml of buffer P1 (50 mM Tris-Cl; pH 8; 10 mM EDTA, 100 µg/ml RNase A) containing RNAase in a 50 ml Falcon tube. The cell suspension was lysed with 4 ml of buffer P2 (200 mM NaOH, 1% SDS). Upon addition the solution was mixed gently by inversion 4-6 times resulting in an increase in viscosity of the suspension. The tube was incubated on ice for 5 mins. For the precipitation of genomic DNA, 4 ml of chilled buffer P3 (3 M potassium acetate, pH 5.5) were added and mixed immediately by gentle inversion. The tube was incubated on ice for a further 15 mins. The supernatant was separated from the precipitate by centrifugation in polypropylene tubes at 20,000 rpm for 30 mins at 4°C in a Sorvall RC-5C centrifuge. The supernatant was re-centrifuged at 20,000 rpm for 15 mins at 4°C and then promptly removed. The clear supernatant was applied to an equilibrated Qiagen-tip 100. Allowing 10 ml of buffer QBT (750 mM NaCl, 50 mM MOPS, pH 7, 15% isopropanol, 0.15% Triton X-100) to flow through the column carried out the equilibration. Following application of the supernatant, the columns were washed with 2 x 30 ml of buffer QC (1 M NaCl, 50 mM MOPS, pH 7, 15% isopropanol) to assist in the removal of contaminants present in the plasmid DNA preparation. DNA was eluted with 15 ml of buffer QF (1.25 M NaCl, 50 mM Tris, Tris-Cl, pH 8.5, 15% isopropanol). The DNA was precipitated by adding 10.5 ml (0.7 volumes) of isopropanol equilibrated to RT (to prevent the co-precipitation of salt). The solution was mixed and centrifuged at 15,000 rpm for 30 mins at 4°C. The supernatant was decanted carefully and the DNA

pellet was washed with 2 ml of RT 70% ethanol and centrifuged at 15,000 rpm for 10 mins at 4°C. The supernatant was decanted from the pellet, to allow the pellet to air-dry for 10 mins. The pellet was resuspend in 400 µl of 1 x TE pH 8.0 overnight at RT.

#### **2.2.1.4. Quantification of DNA in solution.**

DNA concentrations and purity were determined by measuring the light absorbance of DNA samples at 260 nm and 280 nm respectively. 5 µl of a DNA sample was diluted into 1 ml of 1 x TE. DNA samples were measured in UV cuvettes in a Bio-Rad spectrophotometer.

#### **2.2.1.5. Qiagen Magic DNA clean-up system.**

DNA fragments in agarose or DNA samples treated with enzymes were purified by incubating in 1 ml of Qiagen resin (6 M guanidine thiocyanate). The mix was incubated at RT on a rotator until the agarose pieces had completely passed through a Qiagen column using a 2 ml syringe. The resin was washed with 2 ml of 80% isopropanol and dried by spinning the tube for 2 mins in a microcentrifuge at RT. The DNA was eluted with 50 µl of 1 x TE buffer (pH 8.0) heated to 80°C.

#### **2.2.1.6. Gel electrophoresis of DNA.**

Linearised DNA was separated on an agarose gels. 1% agarose gels were cast by dissolving 1 g agarose into 100 ml of 1 x TBE in a microwave. The clear transparent solution was left to cool before it was poured into a sealed rectangular mould. A Teflon comb was positioned at the top of the mould to form the wells. The gel was left to

solidify at RT for 30-45 mins. The comb and seals were then removed and the gel was placed into an electrophoresis tank containing enough electrophoresis buffer (1 x TBE) to cover the surface of the gel. DNA samples were mixed with 1:5 volume of 6 x loading buffer (0.25% bromophenol blue, 0.25% xylene cyanol FF, 30% glycerol in water) and loaded into the wells. Either HaeIII-digested  $\Phi$ x174 or HindIII-digested bacteriophage DNA markers or a mixture of the two were loaded in a separate well to determine the fragment sizes of the DNA sample. Agarose gels were run at 140 V for 45 mins or until the dye front had run approximately 80% through the gel.

#### **2.2.1.7. Visualization of DNA with ethidium bromide.**

DNA fragments were visualized by incubating agarose gels in 1 x TBE containing 1% ethidium bromide for 15-30 mins. Gels were washed briefly in 1 x TBE to remove excess ethidium bromide solution and then placed on UV box. Images were captured on Polaroid film.

#### **2.2.1.8. Isolation of DNA fragments from agarose gels.**

DNA fragments required for ligation purposes or for probe preparation were purified in the appropriate percentage agarose gel. Wells were formed to accommodate the increased sample volume 50-100  $\mu$ l. An additional 10  $\mu$ l of sample were also loaded into a separate well that could be separated and incubated in ethidium bromide for visualization as described above. The whole gel was then placed onto a low wavelength UV box and fragment excised with a razor following the position of the corresponding visible fragment. The fragment of interest was then purified as described 2.2.1.5.

### **2.2.1.9. Enzymatic modification of DNA.**

#### **2.2.1.9.1. Digestion of DNA with restriction enzymes.**

Plasmids, vectors and fragments were digested with various endonucleases using the buffers provided with the enzymes at a 10-fold dilution. Most digests were carried out in 10  $\mu$ l volumes for diagnostic purposes and in greater volumes of 20-100  $\mu$ l when preparing fragments or vectors for ligation. Enzymes units were used according to the amount of DNA present in sample ensuring that the enzyme concentration was not in excess to prevent star activity. Most digestions were carried out at 37°C for 1-2 hours unless otherwise recommended by the manufacturers. Double digest were performed using the buffer with the lower salt concentration if a compatible buffer was not available.

#### **2.2.1.9.2. Stratagene Klenow fill-in kit.**

The Klenow fill-in kit is designed for complete and partial fill-in reactions of 5' DNA overhangs. The following reaction was typically performed with a 50  $\mu$ l DNA sample, to which the following components were added. 6.5  $\mu$ l of 10 x Klenow buffer (60 mM Tris-HCl (pH 7.5), 60 mM NaCl, 60 mM MgCl<sub>2</sub>, 0.5% gelatin, 10 mM DTT), 8  $\mu$ l of 10mM dNTPs 1:1:1:1 (A:T:G:C) and 2  $\mu$ l of Klenow enzyme (5 u/ $\mu$ l). The reaction was incubated at RT for 15 mins and then incubated at 65°C for 10 mins to inactivate the Klenow enzyme. DNA was purified by using the Qiagen "Magic DNA "clean-up" kit (see section 2.2.1.5). The purified sample was then used in the ligation reactions described below.

#### **2.2.1.10. DNA ligation.**

T4 DNA ligase (Promega) catalyzes the formation of phosphodiester bonds between adjacent 5' phosphate and the 3' hydroxyl residues of adjacent nucleotides in either cohesive-ended or blunt-ended fragments. To perform DNA ligations, the following components were added; 20 ng of insert DNA, 100 ng of linearised vector, 2  $\mu$ l of 10 x T4 reaction buffer (30 mM Tris-HCl (pH 7.8), 10 mM MgCl<sub>2</sub>, 10 mM DTT, 1 mM ATP), ddH<sub>2</sub>O to a final volume of 20  $\mu$ l and 1  $\mu$ l of T4 DNA ligase (3 u/ $\mu$ g). Cohesive-end ligations were incubated at 23°C for 3-4 hours. Blunt-ended ligations were performed at 15°C for 4-18 hours. 10  $\mu$ l of ligation mix were used to transform 100  $\mu$ l of XL1-Blue competent cells.

#### **2.2.1.11. Inactivation and removal of enzymes.**

Heat inactivation of enzyme activity was achieved by heating the digest mixture at 65°C for 15 mins. With larger preparations, the DNA samples were cleaned using the DNA clean-resin as described in 2.2.1.5.

#### **2.2.1.12. Polymerase chain reaction (PCR).**

Polymerase chain reaction (PCR) uses single stranded DNA as a template to amplify required DNA sequences. This *in vitro* technique amplifies a required DNA sequence by the use of two oligonucleotides, which are complementary to opposite strands of the DNA template at either end of the DNA sequence to be amplified. The Vent DNA polymerase (NEBL) extends these oligonucleotides by incorporating complementary nucleotides to the template DNA between the two primers. The DNA is heat denatured



and the whole process of annealing and synthesis is repeated. This technique proceeds to produce the required DNA sequence in an exponential manner as both the original DNA template and subsequently formed DNA sequences can act as a template for the oligonucleotides to anneal to forming new complementary DNA sequences.

A typical PCR reaction tube will contain the following;

10  $\mu$ l of 10 x ThermoPol buffer

3  $\mu$ l of 25 mM dNTP mix (ATP, TTP, CTP, GTP)

2  $\mu$ l of DNA Template

0.5  $\mu$ l of VANT polymerase

2.5  $\mu$ l of Oligomers

81  $\mu$ l of ddH<sub>2</sub>O to make up a volume of 100  $\mu$ l

Tubes were placed into a MJ Research PCR machine for the following cycles;

94°C for 4 mins to denature template DNA

94°C for 1 min to denature template DNA in later amplification cycles

X°C for 1 min to allow annealing of oligomers to template DNA

72°C for 5 mins to allow extension of oligomers so as to copy template DNA

This part of the cycle was repeated 25-30 times in order to amplify the required section of the template DNA.

72°C for 5 mins to allow final extension of oligomers

4°C to store PCR products overnight and to end reaction

The value of X is based on the  $T_m$  value of the oligonucleotides used in the reaction

$$T_m = 2(A+T) + 4(G+C)$$

where A, T, G, and C refer to the nucleotide base content.

PCR products were analysed by running 10  $\mu$ l on either a 1% agarose gel or a 16% acrylamide gel depending on the size of the products.

#### **2.2.1.13. siRNA.**

Long double-stranded RNAs (dsRNAs; typically >200 nt) can be used to silence the expression of target genes in a variety of organisms and cell types (e.g., worms, fruit flies, and plants). Upon introduction, the long dsRNAs enter a cellular pathway that is commonly referred to as the RNA interference (RNAi) pathway. First, the dsRNAs get processed into 20-25 nucleotide (nt) small interfering RNAs (siRNAs) by an RNase III-like enzyme called Dicer (initiation step). Then, the siRNAs assemble into endoribonuclease-containing complexes known as RNA-induced silencing complexes (RISCs), unwinding in the process. The siRNA strands subsequently guide the RISCs to complementary RNA molecules, where they cleave and destroy the cognate RNA (effector step). Cleavage of cognate RNA takes place near the middle of the region bound by the siRNA strand.

In mammalian cells, introduction of long dsRNA (>30 nt) initiates a potent antiviral response, exemplified by nonspecific inhibition of protein synthesis and RNA degradation. The mammalian antiviral response can be bypassed, however, by the introduction or expression of siRNAs.

#### **2.2.1.14. Cloning of WAVE1/2 RNAi fragment into pSUPER vector.**

Reduction of endogenous WAVE1 and WAVE2 expression in N1E115 cells was performed using the pSUPER RNAi system (Oligoengine, Seattle, WA, USA) according to the manufacturer's instructions. Oligonucleotides within the open reading frame of mouse WAVE1 or WAVE2 were used as target sequences. Inserts coding for short hairpin RNA (shRNA) against WAVE1 or WAVE2 transcript were cloned between EcoR1 and Hind III restriction site of the pSUPER vector. A scramble RNAi containing a mock shRNA sequence was generated as a control. WAVE RNAi in pSUPER vectors was provided by Tan Yueh-Li (SA lab.).

The following sequences were used for WAVE1, WAVE2 RNAi and scramble sequence;

WAVE1: CGATGAGAAAGGCTTTCCG  
WAVE2: TACTCGGAAGGCCTTCAGA  
Scramble: CGCTATGAACGGTAGCTGA

The following oligos were generated:

WAVE 1 Sense:

5'' – gATCCCCgCgATgAgAAAggCTTTCCgTTCAA  
gAgACggAAAgCCTTTCTCATCATCgTTTTTA –3''

WAVE1 antisense:

5'' – AgCTTAAAAACgATgAgAAAggCTTTCCgTCT  
CTTgAACggAAAgCCTTTCTCATCgCggg – 3''

WAVE2 Sense:

5'' – gATCCCCgTACTCggAAggCCTTCAgATTCAA  
gAgATCTgAAggCCTTCCgAgTATTTTTA –3''

WAVE2 antisense:

5' – AgCTTAAAAATACTCggAAggCCTTCAgATCT  
CTTgAATCTgAAggCCTTCCgAgTACggg –3'

Scramble sense:

5' – gATCCCCgCgCTATgAACggTAgCTgATTCAA  
gAgATCAgCTACCgTTCATAgCgTTTTTA –3'

Scramble antisense:

5' – AgCTTAAAAACgCTATgAACggTAgCTgATCT  
CTTgAATCAgCTACCgTTCATAgCgCggg –3'

## **2.2.2. Protein expression and purification.**

### **2.2.2.1. Expression of recombinant GST-fusion proteins.**

The glutathione s-transferase (GST) Gene Fusion System is an integrated system for the inducible expression of fusion proteins in *E.coli*. pGEX plasmids are designed for the expression of genes or gene fragments with *Schistosoma Japonicum* GST. Protein expression from the pGEX plasmid is under the control of the *tac* promoter, which is induced using the lactose analog isopropyl-D-thiogalactoside (IPTG). Rapid purification can be achieved using Glutathione Sepharose 4B beads where fusion proteins can be purified to >90% in a single chromatographic step. Fusion proteins can then be recovered from beads under competitive elution conditions using excess reduced glutathione.

Single *E.coli* colonies transformed with recombinant pGEX plasmid were used to inoculate 2 ml of L-Broth-amp. Cultures were grown overnight at 37°C with agitation and then were diluted at 1:100 with pre-warmed L-Broth-amp and allowed to continue growing to an optical density (O.D.) of 0.5 at 600nm. Adding IPTG at 1 mM induced fusion protein expression and cells were grown for a further 5-6 hours and then harvested.

Cells were then centrifuged for 10 mins to form a pellet. Pellets were washed in PBS to remove residual media and re-pelleted and left overnight at -20°C.

#### **2.2.2.2. Purification of recombinant GST-fusion proteins.**

Pellets were thawed on ice and completely resuspended in PBS 1% Triton x-100 containing protease inhibitors; 0.5 mM PMSF, 1 µg/ml aprotinin and 1 µg/ml pepstain. The “freeze-thaw” step assists the lysis of the cells. For complete lysis, the cell suspension was sonicated using an Ultrasonic liquid processor (XL series) for 3 x 25 secs on ice until the cloudy suspension becomes semi-translucent. The bacterial lysate was cleared of cellular debris by centrifugation at 20,000 rpm for 15 mins at 4°C. Before incubation with cleared lysate the glutathione-Sepharose 4B beads are washed 3 x in 10 ml of cold 1 x PBS to remove the 20% ethanol storage solution. Approximately 100 µl of the beads slurry is used per 100 ml of bacterial culture. The clear supernatant was then incubated with glutathione-Sepharose 4B beads for 1 hour at 4°C in 50 ml falcon tubes on a rotator. The beads were pelleted briefly and the supernatant, containing the unbound protein removed. The beads were then washed 3 x for 20 mins in PBS 1% Triton x-100. Purified GST-fusion protein was eluted from the beads by incubating with 10 ml of 5 mM Glutathione in 50 mM Tris-HCl, pH 7.5, 0.1 mM EDTA for 10 mins at RT. The suspension was passed down a column to separate the beads from the eluted protein.

#### **2.2.2.3. Dialysis and concentration of GST-fusion proteins.**

Purified fusion proteins was dialysed first against 2 litres of dialysis buffer (50 mM Tris-HCl pH 7.5, 150 mM NaCl, 2.5 mM CaCl<sub>2</sub>) for 1 hour, then again overnight and once more for 1 hour. The protein was then concentrated by ultrafiltration using Centricon-10 tubes (Amicon) by spinning at 3-4 x at 3,000rpm for 10 mins at 4°C until 10 ml is reduced to 500 µl.

#### **2.2.2.4. Quantification of protein concentrations.**

Protein concentrations were determined photometrically on a Bio-Rad spectrophotometer using Bio-Rad reagent. 1-10 µl of protein sample resuspended with 200 µl of Bio-Rad reagent with 0.8 ml of ddH<sub>2</sub>O and left at RT for 5 mins before measuring the OD at 595 nm. Protein concentrations were determined using a BSA standard curve.

#### **2.2.2.5. Preparation of SDS-PAGE.**

SDS polyacrylamide gel electrophoresis (PAGE) was used to separate proteins on the basis of their molecular weight. This was performed using polyacrylamide gels in a discontinuous buffer system. The final acrylamide concentration in the resolving gel is determined by the molecular weight of the proteins that require separation. The composition of a 22% acrylamide resolving gel for separation of proteins typically ranging from 20 kDa to 1 kDa is as follow:

7.3 ml 30% acrylamide/bis-acrylamide

2.5 ml 1.5 M Tris-HCl pH 8.8

100  $\mu$ l 10% (w/v) SDS

50  $\mu$ l 10% APS

7  $\mu$ l TEMED

Approximately 7.5 ml of this mix was pipetted into a minigel apparatus (Bio-Rad) allowing space for a stacking gel. ddH<sub>2</sub>O was applied to the top of the acrylamide mix and left to polymerize at RT for 45 mins. Once polymerized the ddH<sub>2</sub>O was poured off and any residual fluid removed using filter paper. A stacking mix was prepared as follow:

1.67 ml 30% acrylamide/bis-acrylamide

1.25 ml 0.5 M Tris-HCl pH 6.8

7 ml ddH<sub>2</sub>O

100  $\mu$ l 10% (w/v) SDS

50  $\mu$ l 10% APS

12  $\mu$ l TEMED

The stacking gel was pipetted onto the polymerized resolving gel, into which a Teflon comb was inserted. The stacking gel was left to polymerize at RT for 30 mins. Once polymerized, the comb was removed and residual non-polymerized acrylamide was removed by washing wells with ddH<sub>2</sub>O.

#### **2.2.2.6. Separation of proteins by SDS-PAGE.**

Protein samples were separated according to their molecular weight. Protein markers of known size were run in parallel to samples to estimate the molecular weight of proteins separated on the acrylamide gel. Samples were mixed with 5 x SDS-gel loading buffer (10% SDS, 50% glycerol, 0.3 M Tris-HCl pH 6.8, 0.124 ml  $\beta$ -mercaptoethanol, bromophenol blue, ddH<sub>2</sub>O top to 5 ml) and heat denatured at 100°C for 5 mins before being loaded onto the denaturing SDS-PAGE. A 22% SDS gel was typically used to separate proteins ranging from 20 kDa to 4 kDa. 10% gels were used to separate proteins of 16 kDa to 68 kDa molecular weight. Proteins were separated using a Bio-Rad vertical gel discontinuous buffer system. Gels were run at 140 V for typically 90 mins in 1 x TGS buffer (dilution of the 10x TGS buffer produces a 1x running buffer containing 25 mM Tris, 192 mM glycine and 0.1% SDS, pH approx. 8.6).

#### **2.2.2.7. Visualization of separated proteins.**

Proteins separated by SDS-polyacrylamide gel electrophoresis were stained with Coomassie Brilliant blue solution (0.25 g of coomassie brilliant blue dissolved in 90 ml of methanol:H<sub>2</sub>O [1:1 v/v] and 10 ml of glacial acetic acid). The solution was filtered through a Whatman No.1 filter to remove any particulate matter). Gels were stained for 1-4 hours on a slow rotating platform and then destained in Destain solution (50% dd H<sub>2</sub>O, 40% methanol, 10% glacial acetic acid) for 4-6 hours, with 3-4 changes of the Destain solution.



#### **2.2.2.8. Gel drying.**

For permanent records, gels were dried on a slab dryer. Gels were rinsed in ddH<sub>2</sub>O and placed in between two layers of cellophane that has been immersed in ddH<sub>2</sub>O. The sandwich was placed in between two layers of 3M filter paper. Gels were dried for 1 hour 40 mins at 60°C under a vacuum.

#### **2.2.2.9. Western transfer of proteins onto nitrocellulose filters by semi-dry blotting.**

Proteins separated by electrophoresis on denaturing SDS-acrylamide gels were transferred onto nitrocellulose for probing with antibodies (Western blotting). The SDS-gels were equilibrated in 1 x transfer buffer (100 ml of 10 x stock (48 mM Tris, 39 mM glycine, 1.3 mM (0.037%) SDS, 20% (v/v) methanol made up to 1 l with ddH<sub>2</sub>O). Four pieces of Whatman filter paper and one piece of PVDF membrane were cut to a size of 10 cm x 7 cm. The PVDF membrane was soaked in methanol for 30 mins, rinsed in ddH<sub>2</sub>O and then equilibrated in 1x transfer buffer along with the Whatman filter paper for 30 mins. The sandwich was prepared following manufacturers guidelines on a Bio Rad semi-dry transfer system. The sandwich consisted of two pieces of Whatman filter paper, PVDF membrane, SDS-acrylamide gel, two pieces of Whatman filter paper. Proteins were transferred overnight at a constant voltage of 8 V.

#### **2.2.2.10. Immunoanalysis of nitrocellulose immobilized proteins.**

Proteins immobilized onto nitrocellulose filters by semi-dry blotting were stained for 30 mins in coomassie blue (0.5g coomassie brilliant blue, 45% methanol, 10% acetic acid, 45% ddH<sub>2</sub>O) and then destained in destain (40% methanol, 50% ddH<sub>2</sub>O, 10% acetic acid)

solution for 30 mins followed by washing for 3 x 10 mins in PBS. Filters were then blocked for 1 hour at RT or overnight at 4 °C in 3% milk powder in PBS. Filters were then washed for 3 x 10 mins in PBS/0.1% Tween 20. Filters were incubated with primary antibodies in 1% milk powder in PBS for 1.5 hour at RT. Filters were washed for 3 x 10 mins in PBS/0.1% Tween-20 prior to incubation with a Horseradish peroxidase (HRP) conjugated secondary antibody (Santa Cruz) used at 1:1000 dilution of stock in 1% milk powder in PBS. Filters were incubated for 1 hour at RT. Again filters were washed for 3 x 10 mins in PBS/0.1% Tween-20 before being probe with ECL western blotting detection reagents (Amersham). The ECL system is a non-radioactive, luminescent reagent used for detection of antibodies conjugated with horseradish peroxidase. Equal volumes of ECL reagents 1 and 2 were mixed briefly before being applied to filters for one min. Excess liquid was removed by blotting on Whatman filter paper. Filters were wrapped in saran wrap before being placed into a film cassette protein side up and exposed to ECL film (Kodak). A series of varying time length exposures were performed to obtain an optimum signal.

#### **2.2.2.11. *In vitro* transcription-translation and binding assay.**

The TNT coupled reticulocyte lysate system (L4610, Promega) was used to assess whether N-WASP and IRSp53 interact *in vitro*. N-WASP and GFP were transcribed and translated *in vitro* using the TNT T7-coupled reticulocyte lysate systems with pXJ40-N-WASP-HA as the template for N-WASP and pXJ40-GFP as the template for GFP following the manufacturer's protocol. The plasmids were individually added to the rabbit reticulocyte lysate containing T7 polymerase and [<sup>35</sup>S]-methionine in a reaction

volume of 50  $\mu$ l at 30 °C for 90 mins. The translation products were verified by SDS-PAGE and autoradiography. GST, GST-Cdc42Q61L and GST-IRSp53-SH3 (amino acid residues, 400-469) proteins were bound to GST beads for 1 hour at 4°C before blocking in 1 mg/ml BSA for 30 mins at 25°C. Beads were resuspended in GST purification buffer before adding N-WASP or GFP transcription/translation mixes (20  $\mu$ l) for 1 hour at 4°C.

### **2.2.3. Cell culture.**

#### **2.2.3.1. Cell culture of N1E115 cells.**

N1E115 neuroblastoma cells are a clone derived from a C-1300 mouse neuroblastoma (Amano et. al., 1971). They are adrenergic neurons with a high level of acetylcholine esterase enzyme present. This cell line also has a relatively high production rate of tyrosine hydroxylase, which is involved in the noradrenaline synthesis pathway.

Cells were cultured in DMEM with high glucose (4500 mg/l; DMEM-high) and 10% FBS/1% anti-microbial cocktail (supplements) and plated in 90 mm tissue culture dishes (Nunc). Cell cultures were grown at 37°C in a humidified atmosphere with 5% CO<sub>2</sub> (Sanyo).

#### **2.2.3.2. Cell culture of N-WASP WT and KO cells.**

N-WASP WT (flox) and N-WASP KO cell line (1h51) were cultured in DMEM with low glucose (1000 mg/l) (DMEM-low) with supplements and plated in 90 mm tissue culture dishes (Nunc). Cell cultures were grown at 32°C in a humidified atmosphere with 5% CO<sub>2</sub> (Sanyo). For more information on N-WASP WT/KO cells see Lommel et. al., 2001.

#### **2.2.3.3. Cell culture of Mena WT and KO cells.**

Mena WT (GMH3.0) and KO (MDV7) cells were cultured in Immorto medium (DMEM with high glucose (4500 mg/l), supplemented with 15 % FBS, 1 % antibiotic cocktail (penicillin-streptomycin) and mouse interferon  $\gamma$  (50 U/ml). Cells were plated in 90 mm tissue culture dishes (Nunc) and were grown at 32 °C in a humidified atmosphere with 5% CO<sub>2</sub> (Sanyo). For more information on the Mena WT/KO cells see Geese et. al., 2002.

#### **2.2.3.4. Cell maintenance.**

Cells were grown to sub-confluence before being passage and plated onto fresh dishes, typically at 1/5, 1/10 and 1/20 densities. Cells were fed every other day and on average passaged 3 times a week.

Media was removed from the dish using a suction line and sterile glass pipette in a Class II biohazard hood (Gelman BH Class II Series). Cells were detached by pipetting 10 ml of fresh media and placed into a 14 ml falcon tube. The cells were then pelleted at 1000 rpm in a (IEC Centra CL2) table centrifuge for 5 mins. The supernatant was removed and cell pellet was resuspended in 10 ml of fresh media by gentle pipetting. Cells were then plated out onto 90 mm dishes or 150 mm dishes at the required density in fresh media.

N-WASP and Mena WT/KO cells were treated in the same manner as N1E115 cells, except that 1 ml of pre-warmed trypsin (0.125% w/v) was used to trypsinize the cells to disrupt cell attachment and facilitate their removal from the dish. This is due to N-WASP and Mena WT/KO cells attaching to the culture dish much more efficiently than N1E115

cells. 6 ml of pre-warmed media was then added to the dish to prevent further actions of the trypsin and cells were collected into a falcon tube and treated as described above.

#### **2.2.3.5. -70°C storage of cells.**

A sub-confluent plate of cells was harvested in 10 ml of fresh media and placed in a 14 ml falcon tube. The cells were then pelleted by centrifuging at 1000 rpm for 5 mins (IEC Centra CL2) on a table centrifuge. The media was aspirated and the cell pellet resuspended in 4 ml of freezing media (20% FBS, 10% DMSO<sub>4</sub>, 70% Media). The cells were then aliquoted into 1 ml portions into screw cap cyro-tubes. The tubes were then wrapped well in tissue paper and placed into a polystyrene box before being stored in the -20 °C freezer for overnight. The cells were then transferred to the -70 °C freezer for 48 hours. Tubes were finally transferred to liquid nitrogen storage, where they can be stored until required.

#### **2.2.3.6. Cell plating from stocks in liquid nitrogen storage.**

Vials of cell stocks are thawed rapidly at 37 °C in a water bath. Cells are transferred to a 14ml falcon tube containing 10 ml of pre-warmed media with appropriate supplements (refer to section 2.2.3 for details on medium composition for each cell type). Cells are pelleted by centrifuging at 750 rpm for 7 min. Media was aspirated and cell pellet was resuspended in 10 ml of fresh media. Cells are then plated out in the appropriate dishes at either 0.33 or 0.25 densities. Cells were incubated at the appropriate temperature in a humid environment and 5% CO<sub>2</sub>.

### **2.2.3.7. Preparation of coverslips.**

#### **2.2.3.7.1. Preparation of laminin-coated coverslips.**

Square coverslips of sizes 18mm x 18mm were autoclaved under standard conditions. These coverslips were then placed in a tissue culture dish and coated with mouse laminin (10 µg/ml) for 4 hours at RT or overnight at 4 °C. The laminin solution was removed and the coverslips were washed once with ddH<sub>2</sub>O and left to air dry in the tissue culture hood for 15 mins. The coverslips were then placed into 35 mm dish or 6 well plates with 3 ml of culture medium, ready for plating out of cells for transfection or stored at 4 °C for up to a week.

#### **2.2.3.7.2. Preparation of fibronectin-coated coverslips.**

Square coverslips of sizes 18mm x 18mm were autoclaved under standard conditions. These coverslips were then placed in a tissue culture dish and coated with mouse fibronectin (1 mg/ml) in 1 x HBSS solution for 5 mins at RT. The coating solution was then removed and the coverslips were left to air dry in the culture hood for 15 mins. The coverslips were then placed into 35 mm dish or 6 well plates with 3 ml of appropriate media with supplements (see earlier sections for medium composition details for different cell type) ready for plating out of cells for transfection.

### **2.2.3.8. Transient transfection of N1E115 neuroblastoma cells.**

Coverslips and glass-bottomed dishes (Mattek) were prepared as detailed in 2.2.3.7.1. N1E115 cells were plated out at approximately  $1 \times 10^5$  cells per laminin coated coverslip and grown overnight at 37 °C in DMEM-high with supplements. Before transfection,

cells were serum starved in 1 ml of DMEM-high. Transfection mixes were made with 200  $\mu$ l DMEM-high medium, 1-1.5  $\mu$ g of DNA and 6-12  $\mu$ l of lipofectAMINE and left at RT for 45 mins for the formation of DNA liposomes. The transfection mixes were added to the cells and incubated at 37 °C. After 4 hours the media was aspirated off and replaced with 2 ml of DMEM-high with supplements. Cells were then left overnight at 37 °C for expression.

#### **2.2.3.9. Transient transfection of N-WASP WT/KO cells.**

Coverslips and glass-bottomed dishes were prepared as detailed in 2.2.3.7.2 or used as. For transient transfection, N-WASP WT and N-WASP KO cells were plated out at  $1 \times 10^5$  cells per coverslip and grown overnight at 32 °C in DMEM-low with supplements. Before transfection, cells were serum starved for 1 hour in 1 ml of DMEM-low. Transfection mixes were made with 200  $\mu$ l DMEM-low with supplements, 0.1-0.5  $\mu$ g DNA, and 3  $\mu$ l lipofectamine and left at RT for 45 mins for the formation of DNA liposomes. For co-transfections the amount of lipofectAMINE was adjusted accordingly. The transfection mixes were added to the cells and incubated at 32 °C. After 4 hours medium was removed and replaced with 2.5 ml of DMEM-low with supplements. Cells were then left overnight at 32 °C for expression.

#### **2.2.3.10. Delivery of RNAi into N1E115 cells.**

Coverslips and glass-bottomed dishes were prepared as detailed in 2.2.3.7.1. N1E115 cells were plated out a approximately  $1 \times 10^5$  cells per laminin coated coverslips and grown overnight at 37 °C in DMEM-high with supplements. Before transfection, cells

were serum starved in 1 ml of DMEM-high. Transfection mixes were made with 200  $\mu$ l DMEM-high, 1-1.5  $\mu$ g of RNAi constructs, 0.5-1  $\mu$ g of other cDNA and 6-12  $\mu$ l of lipofectAMINE and left at RT for 45 mins for the formation of DNA liposomes. The transfection mixes were added to the cells and incubated at 37°C. After 4 hours the media was aspirated off and replaced with 2 ml of DMEM-high with supplements. Cells were then left at 37°C to express for 20 to 38 hours.

#### **2.2.3.11. Microinjection of N-WASP WT and KO cells.**

N-WASP WT and KO cells were plated out at approximately  $1 \times 10^5$  cells per glass-bottom dishes and grown overnight at 32°C in DMEM-low with supplements. cDNA of required constructs were prepared at 50ng/ $\mu$ l in ddH<sub>2</sub>O and centrifuged at 14,000 rpm for 30 mins. 6  $\mu$ l of DNA mix was loaded into a microinjection needle and cells were injected at a constant pressure of 20 psi for 100 ms duration. Microinjection was performed on a custom microinjection setup and Olympus microscope (IMT-10). Between 100-150 cells were injected per dish and cells were left to express protein for 1 to 6 hours before they were imaged or fixed and stained.

#### **2.2.3.12. Microinjection of Mena WT/KO cells.**

Mena WT/KO cells were plated out at approximately  $1 \times 10^5$  cells per glass-bottom dishes and grown overnight at 37°C in Immorto medium. cDNA of required constructs were prepared at 50 ng/ $\mu$ l in ddH<sub>2</sub>O and centrifuged at 14,000 rpm for 30 mins. 6  $\mu$ l of DNA mix was loaded into a microinjection needle and cells were injected at a constant pressure of 20 psi for 100 ms duration. Microinjection was performed on a custom



microinjection setup and Olympus microscope (IMT-10). Between 100-150 cells were injected per dish and cells were left to express protein for 1 to 6 hours before they were imaged or fixed and stained.

#### **2.2.3.13. Fluorescence microscopy.**

Before fixing cells were washed briefly with PBS to remove residual media. Cells were incubated with 4% paraformaldehyde in PBS for 10 mins at RT. Coverslips were then washed twice in PBS for 10 mins. Cells were then permeabilized in PBS containing 0.5% Triton x-100 for 1 min. Coverslips were then washed again in PBS twice for 10 mins. Coverslips were then blocked using 3% BSA in PBS for 15 mins. Coverslips were incubated with the primary antibodies (Sigma, Santa Cruz) at 1:200 dilution. 50  $\mu$ l of diluted antibody solution was added to each cover slip, overlaid with parafilm and incubated 37°C for 1 hour in a humid chamber. Coverslips were washed in PBS/0.1% Tween-20 for 2 x 10 mins. Coverslips were then incubated with secondary antibodies, which have a fluorescence tag (Cyc5/Alexa350/488/594/640, Molecular Probes) attached. Secondary antibodies were diluted in 1% BSA in PBS solution. Coverslips were incubated at 37°C for 1 hour in a humid chamber. Coverslips were washed as before in PBS/0.1% Tween-20 for 2 x 10 mins. Coverslips were left to air dry for 10 mins and then mounted onto glass slides using 50  $\mu$ l of immunofluor mountant. Cells were then visualized and analyzed on a fluorescence microscope (Zeiss Axiovert 200M). Images were obtained with a CoolSNAP CCD camera (Roper Scientific).

#### **2.2.3.14. Live imaging studies.**

##### **2.2.3.14.1. Actin dynamics of N1E115 cells.**

30 mm glass-bottomed dishes (Mattek) were coated with mouse laminin as described in 2.2.4.7.1.  $1 \times 10^5$  cells were seeded onto these dishes in 2.5 ml of DMEM-high with supplements. Cells were incubated overnight at 37°C and 5% CO<sub>2</sub>. Cells were then transiently transfected with required construct and GFP-actin as described in 2.2.3.8. or for RNAi analysis, cells were transfected as described in 2.2.3.10.

For DIC/fluorescence time-lapse analysis, cells were incubated on a heated stage at 37°C and 5% CO<sub>2</sub> chamber. The imaging was carried out with a monochromator on a Zeiss Axiovert 200 microscope enclosed in an incubator box with a CoolSNAP CCD camera. Generally, images were taken over a period of 10 mins at 10 secs intervals. Movies were compiled using the Metamorph software.

##### **2.2.3.14.2. Actin dynamics of N-WASP WT/KO cells.**

$1 \times 10^5$  cells were seeded onto 30 mm glass-bottomed dishes in 2.5 ml of DMEM-low with supplements. Cells were incubated overnight at 32°C and 5% CO<sub>2</sub>. Cells were then transiently transfected with GFP-actin or other constructs as described in 2.2.4.8. or microinjected as described in 2.2.4.10.

For DIC/fluorescence time-lapse analysis, cells were incubated on a heated stage at 37°C and 5% CO<sub>2</sub> chamber. The imaging was carried out with a monochromator on a Zeiss Axiovert 200 microscope enclosed in an incubator box with a CoolSNAP CCD camera.

Generally, images were taken over a period of 10 mins at 10 secs intervals. Movies were compiled using the Metamorph software.

#### **2.2.3.14.3. Actin dynamics of Mena WT/KO cells.**

$1 \times 10^5$  cells were seeded onto 30 mm glass-bottomed dishes (Matek) in 2.5 ml of Immorto medium. Cells were incubated overnight at 32°C and 5% CO<sub>2</sub>. Cells were then transiently transfected with GFP-actin or other constructs as described in 2.2.4.8. or microinjected as described in 2.2.4.10.

For DIC/fluorescence time-lapse analysis, cells were incubated on a heated stage at 37°C and 5% CO<sub>2</sub> chamber. The imaging was carried out with a monochromator on a Zeiss Axiovert 200 microscope enclosed in an incubator box with a CoolSNAP CCD camera. Generally, images were taken over a period of 10 mins at 10 secs intervals. Movies were compiled using the Metamorph software.

#### **2.2.4. *S. cerevisiae* (yeast) two hybrid.**

##### **2.2.4.1. Preparation of competent cells.**

A stationary phase of Y190 was established following overnight growth at 30°C with agitation in YPD, or for transformed yeast, cells were grown in minimal media for up to 48 hours. The cells were subcultured into 100 ml of fresh pre-warmed media and grown to O.D. at 600 nm of 0.2 (100 ml of culture generates 1 ml of competent cells). The culture was grown with agitation at 30°C until an O.D.<sub>600</sub> of 0.6-1.0 was reached. The cells were examined using light microscopy to check that the culture is free of

contaminants and is actively growing. The cells were transferred to 50ml falcon tubes and pelleted at 2,000 rpm for 2 mins at RT. The supernatant was discarded and the cell pellet was washed twice in 1 ml of LiAc/TE and transferred to a sterile eppendorf tube. The cells were re-pelleted at 12,000 rpm in a microcentrifuge at RT for 2 mins. The pellet was then resuspended in 1 ml of LiAc/TE.

#### **2.2.4.2. *S. cerevisiae* transformation.**

To transform competent Y190 cells the following components were added together; between 200 ng-1 $\mu$ g of plasmid DNA was used for a single transformation in a volume no greater than 10  $\mu$ l, 5  $\mu$ l of salmon sperm carrier DNA (10 mg/ml), 50  $\mu$ l of competent cells and 300  $\mu$ l of 40% PEG/LiAc/TE solution. The suspension was mixed by gentle inversion. The transformation mix was then placed at 30°C for 30 mins without agitation and then transferred to 42°C for a further 20 mins. The cells were centrifuged for 2 mins at 12,000 rpm in a microcentrifuge at RT. The supernatant was decanted and the cells were resuspended into 150  $\mu$ l of sterile water. The cell suspension was divided 3:7 and spread over two pre-warmed selective plates to allow for overcrowding of transformants. The plates were incubated at 30°C for 2-3 days.

#### **2.2.4.3. Isolation of plasmid DNA from *S. cerevisiae*.**

Plasmid DNA was isolated from yeast colonies that tested positive for both reporter genes. Single colonies were inoculated into 2 ml of YPD medium and incubated overnight at 30°C with shaking until the culture reached saturation. 1.5 ml of the culture was spun in a table top centrifuge at top speed for 5 sec at RT in an eppendorf tube to

pellet the cells. The supernatant was decanted and the remaining liquid was used to resuspend the cells. 200  $\mu$ l of yeast lysis solution was added to the cell suspension. 200  $\mu$ l of phenol/chloroform/isoamyl alcohol (25:24:1) and 0.3 g of acid-washed glass beads were added. The tube was vortexed for 2 mins and then spun at 14,000 rpm for 5 mins at RT. The supernatant was transferred to a clean eppendorf tube, to which 1/10 volume of 3M NaAc and 2.5 volumes of ethanol was added. The DNA was precipitated and washed with 70% ethanol and air dried.

#### **2.2.4.4. Recovery of target protein cDNA by electroporation.**

The *E. coli* strain of KC8 carries *trpC*, *leuB* and *hisB* mutations which can be complemented by the yeast TRP1, LEU2 and HIS3 wild-type genes. Therefore the GAL4AD plasmid of pACT-2 carrying the LEU2 gene and cDNA encoding the interacting target protein can be selected on this basis from yeast plasmid preparation described in section 2.2.4.3. Electroporation is recommended to achieve high transformation efficiency, as the plasmid DNA preparations from yeast tend to contain genomic DNA. KC8 cells were electroporated with yeast plasmid DNA. DNA samples were resuspended in ddH<sub>2</sub>O rather than TE to perform electroporation and all samples were chilled before use. KC8 cells were thawed on ice of which 40-80  $\mu$ l were used per reaction. Cells were mixed with <100 ng of DNA in a 5% volume of the cells and left on ice for 1 min. The following settings were use for the Electroporator II (capacitance 50  $\mu$ F, resistance 150  $\Omega$ , voltage 1500 V). Cells were added to pre-chilled 0.2 cm electroporation cuvettes and placed into the pulse chamber and a pulse was applied after which 480  $\mu$ l of YPD media (at RT without antibiotics) was immediately added. The

suspension was gently mixed in the cuvette before it was transferred to a 15 ml falcon tube for incubation at 37°C in a rotary incubator at 225 rpm for 1 hour. Cells were then pelleted by centrifugation at 2500 rpm for 5 mins and then washed twice in M9 minimal media. Cells were plated on M9 agar media containing leu<sup>-</sup> dropout solution. Plasmid DNA was isolated from *Leu*<sup>+</sup>-KC8 transformants using the miniprep procedure described in section 2.2.1.2.

#### **2.2.4.5. Filter assay for $\beta$ -Galactosidase activity.**

To test for transcriptional activation of the *LacZ* reporter gene a filter assay for  $\beta$ -galactosidase activity was performed. *LacZ* gene expression results in the formation of  $\beta$ -galactosidase, which drives the conversion of 5-bromo-4-chloro-3-indoly-D-galactopyranoside (X-gal) into an analogue that results in blue colonies. Yeast colonies were grown to 1-2 mm in diameter before they were assayed for  $\beta$ -galactosidase activity. Whatman filters were pre-soaked in Z buffer/X-gal solution in Petri dishes. Fresh filters were placed over the surface of the agar plates containing the yeast transformants. The filters and plates were marked for orientation by poking asymmetric holes through the filter into the agar with a needle. Filters were lifted off the agar plates with forceps and placed into a pool of liquid nitrogen for 10 secs until completely frozen. Filters were removed and placed colony-side up on 3MM paper to thaw at RT. The freeze-thaw step permeabilized the cells. The thawed filters were then sealed and incubated at 30°C and checked periodically for the appearance of blue colonies. Colonies producing  $\beta$ -galactosidase were expected to turn blue in 30 mins to 30 hours. Aligning the filters to the agar plate using the orientation marks identified the  $\beta$ -galactosidase producing

colonies. The corresponding colonies were isolated and streaked onto fresh plates or grown in liquid cultures.

#### **2.2.4.6. Generation of the mating pairs.**

IRSp53-SH3-pGBKT7 construct was generated by bacterial (KC8) recombination and confirmed by DNA sequencing.

The forward primer was;

5'GGAGGACCTGCATATGGCCATGGAGGCCGAAATGGCAGCCGGCCTGGAGC

GC-3' and the reverse primer was

5'AGTTATGCGGCCGCTGCAGGTCGACGGATCTCACACTGTGGACACCAGCGT

G-3'. The DNA encodes the C-terminal of IRSp53 (154 amino acid residues).

IRSp53-SH3-pGBKT7 was transformed into AH109. N-WASP-pACT2 was derived from the yeast-two hybrid screening of the human brain library as bait. N-WASP-pACT2 was transformed into Y187. A yeast mating was performed using IRSp53-SH3-pGBKT7 (AH109) and N-Wasp-pACT2 (Y187). The mating mixture was plated on QDO plate and a  $\beta$ -gal colony lift assay was performed on the colonies that grew. The mating between IRSp53-SH3-pGBKT7 (AH109) and pACT2 (Y187) was used as a control. Yeast mating and other assays were carried out as described in the Clontech manuals. Y2H work was done in collaboration with Bu Wenyu (SA lab).

### **2.2.5. Mass spectrometry analysis.**

Proteins associated with the SH3 domain of IRSp53 were isolated by affinity purification from lysates of adult rat brain with GST fusion protein of the SH3 domain of IRSp53 immobilized on sepharose beads. The protein complex was eluted and resolved by 10% SDS-PAGE and detected by Coomassie colloidal blue (Pierce). Protein bands detected by colloidal Coomassie blue were excised and subjected to in-gel reduction, S-alkylation and trypsin hydrolysis. Liquid chromatography tandem mass spectrometry (LC-MS/MS) analysis of the peptides was performed on a Finnigan LCQ Deca ion trap mass spectrometer (Thermo Finnigan) fitted with a Nanospray source (MDS Proteomics). Chromatographic separation was conducted using a Famos autosampler and an Ultimate gradient system (LC Packings) over Zorbax SB-C18 reverse phase resin (Agilent) packed into 75  $\mu$ M ID PicoFrit columns (New Objective). Protein identifications were made using the search engines Mascot (Matrix Sciences) and Sonar (ProteoMetrics). 44 peptides were obtained for N-wasp, with 60% coverage of the protein. Mass Spec. analysis was done in collaboration with Dr. Ong Siew Hwa and Dr. Tony Pawson (Toronto).



### **2.2.6. Statistical analysis of morphology.**

Morphological phenotypes were quantitated using the following definitions;

1. Filopodia - protrusions that contains GFP-actin, are dynamic, with a width of 1.5  $\mu\text{m}$  and an average length of between 6-15  $\mu\text{m}$ . The number of filopodia per cell was determined.

2. Neurite or neurite like-structures - processes longer than one body length. The number of neurites per cell was determined.

3. Lamellipodia/membrane ruffling - areas of cell flattening/wavy membrane thickening. Each cell was divided into eight sectors and each sector assessed for the presence of lamellipodia or membrane ruffling. Each sector contributes a maximum of 12.5% morphological activity. The eight sector values for each cell were then combined to give % lamellipodia/membrane ruffle per cell.

For each experiment approx. 12 cells were evaluated for filopodia, neurites/neurite-like structures and lamellipodia/membrane ruffles. At least 3 independent experiments were carried out for any one set of conditions giving an n value of approx. 36. Values presented in bar charts and tables represent mean +/- S.D.

### **2.2.7. Forster resonance energy transfer (FRET) analysis.**

#### **2.2.7.1. Tissue culture.**

CHO-1 cells were obtained from ATCC (Manassas, VA) and grown in 75  $\text{cm}^2$  tissue culture flask up to 90% confluency in the complete growth media, 1 x F-12 Nutrient mixture (Kaighn's modification) media containing 10% Fetal Bovine Serum (FBS) and

1% antibiotics (penicillin and streptomycin). All the tissue culture reagents were obtained from Invitrogen (Singapore). Transient transfection was performed using Fugene 6 (Roche). For transfection, cells were seeded in a 6-well tissue culture plate containing the pre-washed and sterilized cover slips at  $1.0 \times 10^5$  cells/well one day before transfection. CHO cells were co-transfected with mRFP-IRSp53 and GFP-actin or GFP-N-WASP plasmids by following the standard Fugene 6 protocol supplied by the manufacturer. Similar transfections were carried out for the control experiments as well. After 36 hours of transfection, cells were washed thrice with 1 x PBS and fixed with paraformaldehyde and mounted on a microscope slide using Hydromount, an aqueous non-fluorescing mounting media (from National Diagnostics, USA) For tissue culture of N1E115 and N-WASP WT/KO cells, please refer to Section 2.2.3.

#### **2.2.7.2. Conditions for FRET.**

FRET occurs when; (i) a pair of spectrally distinct fluorescent molecules are sufficiently close (between 1 and 10 nm), (ii) their dipole moments are aligned to allow a radiationless transfer of energy and (iii) the emission profile of the donor must be such as to allow excitation of the acceptor. If these three conditions are met then FRET may occur. The FRET efficiency is dependent upon the distance between the acceptor and donor. The Förster distance, defined as the distance between the donor and acceptor, where the average efficiency of energy transfer is 50%, is used to estimate the intramolecular distances between the two molecules. Commonly, FRET is employed to visualize protein-protein interactions by targeting the desired cellular constituents with fluorescent dyes, fluorescent antibodies and/or fluorescent proteins (Figure 2.1).

7 There are two common methods used to determine whether FRET is occurring between two molecules.

- (i) Sensitized emission and
- (ii) Acceptor photobleaching.

In this thesis I have used acceptor photobleaching using GFP as the donor and mRFP as the acceptor as illustrated in figure 2.1.

### **2.2.7.3. Acceptor photo-bleaching (AP)-FRET measurement.**

FRET was measured by acceptor photobleaching method by making necessary settings on a Zeiss LSM 510 confocal microscope with the C-Apochromat 63 x 1.2 W objective. The fusion proteins of GFP and mRFP were excited using 488 and 561 nm laser lines, respectively, by selecting 405/488/561 dichroic mirror and 490,565 secondary dichroic mirrors for GFP and mRFP emission, respectively. The emission was monitored by selecting GFP (BP 505-550) and Red (LP 575) emission filters to record the fluorescence intensity. The ROI was selected and mRFP bleached using 70% of 561 nm laser power by selecting 50 iterations. Bleaching was performed following pre- and post- scan images. The increase in GFP fluorescence intensity followed by mRFP bleaching was measured as FRET. FRET efficiency was calculated using the change in background subtracted fluorescence intensity as  $100 \times [(post-bleach\ intensity)-(pre-bleach\ intensity) / (post-bleach\ intensity)]$ . In order to verify the increase in GFP intensity due to any possible artifact we obtained the Pearson product moment correlation coefficient  $r$ , a dimensionless index that ranges from -1.0 to 1.0 inclusive and reflects the extend of a linear relationship between the two fluorescence intensity data of GFP and mRFP while

bleaching. In our case we expect -1.0 as the perfect fitting of the linear relation. The range between -0.7 to -1.0 was selected as positive FRET based on values obtained from negative controls (cyto-mRFP/cyto-GFP pair) which range between -0.1 to 0.3.

$$r = \frac{\sum(x-\bar{x})(y-\bar{y})}{\sqrt{\sum(x-\bar{x})^2 \sum(y-\bar{y})^2}}$$

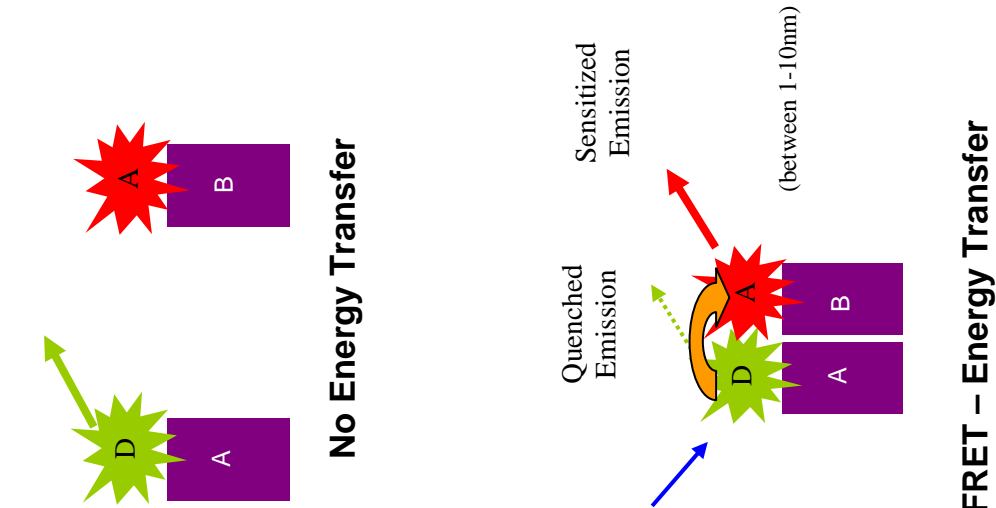
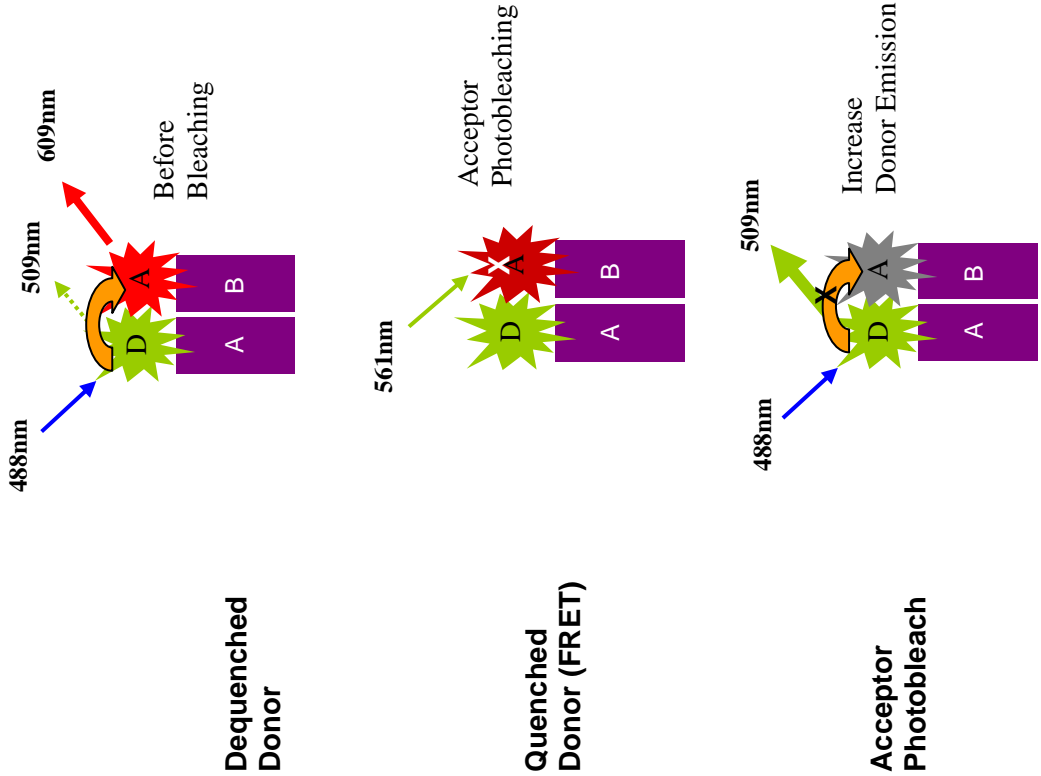
Where x and y are the sample means average (array1, GFP intensity) and average (array2, mRFP intensity).

FRET analysis work was done in collaboration with Dr. Thankiah Sudhaharan (SA Lab).

**Figure 2.1 FRET analysis by acceptor photobleaching (AP-FRET).**

A schematic illustrating the theory of FRET is shown in the left panel. If two protein molecules are within 1-10 nm of each other, i.e. directly binding each other, and the dipole moments of the two fluorescent molecules are in the correct orientation, FRET may occur. In the right panel acceptor photobleaching is shown as a means to determine whether FRET is occurring. In this method the acceptor is destroyed by bleaching eliminating a potential energy transfer from the donor. Increase in donor emission on acceptor photobleaching is an indicator that FRET is occurring (AP-FRET).

Figure 2.1



# **RESULTS**

## **RESULTS**

### **Chapter 3. The IRSp53 phenotype.**

#### **3.1. Introduction.**

The adaptor protein IRSp53 was identified in a yeast-two hybrid screen using the WAVE1 polyproline sequence as bait (Miki, 2000). It was also identified in Cdc42 and Rac1 yeast two-hybrid screens (Govind et. al., 2000; Krugmann et. al., 2001, respectively) and shown to be an effector of Cdc42. It contains a potential Rac1-binding (RCB) domain (residues 1-228), a Cdc42-binding (CRIB) and a Src homology 3 (SH3) domain as well as other protein interaction sites. The mechanism by which IRSp53 induces morphological change and in particular filopodia formation is the subject of this thesis.

In this chapter, to further understand the functions of IRSp53, I used sequential time-lapse DIC/fluorescence microscopy of N1E115 neuroblastoma cells (a model for neuronal cells) transfected with GFP-actin and tdRed-IRSp53.

#### **3. 2. Study of cytoskeletal dynamics using GFP-actin in N1E115 cells.**

To study the cytoskeleton dynamics of filopodia/lamellipodia in mammalian cells, GFP-actin cDNA constructs were transfected in N1E115 cells under live conditions. Actin cytoskeleton changes were observed with time-lapse microscopy, carried out on a heated stage (37°C) on an inverted microscope (Axiovert 200M, Zeiss) equipped for fluorescence and DIC microscopy. Data were acquired with a back-illuminated CCD camera (Roper Scientific), and Metamorph software.



The cells appeared to be morphologically active. The actin network was found to be dynamic with cells having a leading edge, filopodia and lamellipodia but no neurites (Figure 3.1). Transfected cells were observed to cycle between a state of membrane ruffling and filopodia protrusion throughout the whole timeframe, with no defined polarity in most cases observed. Thus I was able to use GFP-actin to follow actin dynamics in live cell imaging studies.

### **3. 3. Phenotype of IRSp53 overexpression in N1E115 cells.**

IRSp53 is a Cdc42 effector and an efficient inducer of filopodia formation in N1E115 cells and Swiss 3T3 cells (Govind et. al., 2001; Krugmann et. al., 2001). IRSp53 may induce membrane ruffling and lamellipodia formation through interaction with WAVE1 and 2 (Miki et. al., 2000). Recent work has suggested that the N-terminal of IRSp53 is sufficient to induce filopodia formation (Yamagishi et. al., 2004; Millard, et. al., 2005). Filopodia are actin-based protrusions that emerge from the periphery of cells and neuronal growth cones. They have distinct morphology; uniform cylinder shape, are of a certain length and sometimes protrude at an angle, waving as they extend. In contrast to retraction fibres and aberrant actin protrusions, filopodia are transient in nature. It is therefore essential to do time-lapse experiments to determine the nature of structures being observed and whether they have all the characteristics of filopodia.

In the experiments described in this thesis a filopodia is defined as an actin containing structure, with a life-time of 120-170s, a width of approximately 1-2  $\mu\text{m}$  and length of

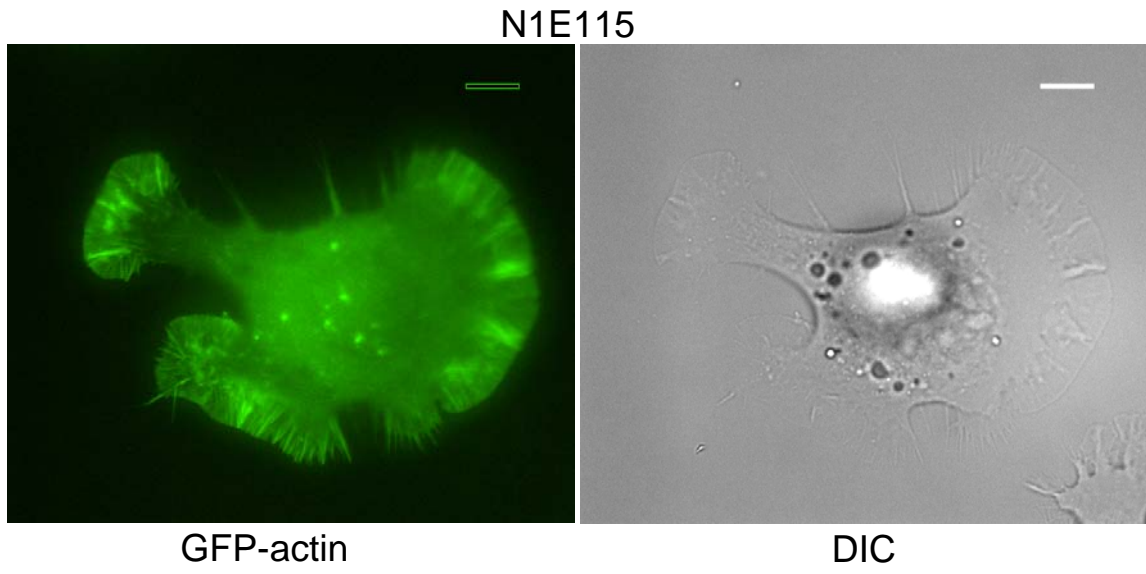
**Figure 3.1 Time-lapse imaging of N1E115 cells transfected with GFP-actin.**

N1E115 cells were transfected with GFP-actin and imaged 18-24 hours later. Live cell imaging was carried by sequential image acquisition using fluorescence and DIC channels (for details, see Materials and Methods section). Images were taken every 10 secs for 10 mins.

(Bar = 10  $\mu\text{m}$ )

(Movie 3.1. GFP-actin transfected N1E115 cells).

**Figure 3.1**



between 6-15  $\mu\text{m}$ . This is based on characterization and statistical analysis of various induced filopodia in mammalian cells (see appendix III for details).

To analyze the phenotypic effect of IRSp53, I carried out time-lapse experiments following the fluorescence using GFP-actin. Cells were observed to undergo successive rounds of actin polymerization, with formation of lamellipodia and filopodia (Figure 3.2).

To analyze the phenotypic effect in more detail I carried out time-lapse experiments following DIC and fluorescence simultaneously, using GFP-actin and tdRed-IRSp53 transfected N1E115 cells. The morphology of cells expressing HA-IRSp53 was similar to those expressing GFP-actin/tdRed-IRSp53 suggesting that the relatively larger 'GFP- or tdRed- fusions' did not alter the IRSp53 phenotype significantly (Figure 3.3). Overexpression of IRSp53 induced a number of phenotypes within the cell population. The general features of overexpressing cells include formation of neurites (with branching), filopodia, lamellipodia with well defined ribs and membrane ruffling. Figure 3.3 shows examples of two cells with these features. Filopodia and lamellipodia formation could be seen along the length of the neurite (Figure 3.3B). In some cells the predominant phenotype was the formation of large lamellipodia with well defined ribs (Figure 3.3A). IRSp53 colocalized with actin in filopodia (Figure 3.3C), the ribs (Figure 3.3D) and lamellipodia (Figure 3.3E). IRSp53 was most strongly enriched with F-actin in filopodia and the rib-like structures. In cells that expressed high levels of IRSp53 the filopodia become stabilized and form star-like clusters. These structures did not appear to turnover.

**Figure 3.2 Time-lapse imaging of N1E115 cells transfected with GFP-actin and HA-IRSp53.**

N1E115 cells were transfected with GFP-actin and HA-IRSp53 by standard transfection procedure and left between 18-24 hours for cDNA expression. Live cell DIC/fluorescence imaging was then carried out (as described in Materials and Methods). (Movie 3.2. N1E115 cells transfected with HA-IRSp53 and GFP-actin)

- (A) GFP-actin image of a N1E115 cell transfected with IRSp53.
  - (B) Time sequence of three regions (panels 1-3) of the cell in (A).
- (Bar = 10  $\mu\text{m}$ )

**Figure 3.2**

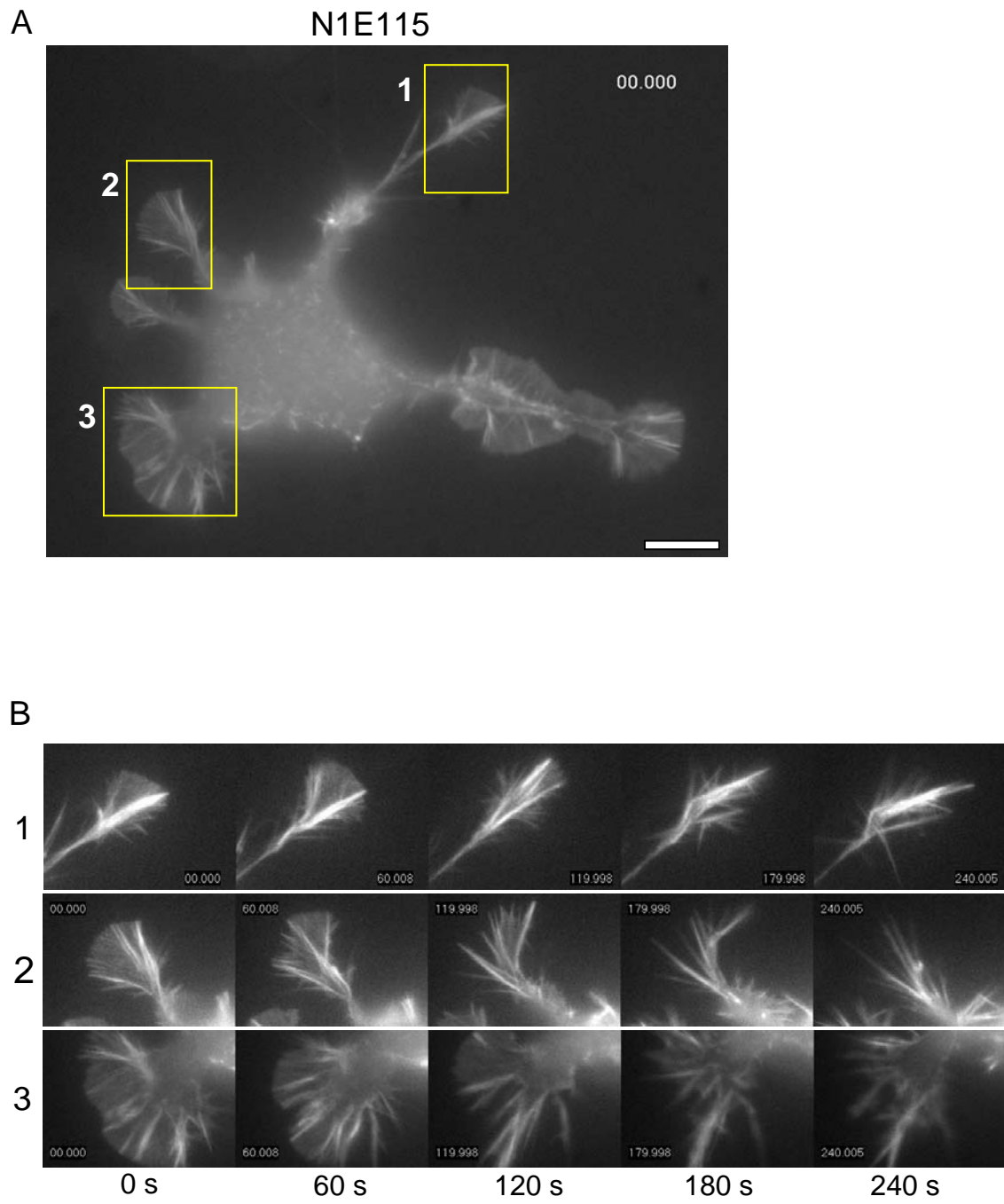


**Figure 3.3 Time-lapse imaging of GFP-actin and tdRed-IRSp53 in N1E115 cells.**

N1E115 cells were transfected with GFP-actin and tdRed-IRSp53 and left for between over 18-24 hours for cDNA expression. Following cDNA expression time-lapse imaging was carried out to visualize GFP, tdRed and DIC (as described in Materials and Methods). (Bar = 10  $\mu$ m)

(Movie 3.3.1. N1E115 transfected with GFP-actin and tdRed-IRSp53 – A)

(Movie 3.3.2. N1E115 transfected with GFP-actin and tdRed-IRSp53 – B)

(A) N1E115 cell with IRSp53 induced lamellipodia and ribs

(B) N1E115 cell with IRSp53 induced neurites

(C) Time sequence showing filopodia

(D) Time sequence showing membrane ruffle and ribs

(E) Time sequence showing lamellipodia

For C-E; lane 1-DIC, lane 2-GFP-actin, lane 3-tdRedIRSp53 and lane 4-Merge images.

Figure 3.3

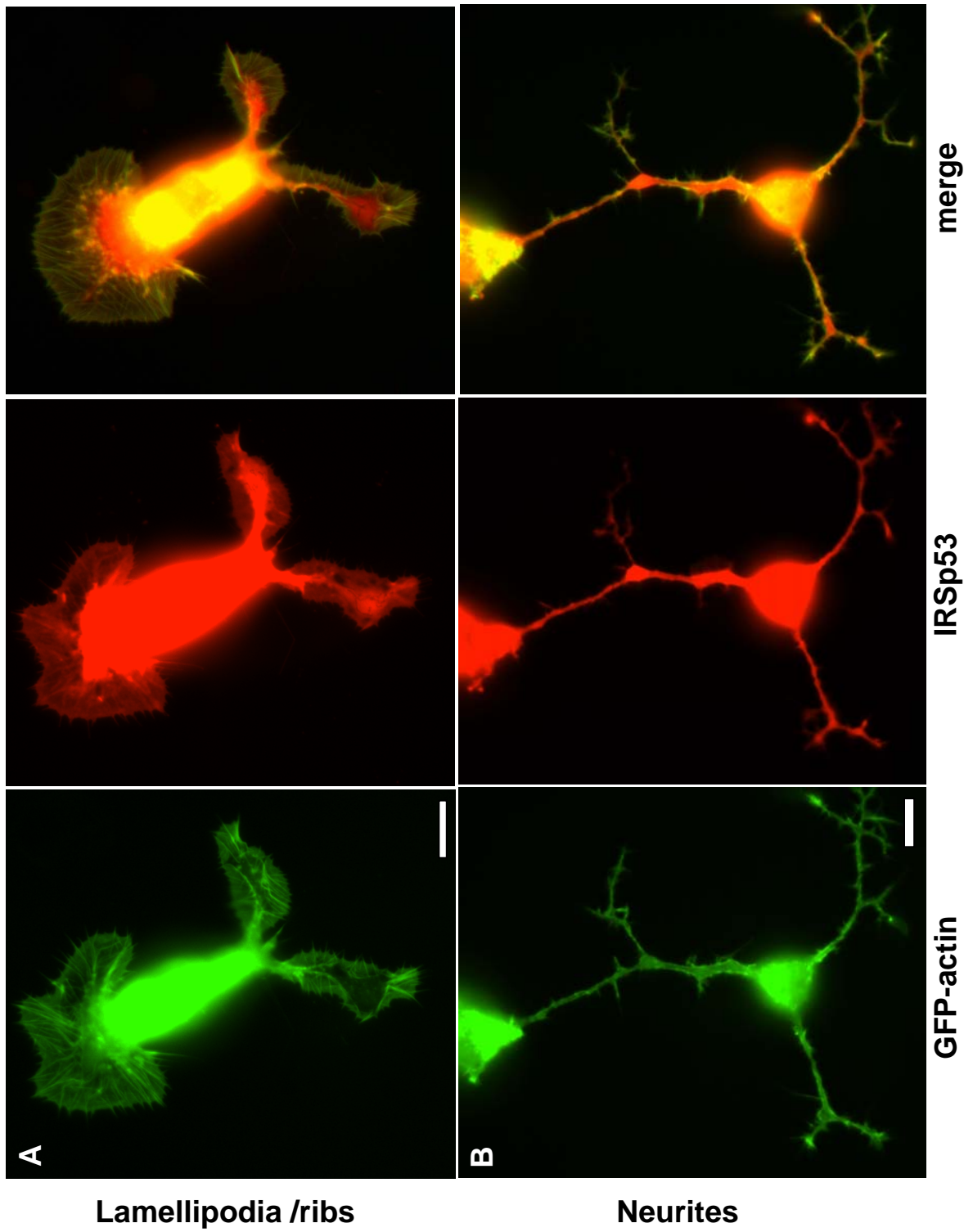
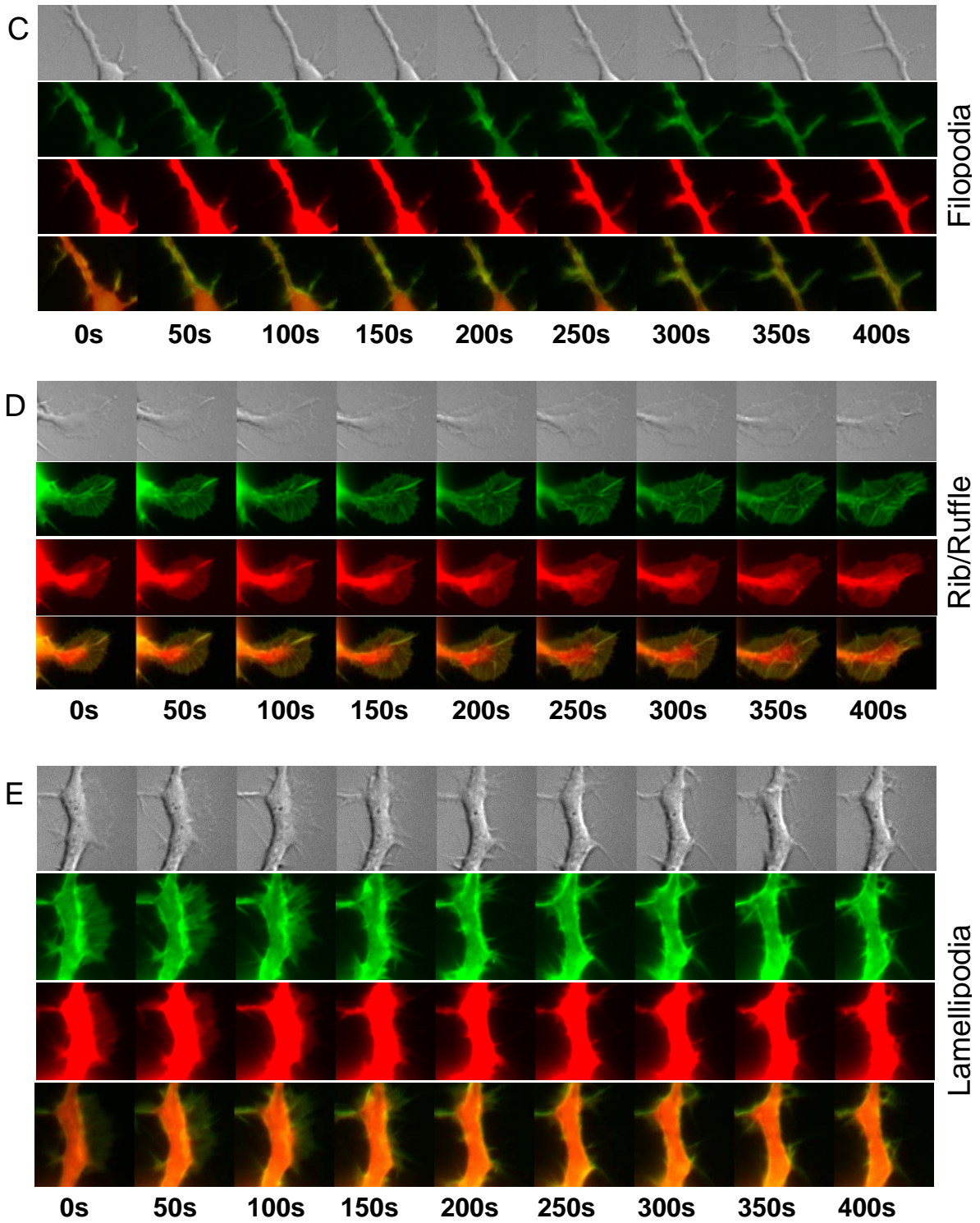




Figure 3.3



### **3. 4. Role of the IRSp53 SH3 domain in filopodia and lamellipodia formation.**

IRSp53 induces complex branched neurites that lack polarity. Induction of complexity (filopodia/lamellipodia) is significantly reduced in an IRSp53 mutant missing the C-terminal domain comprising the SH3 domain (Govind et. al., 2001). The C-terminal of IRSp53 contains at least three protein binding domains, the SH3 domain, a potential WW domain binding motif, and a PDZ domain binding motif that could be responsible for the neurite complexity. The IRSp53 SH3 domain is known to interact with a number of proteins, including, WAVE1/2, Mena, Espin, and Eps8 (Miki et. al., 2000, Krugmann, et al., 2001; Sekerkova et. al., 2003). To determine if the SH3 domain was responsible for the neurite complexity, I compared the phenotypes of wild-type protein with that of two mutants defective in binding to ligands (W/R and FP/AA) of the SH3 domain (expressed as GFP fusions). N1E115 neuroblastoma cells were transfected with the GFP-tagged fusion constructs of W/R and FP/AA (Phe<sup>427</sup>Pro<sup>428</sup>/Ala<sup>427/428</sup>). The two SH3 domain mutants did not affect neurite formation significantly (Figure 3.4). However, filopodia formation was reduced in the W/R mutant and absent in the FP/AA mutant (Figure 3.4D). Lamellipodia formation was reduced by 80% in both mutants but was still detectable (Figure 3.4E). Neurite branching was reduced in the SH3 domain mutants by approximately 50%. Thus the SH3 domain plays a major role in filopodia and lamellipodia formation induced by IRSp53.

**Figure 3.4 Effect of mutations of the SH3 domain (W/R and FP/AA) on IRSp53 phenotype in N1E115 cells.**

N1E115 cells were transfected with GFP-IRSp53, GFP-IRSp53-W/R and GFP-IRSp53-FP/AA and left for 18-24 hours for cDNA expression. Whole cell images are shown in (A). In (B) areas of lamellipodia formation and in (C) structure of neurites are shown.

Bar chart in (D) and (E) shows statistical data after scoring for filopodia per cell and lamellipodia/membrane ruffle per cell (see Materials and Methods for details). Data presented as mean  $\pm$  S.D. (n=6) (Experiments=3). (Bar = 10  $\mu$ m).

Figure 3.4

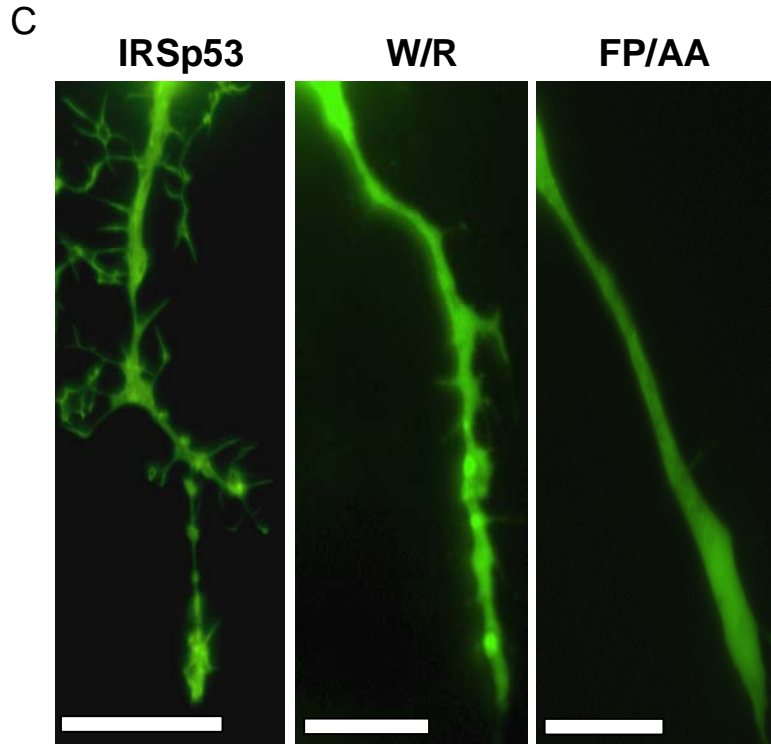
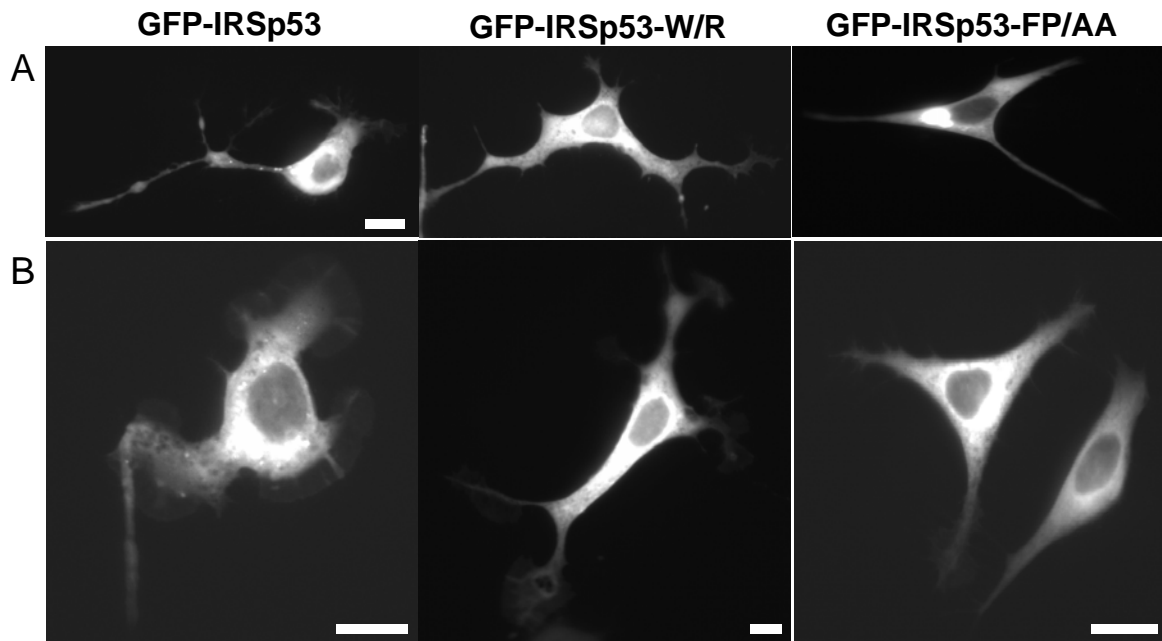
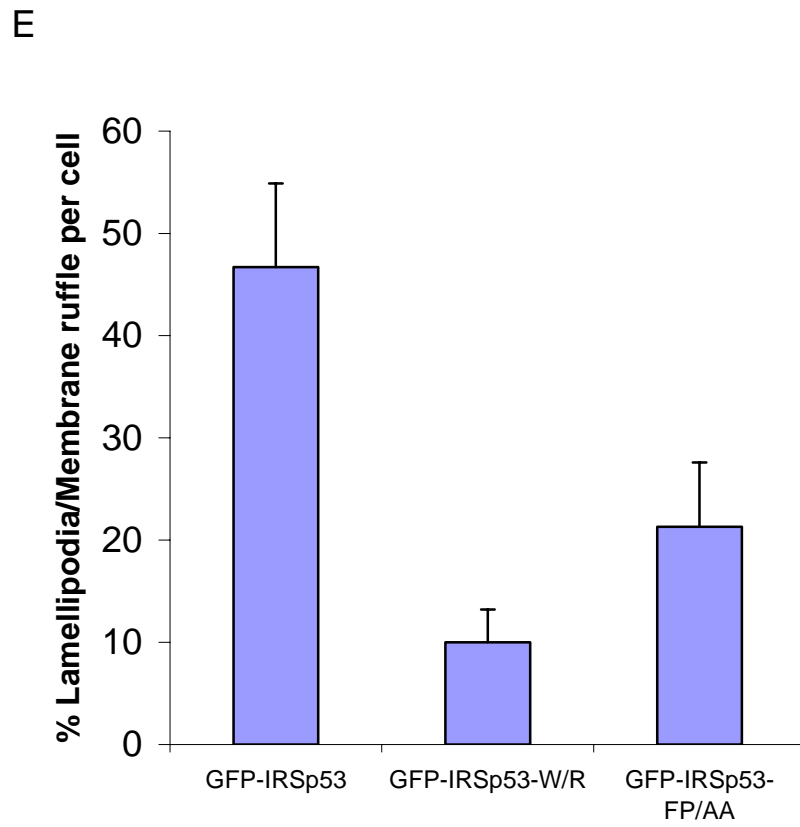
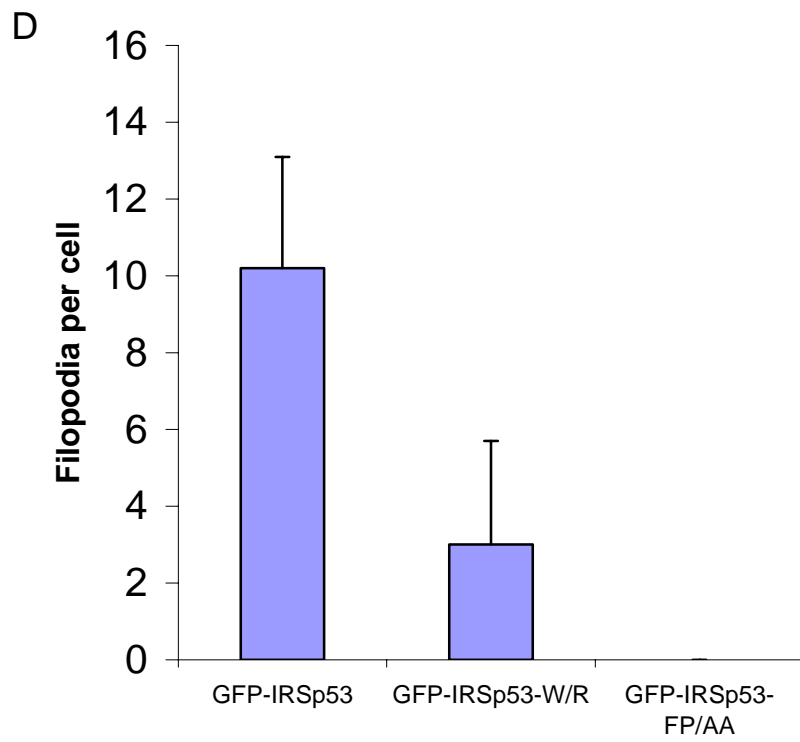


Figure 3.4



## **Chapter 4. IRSp53 SH3 domain binding partners.**

### **4.1. Introduction.**

IRSp53 SH3 domain is known to interact with a number of proteins, including, WAVE1/2, Mena, Espin, and Eps8 (Miki et. al., 2000, Krugmann et. al., 2001, Sekerkova et. al., 2003). Mena was initially thought to be the strongest candidate to play a role in filopodia formation downstream of Cdc42-IRSp53 (Krugmann et. al., 2001). However, experiments with MDV7 Mena/VASP KO cells suggest that Mena is not essential for IRSp53 induced filopodia formation although quantitative data from these experiments were not presented (Nakagawa et. al., 2003). To identify new partners of IRSp53, a Mass Spectrometry analysis was carried out to isolate proteins interacting with IRSp53 SH3 domain.

### **4.2. IRSp53 SH3 domain associates with both N-WASP and WAVE1/2 protein complexes.**

A GST-IRSp53 SH3 domain affinity column was set up and brain proteins that bound were analyzed. Interestingly, WAVE1 and the WAVE2 complex proteins, Abi1/2b, p125Nap-1 and p140sra-1 were present on the GST-SH3 column (Figure 4.1). In addition to the WAVE1 complex I found N-WASP and CR-16 binding to the affinity column (Figure 4.1). Actin, tubulin, dynamin and mDia1 were also present on the column. In similar experiments using T-cell lysates instead of brain I detected Mena and WAVE2 as found previously (Krugmann, et. al., 2001; Miki et. al., 2000; Ong, S-W. and Ahmed, S., unpublished data).

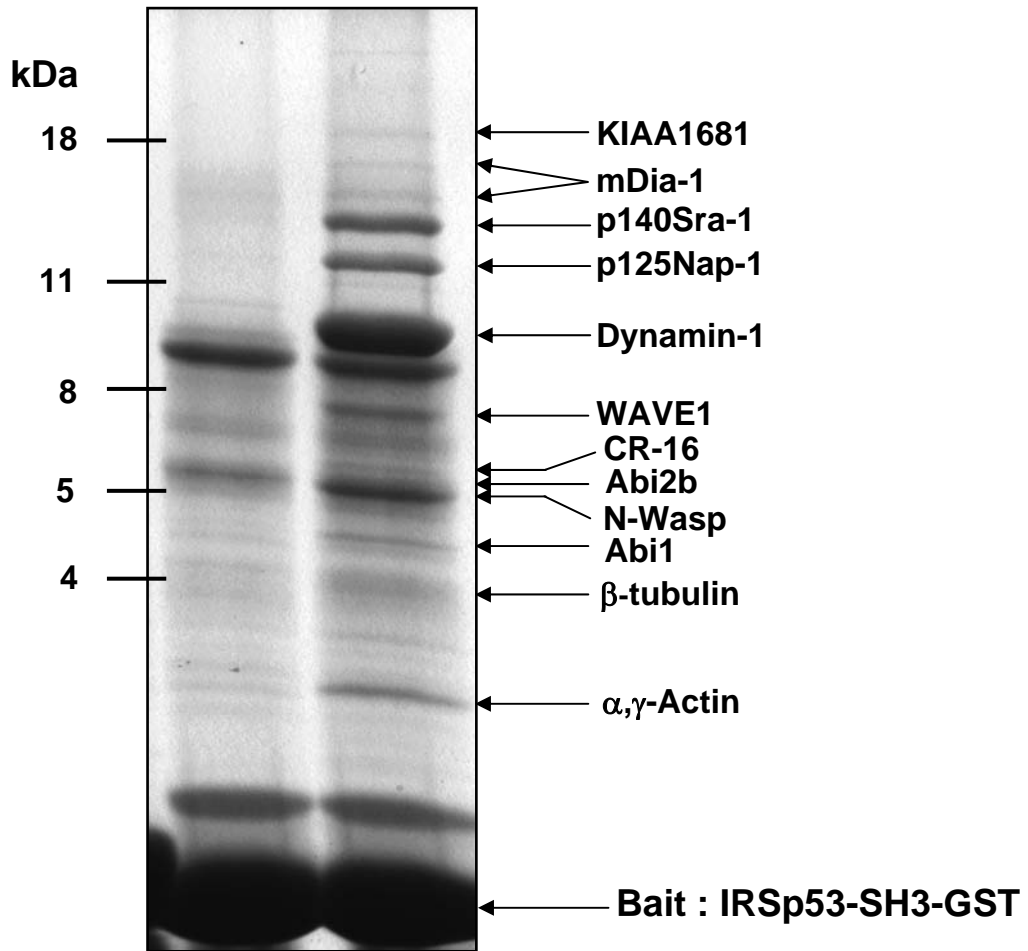
**Figure 4.1 Mass Spectrometry analysis of brain proteins binding to the IRSp53 SH3 domain affinity column.**

Brain lysates were loaded onto GST-SH3 domain affinity columns and after washing, run on SDS-PAGE gels. Protein bands of distinct molecular mass were then excised and the peptide sequence determined as described in the Materials and Methods section.

Lane 1- GST affinity column

Lane 2- GST-IRSp53 SH3 domain affinity column

Figure 4.1





KIAA1681, known as the Ras association (RalGDS/AF-6) and pleckstrin homology domain was also among the proteins been pulled down.

#### **4. 3. IRSp53 interacts with N-WASP directly.**

The presence of N-WASP and CR-16 on SH3 domain affinity columns suggested that IRSp53 might induce filopodia formation by direct interaction with N-WASP. To investigate this, I used *in vitro*-transcription/translation to produce <sup>35</sup>S-labelled N-WASP protein for use in binding with IRSp53 SH3 expressed as GST and bound on glutathione sepharose beads. Cdc42-GST binding was used as positive control (Figure 4.2.B, lane 1) and GFP as a negative control (Figure 4.2.B, lane 4). The SH3 domain of IRSp53 indeed interacted specifically with N-WASP (Figure 4.2.B, lane 2). A weak interaction between amino acid residues 1-1295 of IRSp53 and N-WASP was also detected (Figure 4.2.B, lane 3).

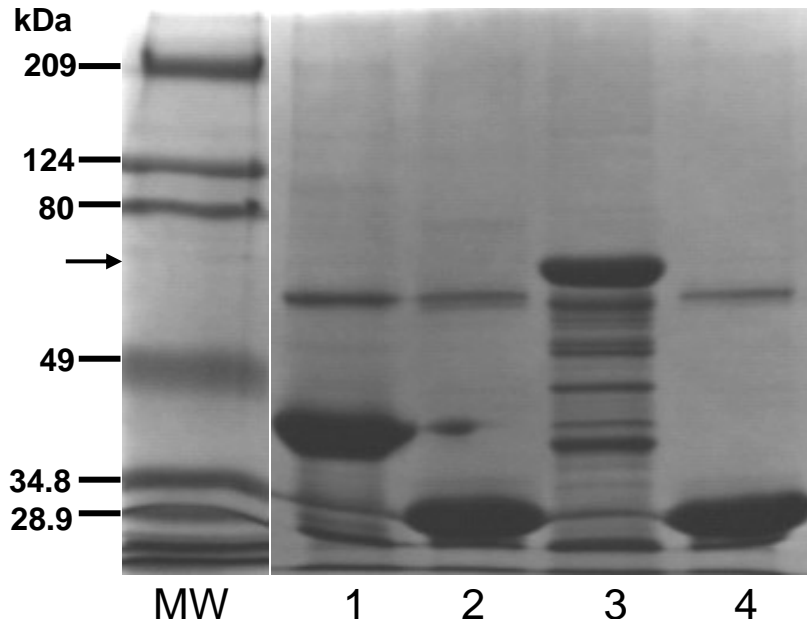
The IRSp53 SH3 domain interaction with N-WASP was also analysed using the yeast two-hybrid system. The SH3 domain was cloned into the bait vector (Clontech, system 3) and mated with a strain carrying the N-WASP cDNA cloned into the prey vector or with a strain carrying an empty prey vector as a control. IRSp53 and N-WASP were found to interact as diploids grew on quadruple dropout plates and possessed significant  $\beta$ -galactosidase activity (Figure 4.3).

**Figure 4.2 IRSp53 SH3 domain interaction with <sup>35</sup>S-labelled N-WASP *in vitro*.**

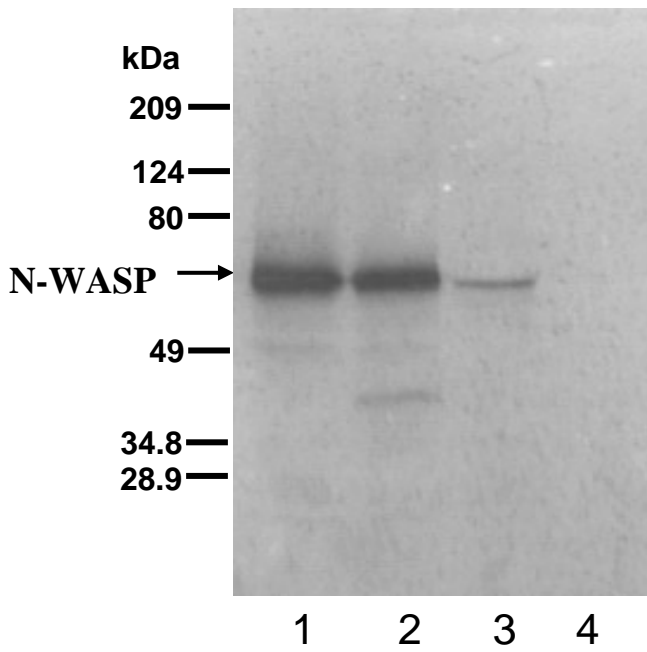
<sup>35</sup>S-labelled N-WASP and GFP were generated using an *in vitro* transcription/translation kit. (A) SDS-PAGE analysis of GST proteins used for pull down and (B) X-ray autoradiograph film of <sup>35</sup>S-N-WASP pull down experiment. (A and B) The GST fusion protein of Cdc42 (lane 1), IRSp53 SH3 (lanes 2 and 4), and IRSp53 lacking the SH3 domain (lane 3) were used to pull down <sup>35</sup>S-labelled-protein from the *in vitro* mix.

Figure 4.2

A



B



1. GST-Cdc42 and  $^{35}\text{S}$ -Met-N-WASP
2. GST-IRSp53 SH3 and  $^{35}\text{S}$ -N-WASP
3. GST-IRSp53-1-1295 and  $^{35}\text{S}$ -N-WASP
4. GST-IRSp53 SH3 and  $^{35}\text{S}$ -GFP

**Figure 4.3 IRSp53 SH3 domain interaction with N-WASP using Yeast Two Hybrid.**

Yeast  $a/\alpha$  strains containing (A) IRSp53 SH3 domain with N-WASP or (B) IRSp53 SH3 and pACT2 (empty vector) were mated and then plated on either quadruple drop out (QDO) plates or his-/trp- plates for  $\beta$ -gal assays. The QDO is the selection plate for protein-protein interaction and the  $\beta$ -gal plate shows protein-protein interaction by enzyme activity (for details of the yeast two hybrid assay see Materials and Methods section).

**Figure 4.3**



QDO

β-gal

**IRSp53 SH3 + N-WASP**



QDO

β-gal

**IRSp53 SH3 + pACT2**

#### **4.4. FRET analysis of the IRSp53-N-WASP interaction.**

To confirm the interaction between IRSp53 and N-WASP, mRFP-tagged full length IRSp53 and GFP-tagged full length N-WASP were overexpressed in N1E115 and CHO-1 cells. FRET analysis (by Acceptor Photo-Bleaching) was carried out. (For the theory on FRET, please refer to Materials and Methods section).

FRET efficiencies (FEs) were calculated as described in the Materials and Methods section. FRET only occurs when the 2 molecules are in close proximity (distance of between 1 and 10 nm). A tandem mRFP-GFP construct was used as a positive control. The mRFP-IRSp53/GFP pair, GFP-N-WASP/mRFP pair and cyto-GFP/cyto-mRFP pair were used as negative controls. All the negative controls gave FEs in the range of 0.96-1.91 (Table 4.1).

In N1E115 cells FRET between N-WASP and IRSp53 was found to occur (FEs) in the filopodia (6.95%), neurites (18.4%) and the cell body (12.6%). In CHO-1 cells N-WASP/IRSp53 FRET was observed in the filopodial tip (Figure 4.4). FRET analysis was also carried out with mRFP-tagged full length N-WASP and GFP-tagged IRSp53 SH3 mutants FP/AA and W/R. The FP/AA mutant cannot bind downstream effectors. FEs values for mutants were 2.95% and 4.34%, respectively, (Table 4.1). To investigate the FRET data in more detail, I used the Pearson product moment correlation coefficient  $r$  (CC), a dimensionless index that ranges from -1.0 to 1.0 inclusive and reflects the extent of a linear relationship between the two fluorescence intensity data of GFP and mRFP while bleaching. In this case, I expect -1.0 as the perfect fitting of the linear relation.

Based on negative controls (see Materials and Methods), I used CC values between  $-0.7$  to  $-1.0$  as FRET positive. CC values were express with a  $\pm$ -SD (Table 4.1).

From the FRET analysis I conclude that N-WASP can interact with IRSp53 *in vivo* at spatially important sites.

**Figure 4.4 AP-FRET assay of mRFP-IRSp53 and GFP-N-WASP.**

N1E115 or CHO-1 cells were transfected with mRFP-tagged IRSp53 and GFP-tagged N-WASP cDNA for around 36 hours to allow complete folding of the fluorescent proteins. A region of interest (ROI) was then selected and both GFP and RFP channels monitored over the time course of the experiment. Once baseline signals for both GFP and mRFP channels was obtained the mRFP was beached using a 561nm laser. Traces show changes in intensity of the GFP and mRFP channels during the experiment. The box in each image indicates the ROI. Full details of the AP-FRET methodology can be found in the Materials and Methods section 2.2.7.3.



Figure 4.4

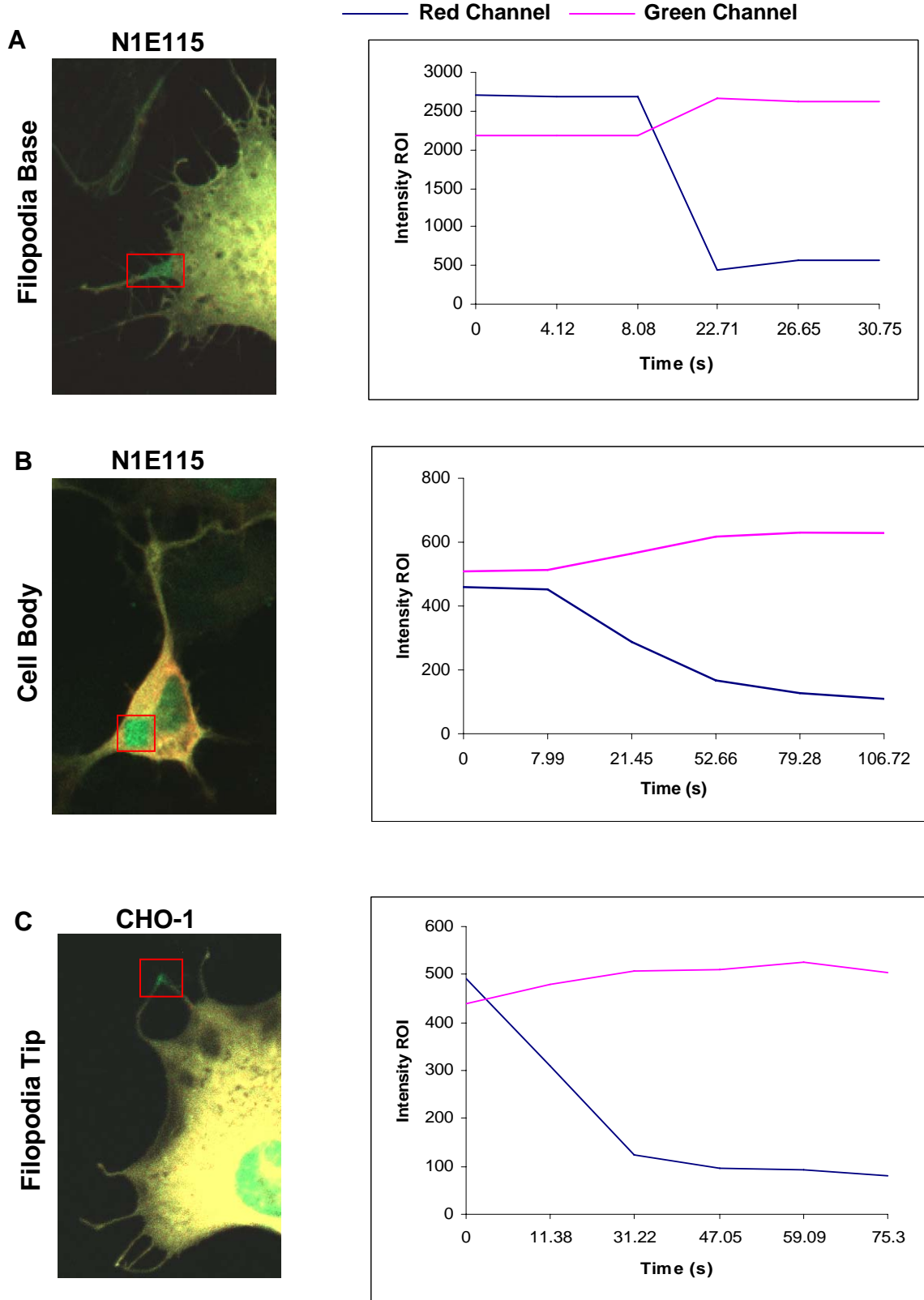


**Table 4.1 AP-FRET assay of mRFP-IRSp53 and GFP-N-WASP.**

AP-FRET analysis was carried out as described in Figure 4.4. FEs and CC were calculated as described in Materials and Methods 2.2.7.3.

**Table 4.1. IRSp53-N-WASP AP-FRET Efficiency with Cross correlation values**

	FRET E%	± SD	CC *	± SD
<b>Controls in N1E115 or CHO-1</b>				
mRFP-IRSp53 and GFP	1.4	1.18	0.29	0.4
GFP-N-WASP and mRFP	0.96	0.59	0.49	0.37
Cytoplasmic-GFP and Cytoplasmic mRFP	1.91	1.49	0.17	0.63
Cytoplasmic-mRFP-GFP (Tandem)	22.34	5.34	-0.99	0.001
<b>mRF-IRSp53 and GFP-N-WASP in N1E15 or CHO-1</b>				
Flippodia like	6.95	2.01	-0.73	0.21
Neurite like	18.4	2.87	-0.97	0.032
Cell body	12.6	3.17	-0.93	0.063
<b>IRSp53 SH3-Mutants in N1E115</b>				
GFP-IRS FP/AA and mRFP-N-WASP	2.95	2.24	-0.63	0.41
GFP-IRS W/R and mRFP-N-WASP	4.34	2.99	-0.58	0.62

\*Cross correlation values between -0.7 to -1 is considered as FRET

## **Chapter 5. IRSp53 phenotype in N-WASP knock out cells.**

### **5.1. Introduction.**

Members of the WASP/WAVE family proteins promote actin polymerization by stimulating the actin-nucleating activity of the Arp2/3 complex (Takenawa and Miki, 2001). Hematopoietic WASP and ubiquitously expressed N-WASP interact directly with the Rho-GTPase Cdc42 through their CRIB domain (Aspenstrom et. al., 1996, Rohatangi et. al., 1999). Cdc42 induces the formation of cell surface projections such as filopodia (Kozma et. al., 1995, Nobes and Hall, 1995) which is enhanced upon the presence of N-WASP (Miki et. al., 1998). This suggests that filopodia formation can result from Cdc42-based activation of N-WASP, which leads to Arp2/3 recruitment and leading to actin filament assembly (Carrier et. al., 1999). In order to examine the functional consequence of the IRSp53-N-WASP interaction, I employed the use of N-WASP control precursors (WT) and N-WASP knock-out (KO) fibroblast cell lines respectively (for details of N-WASP WT and KO fibroblasts see Lommel et. al., 2003 and Materials and Methods).

### **5.2. IRSp53 requires N-WASP for filopodia formation.**

In the first set of experiments I compared the effect of IRSp53 cDNA microinjection on the morphology of the N-WASP WT and KO cells. cDNA for GFP-actin was included in the microinjection to identify expressing cells and to facilitate imaging of the actin dynamics (Figure 5.1). When cells were injected with GFP-actin cDNA alone, and scored for filopodia and membrane ruffling, there was no difference between N-WASP WT and

**Figure 5.1 IRSp53 phenotypes in N-WASP WT and KO cells.**

(A) N-WASP WT (b,d,e) and N-WASP KO fibroblast (a,c) were microinjected with (a,b) GFP-actin, or (c,d) GFP-actin with IRSp53 cDNA. Cells were left for 1-6 hours for cDNA expression. Images show a time sequence from time-lapse experiments of; GFP-actin/IRS-53 microinjection in N-WASP WT cells (f), and N-WASP KO cells (g).  
(Bar = 10  $\mu$ m)

(B) and (C) Statistical analysis of experiments illustrated in A. Filopodia per cell and % lamellipodia/membrane ruffle per cell were scored (refer to section 2.2.6 in Materials and Methods).

(Movie 5.1.1. N-WASP WT microinjected with IRSp53).

(Movie 5.1.2. N-WASP KO microinjected with IRSp53).

Figure 5.1

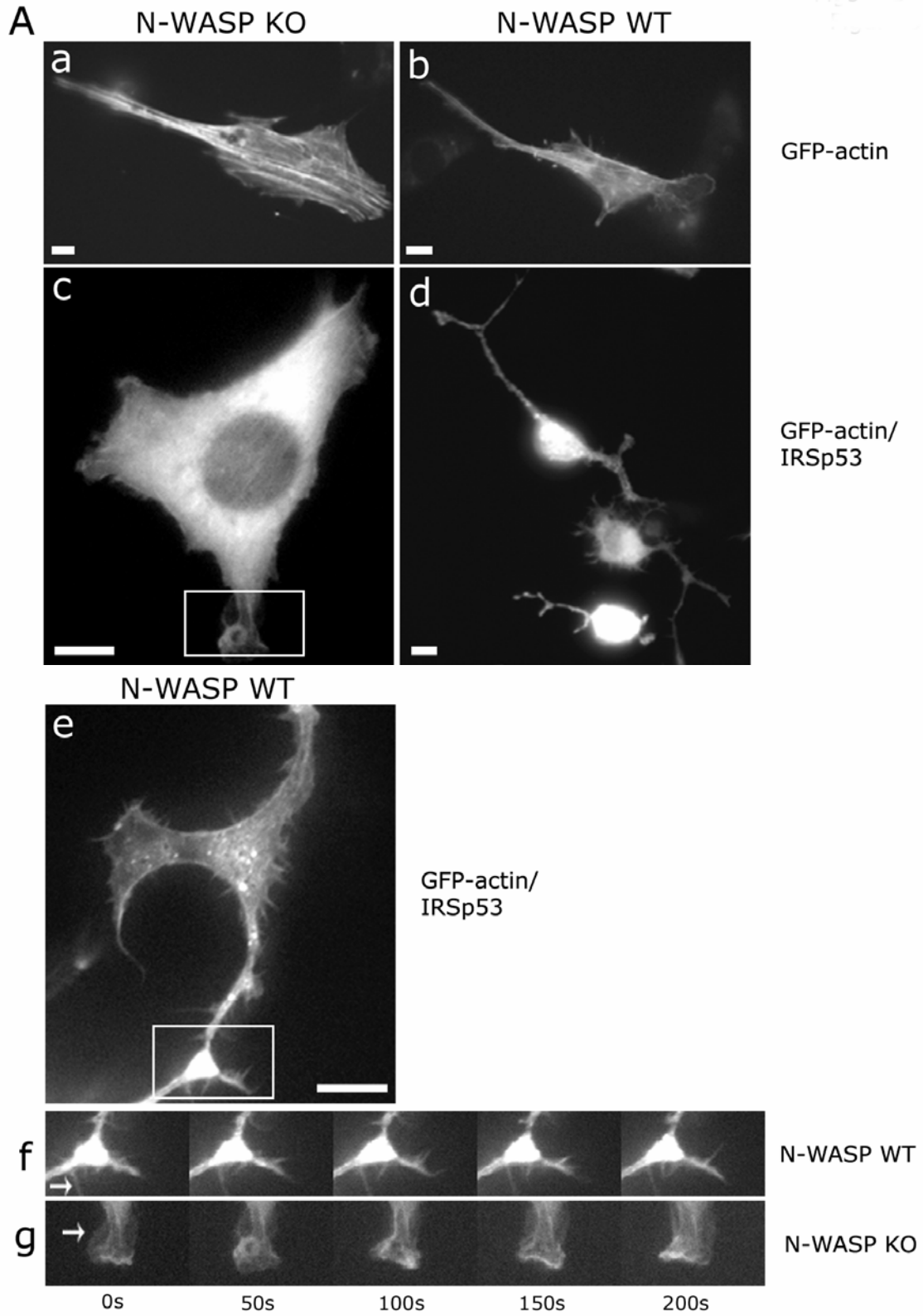
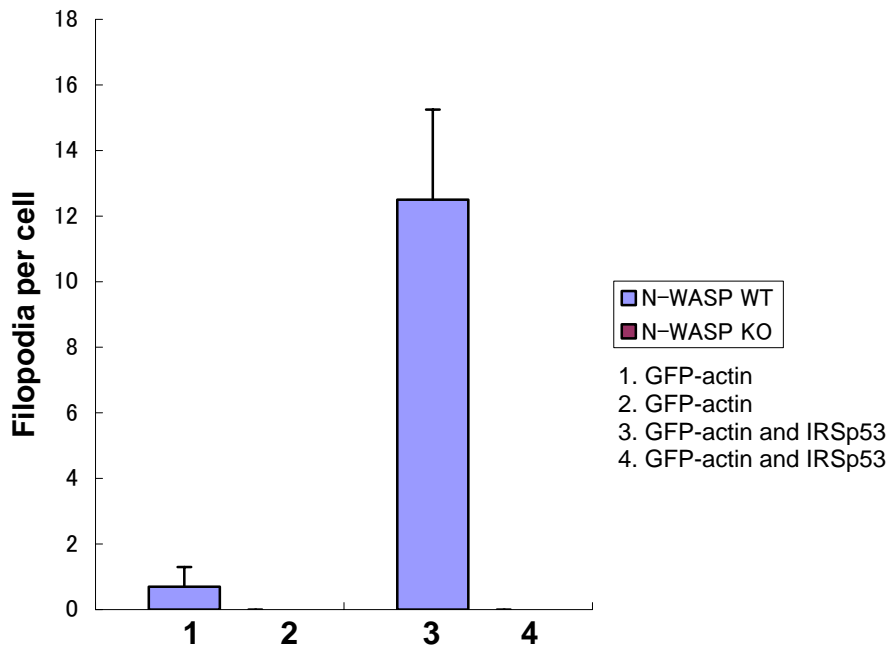
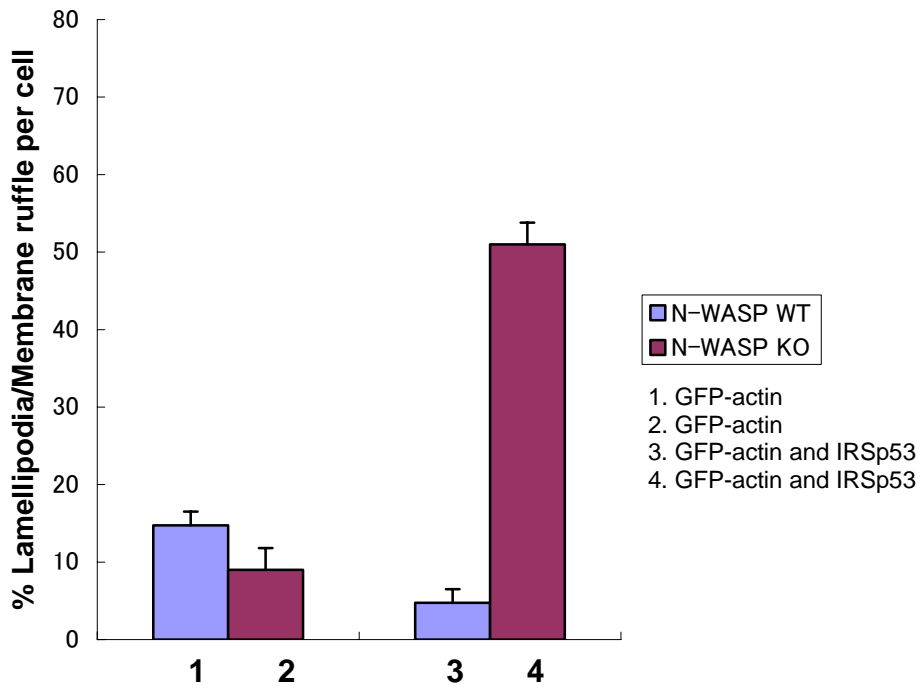


Figure 5.1

B



C



N-WASP KO cells (Figure 5.1A, a and b). IRSp53 induced strong filopodia formation in N-WASP WT and caused the formation of neurite-like projections (Figure 5.1A, d). In N-WASP KO cells no filopodia or neurite-like processes were seen. However, membrane ruffling (and lamellipodia formation) was strongly stimulated when IRSp53 was expressed in N-WASP KO cells. (Figure 5.1A, c). These results suggested that N-WASP is essential for IRSp53 induced filopodia formation, and when it was absent secondary morphological activities were revealed.

### **5.3. The Effect of Rac1N17 on IRSp53 Phenotype in N-WASP KO cells.**

IRSp53 induces a strong filopodial response in N-WASP WT cells but not in KO cells. However, IRSp53 does induce a membrane ruffling response in the N-WASP KO cells. To eliminate the possibility that the membrane ruffling was masking potential filopodial activity in the N-WASP KO cells, I examined the effect of Rac1N17 on the IRSp53 induced phenotype. In the presence of Rac1N17, IRSp53-induced ruffling is kept to minimum in both cell types (Figure 5.2C, lanes 5-6). A significant increase in filopodia number was observed in the WT cells with IRSp53/Rac1N17 (Figure 5.2B, lane 5) as compared to IRSp53 alone (Figure 5.2B, lane 3). In KO cells, no filopodia were observed despite ruffling activity been reduced significantly by Rac1N17 (Figure 5.2B, compare lanes 4 and 6, and Figure 5.2C, lanes 4 and 6).



**Figure 5.2 Effect of Rac1N17 on IRSp53 induced phenotype.**

(A) N-WASP WT and KO cells were microinjected with either (a,b) IRSp53 or (c,d) IRSp53 with Rac1N17 and GFP-Actin cDNA. The cells were then left to express the cDNA for between 1-6 hours. GFP-actin positive cells were imaged using DIC time-lapse microscopy as described in the Material and Methods section.

(Bar = 10  $\mu$ m)

(B) and (C) Statistical analysis of experiments illustrated in A. Filopodia per cell and % lamellipodia/membrane ruffle per cell were scored (refer to section 2.2.6 in Materials and Methods).

Figure 5.2

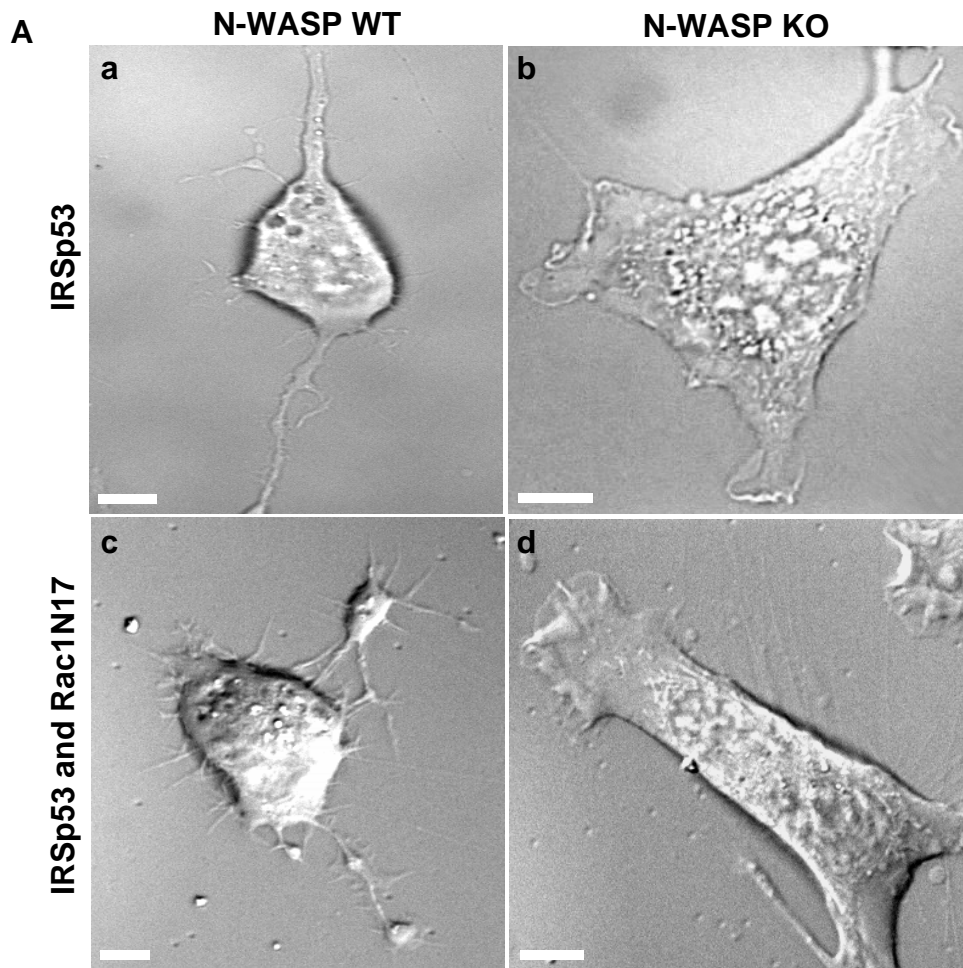
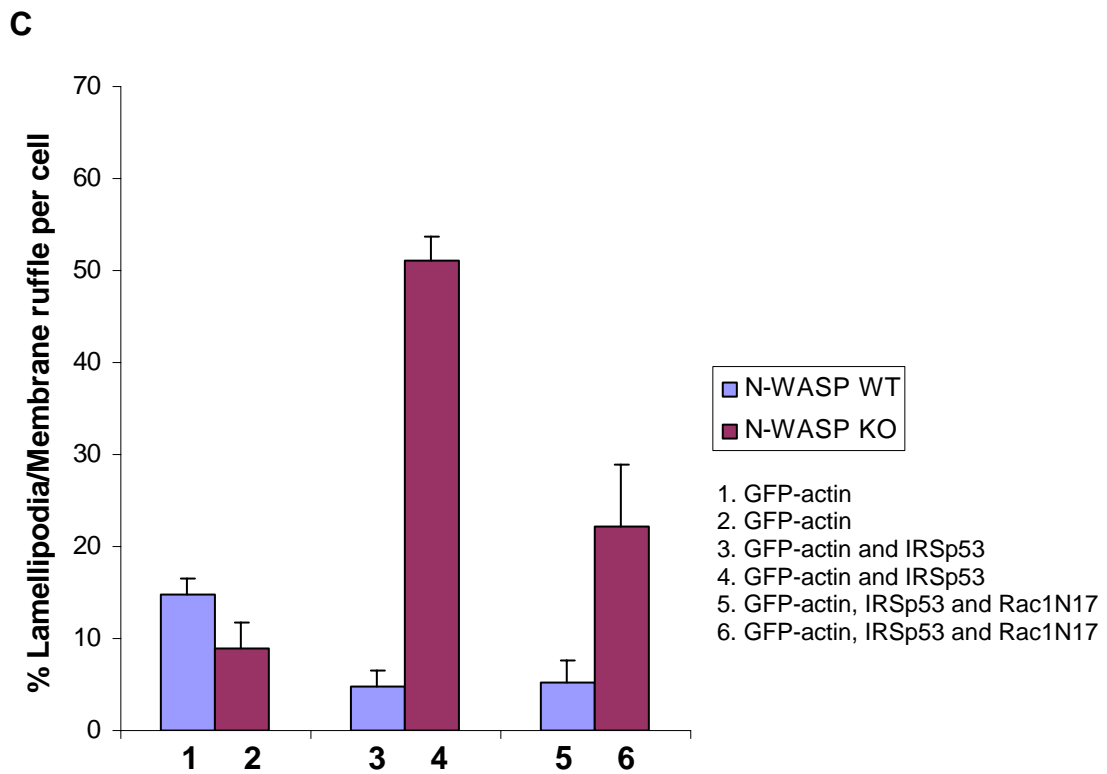
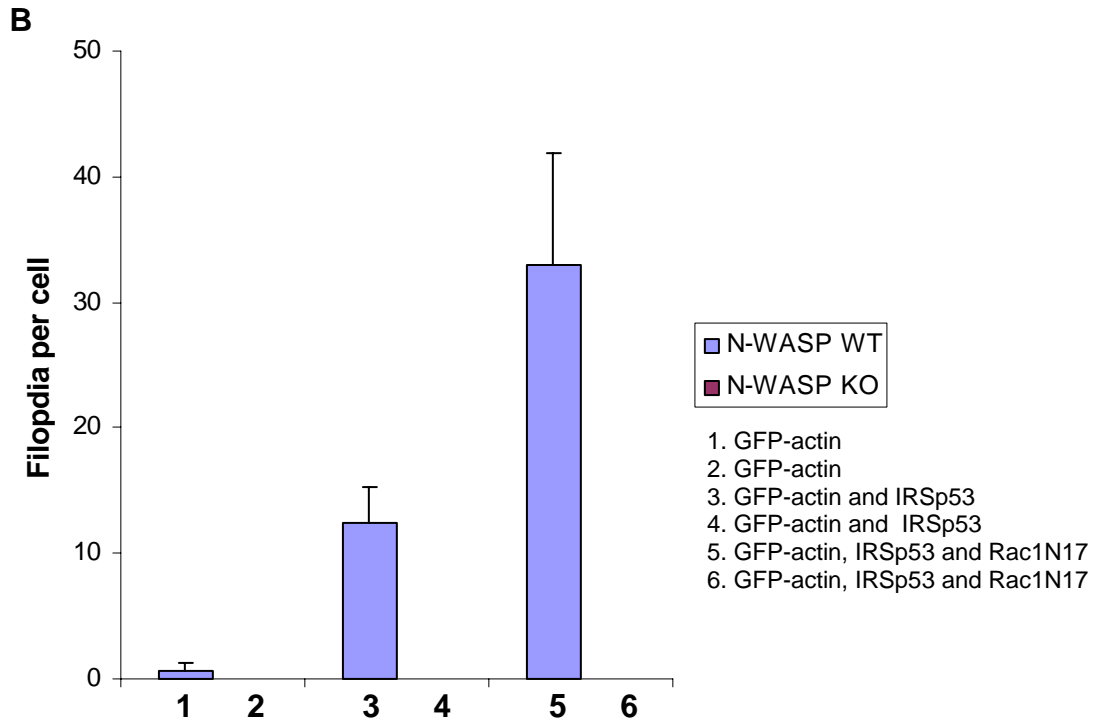


Figure 5.2



#### **5.4. IRSp53 overexpression is comparable in both N-WASP WT and KO cells.**

The expression level of a protein can affect the function. To determine if the expression level of the IRSp53 proteins in the two cell types was the same IRSp53 fluorescence intensity was measured in both N-WASP WT and KO cells. The expression level of IRSp53 was found to be of comparable levels in both cell types. (Figure 5.3)

#### **5.5. Effect of N-WASP reconstitution in KO fibroblasts of IRSp53 phenotype.**

In the next set of experiments I titrated in N-WASP cDNA to the KO cells with IRSp53 cDNA. Low levels of N-WASP cDNA were tolerated by the cells and allowed me to carry out reconstitution experiments. N-WASP KO cells microinjected with N-WASP cDNA responded to IRSp53 by filopodia formation (Figure 5.4B) and neurite-like processes were also formed. These results support the idea that IRSp53 requires N-WASP for its filopodia formation.

N-WASP contains a WA domain that is important for binding to and activation of the Arp 2/3 complex that is required for actin branching networks. To investigate if Arp2/3 activation is essential for the filopodia formation observed, I used an N-WASP $\Delta$ WA mutant that had a WA ( $\Delta$ VCA) deletion and carried out reconstitution experiments. This N-WASP- $\Delta$ WA mutant protein would not be able to bind or activate the Arp2/3 complex. The N-WASP $\Delta$ WA-IRSp53 combination was able to reconstitute filopodia formation in KO cells but neurite-like processes were not observed. Furthermore, filopodia formation with the  $\Delta$ WA mutant was more robust than that observed with cDNA encoding wild-type protein. Reconstitution with the N-WASP- $\Delta$ WA mutant induced filopodia on the dorsal surface of the KO cells as well as on the periphery (Figure 5. 4C).

**Figure 5.3 IRSp53 expression in N-WASP WT and KO cells.**

(A) N-WASP WT and KO cells were transfected with HA-IRSp53 and GFP-actin. Cells were left for between 18-24 hours for cDNA expression. They were then fixed and stained. Anti-HA antibodies were used to detect IRSp53.

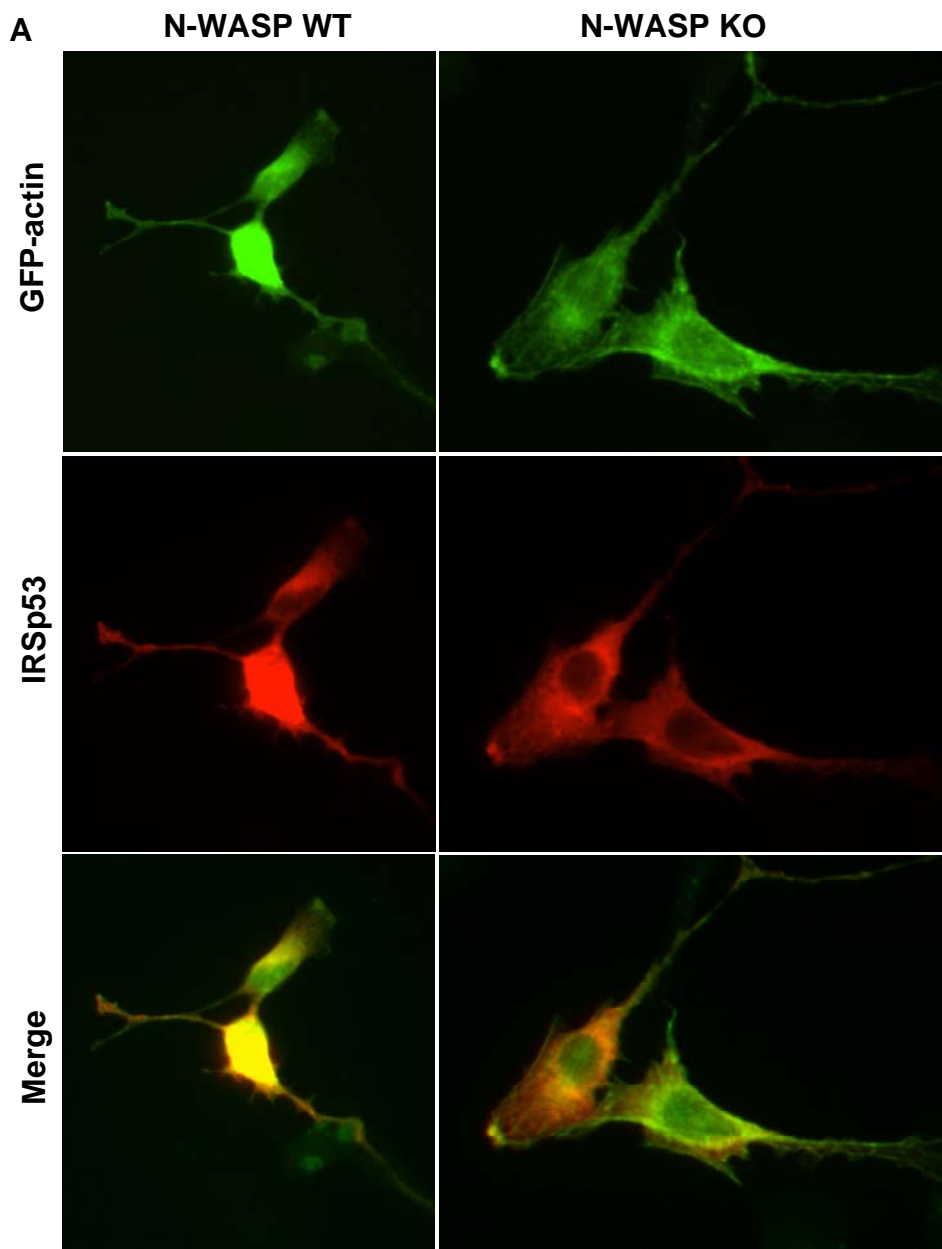
(Bar = 10 $\mu$ m)

(B) Quantification of fluorescence signal was carried out using Metamorph software and Microsoft Excel. A semi-automated procedure was employed in the analysis.

1. Load images into Metamorph.
2. Define the ROI (region of interest) (under Regions/Region Tools).
3. Connect to Excel through Dynamic Data Exchange (Under Measure Menu/Region Measurements/Open log/DDE/Excel).
4. Choose "all regions" (in Region Measurements window).
5. Log data. This will generate a table containing image number, average intensity, and other values as specified in Metamorph.

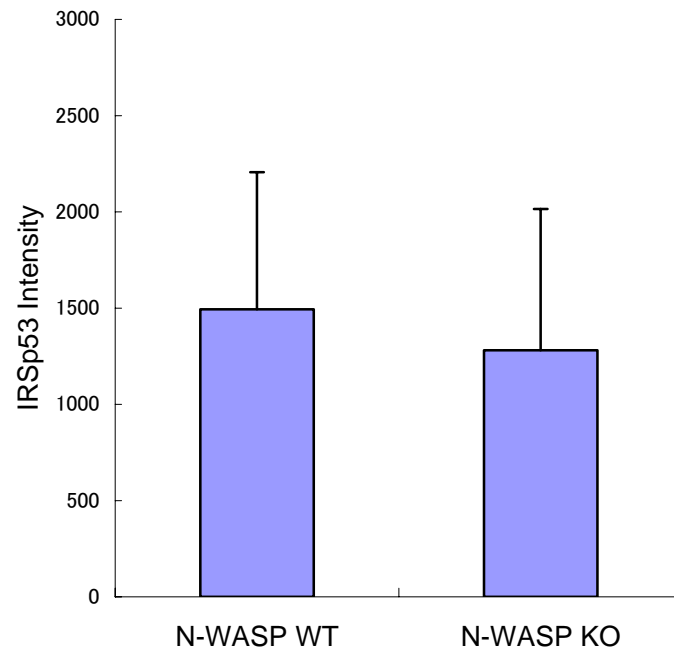
The values obtained were presented in graphical form.

Figure 5.3



**Figure 5.3**

**B**



**Figure 5.4 Reconstitution of N-WASP KO cells with N-WASP and N-WASP $\Delta$ WA.**

The IRSp53 phenotype was assessed in N-WASP KO cells, after reconstitution with (B) N-WASP or (C) N-WASP $\Delta$ WA. Cells were left for between 1-6 hours for cDNA expression. GFP-actin positive cells were imaged using DIC time-lapse microscopy as described in the Material and Methods section. (D and E) Statistical analysis of the experiment illustrated in A-C. Cells were scored for the number of filopodia per cell and % lamellipodia/membrane ruffle per cell (refer to section 2.2.6 in Materials and Methods). (Bar = 10  $\mu$ m)

(Movie 5.4.1. N-WASP KO microinjected with IRSp53).

(Movie 5.4.2. N-WASP KO microinjected with IRSp53 and N-WASP).

(Movie 5.4.3. N-WASP KO microinjected with IRSp53 and N-WASP $\Delta$ WA).



**Figure 5.4**

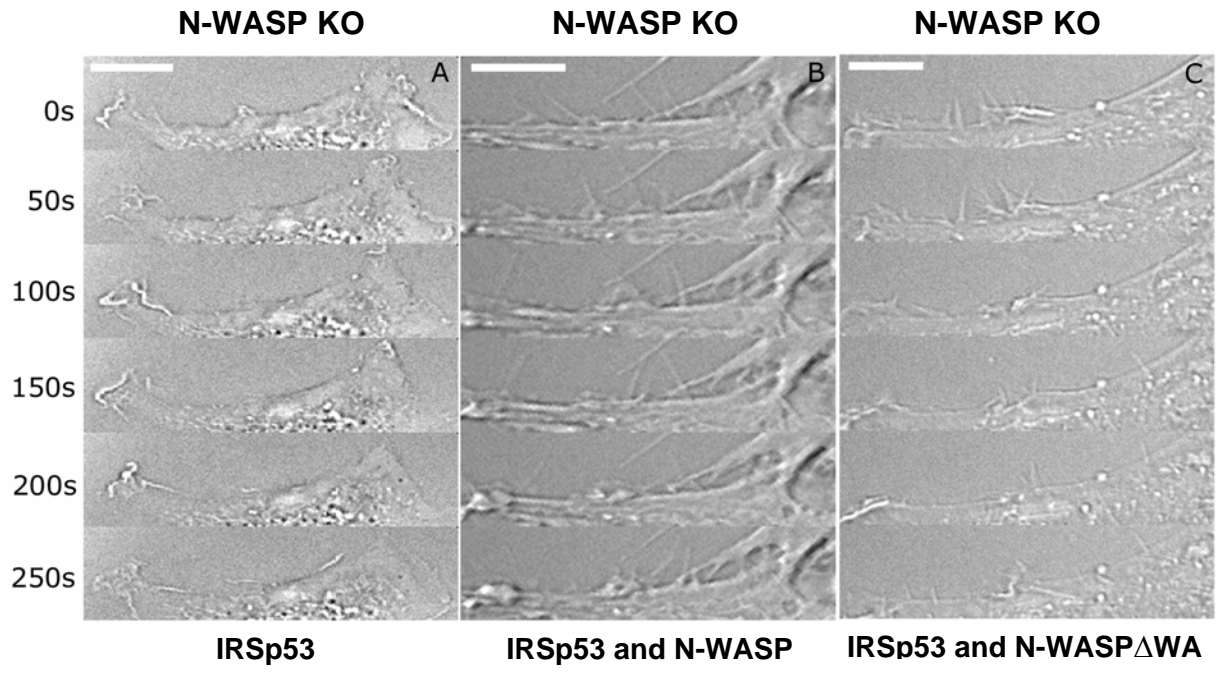
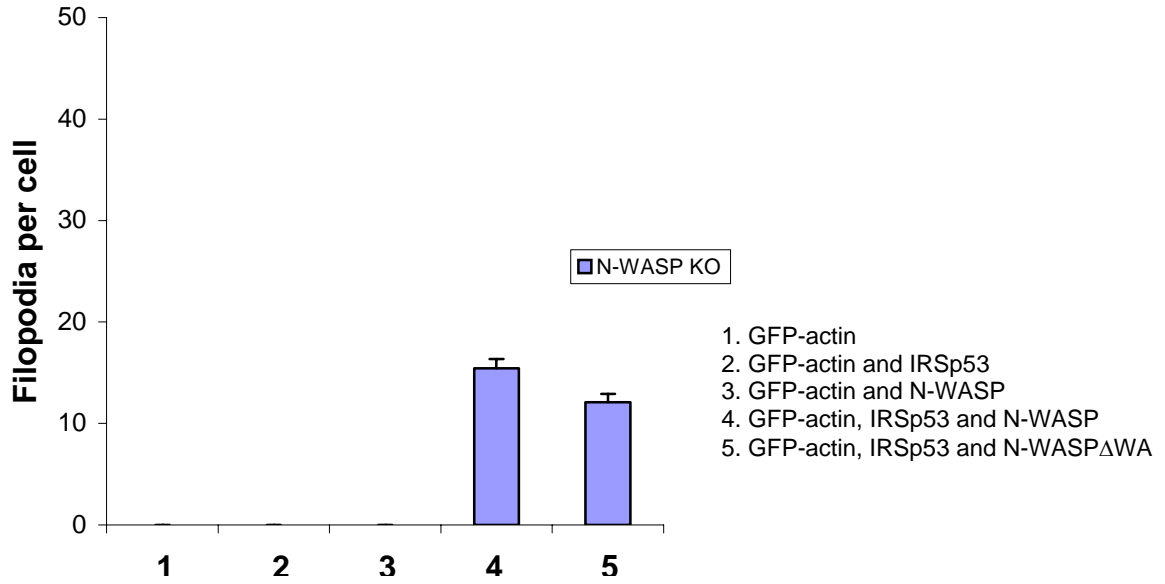
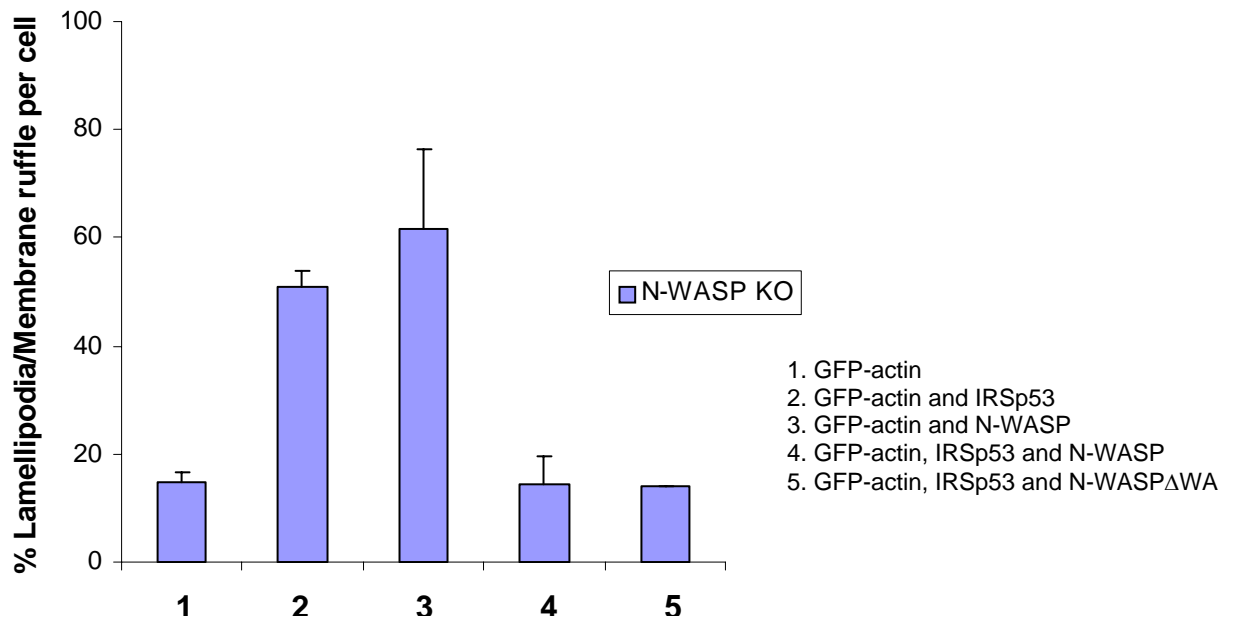


Figure 5.4

D



E



## **5.6. Characteristics of filopodia induced in N-WASP reconstitution experiments.**

I compared filopodia induced by IRSp53/N-WASP pair and IRSp53/NWASP $\Delta$ WA pair in reconstitution experiments for size and turnover time (Figure 5.5C and D). The filopodia induced in the two situations differed significantly only in turnover time (Figure 5.5D). The effect of the WA deletion was to increase the half-life of the filopodia from 30 sec to 120 sec (Figure 5.5E) which was caused by an increase in time taken for disassembly.

## **5.7. WAVE1 (SCAR) and WAVE1 $\Delta$ WA can reconstitute IRSp53 induced filopodia formation in N-WASP KO cells.**

N-WASP contains a number of domains, including an N-terminal sequence that has been shown to be important for interacting with the WASP interacting protein (CR16, WIP) forming a complex. To determine whether the N-terminal sequence of N-WASP was required for reconstitution, I used SCAR (a WASP family homolog, WAVE1 homolog in *Drosophila*) and SCAR  $\Delta$ WA construct and investigated whether these proteins can reconstitute IRSp53 induced filopodia formation in N-WASP KO cells. (The SCAR constructs will be referred to as WAVE1 and WAVE1  $\Delta$ WA throughout rest of the thesis.) The combination of IRSp53 and WAVE1 or WAVE1  $\Delta$ WA mutant was able to reconstitute filopodia formation in the KO cells (Figure 5.6). The level of filopodia formation obtained by WAVE1 and WAVE1 $\Delta$ WA reconstitution was comparable to that obtained with N-WASP (Figure 5.6C, lanes 3, 4 and 5).

**Figure 5.5 IRSp53 induced filopodia dynamics in N-WASP KO cells reconstituted with either N-WASP or N-WASP $\Delta$ WA.**

N-WASP KO cells were transfected with GFP-actin/IRSp53 and (A) N-WASP cDNA or (B) N-WASP $\Delta$ WA cDNA and cells left for 1-6 hours for cDNA expression. GFP-actin positive cells were imaged using DIC time-lapse microscopy as described in the Material and Methods section. The time-lapse series shown gives an example of one such measurement. Filopodia were measured for (C) size, (D) half-life, and (E) assembly/disassembly.

(Bar=5  $\mu$ m)

Figure 5.5

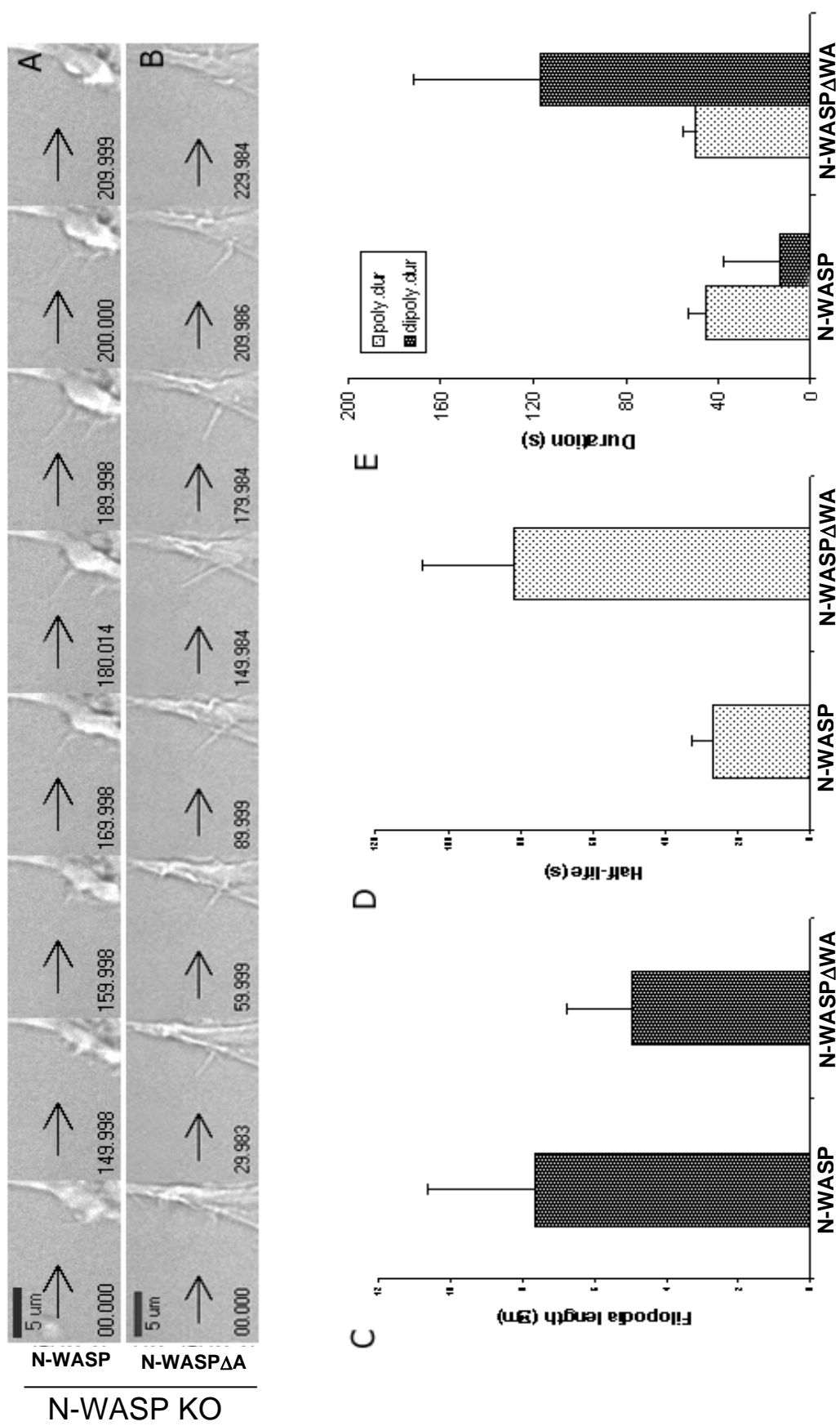


**Figure 5.6 IRSp53 induced filopodia dynamics in N-WASP KO cells transfected with either WAVE1 (SCAR) or WAVE1 $\Delta$ WA (SCAR mutant).**

N-WASP KO cells were microinjected with GFP-actin and (A) IRSp53 and WAVE1 cDNA or (B) IRSp53 and WAVE1 $\Delta$ WA cDNA and cells were left for 1-6 hours for cDNA expression. GFP-actin positive cells were imaged using DIC time-lapse microscopy as described in the Material and Methods section. (C,D) Statistical analysis of the experiment illustrated in A. Cells were scored for the number of filopodia per cell and % lamellipodia/membrane ruffle per cell (refer to section 2.2.6 in Materials and Methods).

(Bar=10  $\mu$ m)

Figure 5.6

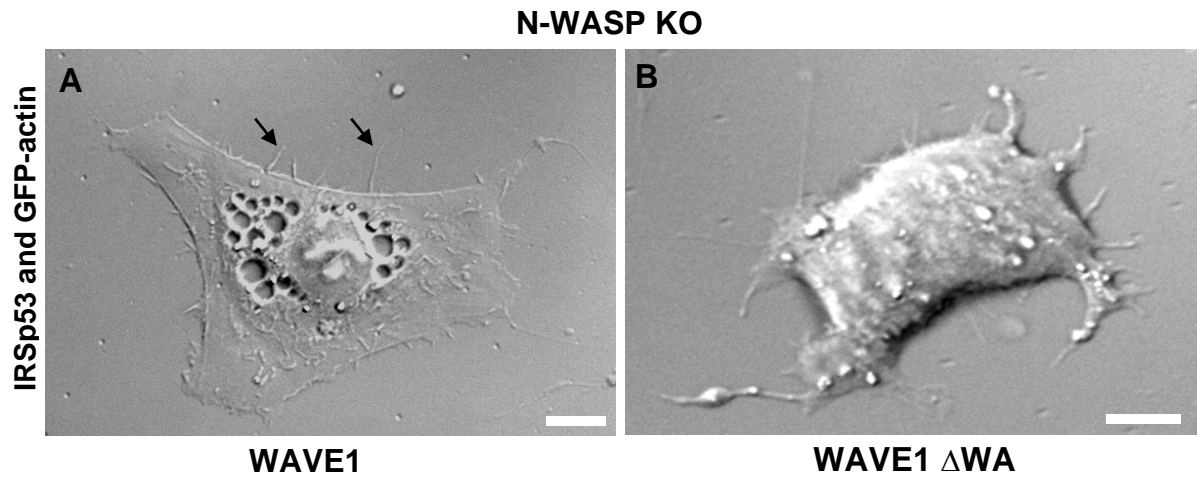
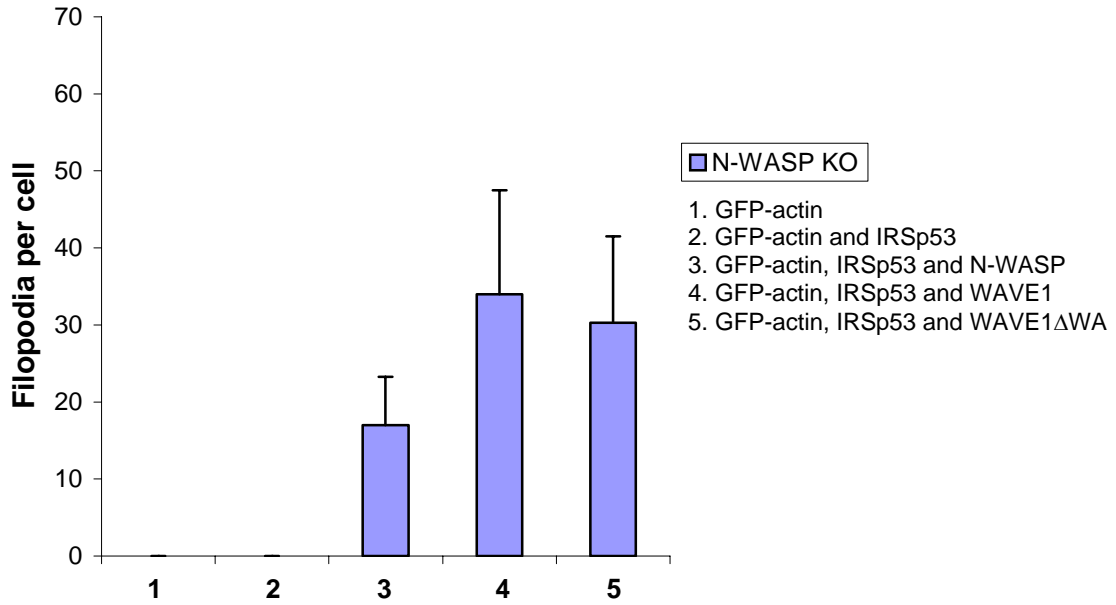
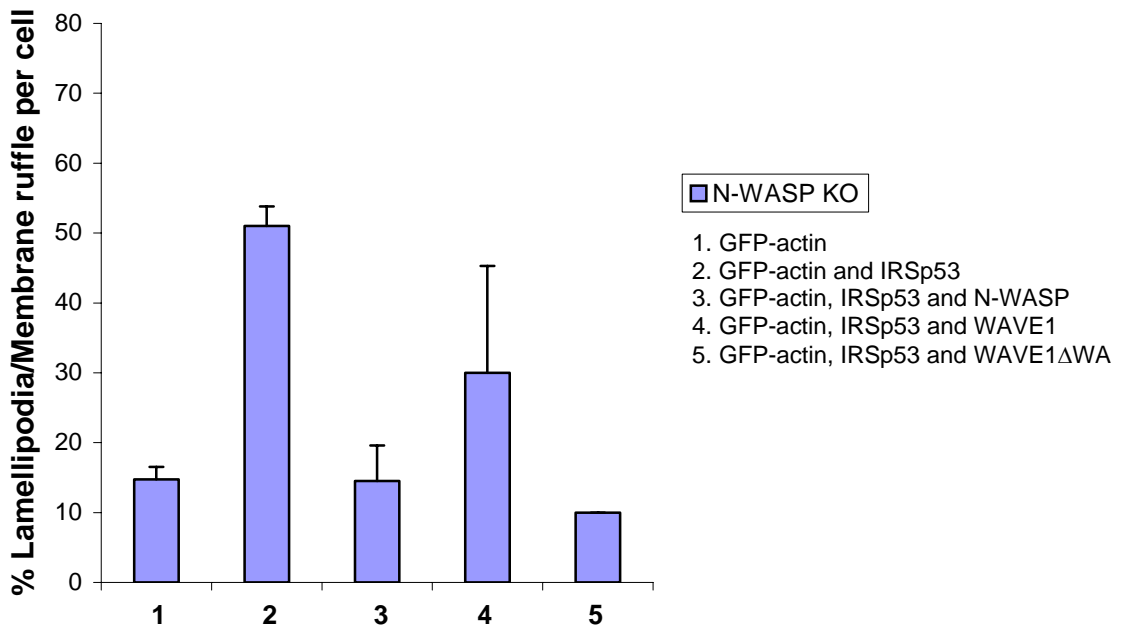


Figure 5.6

C



D





These data suggest that the N-terminal sequence of N-WASP may not be essential for IRSp53 induced filopodia formation in this system, making a role for WIP unlikely.

### **5.8. The SH3 domain is required for IRSp53 induced filopodia formation.**

To determine the role of the SH3 domain in IRSp53 induced filopodia formation, a SH3 deletion mutant FP/AA was employed in the study. The FP/AA mutant would not be able to bind to N-WASP or other interacting proteins like WAVE/SCAR family. In FRET experiments the FP/AA mutation eliminated IRSp53 binding to N-WASP (Table 4.1). The FP/AA mutant failed to induce any filopodia formation in both the WT and KO cells (Figure 5.7). N-WASP reconstitution experiments on the KO cells were also done using the FP/AA mutant. This combination of the FP/AA mutant and N-WASP was not able to re-constitute the filopodia activity in the KO cells (Figure 5.8C, lane 4). These results strongly support the idea that the SH3 domain is required for N-WASP to reconstitute IRSp53 induced filopodia formation in N-WASP KO cells.

### **5.9. FRET analysis of the IRSp53-N-WASP interaction in the KO cells.**

To confirm that the IRSp53-N-WASP interaction described in Chapter 4.4 also occurs in the N-WASP KO cell line, I overexpressed mRFP-tagged full length IRSp53 and GFP-tagged full length N-WASP in the N-WASP WT and KO cell and AP-FRET analysis was carried out. A positive FRET result with FE values of 22% and 20% in N-WASP WT and KO cells were obtained, respectively. CC values of -0.99 was also obtained for both WT and KO cells respectively. These results fall within the acceptable range of -0.7

to -1, confirming that the observed increase in GFP signal was not an artifact (for details, refer to Materials and Methods).

**Figure 5.7 Morphological activity of the SH3 domain mutant IRSp53-FP/AA.**

(A) N-WASP WT and KO cells were microinjected with IRSp53-FP/AA cDNA and GFP-actin. Cells were left for between 1-6 hours for cDNA expression. GFP-actin positive cells were imaged using fluorescence and DIC time-lapse-microscopy as described in the Material and Methods section. (B,C) Statistical analysis of cells from the experiment illustrated in (A). Cells were scored for number of filopodia per cell and % lamellipodia/membrane ruffle per cell (refer to section 2.2.6 in Materials and Methods). (Bar = 10  $\mu$ m)

**Figure 5.7**

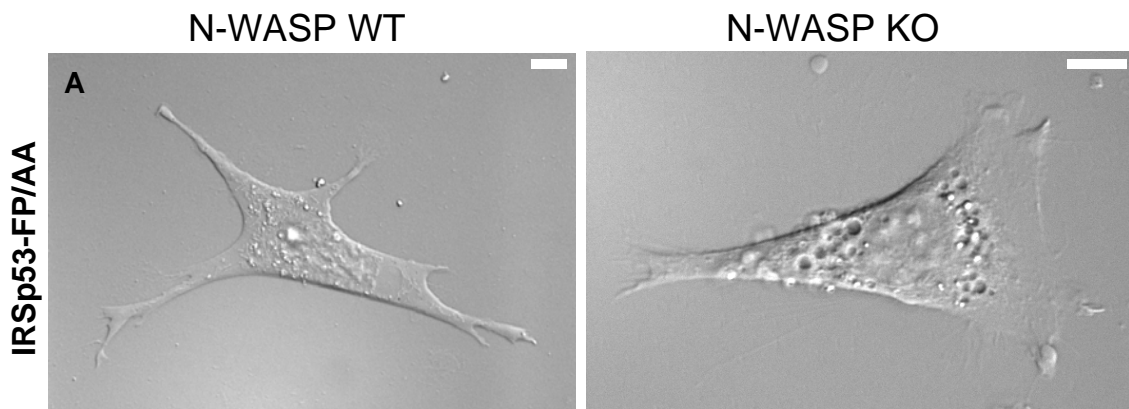


**Figure 5.7**

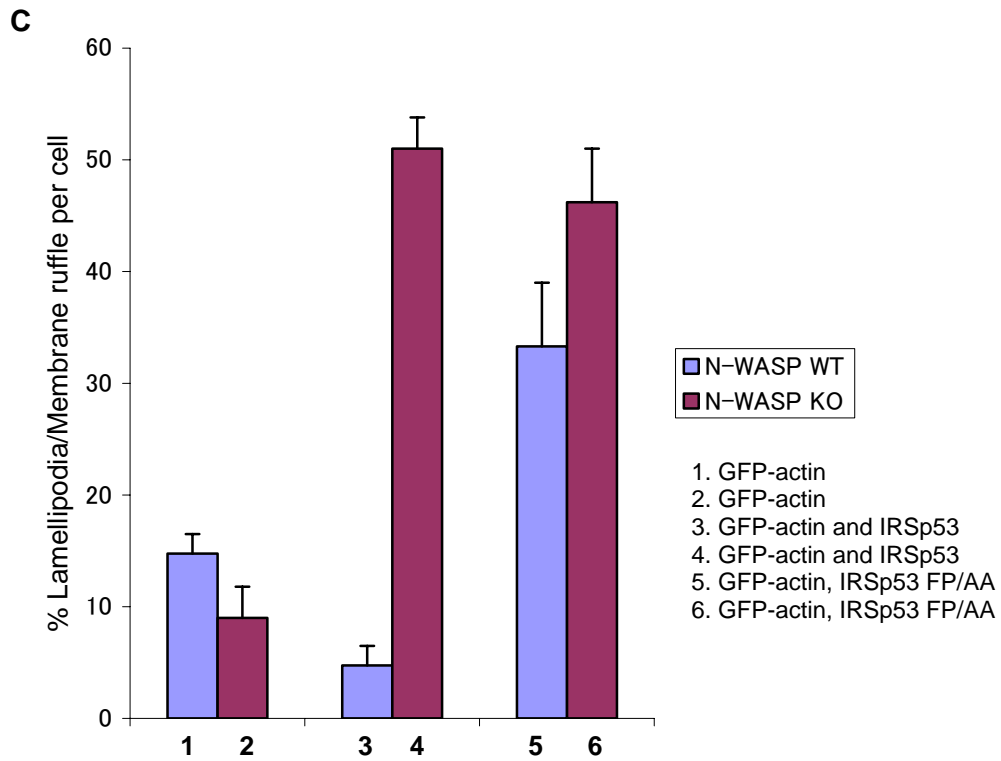
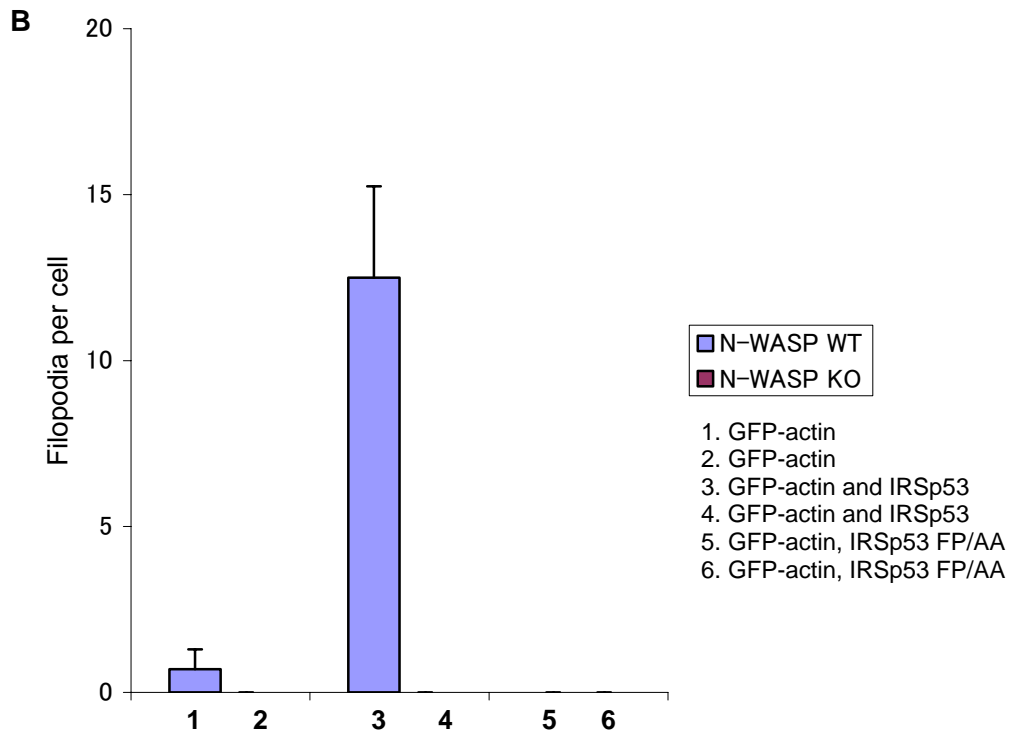


**Figure 5.8 IRSp53-FP/AA induced morphological effects in N-WASP KO cells reconstituted with N-WASP.**

(A) A reconstitution experiment was carried out with the IRSp53-FP/AA mutant. N-WASP KO cells were micro-injected with GFP-IRSp53-FP/AA and N-WASP (approximately 100 ng cDNA). Cells were then left for between 1-6 hours for cDNA expression. GFP-actin positive cells were then imaged as described in Materials and Methods. (B,C) Statistical analysis of the experiment illustrated in (A). The cells were scored for number of filopodia per cell and % lamellipodia/membrane ruffle per cell (refer to section 2.2.6 in Materials and Methods). (Bar = 10  $\mu$ m).

**Figure 5.8**

**A**

**N-WASP KO**

**IRSp53 -FP/AA and N-WASP**

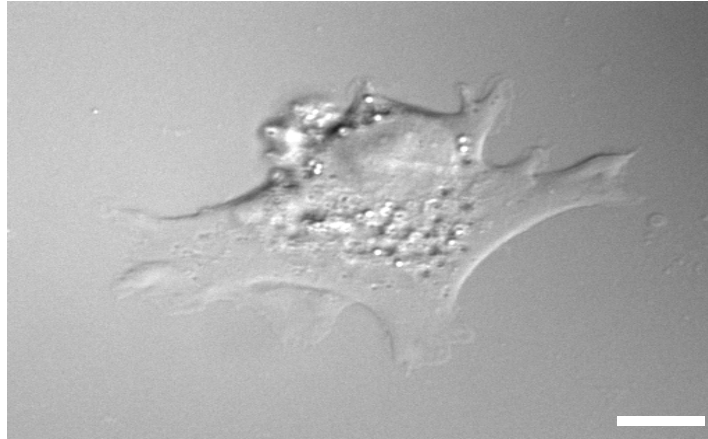
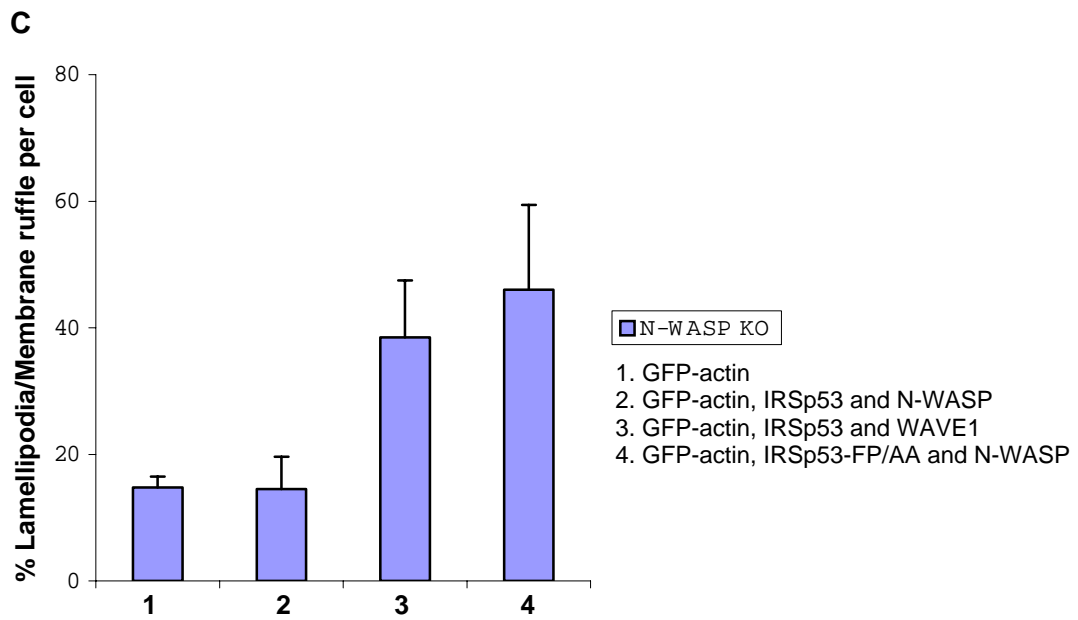
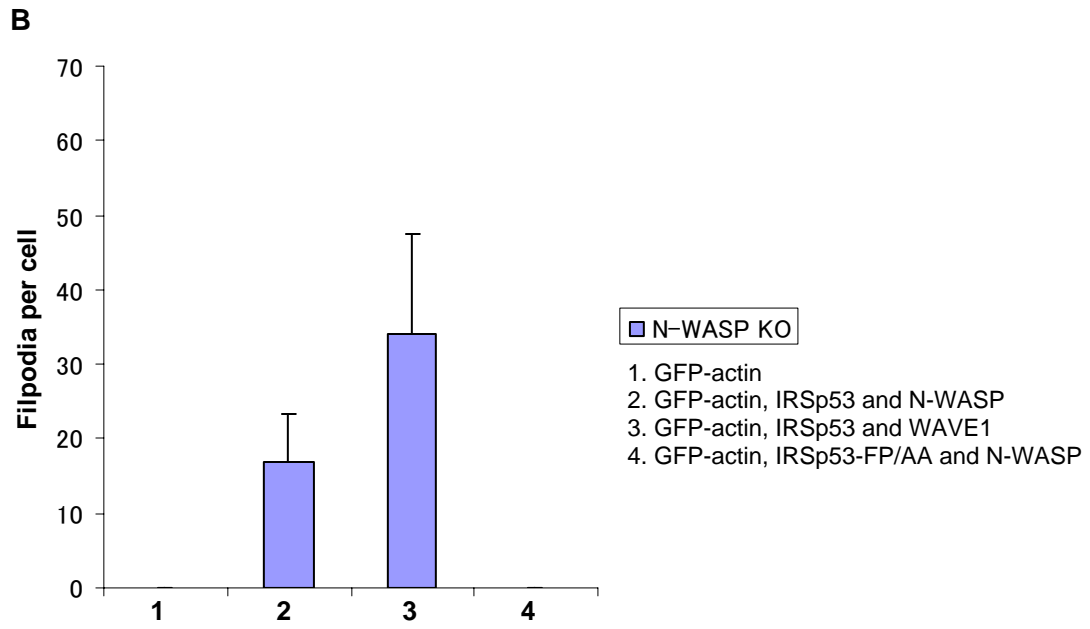


**Figure 5.8**





## **Chapter 6. The IRSp53 IMD**

### **6.1. Introduction.**

The predicted N-terminal helical stretch of 250 amino acids of IRSp53 has been reported to be an evolutionarily conserved F-actin bundling domain involved in filopodia formation (Millard et. al., 2005). A number of proteins including IRSp53 and missing in metastasis (MIM) protein share this unique domain termed the IRSp53/MIM homology domain (IMD/BAR domain). The IMD domain is highly conserved in vertebrates and has domain relatives in invertebrates which do not show obvious homology to any known actin interacting proteins. A previous report (Yamagashi et.al, 2004) has shown that the IMD domain derived from both IRSp53 and MIM can induce “filopodia” (for definition of filopodia, please refer to section 6.2 below) in cultured cells and form tightly packed F-actin bundles *in vitro*. On the other hand, findings from work on MIM that suggested the domain does not bundle F-actin (Dr. Pekka Lappalainen, University of Helsinki, personal communications). In this chapter I set out to investigate the role of IMD domain in IRSp53 function. Is the IMD sufficient for filopodia formation?

### **6.2. IRSp53 IMD domain produces protrusions.**

To establish the role of IMD in IRSp53 function, I carried out overexpression studies in N-WASP WT and KO cells. GFP-IMD and mRFP-actin cDNA were microinjected into N-WASP WT and KO cells and time-lapse microscopy was carried out. The IMD domain was indeed able to drive protrusions. However, upon further examination, I determined that the IMD-driven protrusions were not filopodia. I defined a filopodium by the following criteria:

1. Contains F-actin
2. Have a length of between 6-15  $\mu\text{m}$
3. Have a thickness of between 1-2  $\mu\text{m}$
4. Have a lifetime of 120 – 170 secs

This is based on observations of filopodia formation induced by IRSp53, N-WASP, Cdc42 and Toca-1 in a variety of mammalian cell lines (for more details, please refer to appendix III).

The IMD-driven protrusions observed fulfil some but not all of the criteria. They can be classified into 3 groups (Figure 6.1; Table 6.1). The first group consist of protrusions that were stable and contained F-actin. They were also of the correct length but with a smaller width (thickness). The second group of protrusions was also stable but did not contain F-actin. These protrusions were also smaller in size in terms of length and thickness. The last group of protrusions were dynamic but they were also smaller in size in terms of length and thickness and most importantly, they did not contain F-actin (Table 6.1).

**Figure 6.1 Characterization of IMD domain driven protrusive structures.**

(A) N-WASP WT or KO cells were microinjected with (a-c) GFP-IMD and mRFP-actin and cells were left for between 1-6 hours for cDNA expression. Positive cells were imaged using time-lapse microscopy as described in the Material and Methods section. (a) Stable protrusions with actin; (b) Stable protrusions without actin; (c) Dynamic protrusions without actin. (d) N-WASP WT cells microinjected with IRSp53 and GFP-actin. (B) Statistical analysis of experiments illustrated in A, together with additional data from experiments carried out with the IMD-4K mutant. Cells were scored for different types of protrusive activity per cell. (Bar = 10  $\mu$ m)

Figure 6.1

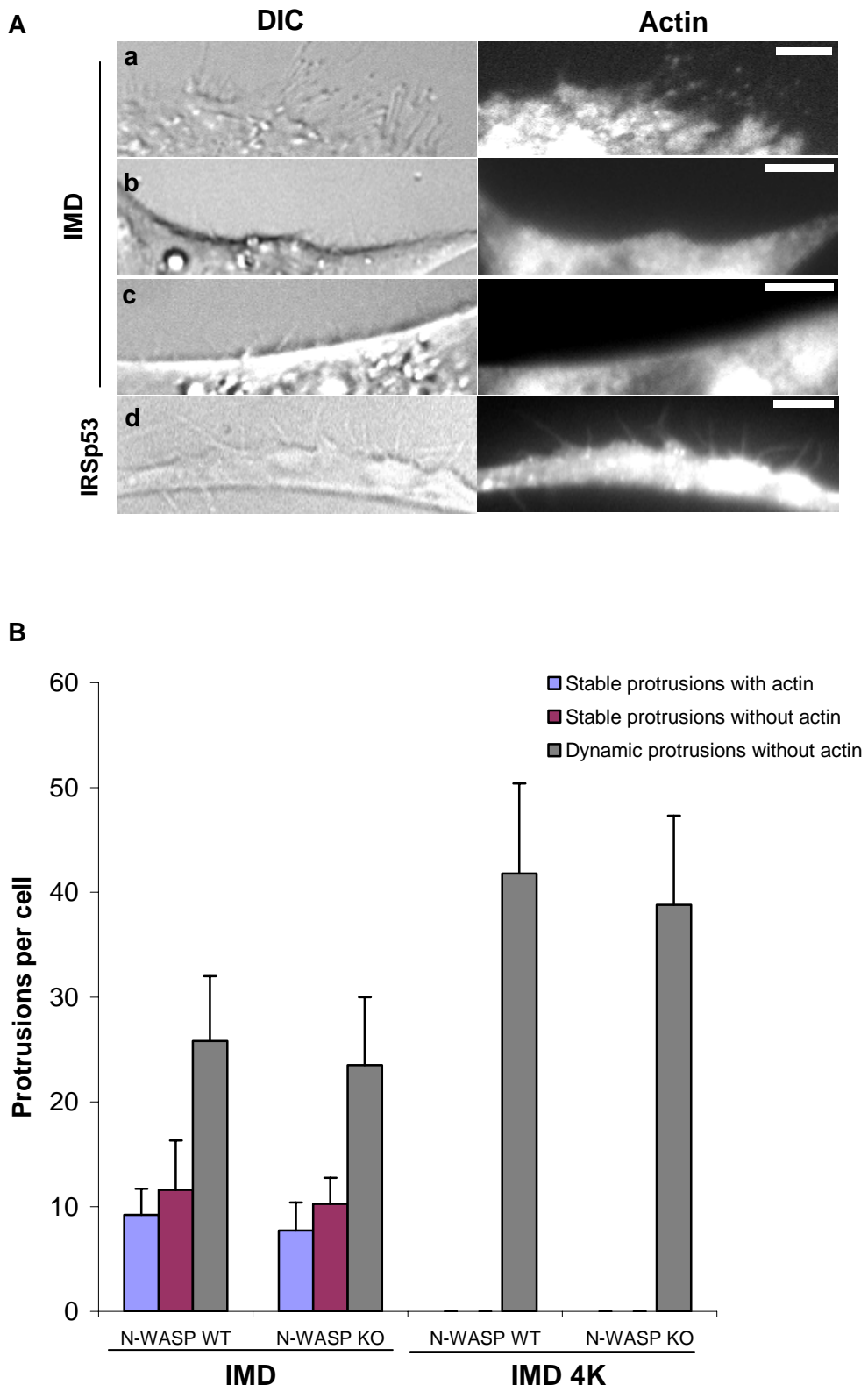


### **Table 6.1 Characterization of IMD/IMD-4K induced protrusions.**

IMD/IMD-4K induced protrusions can be classified into 3 groups:

1. Stable structures with actin
2. Stable structures without actin
3. Dynamic structures without actin

Filopodia produced by IRSp53 is used for comparison as group 4

N-WASP WT and KO cells were microinjected with GFP-IMD or GFP-IMD-4K with mRFP-actin. Cells were left for 1-6 hours for cDNA expression before live cell imaging was carried out. Protrusions were imaged for 10 mins with frames taken every 10 secs. Stable structures (1,2) did not turnover during the 10 mins and are scored as having a lifetime of more than 10 mins. Dynamic structures (3,4) are those that are appearing/disappearing over the 10 mins. Lifetime is determined as the time taken from appearance to disappearance.

F-actin was followed with mRFP signal. All measurements are presented as an average  $\pm$  SD. (n=7). Three experiments were carried out.

**Table 6.1. Characterization of IMD-induced protrusions**

Protrusions	IMD			IMD-4K			IRSp53		
	Lifetime (s)	Length ( $\mu\text{m}$ )	Width ( $\mu\text{m}$ )	Lifetime (s)	Length ( $\mu\text{m}$ )	Width ( $\mu\text{m}$ )	Lifetime (s)	Length ( $\mu\text{m}$ )	Width ( $\mu\text{m}$ )
1. Stable Structure with Actin	>10 Mins	10.3 $\pm$ 0.8	0.89 $\pm$ 0.06	ND	ND	ND	ND	ND	ND
2. Stable Structure without Actin	>10 Mins	4.5 $\pm$ 1.09	0.69 $\pm$ 0.11	ND	ND	ND	ND	ND	ND
3. Dynamic Structure without actin	174 $\pm$ 40	4.5 $\pm$ 0.62	0.74 $\pm$ 0.09	176 $\pm$ 32	5.7 $\pm$ 0.9	1.08 $\pm$ 0.15	ND	ND	ND
4. Dynamic Structure with actin	ND	ND	ND	ND	ND	ND	187 $\pm$ 38	6.83 $\pm$ 1.8	1.25 $\pm$ 0.12

\*ND – Not Detected

The IRSp53-IMD was reported to have intrinsic actin-bundling activity and four lysine (4K) residues have been identified to be important for interaction with actin (Millard et al., 2005). It was reported that mutation of these four residues resulted in loss of “filopodia” formation and reduced F-actin bundling activity. To investigate if the 4K of the IMD is indeed required for filopodia formation, I employed the use of an IMD mutant, GFP-IMD-4K. The IMD-4K has 4 lysines (K142,143,146 and 147) mutated to glutamic acid (D). I microinjected GFP-IMD-4K and mRFP-actin cDNA into N-WASP WT and KO cells and carried-out time-lapse microscopy. I was able to detect dynamic protrusions that resemble filopodia but they did not contain any F-actin (Figure 6.1B, Table 6.1). These structures were also of a smaller size in terms of length and thickness. IMD-4K did not induce stable protrusions with or without actin. (Figure 6.1B; Table 6.1). Taken together, these results suggested that the IMD domain is able to drive protrusions. However, these protrusions either lack the dynamics of a real filopodium or do not contain F-actin. I will refer to these IMD induced protrusions as “partial filopodia”; dynamic membrane protrusions that lack F-actin.

### **6.3. The IMD-4K is important for IRSp53 filopodia formation.**

The IMD domain was microinjected into N-WASP WT and KO cells and found to induce “partial filopodia in both cases (Figure 6.2A). N-WASP does not play a role in IMD function on its own.

To investigate if the 4 lysines of the IMD domain are required for IRSp53-induced filopodia formation, I employed the use of a full length IRSp53 protein with an IMD-4K

mutation (IRSp53-4K). IRSp53-4K did not induce filopodia in either WT or KO cells (Figure 6.2B; Figure 6.2C, lane 5-8). Thus, the data are consistent with IMD activity being important for IRSp53 function.

#### **6. 4. IRSp53 interacts directly with F-actin but IMD does not.**

To determine if IRSp53 and IMD interact directly with F-actin, AP-FRET experiments were carried out. Cells were transfected with GFP-IRSp53 or GFP-IMD with mRFP-actin and AP-FRET analysis was carried out. FRET was observed between GFP-IRSp53/mRFP-actin in the filopodia, neurite, rib, ruffles and cell body. FE values ranging from 5.4 to 7.7 % was obtained (Table 6.2). Corresponding CC values also fall within the acceptable range of between  $-0.7$  to  $-1$ , confirming the positive FRET results. On the other hand, I failed to observe any FRET between GFP-IMD/mRFP-actin or the GFP-IMD-4K/mRFP-actin pair (Table 6.2).



**Figure 6.2 Phenotype of the IRSp53-4K in N-WASP WT and N-WASP KO cells.**

(A) Cells were microinjected with GFP-IMD and mRFP-actin or (B) GFP-IRSp53-4K and mRFP-actin and were cells left for between 1-6 hours for cDNA expression. Positive cells were imaged using time-lapse microscopy as described in the Material and Methods section. (a,c) N-WASP WT cells and (b,d) N-WASP KO cells. (C and D) Statistical analysis of the experiments illustrated in A and B. Cells were scored for protrusions per cell and % lamellipodia/membrane ruffle per cell (refer to section 2.2.6 in Materials and Methods).

(Bar = 10  $\mu$ m)

Figure 6.2

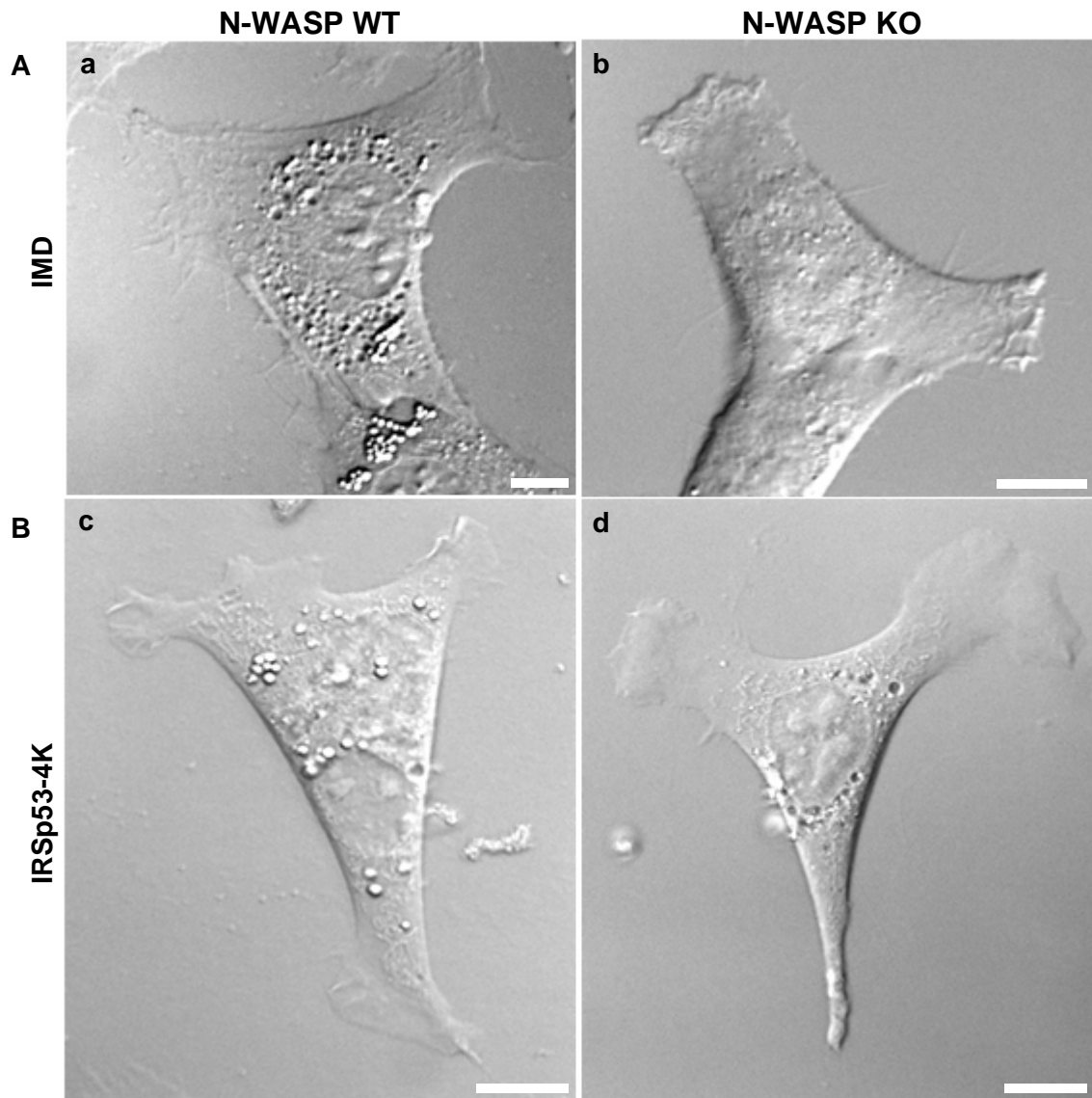
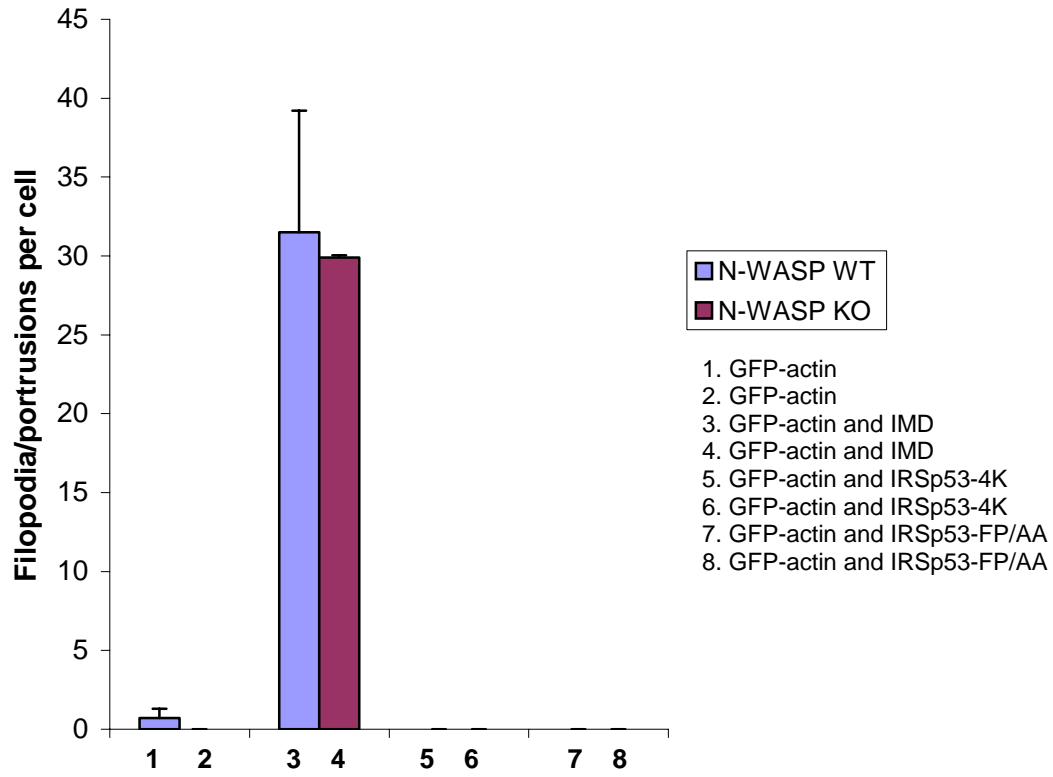
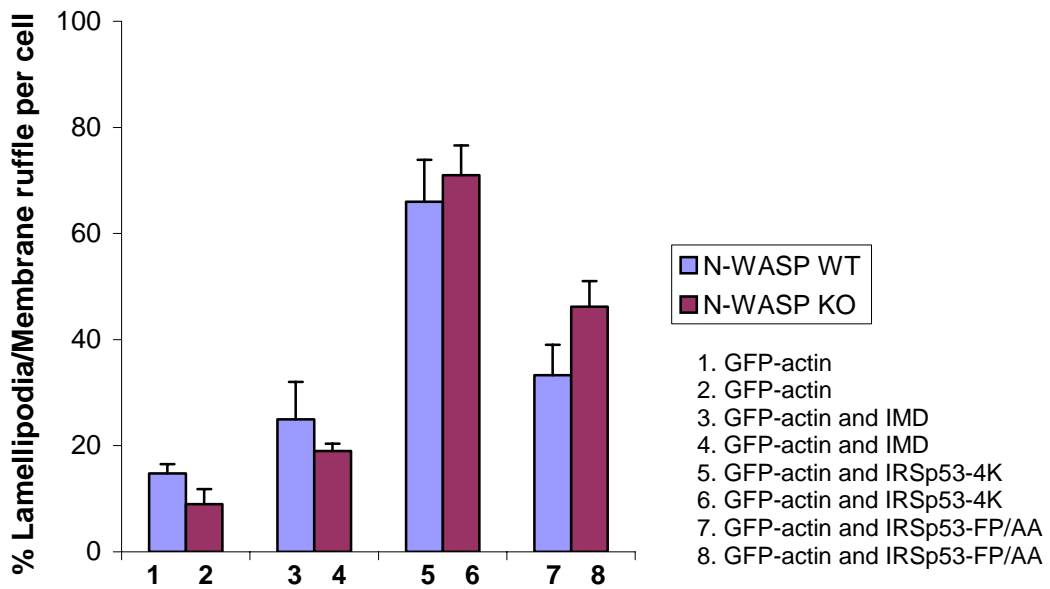


Figure 6.2

C



D



**Table 6.2 AP-FRET assay of mRFP-IRSp53, mRPF-IMD and GFP-actin.**

AP-FRET analysis was carried out as described in Figure 4.4. FEs and CC were calculated as described in Materials and Methods 2.2.7.3.

**Table 6.2. Actin-IRSp53 AP-FRET Efficiency with Cross correlation values**

	FRET E%	± SD	CC *	± SD
<b>Controls</b>				
mRFP-IRSp53 + GFP	1.4	1.18	0.29	0.4
GFP-actin + mRFP	1.54	1.32	-0.12	0.57
Cytoplasmic-GFP + mRFP	1.91	1.49	0.17	0.63
Cytoplasmic-mRFP-GFP (Tandem)	22.34	5.34	-0.99	0.001
<b>GFP-actin + mRFP-IRSp53 in N1E115 or CHO-1</b>				
Filopodia	7.7	0.94	-0.85	0.1
Neurite	5.86	2.09	-0.86	0.067
Rib	6.51	2.97	-0.76	0.084
Ruffling	5.4	1.67	-0.95	0.053
Cell Body	7.27	3.05	-0.93	0.081
<b>Actin + IMD in N1E115</b>				
mRFP-actin + GFP-IMD	3.1	1	-0.35	0.48
mRFP-actin + GFP-IMD-4K	1.88	1.6	-0.27	0.66

\*Cross correlation values between -0.7 to -1 is considered as FRET

## **Chapter 7. The role of G-Proteins.**

### **7.1. Introduction.**

Cdc42 is a ubiquitously expressed protein that belongs to the family of Rho GTPases (Bishop & Hall, 2000). Rho GTPases control many processes including the organization of the actin and microtubule cytoskeleton, proliferation and apoptosis. They exist in an inactive GDP-bound and an active GTP-bound state. Activation of the Rho GTPases is mediated by GEFs that catalyze the replacement of the GDP by GTP. Expression of constitutively active Cdc42, Cdc42V12, induces the formation of actively protruding filopodia with or without concomitant lamellipodia formation depending on the cell type (Kozma, et. al., 1995; Nobes et. al., 1995). N-WASP is one of the downstream effectors of Cdc42 that has been implicated to be involved in filopodia formation (Miki et. al., 1998). N-WASP was shown to bind directly to Cdc42 through its CRIB motif. When co-expressed with active Cdc42, the formation of filopodia was observed. Binding of active Cdc42 to the CRIB region of N-WASP disrupts the inhibitory interaction between N- and C- terminal moieties of the N-WASP molecule to reveal the binding sites to several proteins (Kim et. al., 2000). On filopodia formation, N-WASP is assumed to activate Arp2/3 complex and recruit actin monomers of profilin-actin complex to the fast growing ends of actin filaments (Rohatgi et. al., 1999).

### **7. 2. The Cdc42 phenotype.**

To analyze the phenotypic effect of Cdc42, I carried out time-lapse experiments following the fluorescence using GFP-actin to observe actin dynamics. N1E115 cells were transfected with Cdc42V12 and GFP-actin cDNA. Overexpression of Cdc42V12

induces a fan shape leading edge with ribs and a thin lamellae (Figure 7.1, compare with Figure 3.1). Cdc42V12-induced filopodia are not clearly seen because the activation of Rac1 induced membrane ruffling.

Previous work (Lommel et. al., 2001) has suggested that Cdc42 is competent to induce filopodia in N-WASP KO cells. However, the experiments were done with Cdc42L61/Rac1N17/C3 toxin combination and not with Cdc42V12 or Cdc42L61 alone. I re-investigated the role of Cdc42 by comparing the effects of Cdc42V12 alone, Cdc42V12/Rac1N17 and Cdc42V12/Rac1N17/C3 toxin in the two cell lines. I could not reproduce the results (Lommel, et. al., 2001) using Cdc42V12/Rac1N17/C3 toxin; the cells invariably died with this combination of reagents. Cdc42V12 induced a strong membrane ruffling response in both cell lines and filopodia could not be detected in the KO cells.

### **7.3. The effect of Rac1N17 on the Cdc42 phenotype in N-WASP KO cells.**

Cdc42 induces a strong membrane ruffling response in N-WASP WT/KO cells (figure 7.2A). To eliminate the possibility that the membrane ruffling was masking potential filopodial activity in these cells, I examined the effect of Rac1N17 on Cdc42V12 induced phenotype. In the presence of Rac1N17, Cdc42V12-induced ruffling is kept to a minimum in both cell types (Figure 7.2D, Lane 7 and 8). A significant increase in filopodia number was observed in the WT cells with Cdc42V12/Rac1N17 (Figure 7.2B; Figure 7.2C, Lane 7). In KO cells, no filopodia were observed despite ruffling activity

### **Figure 7.1 Phenotype of Cdc42V12 in N1E115 cells**

GFP-actin phenotype of N1E115 cells overexpressing Cdc42V12. A typical fan shape spread of thin lamellae and ribs are observed with a directional progression of polymerization. Panel on the right shows the details in DIC channel.  
(Bar = 12  $\mu\text{m}$ )

(Movie 7.1. N1E115 transfected with Cdc42V12 and GFP-actin).



**Figure 7.1**

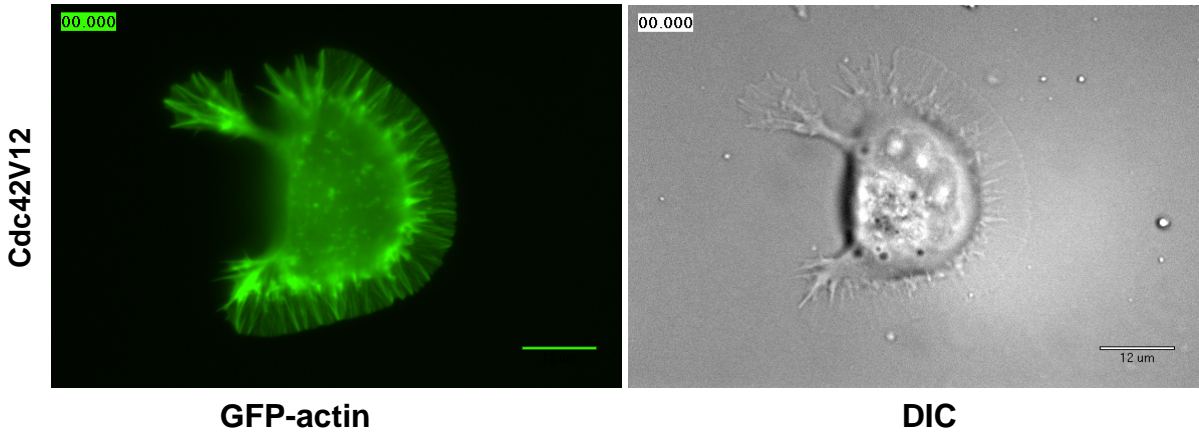


**Figure 7.2 Phenotype of Cdc42V12 in N-WASP WT and KO cells.**

N-WASP WT and KO cells were (A) microinjected with Cdc42V12 cDNA or (B) with Cdc42V12 and Rac1N17 cDNA as per described in Materials and Methods. Cells were left for between 1-6 hours for cDNA expression. Positive cells were imaged using time-lapse microscopy as described in the Material and Methods section. (C and D) Statistical analysis of experiments illustrated in A and B. Cells were scored for protrusions/ruffling and compared to various conditions (refer to section 2.2.6 in Materials and Methods).

(Bar = 10  $\mu$ m)

Figure 7.2

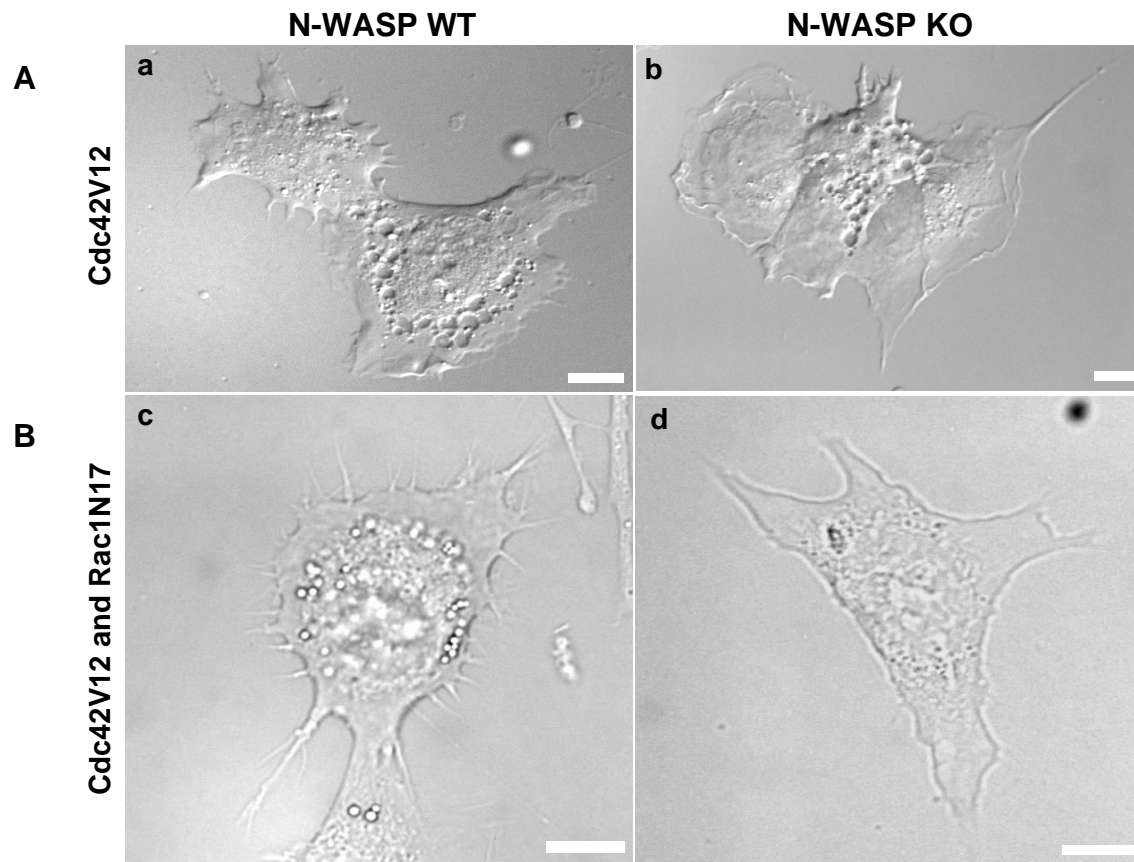
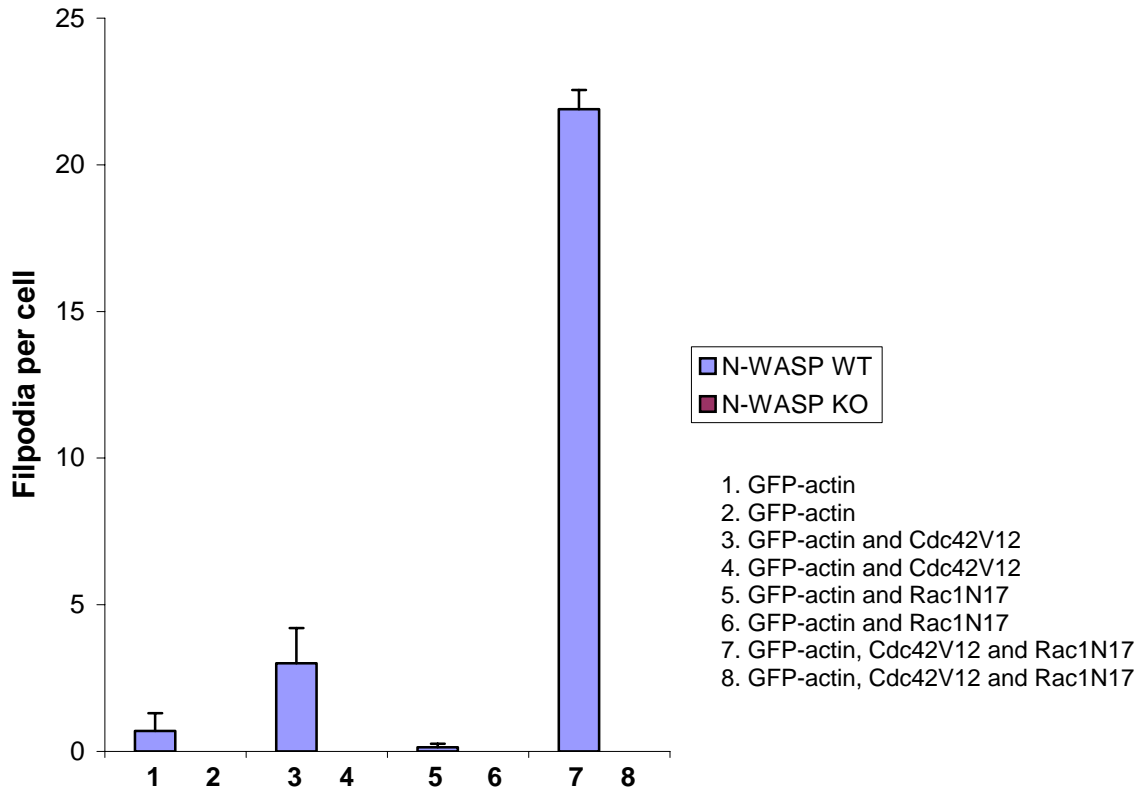
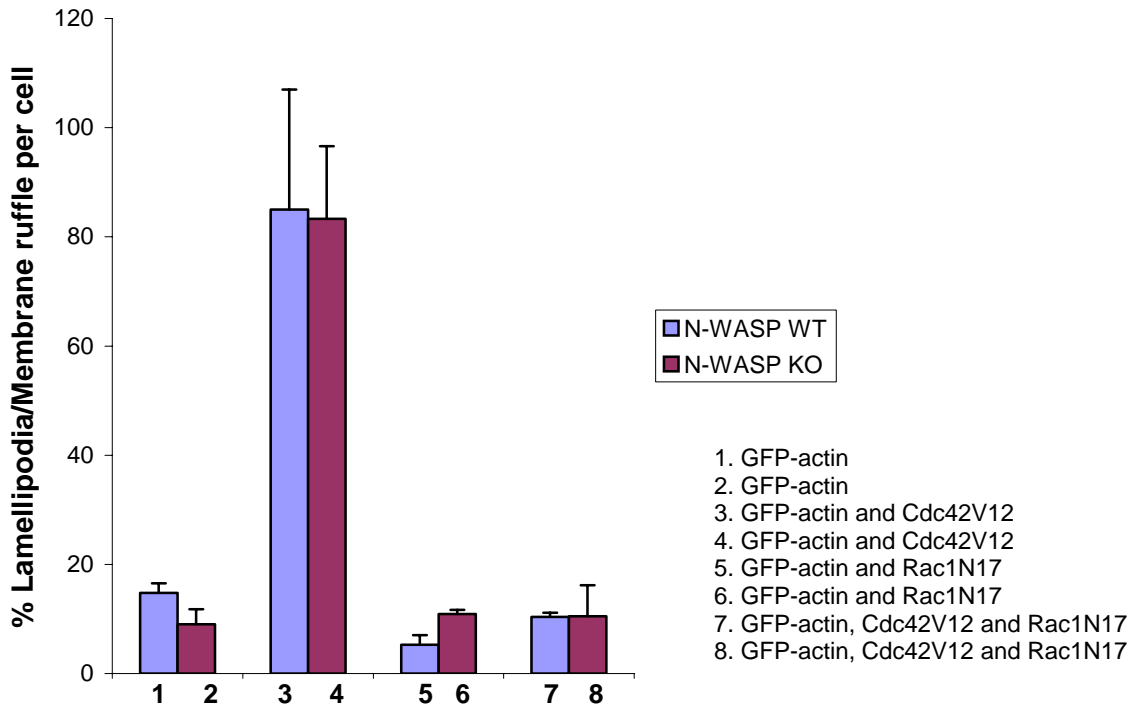


Figure 7.2

C



D



having been reduced significantly by Rac1N17 (Figure 7.2B, panel d; Figure 7.2C, Lane 8). These results suggested that N-WASP is likely to be required for Cdc42-induced filopodia formation.

#### **7. 4. Cdc42 requires N-WASP for filopodia formation.**

In the next set of experiments, I titrated in N-WASP cDNA to the KO cells with Cdc42 V12/Rac1N17 cDNA to carry out reconstitution experiments. N-WASP KO cells microinjected with N-WASP cDNA responded to Cdc42V12/Rac1N17 and filopodia formation was observed (Figure 7.3A). As a control, N-WASP cDNA was titrated into the N-WASP KO cells and time-lapse microscopy was carried out (Figure 7.3B). A ruffling phenotype was observed but no filopodia were detected. Taken together, these results support the idea that N-WASP is essential for Cdc42 driven filopodia formation.

**Figure 7.3 Cdc42V12/Rac1N17 phenotype in N-WASP KO cells with N-WASP reconstitution.**

N-WASP KO cells were microinjected with N-WASP cDNA (100ng/ $\mu$ l)/GFP-actin and with (A) Cdc42V12/Rac1N17 cDNA mix or (B) without. Cells were then left for between 1-4 hours for cDNA expression. GFP-actin positive cells were imaged using DIC time-lapse-microscopy as described in the Material and Methods section. (C,D) Statistical analysis of experiments illustrated in A and B. Cells were scored for the number of filopodia per cell and % lamellipodia/membrane ruffle per cell (refer to section 2.2.6 in Materials and Methods).

(Bar = 10  $\mu$ m)

**Figure 7.3**

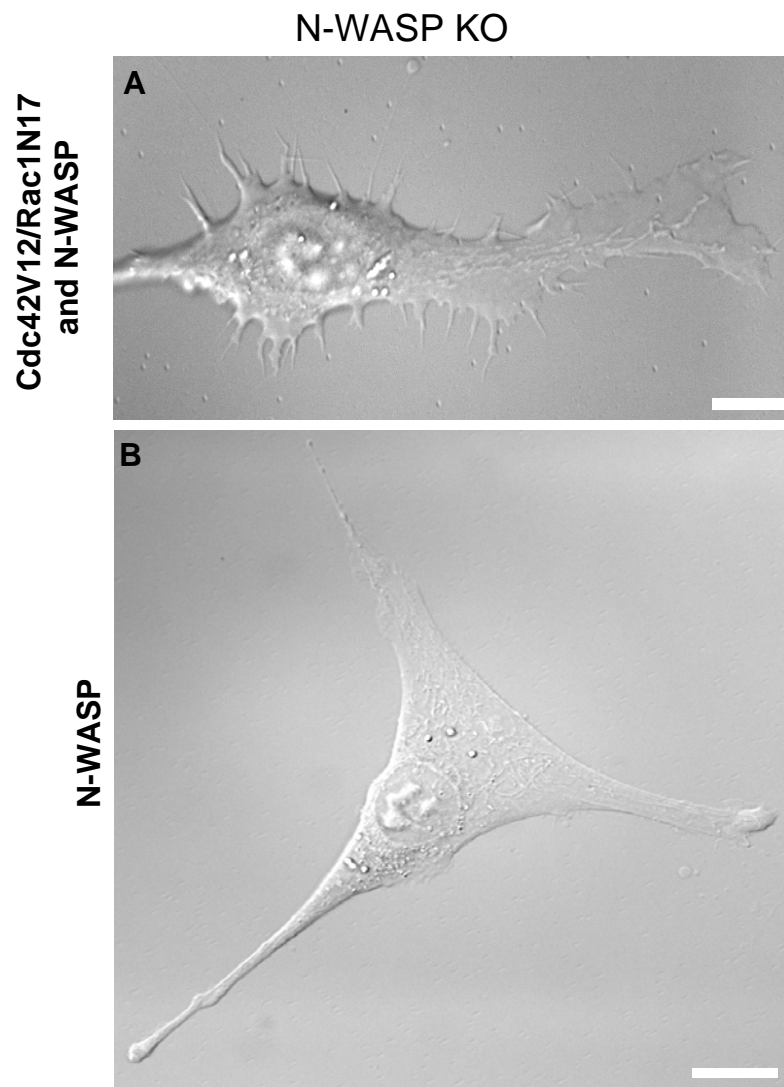
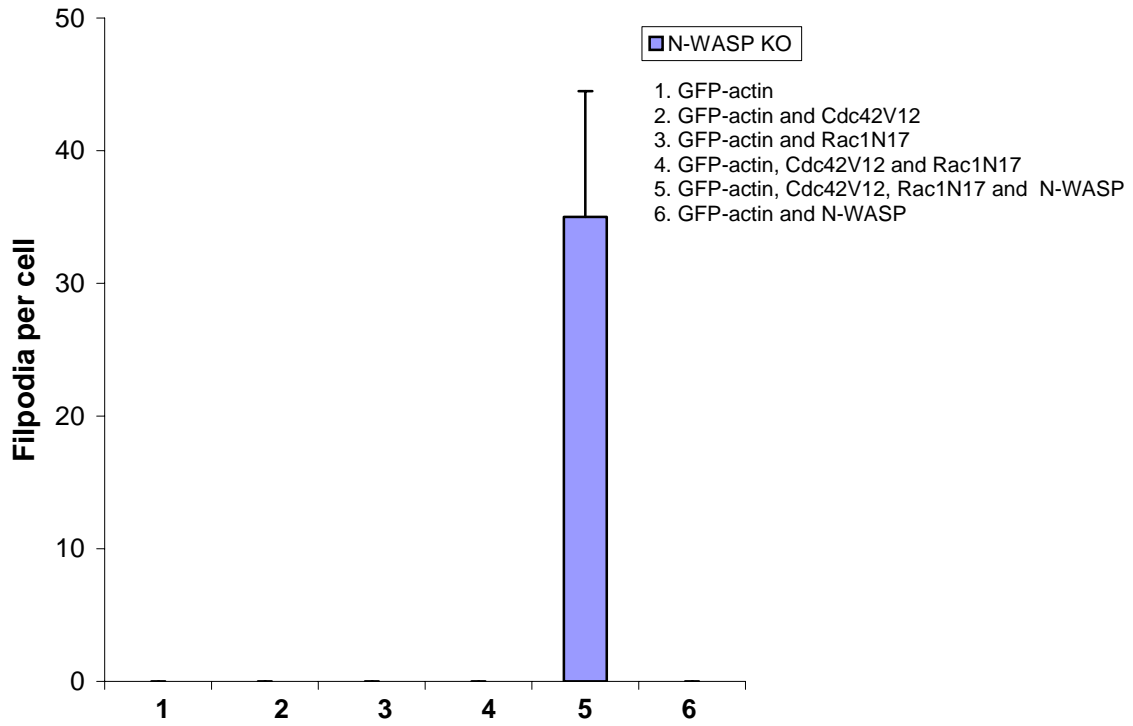
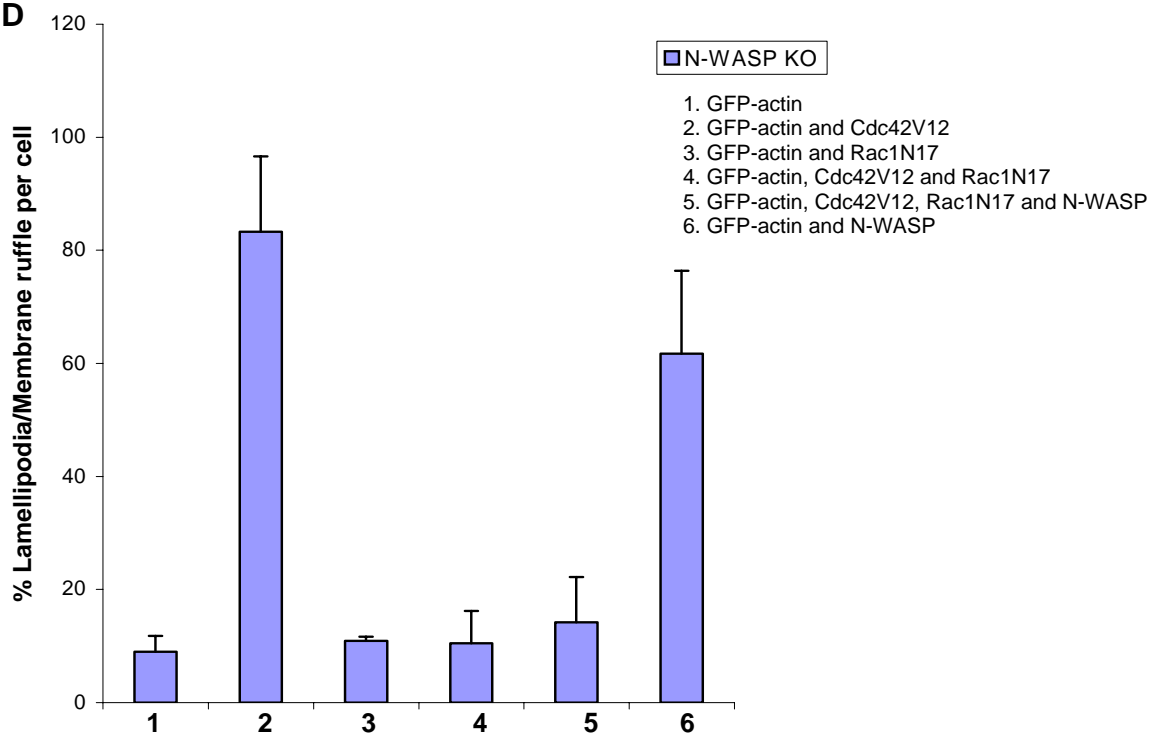


Figure 7.3

C



D





## **Chapter 8. Role of WAVE1, WAVE2 and Mena in IRSp53 induced filopodia formation.**

### **8.1 Introduction.**

WASP/WAVE-and Ena/VASP-family proteins have been reported to regulate the actin cytoskeleton as downstream effectors of the Rho-family small GTPases, Rac1 and Cdc42 (Aspenstrom et. al., 1996; Kolluri et. al., 1996; Miki et. al., 1998; Symons et. al., 1996). These proteins have common binding sites for actin, profilin and Arp2/3 complex (Egile et. al., 1999; Machesky and Insall, 1998, Machesky et. al., 1999; Miki et. al., 1996; Miki et. al., 1998; Rohatgi et. al., 1999; Suetsugu et. al., 1998), but have unique amino acid sequences around their N-terminus. The C-terminal acidic domain of WASP family proteins stimulates the actin filament nucleation activity of Arp2/3 complex (Machesky and Insall, 1998; Rohatgi et. al., 1999). Like N-WASP, WAVE1-3 are ubiquitously expressed in mammalian organs (Miki et. al., 1996; 1998b). Studies have shown that WAVE1 is localized to the lamellipodium edge whereas WAVE2 has been shown to localized to filopodia tips with IRSp53 (Nakagawa et. al., 2001). KO studies on WAVE1 and WAVE2 have suggested that they are responsible for different types of ruffling activity observed in cells (Suetsugu et. al., 2003). Mena belongs to the family of Ena/VASP and has been shown to localize to the tip of lamellipodia and filopodia (Rottner et. al., 1999; Nakagawa et. al., 2001). To further understand the functions of WAVE1, WAVE2 and Mena as binding partners of IRSp53, I used RNAi technology, KO cells and time-lapse microscopy.

## **8.2. Phenotype of WAVE1, WAVE 2 and Mena overexpression in N1E115 cells.**

To analyze the phenotypic effect of WAVE1, WAVE2 and Mena I carried out overexpression studies in N1E115 cells. WAVE1 overexpression induced a phenotype that is relatively flat, with large lamellipodia and small protrusions (Figure 8.1). WAVE2 overexpressing cells possessed multiple short protrusions resembling a potential neuronal phenotype. Overexpression of Mena induced a phenotype where the cells adopt a flattened morphology with short protrusions and many dynamic filopodia decorating the protrusions and cell body (Figure 8.1). Like IRSp53, WAVE1 and Mena induced lamellipodia/membrane ruffling and increases filopodia formation (Figure 8.2B and C). WAVE2 only affected filopodia formation (Figure 8.2 B and C, lane 4). Mena but not WAVE1 and WAVE2 induced neurites (Figure 8.2D).

## **8.3. Localization of WAVE1 and WAVE2 with IRSp53 overexpression in N1E115 cells.**

Both WAVE1 and WAVE2 proteins contain a proline rich region and are thus capable of binding to SH3 domain containing proteins such as IRSp53 (Miki et. al., 2000). IRSp53 phenotype in N1E115 cells is described in Chapter 3. In addition to filopodia, IRSp53 induced membrane ruffling and lamellipodia formation perhaps through interaction with WAVE1 and WAVE2. To examine IRSp53, WAVE1 and WAVE2 interactions in more detail, I carried out immunostaining studies to look at the distribution of the endogenous WAVE1 and WAVE2 in N1E115 cells overexpressing IRSp53.

**Figure 8.1 Phenotypes of WAVE1, WAVE2 and Mena overexpression in N1E115 cells.**

N1E115 cells were transfected with A (a) GFP-WAVE1 and (b) GFP-WAVE2 and (c) GFP-Mena. Cells were then left for between 16-24 hours for cDNA expression. GFP positive cells were imaged using DIC time-lapse-microscopy as described in the Material and Methods section. (B, C and D) Statistical analysis was carried out on experiments illustrated in a-c. Cells were scored for the number of filopodia per cell, % lamellipodia/membrane ruffle per cell and neurites (refer to section 2.2.6 in Materials and Methods).

(Bar = 10  $\mu$ m)

Figure 8.1

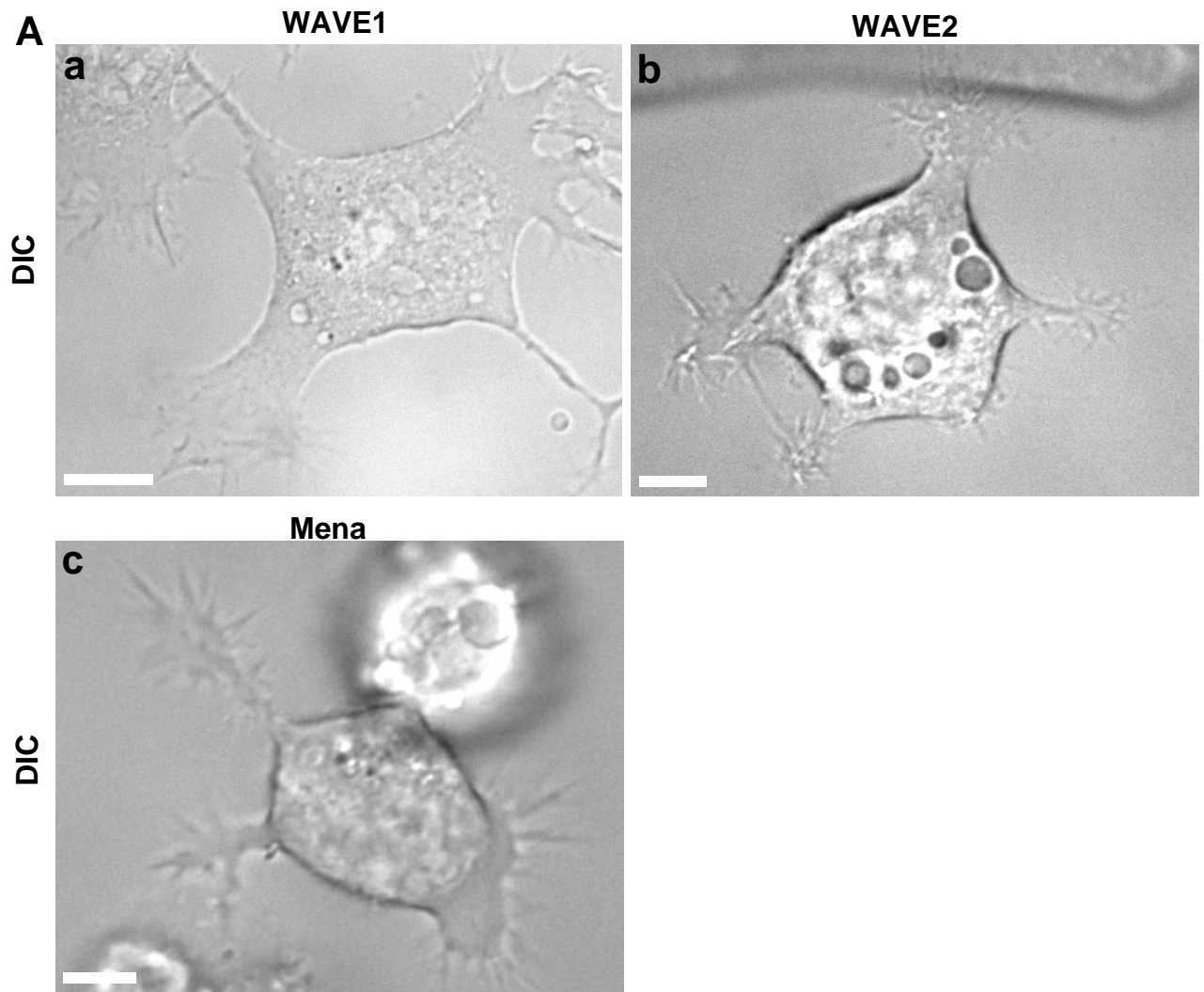
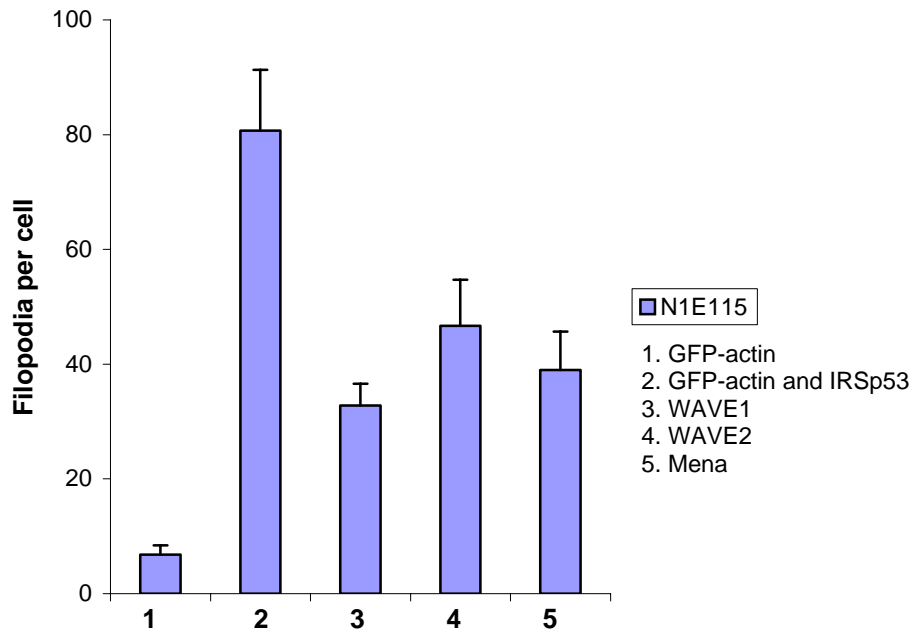
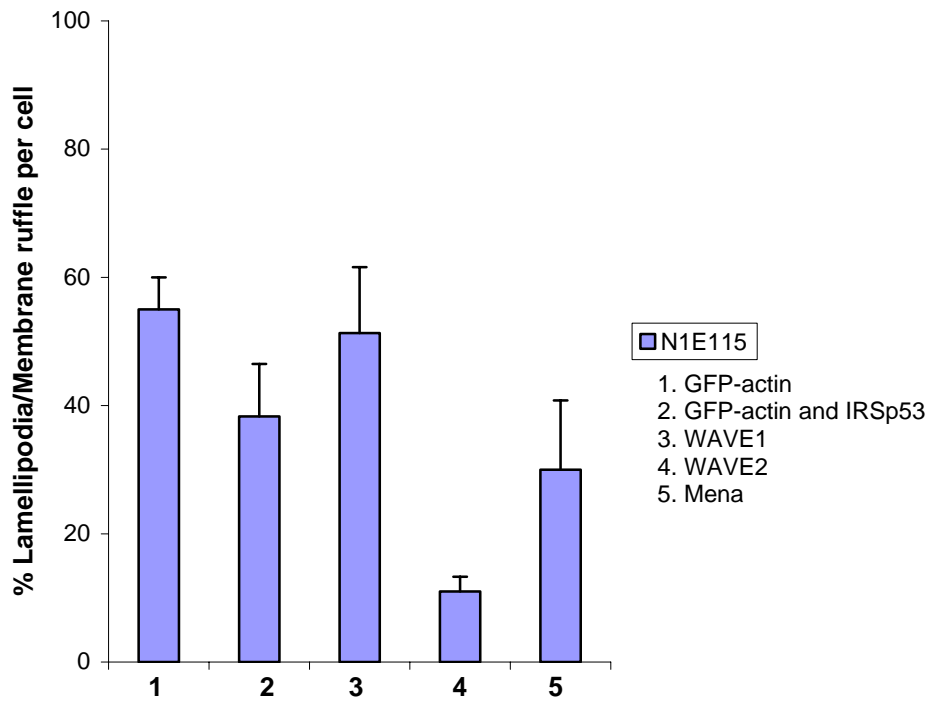


Figure 8.1

B

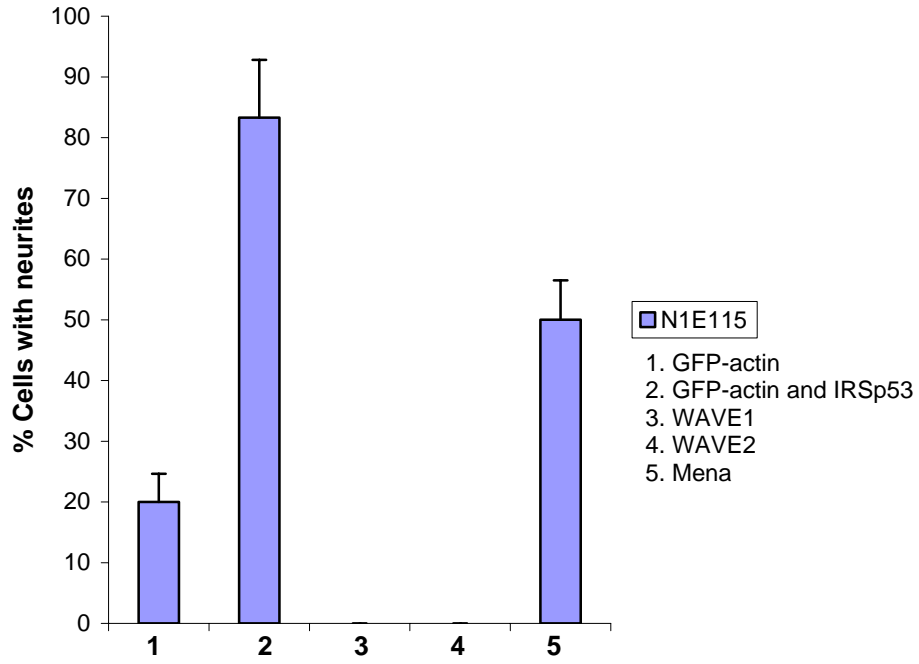


C



**Figure 8.1**

**D**



WAVE1 was observed to be distributed throughout the cell body and along the neurites. But most strikingly, WAVE1 is highly concentrated along the edges of extending lamellipodia (Figure 8.2). WAVE2 was observed to be highly concentrated in the cell body and distributed along the length of neurites. It also appears to be localized to tips of some filopodia (Figure 8.2C and D).

#### **8.4. Effect of WAVE1 and WAVE 2 knockdown on IRSp53 phenotype in N1E115 cells.**

In order to examine the functional consequences of the IRSp53-WAVE1/2 interaction, I employed the use of RNAi. WAVE1 and WAVE2 RNAi were delivered into N1E115 cells by co-transfection with IRSp53 and GFP-actin cDNA as described in the Materials and Methods section. Knock down was assessed by intensity of WAVE1 and WAVE2 staining in GFP-actin positive cells (Figure 8.3). In WAVE1 knockdown cells, IRSp53 induced a phenotype of branching neurites with filopodia seen along the length of the neurite. However, no ruffling or lamellipodia were observed (Figure 8.4). In WAVE2 knockdown cells, IRSp53 did not induce neurite formation. In place were short stumps or extensions. Ruffling, lamellipodia and filopodia formation do not seem to be affected by WAVE2 knockdown (Figure 8.4). As a control, a scramble RNAi transfection was also carried out. Normal IRSp53 phenotypes were observed in these cells, confirming that the distinct phenotypes observed with the WAVE1/2 RNAi knockdown were specific (Figure 8.4).

**Figure 8.2 Localization of WAVE1 and WAVE2 in IRSp53 overexpression N1E115 cells.**

Cells were transfected with HA-IRSp53 and GFP-actin, and were then fixed and stained with (A) anti-WAVE1 and (B) anti-WAVE2 antibodies See Materials and methods for details. (C, D) Areas of the cells enlarged to allow localization of WAVE1 and WAVE2 to be determined. C (a-c, d-f) WAVE1 localization in the lamellipodia and (g-i) filopodia. D(a-c) WAVE2 localization in the lamellipodia and (d-f, g-i) in filopodia.

(Bar = 10  $\mu$ m)



Figure 8.2

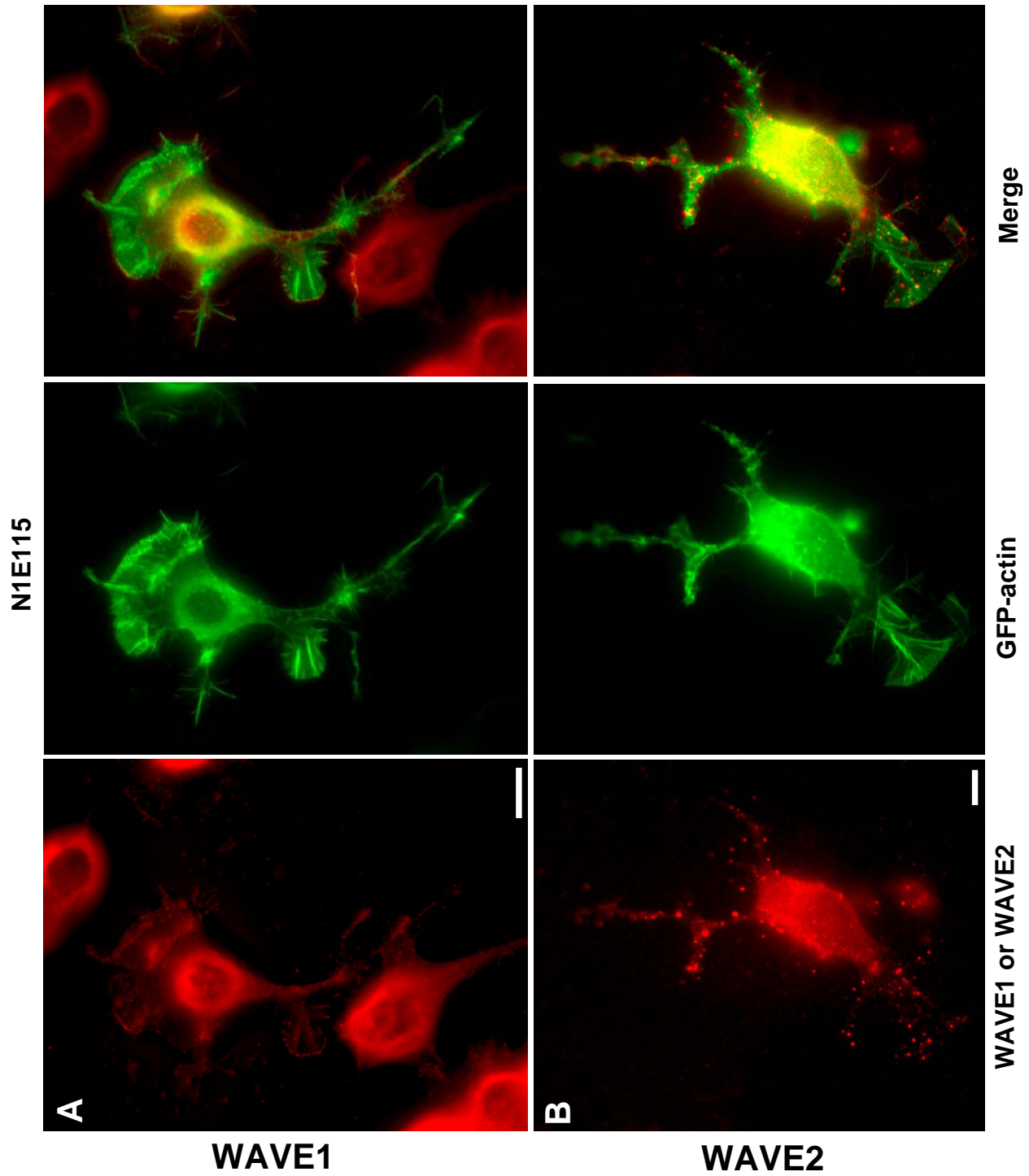
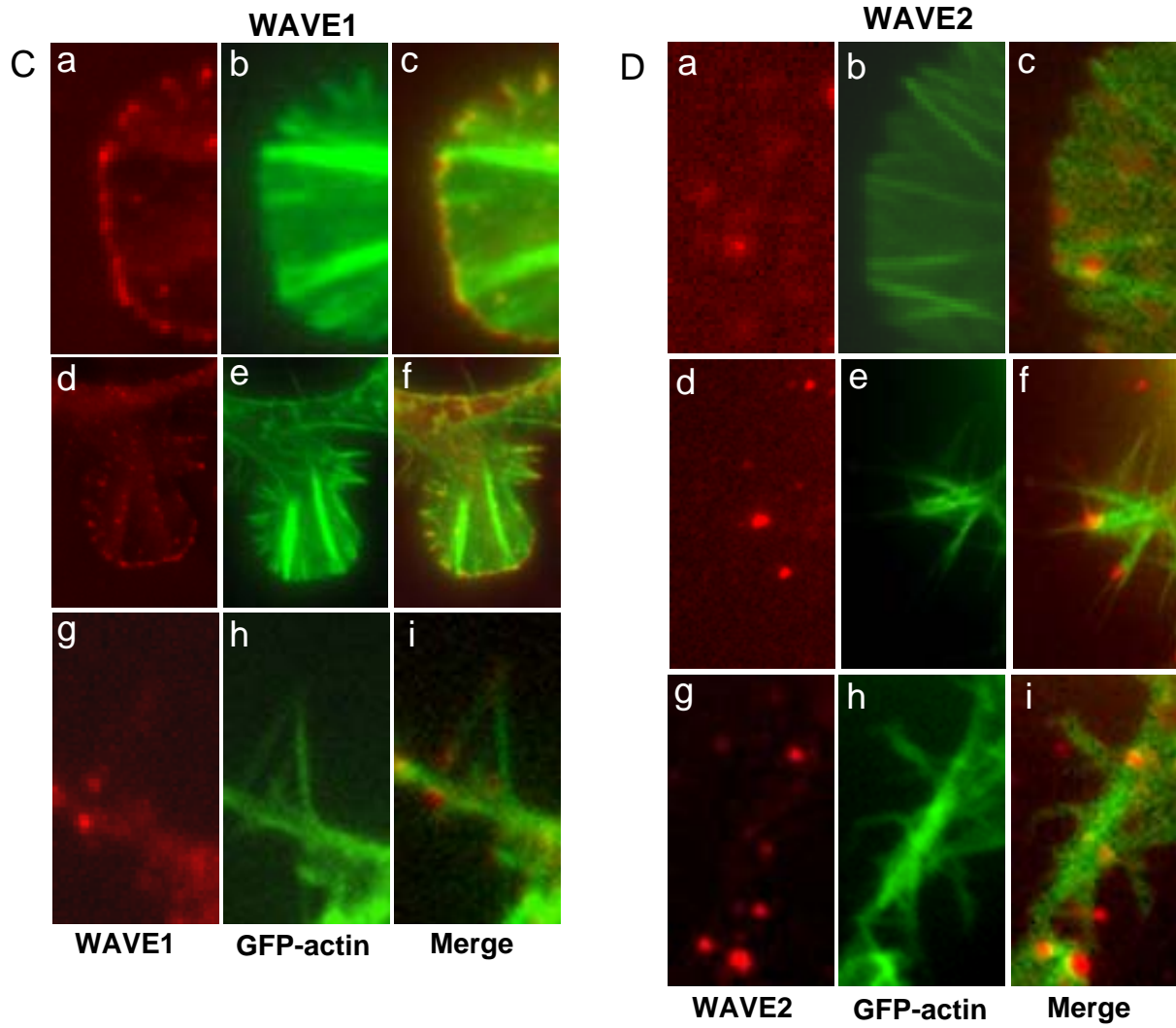


Figure 8.2



**Figure 8.3 Effect of WAVE1 and WAVE2 RNAi treatment on IRSp53 induced morphology.**

Cells were transfected with HA-IRSp53 and GFP-actin and (a,b,c) WAVE RNAi or (d,e,f) WAVE2 RNAi. (a,d) WAVE1/2 expression. (b,e) GFP-actin expression and (c, f) Merge. Cells were left for between 20-24 hours for RNAi/cDNA expression and were then fixed and stained with (a,b,c) anti-WAVE1 and (d,e,f) anti-WAVE2.  
(Bar = 10  $\mu$ m)

Figure 8.3

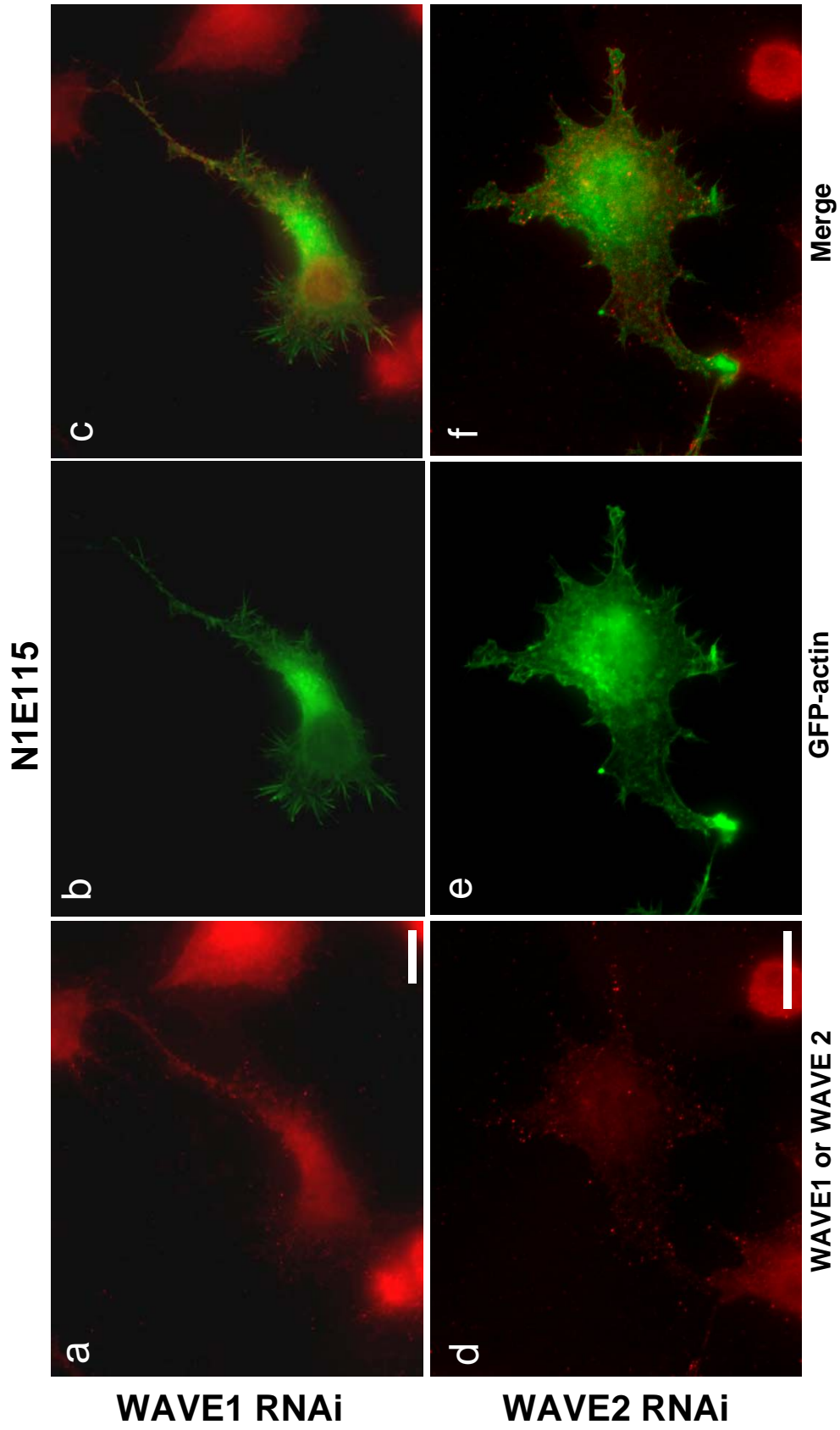


**Figure 8.4 Effect of WAVE1 and WAVE2 knockdown on IRSp53 phenotype.**

N1E115 cells were transfected with HA-IRSp53 and GFP-actin and (a, a') WAVE1 RNAi, (b,b') WAVE2 RNAi and (c,c') scramble RNAi. (A) GFP-actin and (B) DIC. Cells were then left for between 20-24 hours for RNAi/ cDNA expression. GFP-actin positive cells were imaged using fluorescence and DIC time-lapse-microscopy as described in the Materials and Methods section. (C, D and E) Statistical analysis was carried out on experiments illustrated in a-c. Cells were scored for the number of filopodia per cell, % lamellipodia/membrane ruffle per cell and neurites (refer to section 2.2.6 in Materials and Methods).

(Bar = 10  $\mu$ m)

(Movie 8.4.1. N1E115 transfected with IRSp53 and WAVE1 RNAi).

(Movie 8.4.2. N1E115 transfected with IRSp53 and WAVE2 RNAi).

(Movie 8.4.3. N1E115 transfected with IRSp53 and scramble RNAi).

Figure 8.4

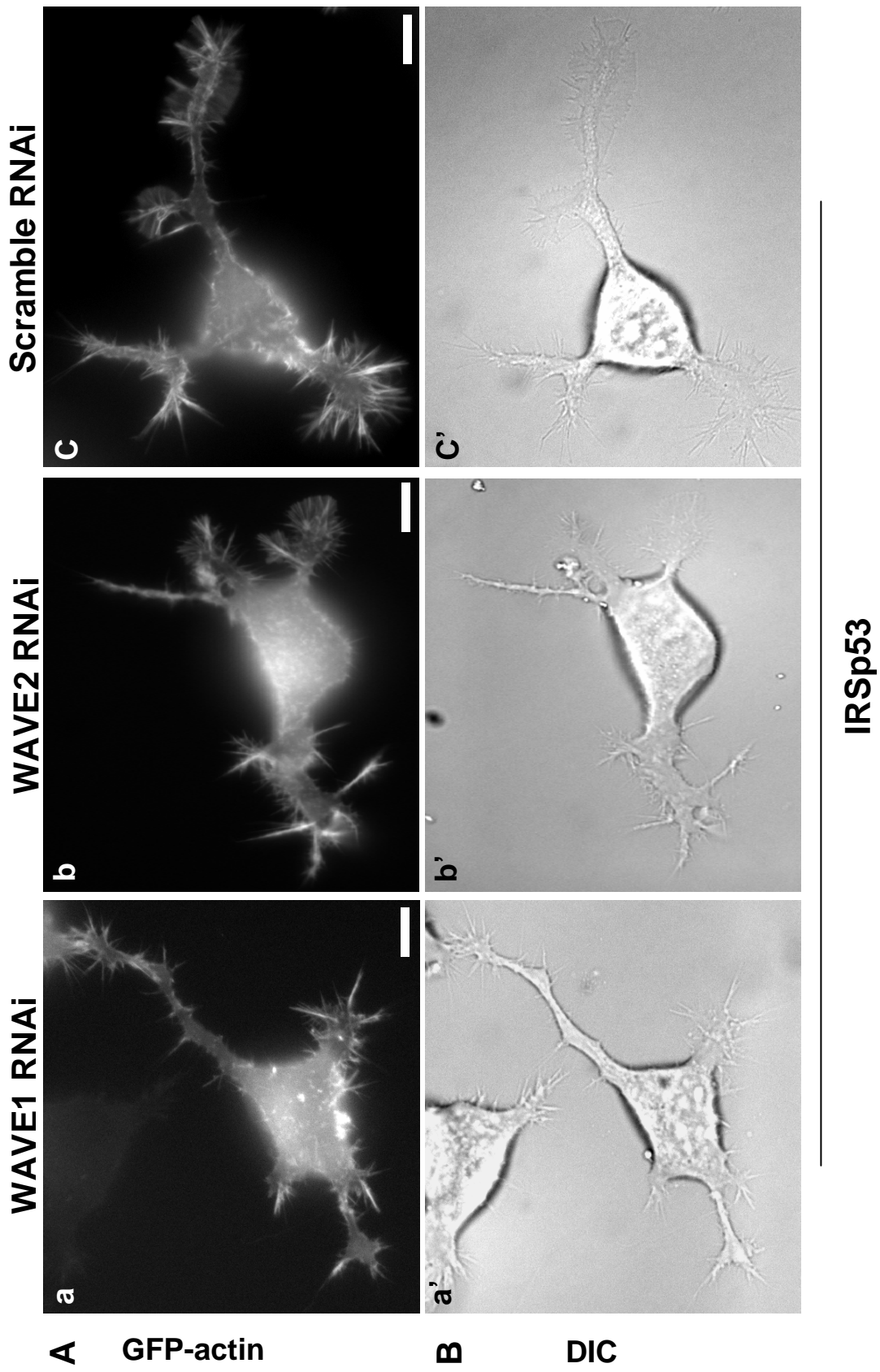
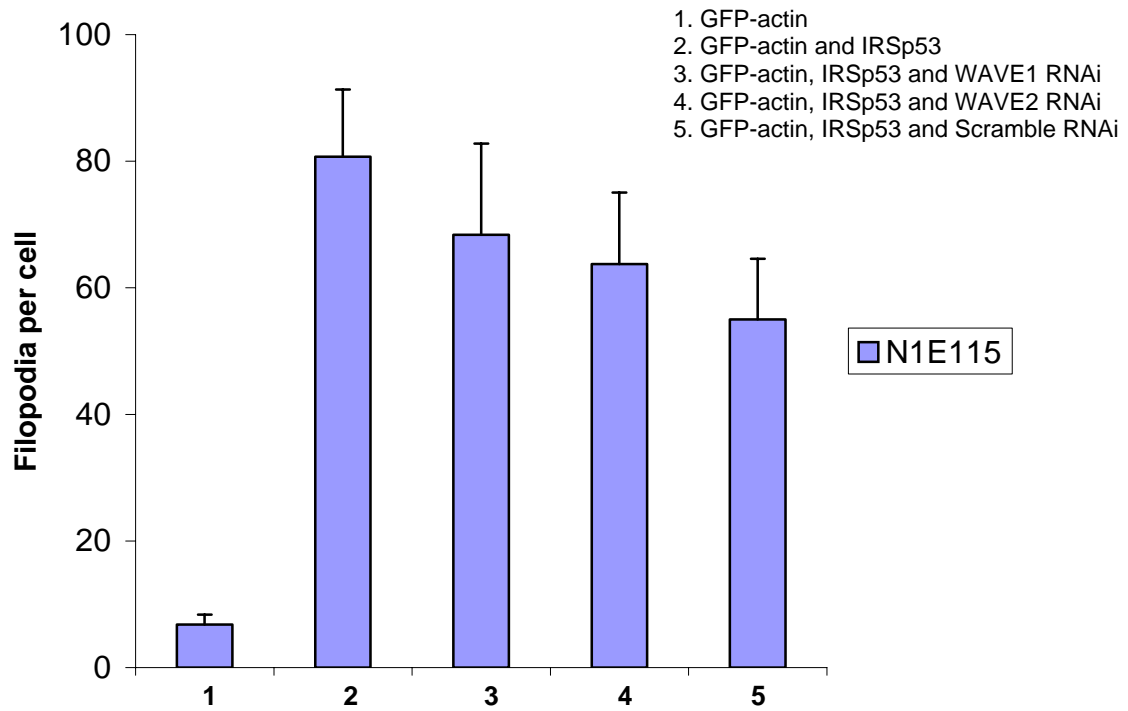
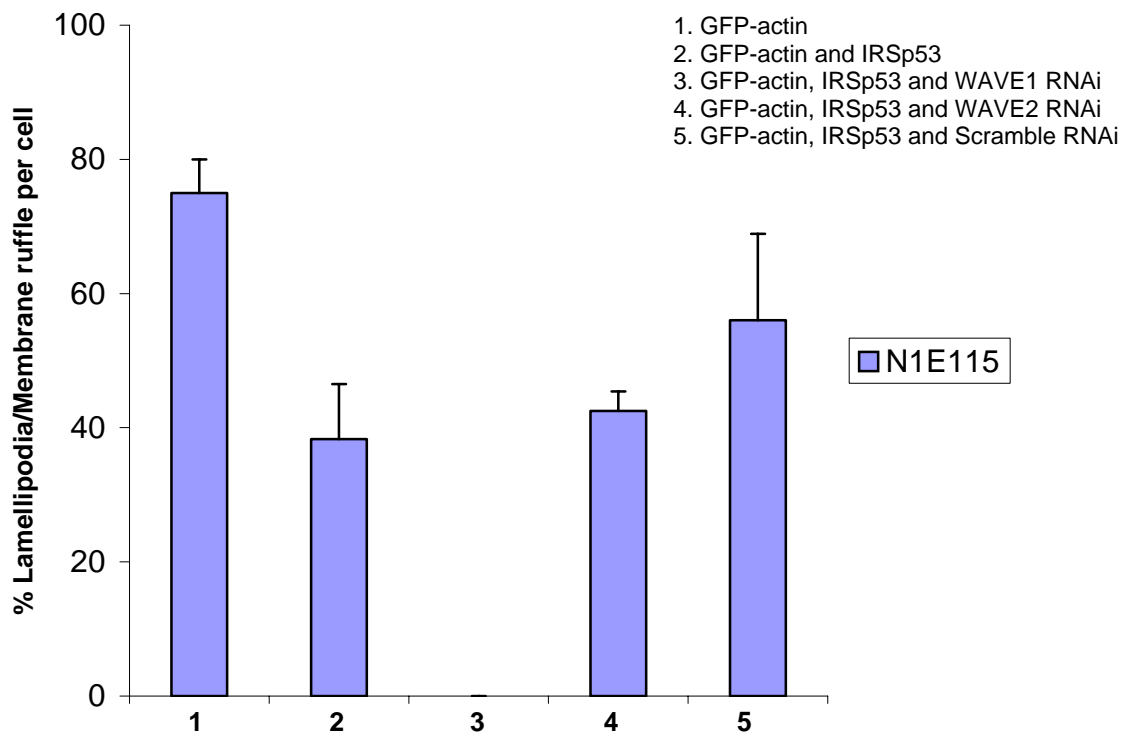


Figure 8.4

C

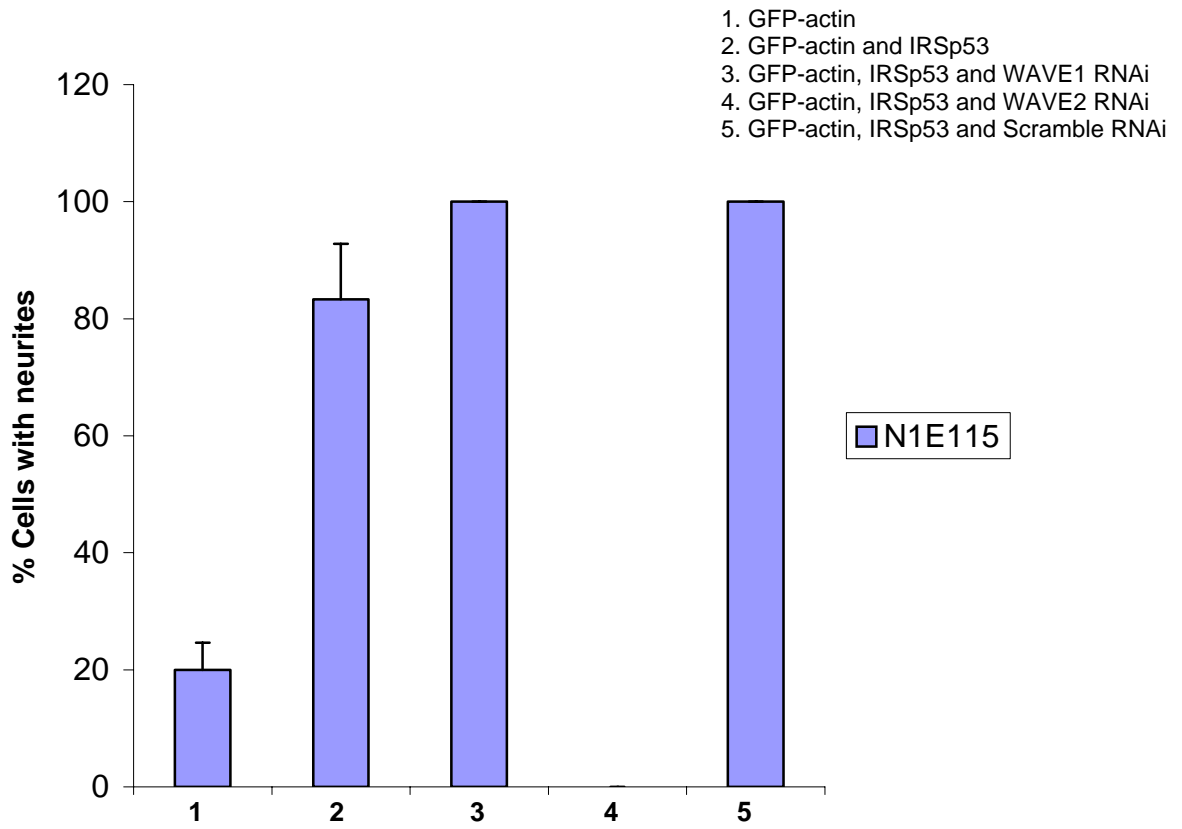


D



**Figure 8.4**

**E**





### **8.5. IRSp53 Phenotype in Mena KO cells.**

The IRSp53-Mena complex has been shown to represent one pathway by which IRSp53 induced filopodia can be derived (Krugmann et. al., 2001). I have shown that IRSp53 induced filopodia requires N-WASP. To determine if Mena too is required for IRSp53 function, I employed the use of Mena control precursor (WT) and Mena knock-out (KO) cells (for details of Mena WT and KO cells see Materials and Methods).

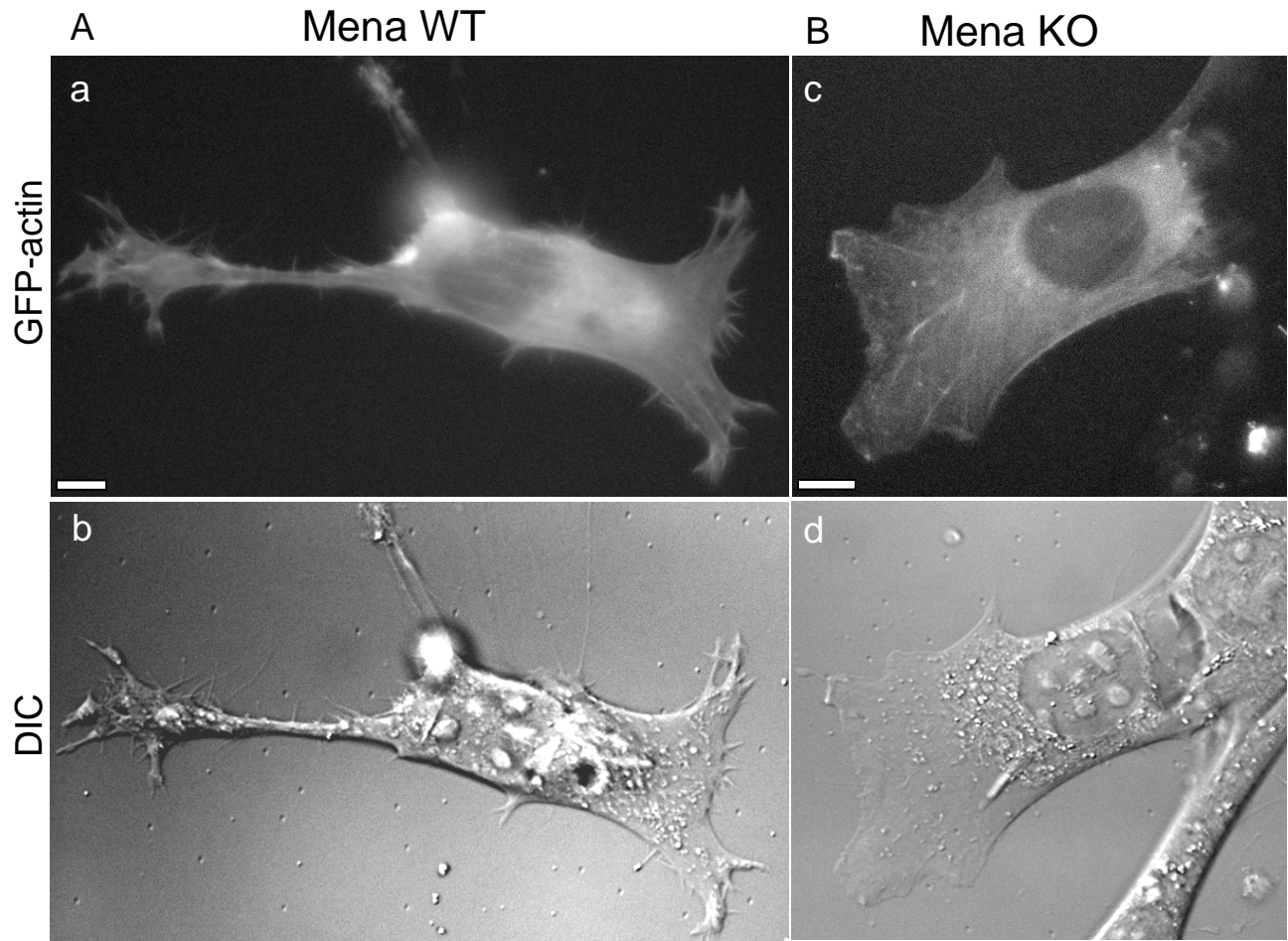
I compared the effect of IRSp53 cDNA microinjection on the morphology of the Mena WT and KO cells. GFP-actin cDNA was included in the microinjection to identify expressing cells and to facilitate the imaging of actin dynamics (Figure 8.5). When cells were injected with GFP-actin cDNA alone, there were no morphological differences between the WT and KO cells . IRSp53 induced strong filopodia formation in Mena WT and causes the formation of neurite-like extensions (Figure 8.5C and D). However, membrane ruffling formation was strongly stimulated when IRSp53 was overexpressed in Mena KO cells (Figure 8.5D). These results are very similar to those observed in N-WASP WT and KO cell lines and suggest that Mena, together with N-WASP are essential for the IRSp53 induced filopodia formation.

**Figure 8.5 IRSp53 phenotypes in Mena WT and KO cells.**

(A) Mena WT and (B) Mena KO cells were microinjected with IRSp53 and GFP-actin cDNA. Cells were left for between 1-6 hours for cDNA expression. Positive cells were imaged using fluorescence and DIC time-lapse-microscopy as described in the Material and Methods section. Images showing time-lapse experiments of GFP-actin/IRSp53 microinjection in WT cells (A) and Mena KO cells (B). (C and D) Statistical analysis was carried out on experiments illustrated in A and B. Cells were scored for the number of filopodia per cell and % lamellipodia/membrane ruffle per cell (refer to section 2.2.6 in Materials and Methods).

(Bar = 10  $\mu$ m)

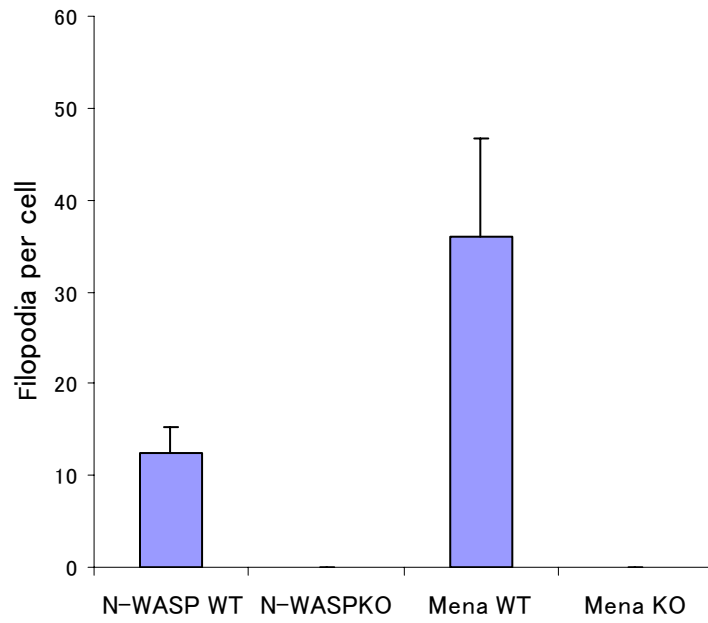
**Figure 8.5**



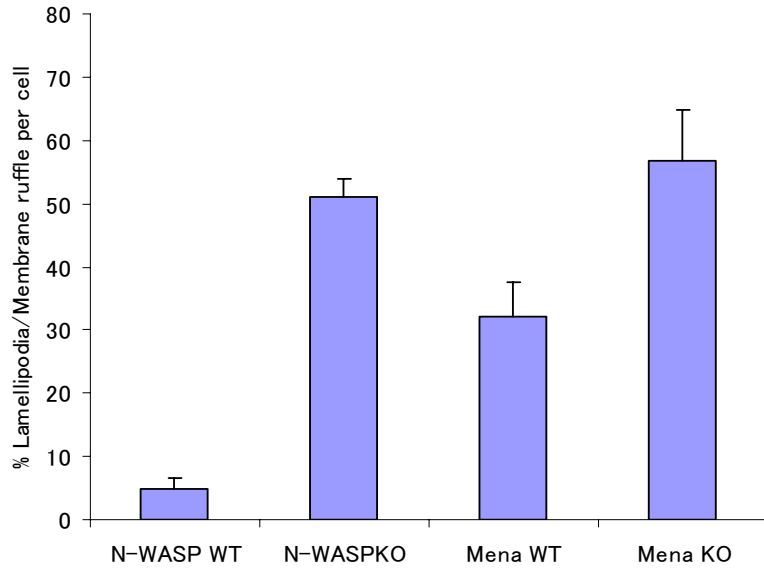
**IRSp53 and GFP-actin**

**Figure 8.5**

**C**



**D**



# **DISCUSSION**

## **9. DISCUSSION**

### **9.1. Are all protrusive structures filopodia?**

F-actin based filopodia are well conserved morphological structure at the periphery of mammalian cells. In particular, neurons have prominent filopodia in their growth cones and these structures are thought to help axons find their targets (Chien et. al., 1993). Filopodia are constructed from parallel bundles of F-actin that lie perpendicular to the cell periphery. Mammalian cells form a number of structures that resemble filopodia. For example, retraction fibres protrude from the cell periphery and have similar overall dimensions to filopodia. However, retraction fibres are tapered while filopodia have uniform thickness along their length. The length of filopodia varies between 6-15  $\mu\text{M}$  in mammalian cells. Retraction fibres are static structures while filopodia are highly dynamic and are characterized by a half-life of approximately 120-170 secs. To distinguish filopodia from other cell protrusions it is essential to compare physical characteristics and to use time-lapse analysis.

### **9.2. Cdc42 effectors in filopodia formation and Rac1 activation.**

The observation that Cdc42 plays a major role in the formation of filopodia and Rac1-dependent lamellipodia/membrane ruffles (as a secondary event) has opened avenues to study mechanisms of cell migration and growth cone guidance (Kozma et. al., 1995; Nobes and Hall, 1995). Cdc42 binds to a number of effectors, including the kinases, PAK, ACK and MRCK, and the adaptor proteins, IQGAP, PAR6, N-WASP and IRSp53 (see Bishop and Hall, 2000, for list of effectors). Of these effectors there is strong evidence

for involvement in filopodia formation only for the latter two (Miki et. al., 1998; Govind et. al., 2001 and Krugmann et. al., 2001).

### **9. 3. IRSp53 phenotype in N1E115 cells.**

Since the identification IRSp53 was initially reported, its specific function has been debated. In the present study I used a time-lapse analysis with GFP-actin and tdRed-IRSp53 overexpression to study IRSp53 function. N1E115 transfected cells developed complex and branched neurites comprising of multiple filopodia, lamellipodia and membrane ruffles. These phenotypes were not seen in untransfected cells or cells transfected with a range of other Cdc42 effectors such as ACK, PAK or MRCK (Sarner et. al., 2000; Ahmed, S., unpublished data). Two typical phenotypes of IRSp53 overexpressing cells were either large lamellipodia with prominent ribs or cells with branched neurites decorated with areas of membrane ruffling, lamellipodia and filopodia. With N1E115 cells membrane ruffling was not a prominent phenotype of IRSp53 overexpression. IRSp53 localizes most significantly with F-actin to the ribs of lamellipodia-like protrusions and filopodia. IRSp53 is poorly localized to membrane ruffles.

### **9. 4. IRSp53 SH3 domain function.**

The SH3 domain of IRSp53 is clearly important in the morphological activities of this molecule. Using mutants of the SH3 domain (W/R and FP/AA mutants) that were unable to bind to its ligands, I was able to show that the SH3 domain of IRSp53 is important for induction of neurite complexity (which includes filopodia and lamellipodia formation).

The double point SH3 domain mutant of IRSp53-FP/AA, which was null for filopodia formation, was nevertheless able to induce neurites and some lamellipodia suggesting that the SH3 domain is not essential for these morphological activities. The binding of Tiam1 to IRSp53 near its partial CRIB motif may explain the phenotypes obtained with SH3 domain mutants.

Yamagishi et. al., (2004) and Millard et. al., (2005) have suggested that the SH3 domain is not essential for filopodia formation and that the N-terminal IMD domain is sufficient. Since time-lapse analysis was not documented in these studies it is difficult to interpret the data presented. I believe the SH3 domain-independent structures described in these studies are not filopodia. However, the data presented do suggest that IRSp53 through the IMD domain is capable of generating protrusions (see below for further discussion on the IRSp53 IMD).

To search for SH3 domain binding proteins, Mass Spectrometry analysis using the IRSp53 SH3 domain as a bait was carried out and a number of candidate proteins were isolated. These include p140-Sra-1, KIAA1681, mDia1, CR-16, Abi1 and N-WASP (for complete analysis, see Results Chapter 4.2) The analysis suggested that N-WASP can bind the SH3 domain of IRSp53 and this was confirmed in both pull-down experiments, yeast two-hybrid analysis and AP-FRET *in vivo*. For the first time I show N-WASP and IRSp53 interact in filopodia and filopodial tips. Thus N-WASP is a not only a bona fide target for IRSp53 *in vivo* but also in the right place. These results reveal the additional



insights obtained from AP-FRET versus more traditional immuno-precipitation experiments.

### **9. 5. IRSp53 phenotypes in N-WASP KO cells**

Mutations in the Cdc42 binding site (Govind et. al., 2001) and the SH3 domain (Krugmann et. al., 2001; present study) significantly affect the ability of IRSp53 to induce filopodia formation. I have identified N-WASP as a candidate IRSp53 SH3 domain binding partner. Taken together, these results suggest that the Cdc42-IRSp53-N-WASP complex is important for filopodia formation. To investigate the role of the Cdc42-IRSp53-N-WASP interaction I employed the use of N-WASP KO fibroblasts. Overexpression of IRSp53 in control fibroblasts N-WASP WT induced strong filopodia formation. However, in N-WASP KO cells overexpression of IRSp53 induced strong membrane ruffling and filopodia were not observed. The possibility that the membrane ruffling was masking filopodia formation in KO fibroblasts was addressed by using IRSp53 in combination with Rac1N17. In N-WASP WT cells the IRSp53 filopodia response was enhanced by using Rac1N17, however, in KO cells filopodia were still not observed.

To determine if N-WASP KO cells were capable of generating filopodia I carried out reconstitution experiments. N-WASP cDNA was included with IRSp53 in the injection/transfection of N-WASP KO cells and filopodia formation was observed. To extend this analysis I carried out the reconstitution with the mutant, N-WASP $\Delta$ WA, which is unable to bind the Arp2/3 complex. N-WASP $\Delta$ WA was fully competent to

reconstitute filopodia formation. The filopodia generated by N-WASP $\Delta$ WA were similar to those generated by N-WASP apart from the rates of disassembly. The slower the disassembly rates seen with N-WASP $\Delta$ WA may be caused by changes in actin depolymerization. Further work examining actin polymerization rates will be required to resolve this issue. These results suggest that the role of N-WASP in IRSp53 mediated filopodia formation is not to recruit the Arp2/3 complex but perhaps other interacting N-WASP proteins are important, e.g. the N-WASP interacting protein, WIP (Ho et. al., 2001). To address this latter point I used WAVE1 and WAVE1 $\Delta$ WA in reconstitution experiments and found that both allowed IRSp53 to induce filopodia in N-WASP KO cells. In addition, I found that the IRSp53 mutant FP/AA could not substitute for IRSp53 in the reconstitution experiments. I conclude that N-WASP interaction with the SH3 domain of IRSp53 is essential for filopodia formation. Further, the role of N-WASP is not to activate the Arp2/3 complex or recruit other interacting proteins. Rather it is to bind to the IRSp53 SH3 domain and perhaps facilitate an “open conformation” (see Model, Figure 9.2).

#### **9.6. The role of IRSp53 IMD in filopodia formation.**

Recent work by Scita’s group (Disanza et. al., 2006) has proposed a model for IRSp53 mediated filopodia formation. They suggest that Eps8 binding to IRSp53 reveals the IMD domain and activates F-actin bundling while Cdc42 recruits the IRSp53-Eps8 complex to the membrane. Interestingly, Eps8 alone was found to have F-actin bundling activity. Like the previous two studies on IRSp53 F-actin bundling activity (Yamagishi et. al., 2004; Millard et. al., 2005), Disanza et. al., (2006) failed to show any *in vivo* time-lapse

experiments on filopodia formation making it difficult to interpret these studies. Further, the amounts of IRSp53 needed to bundle F-actin are approximately 50-fold higher than well-established F-actin bundling proteins such as Fascin. Under physiological conditions it is unlikely that cellular concentrations of IRSp53 will reach the levels required for F-actin bundling.

I overexpressed the GFP-actin and the IMD domain in cells and monitored morphological activity by timelapse microscopy. Interestingly, a variety of protrusive structures were seen. Firstly, protrusive structures containing actin similar to that already reported (Yamagishi et. al., 2004; Millard et. al., 2005) were observed. However, these were static. Secondly, IMD also induced protrusive structures that are either dynamic or static but lacked actin. The IMD induced structures lacking actin were thinner and shorter than filopodia. The IMD-4K mutant, which has reduced efficiency in F-actin binding and bundling, only induced dynamic structures lacking actin. Thus the IMD has at least two activities, it is able to cause membrane protrusion (4K mutant) and can link to F-actin changes. I conclude that IMD generates “partial filopodia” but is not capable of generating complete filopodia.

Unlike IRSp53, IMD was not sensitive to the presence of N-WASP. Similar protrusive structures were generated by the IMD in both N-WASP WT and KO cells. This is not unexpected since I have already shown that IRSp53 SH3 domain is essential for its interaction with N-WASP.

### **9.7. Cdc42 does not induce filopodia in N-WASP KO cells.**

The original study on N-WASP KO cells investigating the ability of Cdc42 to generate filopodia concluded that N-WASP was not required (Lommel, et.al., 2001). However, Cdc42 alone was not used in this work. DIC time-lapse experiments were carried out after microinjection of Cdc42L61 protein with Rac1N17 protein and C3 toxin. I repeated these experiments but the combination of Cdc42V12/Rac1N17/C3 caused cell retraction, blebbing and death. To address the issue of whether Cdc42 could induce filopodia in N-WASP KO cells I compared Cdc42V12 and Cdc42V12/Rac1N17 transfections. Using Cdc42V12 alone in either N-WASP WT or KO cells generate membrane ruffling and lamellipodia formation with few visible filopodia. However, with the Cdc42V12/Rac1N17 combination filopodia could be clearly seen in N-WASP WT but not in N-WASP KO cells, while membrane ruffling/lamellipodia formation was reduced significantly in both cell types.

To confirm that N-WASP KO cells were capable of generating filopodia I reconstituted the cells with N-WASP cDNA and found that Cdc42V12/Rac1N17 was able to induce filopodia formation in these cells. I conclude that N-WASP is essential for Cdc42 induced filopodia formation. One possible explanation for the results reported by Lommel et. al., 2001, is that C3 toxin, a RhoA inhibitor, may induce dissociation of a RhoA-mDia2 complex making mDia2 available for Cdc42. The Cdc42-mDia2 may be sufficient to drive filopodia formation in N-WASP KO cells. Peng et. al. (2003) has shown that depletion of Drf3 (mDia2) could interfere with and block Cdc42 induced filopodia. Drf3 was also reported to contain a previously unidentified CRIB-like motif

within its GTPase binding domain (GBD). This motif was shown by FRET analysis to be required for Cdc42 binding and Drf3 recruitment to the leading edge. These results suggested that Cdc42-mDia2 is another candidate pathway leading to filopodia formation.

### **9. 8. Relationship between IRSp53 and WAVE1, WAVE2 and Mena.**

IRSp53 binding partners include WAVE1, WAVE2 and Mena. What role, if any, do these proteins play in the IRSp53 phenotype? To address this question I overexpressed these proteins in N1E115 cells and followed changes in morphology by time-lapse microscopy. WAVE1 overexpression induced a phenotype that is relatively flat and with large lamellipodia protrusions and small extensions while cells overexpressing WAVE2 adopt a neuronal phenotype, with multiple short extensions. Mena, WAVE1 and WAVE2 induced a significant number of filopodia. Mena and WAVE1 induce lamellipodia/membrane ruffling but not WAVE2.. WAVE1 and WAVE2 did not induce neuritis while Mena did.

Next I used IRSp53 overexpression in combination with RNAi for WAVE1 and WAVE2 and Mena KO cells to determine whether these proteins were required for the IRSp53 phenotype. The RNAi was able to reduce expression of WAVE1/2 protein at the single cell level as seen by reduced in situ staining. I selected cells that had the greatest reduction in WAVE1/2 expression and examined their phenotype. Neither RNAi affected IRSp53 induced filopodia formation. However, the WAVE1 RNAi affected lamellipodia/membrane ruffling while WAVE2 RNAi affected neurite formation.

### **9. 9. Relationship between IRSp53 and Mena.**

IRSp53 failed to induce filopodia in Mena KO cells. This result extends data initially presented by Krugmann, et. al. 2001, identifying Mena as an IRSp53 binding partner and a protein that synergizes with IRSp53-mediated filopodia formation.

### **9. 10. Is IRSp53 a Cdc42 or Rac1 effector?**

Takenawa's group initially reported that IRSp53 is a Rac1 binding protein and an essential mediator of membrane ruffling via WAVE2 (Miki et. al, 2000). In a follow-up paper it is suggested that Rac1 binding to the N-terminus of IRSp53 (RCB domain, 1-226) is stimulated by unfolding of the protein and WAVE2 interaction (Miki and Takenawa, 2002). Attempts to confirm direct Rac1 binding to N-terminus of IRSp53 have been unsuccessful (Govind, S., and Ahmed, S., unpublished data). Similarly, other studies have failed to show direct Rac1 interaction with IRSp53 (Krugmann et. al., 2001; Soltau et. al., 2002). The reason for this discrepancy is unclear.

Nevertheless, it is possible that IRSp53 may bind Rac1 indirectly through SH3 domain interactions with the WAVE1/2 complexes or the Rac1 exchange factor Eps8 (Funato et. al., 2004). Most recently, Connolly et. al., 2005, has found that IRSp53 interacts directly with the Rac1 exchange factor Tiam1 via a region near the partial CRIB motif. Two other Cdc42 effectors are also linked to Rac1 exchange factors: PAK binds to PIX (Obermeir et. al., 1998) and PAR6 binds to Tiam1 (Chen et. al., 2005; Nishimura et. al; 2005). In both cases lamellipodia/membrane ruffling is stimulated by the interaction.

IRSp53 point mutants of the partial CRIB motif lack Cdc42-binding activity and are not able to induce neurites and associated morphologies in N1E115 cells (Govind et. al., 2001). This result strongly supports the idea that IRSp53 is primarily a Cdc42 effector.

### **9.11. The relation between IMD and BAR domains.**

The BAR domain was first identified in vertebrate Bin1 and Amphiphysins and in the *S. cerevisiae* Rvs proteins (Sakamuro et. al., 1996) due to its common occurrence. The BAR domain is highly conserved across species and evolution. The family has since expanded to include many other BAR-containing proteins, such as endophilins and sorting nexins, proteins that are mostly involved in membrane binding or remodeling events (Peter et. al., 2004).

The structures of BAR domains in *Drosophila* Amphiphysin, human Arfaptin2, and murine Endophilin have been published. These structural studies have revealed that the BAR domain adopts a banana-shaped  $\alpha$ -helical dimer that functions to sense highly curved membranes (Gallop et. al., 2006; Masuda et. al., 2006; Weissenhorn et. al., 2006; Peter et. al., 2004). The banana shape of the BAR domain favors curved membranes with an outer radius of 11-15 nm and primarily uses electrostatic forces to bind negatively charged lipids, such as phosphatidyl serine (PS) or PIP<sub>2</sub>.

BAR domains can also induce lipids to form tubules (tubulate) *in vitro* and *in vivo* (Itoh et. al., 2005). BAR domains form higher order structures and are capable of polymerizing to give rise to long filamentous structures *in vitro* (Itoh et. al., 2005).

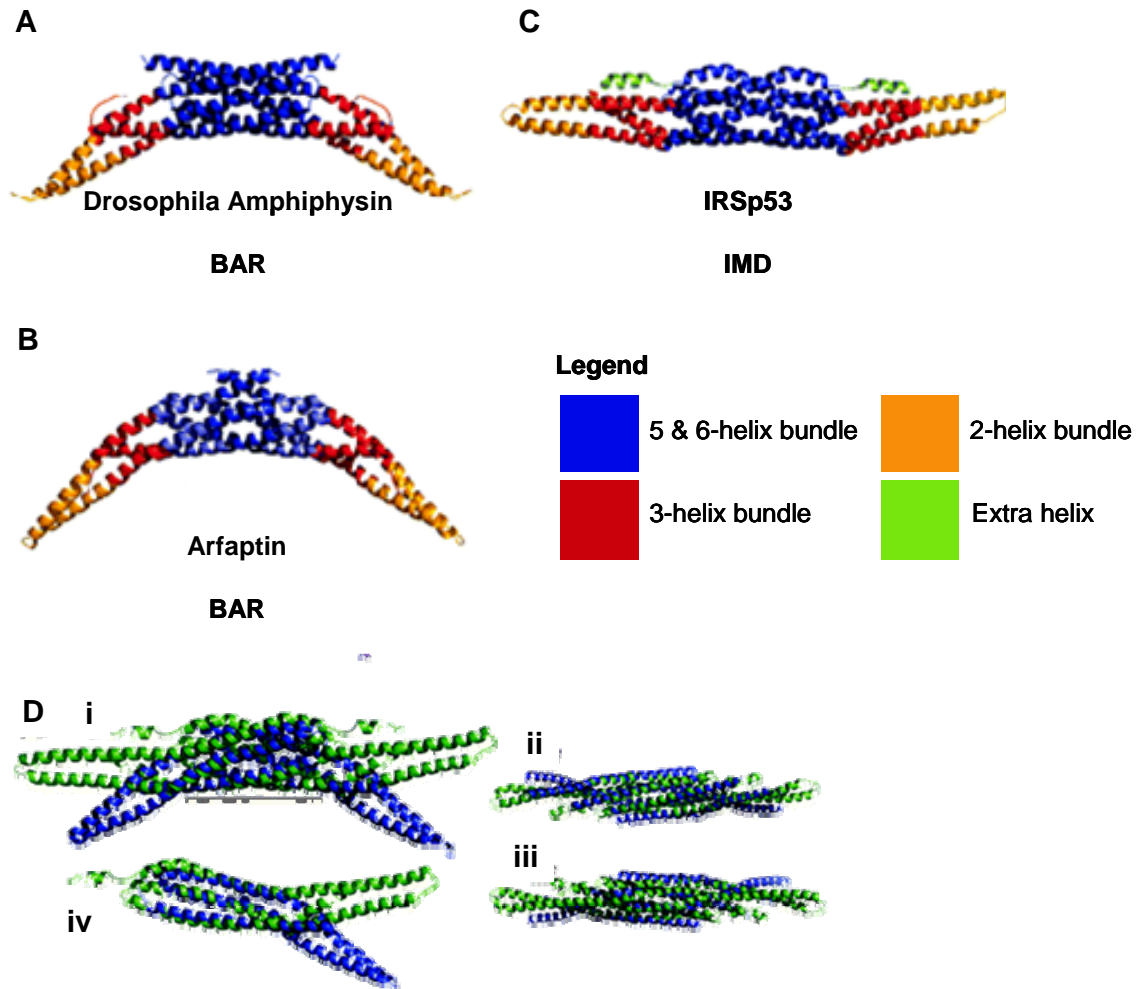
Most recently, the structure of IMD has been solved and was shown to share striking similarities to the BAR domain (Millard et. al., 2005). IMD was found to share the same turns and folds seen in BAR proteins (Figure 9.1). Interestingly, the IMD structure differs only in the shape; instead of the typical banana-shaped BAR domain, the IMD domain is almost straight. This has led to the suggestion that the IMD domain is able to drive membrane protrusion rather than membrane invagination. This implication of IMD having the potential to play a role in membrane deformation is supported with my observations that IMD induces “partial filopodia”. The IMD/BAR domains are likely to provide an important link between membrane deformation and the actin cytoskeleton.



**Figure 9.1 Comparison of the IMD with known structures of different BAR domains.**

Ribbon representation of the different BAR domains of known structures. (A-B) BAR domains (*Drosophila* Amphiphysin and Arfaptin) consists of a central 6-helix bundle (blue), flanked by a 3-helix bundle (orange-red) and a 2-helix coiled-coil at the periphery (yellow). (C) IRSp53 IMD domain contains the exact folds and turns, except that it contains an extra helix (green). The BAR domains adopts the typical banana-shaped conformation whereas IMD has a straight structure, with not much curvature. (D) Bin1BAR (blue) superimposed with the IMD domain of IRSp53 (green). The numbers i-iii correspond to the side, concave and convex views of the dimer, respectively. Number iv corresponds to the superposed images of the protomers alone.

Figure 9.1



## **9.12. Conclusion**

### **A Proposed Model.**

In this study I have demonstrated that IRSp53 and N-WASP interact directly. Taken together with observations made previously (Govind et al, 2001) and by other groups (Krugmann et. al., 2001; Miki et. al., 2000; Funato et. al., 2004; Connolly et. al., 2005), a mechanism of IRSp53 induced filopodia formation emerges (Figure 9.2).

### **IMD.**

The simplest morphological activity generated by IRSp53 was by the mutant IMD-4K. This mutant domain induced membrane protrusion without actin involvement. Strikingly, the size and dynamics of the protrusions generated by IMD-4K resembled filopodia. The wild-type IMD generated in addition a static protrusion, with aberrant morphology, that contained F-actin. FRET analysis showed that IRSp53 interacted directly with F-actin but the IMD domain did not. The relationship between IMD and F-actin is unclear. When the IMD-4K mutation was inserted into full length IRSp53 it was no longer able to induce filopodia, suggesting that this region of IRSp53 is important for filopodia formation.

### **Cdc42.**

Activated Cdc42 binds IRSp53 and N-WASP through their CRIB motifs, localizing these proteins to the plasma membrane, and revealing the SH3 domain and polyproline sequence, respectively, which in turn leads to IRSp53 binding to N-WASP. The Cdc42-IRSp53-N-WASP-Cdc42 complex initiates filopodia formation first as both IRSp53 and N-WASP are Cdc42 binding proteins. Subsequently, IRSp53 recruits Mena (and other

interacting proteins) which may help influence the dynamics of filopodia formation. Next, IRSp53 recruits WAVE2 (and WAVE1) or Eps8 and simultaneously Tiam1. The coordination of recruitment of proteins by IRSp53 involved in filopodia formation and lamellipodia formation/membrane ruffling ensures the continuous cycling of these structures in particular locations.

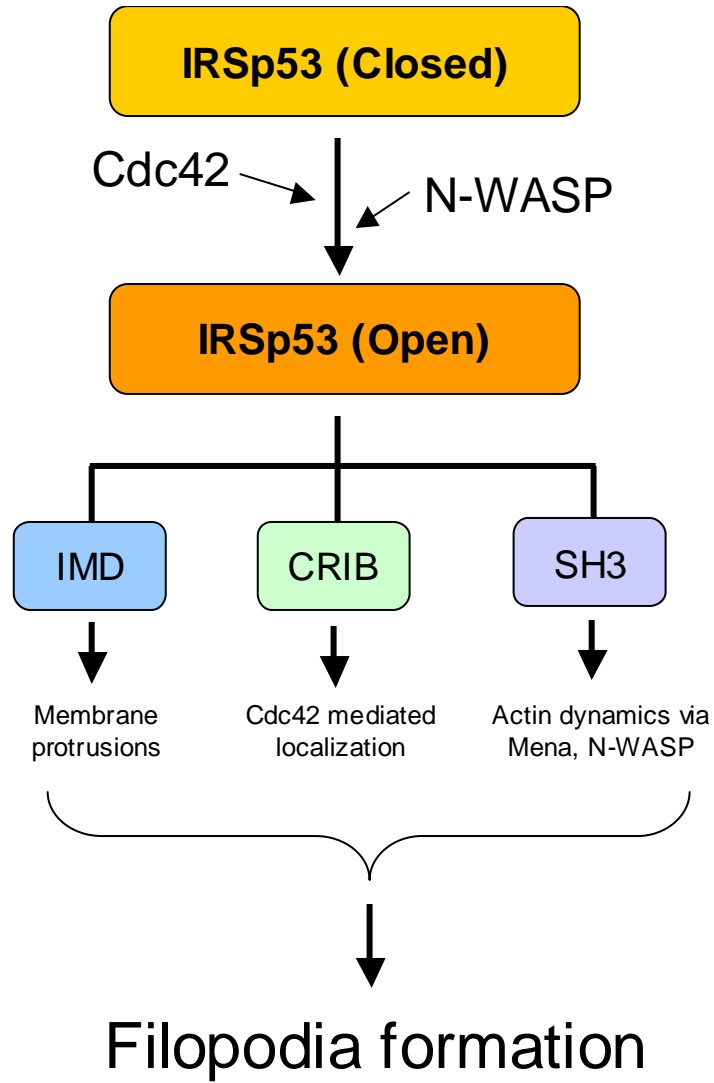
### **SH3 domain.**

Filopodia formation requires full length IRSp53. I suggest that the SH3 domain works in concert with the IMD domain by providing the dynamic actin components of filopodia through proteins such as N-WASP and Mena. The exact molecular mechanism by which the IRSp53 SH3 domain binding partners control actin dynamics requires further work. Nevertheless, I think it reasonable to suggest that Mena may contribute to the filament anti-capping activity, thereby stimulating actin polymerization, while N-WASP may sequester free actin through its WA domain, and influence depolymerization. Results obtained from the RNAi study supports the idea that WAVE1 and WAVE2 interaction with SH3 is not required for the filopodial activity of IRSp53. Eps8 that binds to IRSp53 SH3 domain may also contribute to the filopodia activity through its F-actin bundling activity (Disanza et. al., 2006).

**Figure 9.2 Proposed model of filopodia formation through IRSp53.**

IRSp53 exist in a closed conformation. N-WASP/Cdc42 binding to IRSp53 allows it to open up at a location determined by Cdc42. SH3 binding proteins, such as N-WASP, Mena, Eps8 and mDia2, along with the IMD/BAR domain allow filopodia formation.

Figure 9.2



## **REFERENCES**

## REFERENCES

Abbott, M. A., Wells, D. G. , Fallon, J. R.. The insulin receptor tyrosine kinase substrate p58/53 and the insulin receptor are components of CNS synapses. *J Neurosci.* (1999) 19:7300-8.

Abercrombie M. Contact inhibition and malignancy. *Nature.* (1979) 281:259-62.

Adra CN, Iyengar AR, Syed FA, Kanaan IN, Rilo HL, Yu W, Kheraj R, Lin SR, Horiuchi T, Khan S, Weremowicz S, Lim B, Morton CC, Higgs DR. Human ARHGDIG, a GDP-dissociation inhibitor for Rho proteins: genomic structure, sequence, expression analysis, and mapping to chromosome 16p13.3. *Genomics.* (1998) 53:104-9.

Ahern-Djamali SM, Comer AR, Bachmann C, Kastenmeier AS, Reddy SK, Beckerle MC, Walter U, Hoffmann FM. Mutations in *Drosophila* enabled and rescue by human vasodilator-stimulated phosphoprotein (VASP) indicate important functional roles for Ena/VASP homology domain 1 (EVH1) and EVH2 domains. *Mol Biol Cell.* (1998) 8:2157-71.

Ahmed S, Lee J, Kozma R, Best A, Monfries C, Lim L. A novel functional target for tumor-promoting phorbol esters and lysophosphatidic acid. The p21rac-GTPase activating protein n-chimaerin. *J Biol Chem.* (1993) 268:10709-12.



Ahmed S, Prigmore E, Govind S, Veryard C, Kozma R, Wientjes FB, Segal AW, Lim L. Cryptic Rac-binding and p21(Cdc42Hs/Rac)-activated kinase phosphorylation sites of NADPH oxidase component p67(phox). *J Biol Chem.* (1998) 273:15693-701.

Alberts B, Bray D, Lewis J, Raff M, Roberts K, Watson JD. *The Cytoskeleton. Molecular Biology of the Cell*, 3<sup>rd</sup> Edition 1994, Chapter 16, 787-906.

Allen WE, Zicha D, Ridley AJ, Jones GE. A role for Cdc42 in Macrophage Chemotaxis. *J. Cell Biol.* (1998) 141:1147-57

Alvarez, C. E., Sutcliffe, J. G., Thomas, E. A. Novel isoform of insulin receptor substrate p53/p58 is generated by alternative splicing in the CRIB/SH3-binding region. *J Biol Chem.* (2002) 277:24728-34.

Alvarez CE, Sutcliffe JG, Thomas EA. Novel isoform of insulin receptor substrate p53/p58 is generated by alternative splicing in the CRIB/SH3-binding region. *J Biol Chem.* (2002) 277:24728-34. Epub (2002)

Amano M, Chihara K, Nakamura N, Kaneko T, Matsura Y, Kaibuchi K. The COOH terminus of Rho-Kinase negatively regulates Rho-Kinase activity. *J. Biol. Chem.* (1999) 274:32418-34242.

Amano M, Mukai H, Ono Y, Chihara K, Matsui T, Hamajima Y, Okawa K, Iwamatsu A, Kaibuchi K. Identification of a putative target for Rho as the serine-threonine kinase protein kinase N. *Science*. (1996)271:648-650.

Anton IM, Lu W, Mayer BJ, Ramesh N, Geha RS. The Wiskott-Aldrich syndrome protein-interacting protein (WIP) binds to the adaptor protein Nck. *J Biol Chem*. (1998) 273:20992-5.

Aspenstrom P, Lindberg U, Hall A. Two GTPases, Cdc42 and Rac, bind directly to a protein implicated in the immunodeficiency disorder Wiskott-Aldrich syndrome. *Curr Biol*. (1996) 6:70-5.

Aszodi A, Pfeifer A, Ahmad M, Glauner M, Zhou XH, Ny L, Andersson KE, Kehrel B, Offermanns S, Fassler R. The vasodilator-stimulated phosphoprotein (VASP) is involved in cGMP- and cAMP-mediated inhibition of agonist-induced platelet aggregation, but is dispensable for smooth muscle function. *EMBO J*. (1999) 18:37-48.

Bachmann C, Fischer L, Walter U, Reinhard M. The EVH2 domain of the vasodilator-stimulated phosphoprotein mediates tetramerization, F-actin binding, and actin bundle formation. *J Biol Chem*. (1999) 274:23549-57.

Bahler M. Myosins on the move to signal transduction. *Curr Opin Cell Biol*. (1996) 8:18-22. Review.

Baldassarre M, Pompeo A, Bezonussenko G, Castaldi C, Cortellino S, McNiven MA, Luini A, Buccione R. Dynamin participates in focal extracellular matrix degradation by invasive cells. *Mol Biol Cell*. (2003) 14:1074-84.

Bamburg JR. Proteins of the ADF/cofilin family: essential regulators of actin dynamics. *Annu Rev Cell Dev Biol*. (1999);15:185-230. Review.

Bagrodia S, Taylor SJ, Jordon KA, Van Aelst L, Cerione RA. A novel regulator of p21-activated kinases. *J Biol Chem*. (1998) 273:23633-6.

Bagrodia S, Derijard B, Davis RJ, Cerione RA. Cdc42 and PAK-mediated Signaling leads to Jun kinase and p38 mitogen-activated protein kinase activation. *J Biol Chem*. (1995) 270:27995-8.

Banzai Y, Miki H, Yamaguchi H, Takenawa T. Essential role of neural Wiskott-Aldrich syndrome protein in neurite extension in PC12 cells and rat hippocampal primary culture cells. *J Biol Chem*. (2000) 275:11987-92.

Bar-Sagi D, Hall A. Ras and Rho GTPases: a family reunion. *Cell*. (2000) 103:227-38. Review.

Barbacid M. ras genes. *Annu Rev Biochem*. (1987) 56:779-827. Review.

Barkalow K, Witke W, Kwiatkowski DJ, Hartwig JH. Coordinated regulation of platelet actin filament barbed ends by gelsolin and capping protein. *J Cell Biol.* (1996) 134:389-99.

Barzik M, Kotova TI, Higgs HN, Hazelwood L, Hanein D, Gertler FB, Schafer DA. Ena/VASP proteins enhance actin polymerization in the presence of barbed end capping proteins. *J Biol Chem.* (2005) 280:28653-62.

Benna J, Ruedi JM, Babior BM. Cytosolic guanine nucleotide-binding protein Rac2 operates in vivo as a component of the neutrophil respiratory burst oxidase. Transfer of Rac2 and the cytosolic oxidase components p47phox and p67phox to the submembranous actin cytoskeleton during oxidase activation. *J Biol Chem.* (1994) 269:6729-34.

Biesova Z, Piccoli C, Wong WT. Isolation and characterization of c3B1, an eps8 binding protein that regulates cell growth. *Oncogene* (1997)14:233-41.

Bishop, A. L, and Hall, A.2000. Rho GTPases and their effector proteins *Biochem. J.* 348, 241-255

Bandtlow CE, Schmidt MF, Hassinger TD, Schwab ME, Kater SB. Role of intracellular calcium in NI-35-evoked collapse of neuronal growth cones. *Science.* (1993) 259:80-3.

Bar-Sagi D, Hall A. Ras and Rho GTPases: a family reunion. *Cell*. (2000) 103:227-38.  
Review.

Bear JE, Svitkina TM, Krause M, Schafer DA, Loureiro JJ, Strasser GA, Maly IV, Chaga OY, Cooper JA, Borisy GG, Gertler FB. Antagonism between Ena/VASP proteins and actin filament capping regulates fibroblast motility. *Cell*. (2002) 109:509-21.

Bear JE, Loureiro JJ, Libova I, Fassler R, Wehland J, Gertler FB. Negative regulation of fibroblast motility by Ena/VASP proteins. *Cell*. (2000) 101:717-28.

Bear JE, Rawls JF, Saxe CL 3rd. SCAR, a WASP-related protein, isolated as a suppressor of receptor defects in late Dictyostelium development. *J Cell Biol*. (1998) 142:1325-35.

Berg JS, Cheney RE. Myosin-X is an unconventional myosin that undergoes intrafilopodial motility. *Nat Cell Biol*. (2002) 4:246-50.

Berg JS, Powell BC, Cheney RE. A millennial myosin census. *Mol Biol Cell*. (2001) 12:780-94. Review.

Bernards A, Settleman J. GAP control: regulating the regulators of small GTPases. *Trends Cell Biol*. (2004) 14:377-85.

Biou V, Cherfils J. Structural principles for the multispecificity of small GTP-binding proteins. *Biochemistry*. (2004) 43:6833-40.

Biyasheva A, Svitkina T, Kunda P, Baum B, Borisy G. Cascade pathway of filopodia formation downstream of SCAR. *J Cell Sci*. (2004) 117:837-48. Epub (2004)

Blagg SL, Stewart M, Sambles C, Insall RH. PIR121 regulates pseudopod dynamics and SCAR activity in *Dictyostelium*. *Curr. Biol*. (2003) 13:1480-87.

Blanchoin L, Pollard TD, Mullins RD. Interactions of ADF/cofilin, Arp2/3 complex, capping protein and profilin in remodeling of branched actin filament networks. *Curr Biol*. (2000) 10:1273-82.

Bockmann, J., Kreutz, M. R., Gundelfinger, E. D., Bockers, T. M. (2002) ProSAP/Shank postsynaptic density proteins interact with insulin receptor tyrosine kinase substrate IRSp53. *J Neurochem*. 83:1013-7.

Bogerd HP, Fridell RA, Benson RE, Hua J, Cullen BR. Protein sequence requirements for function of the human T-cell leukemia virus type O Rex nuclear export signal delineated by a novel in vivo randomization-selection assay. *Mol Cell Biol*. (1996) 16:4207-14.

Boguski MS , McCormick F. Proteins regulating Ras and its relatives. *Nature* (1993)366:643-54.

Bokoch GM. Biology of the p21-activated kinases. *Annu Rev Biochem.* (2003);72:743-81.

Bokoch GM, Vlahos CJ, Wang Y, Kanus UG, Traynor-Kaplan AE. Rac GTPase interacts specifically with phosphatidylinositol 3-kinase. *Biochem J.* (1996)315:775-79.

Bompard G, Sharp SJ, Freiss G, Machesky LM. Involvement of Rac in actin cytoskeleton rearrangements induced by MIM-B. *J Cell Sci.* (2005) 118:5393-403.

Borisy GG, Svitkina TM. Actin machinery: pushing the envelope. *Curr Opin Cell Biol.* (2000) 12:104-12. Review.

Bos JL. ras oncogene in human cancer: a review [published erratum appears in *Cancer Res* (1990) 50:1352. *Cancer Res.* 49:4682-69

Bourne HR, Sanders DA, McCormick F. The GTPase superfamily: a conserved switch for diverse cell functions. *Nature.* (1990) 348:125-32. Review.

Bray, D. 2001. *Cell Movements. From Molecules to Motility.* Second edition. Garland Publishing.

Brook JD, McCurrach ME, Harley HG, Buckler AJ, Church D, Aburatani H, Hunter K, Santon VP, Thirion JP, Hudson T. Molecular basis of myotonic dystrophy: expansion of a trinucleotide (CTG) repeat at the 3' end of a transcript encoding a protein kinase family member. *Cell*. (1992) 69:385.

Brunet N, Morin A, Olofsson B. RhoGDI-3 regulates RhoG and targets this protein to the Golgi complex through its unique N-terminal domain. *Traffic*. (2002) 3:342-57.

Buccione R, Orth JD, McNiven MA. Foot and mouth: podosomes, invadopodia and circular dorsal ruffles. *Nat Rev Mol Cell Biol*. (2004) 5:647-57.

Burbelo PD, Drechsel D, Hall A. A conserved binding motif defines numerous candidate target proteins for both Cdc42 and Rac GTPases. *J Biol Chem*. (1995) 270:29071-4.

Burns S, Thrasher AJ, Blundell MP, Machesky L, Jones GE. Configuration of human dendritic cell cytoskeleton by Rho GTPases, the WAS protein, and differentiation. *Blood*. (2001) 98:1142-9.

Burridge, K., and Chrzanowska-Wodnicka M. Focal adhesions, contractility, and Signaling. *Annu Rev Cell Dev Biol*. (1996)12:463-518.

Calle Y, Chou HC, Thrasher AJ, Jones GE. Wiskott-Aldrich syndrome protein and the cytoskeletal dynamics of dendritic cells. *J Pathol*. (2004) 204:460-69.



Carlier MF, Ducruix A, Pantaloni D. Signaling to actin: the Cdc42-N-WASP-Arp2/3 connection. *Chem Biol.* (1999) 6:R235-40. Review.

Carlier MF, Pantaloni D. Control of actin dynamics in cell motility. *J Mol Biol.* (1997) 269:459-67. Review.

Carlier MF, Laurent V, Santolini J, Melki R, Didry D, Xia GX, Hong Y, Chua NH, Pantaloni D. Actin depolymerizing factor (ADF/cofilin) enhances the rate of filament turnover: implication in actin-based motility. *J Cell Biol.* (1997) 136:1307-22.

Carl UD, Pollmann M, Orr E, Gertlere FB, Chakraborty T, Wehland J. Aromatic and basic residues within the EVH1 domain of VASP specify its interaction with proline-rich ligands. *Curr Biol.* (1999) 9:715-8.

Cassimeris L, Safer D, Nachmias VT, Zigmond SH. Thymosin beta 4 sequesters the majority of G-actin in resting human polymorphonuclear leukocytes. *J Cell Biol.* (1992) 119:1261-70.

Castellano F, Montcourrier P, Guillemot JC, Gouin E, Machesky L, Cossart P, Chavrier P. Inducible recruitment of Cdc42 or WASP to a cell-surface receptor triggers actin polymerization and filopodium formation. *Curr Biol.* (1999) 9:351-60.

Cerione RA, Zheng Y. The Dbl family of oncogenes. *Curr Opin Cell Biol.* (1996) 8:216-22. Review.

Chambers AF, Groom AC, MacDonald IC. Dissemination and growth of cancer cells in metastatic sites. *Nat Rev Cancer.* (2002) 2:563-72. Review.

Chapman ER, An S, Barton N, Jahn, R. SNAP-25. a SMARE which binds to both syntaxin and synaptobrevin via domains that may form coiled coils. *J. Biol. Chem.* (1994) 269:27427-32.

Chen X. and Macara, I. G Par-3 controls tight junction assembly through the Rac exchange factor Tiam1. *Nature Cell Biology* (2005) 7:262-269.

Chen YA, Scheller RH. SNARE-mediated membrane fusion. *Nat. Rev. Mol. Cell Biol.* (2001) 22:98-106.

Chien CB, Rosenthal DE, Harris WA, Holt CE. Navigational errors made by growth cones without filopodia in the embryonic *Xenopus* brain. *Neuron.* (1993) 11:237-51.

Chan W, Kozma R, Yasui Y, Inagaki M, Leung T, Manser E, Lim L. Vimentin intermediate filament reorganization by Cdc42: involvement of PAK and p70 S6 kinase. *Eur J Cell Biol.* (2002) 81:692-701.

Chang JH, Gill S, Settleman J, Parsons SJ. c-Src regulates the simultaneous rearrangement of actin cytoskeleton, p190RhoGAP, and p120RasGAP following epidermal growth factor stimulation. *J Cell Biol.* (1995) 130:355-68.

Choi J, Ko J, Racz B, Burette A, Lee J. R., Kim S, Na M, Lee H. W., Kim K, Weinberg R. J., Kim E. Regulation of dendritic spine morphogenesis by insulin receptor substrate 53, a downstream effector of Rac1 and Cdc42 small GTPases. *J Neurosci.* (2002) 25:869-79.

Chong C, Tan L, Lim L, Manser E. The mechanism of PAK activation. Autophosphorylation events in both regulatory and kinase domains control activity. *J Biol Chem.* (2001) 276:17347-53.

Citi S, Kendrick-Jones J. Regulation of non-muscle myosin structure and function. *Bioessays.* (1987) 7:155-59.

Clark EA, Golub TR, Lander ES, Hynes RO. Genomic analysis of metastasis reveals an essential role for RhoC. *Nature.* (2000) 406:532-5.

Clark EA, King WG, Brugge JS, Symons M, Hynes RO. Integrin-mediated signals regulated by members of the rho family of GTPases. *J Cell Biol.* (1998) 142:573-86.

Condeelis J, Segall JE. Intravital imaging of cell movement in tumours. *Nat Rev Cancer.* (2003) 3:921-30. Review.

Condeelis J. Life at the leading edge: the formation of cell protrusions. *Annu. Rev. Cell Biol.* (1993) 9:411-44.

Connolly BA, Rice J, Feig LA, Buchsbaum RJ. Tiam1-IRSp53 complex formation directs specificity of rac-mediated actin cytoskeleton regulation. *Mol Cell Biol.* (2005) 25:4602-14.

Cooper JA, Schafer DA. Control of actin assembly and disassembly at filament ends. *Curr Opin Cell Biol.* (2000) 12:97-103. Review.

Cozier GE, Lockyer PJ, Reynolds JS, Kupzig S, Bottomley JR, Millard TH, Banting G, Cullen PJ. GAP1IP4BP contains a novel group 1 pleckstrin homology domain that directs constitutive plasma membrane association. *J. Biol. Chem.* (2000)275:28261-68.

Crespo P, Schuebel KE, Ostrom AA, Gutkind JS, Bustelo XR. Phosphotyrosine-dependent activation of Rac-1GDP/GTP exchange by the vav proto-oncogene product. *Nature* (1997)385:169-72.

Cullen PJ, Hsuan JJ, Truong O, Letcher AJ, Jackson TR, Dawson AP, Irvine RF. Identification of a specific ins (1,3,4,5)P4-binding protein as a member of the GAP1 family. *Nature.* (1995)376:527-30.

Dai Z, Pendergast AM. Abi-2, a novel SH3-containing protein interacts with the c-Abl tyrosine kinase and modulates c-Abl transforming activity. *Genes Dev.* (1995)9:2569-82.

Dasgupta B, Gutmann DH. Neurofibromatosis 1: closing the GAP between mice and men. *Curr. Opin. Genet. Dev.* (2003) 13:20-27.

Dawson JC, Legg JA, Machesky LM. Bar domain proteins: a role in tubulation, scission and actin assembly in clathrin-mediated endocytosis. *Trends Cell Biol.* (2006) 16:493-8.

Derry JM, Ochs HD, Francke U. Isolation of a novel gene mutated in Wiskott-Aldrich syndrome. *Cell.* (1994) 78:635-44.

Dickson BJ. Rho GTPases in growth cone guidance. *Curr. Opin. Neurobiol.* (2001)11:103-110.

Diekmann D, Abo A, Johnston C, Segal AW, Hall A. Interaction of Rac with P67phox and Regulation of Phagocytic NADPH Oxidase Activity. *Science.* (1994) 265:531-533.

Diekmann D, Brill S, Garrett MD, Totty N, Hsuan J, Monfries C, Hall C, Lim L, Hall A. Bcr encodes a GTPase-Activating Protein for p21rac. *Nature.* (1991) 351:400-402.

Disanza A, Mantoani S, Hertzog M, Gerboth S, Frittoli E, Steffen A, Berhoerster K, Kreienkamp HJ, Milanesi F, Di Fiore PP, Ciliberto A, Stradal TE, Scita G. Regulation of cell shape by Cdc42 is mediated by the synergic actin-bundling activity of the Eps8-IRSp53 complex. *Nat Cell Biol.* (2006) 8:1337-47.

DePina AS, Langford GM. Vesicle transport: the role of actin filaments and myosin motors. *Microsc Res Tech.* (1999) 47:93-106. Review.

DesMarais V, Ghosh M, Eddy R, Condeelis J. Cofilin takes the lead. *J Cell Sci.* (2005) 118:19-26.

Desai A, Mitchison TJ. Microtubule polymerization dynamics. *Annu Rev Cell Dev Biol.* (1997) 13:83-117. Review.

Downey GP. Mechanism of leukocyte motility and chemotaxis. *Curr. Opin. Immunol.* (1994) 6:113-24.

Downward J. Ras signaling and apoptosis. *Curr Opin Genet Dev.* (1998) 8:49-54. Review.

Dransart E, Olofsson B, Cherfils J. RhoGDIs revisited: novel roles in Rho regulation. *Traffic.* (2005) Nov;6(11):957-66. Review. Erratum in: *Traffic.* (2006) 7:108.

Drechsel DN, Hyman AA, Cobb MH, Kirschner MW. Modulation of the dynamic instability of tubulin assembly by the microtubule-associated protein tau. *Mol Biol Cell.* (1992) 3:1141-54.

Du J, Frieden C. Kinetic studies on the effect of Yeast Cofilin on yeast actin polymerization. *Biochemistry* (1998) 37:13276-84.

DuHadaway JB, Prendergast GC, Luisi BF, Laue ED. The crystal structure of the BAR domain from human Bin1/amphiphysin II and its implications for molecular recognition. *Biochemistry.* (2006) 45:12917-28.

Dustin ML, J Garcia-Aguilar ML, Hibbs RS, Larson SA, Stacker DE, Staunton AJ, Wardlaw and Springer TA. Structure and regulation of the leukocyte adhesion receptor LFA-1 and its counterreceptors, ICAM-1 and ICAM-2. *Cold Spring Harbor Symp. Quant. Biol.* (1989) 54:753-66.

Eden S, Rohatgi R, Podtelejnikov AV, Mann M, Kirschner MW. Mechanism of regulation of WAVE1-induced actin nucleation by Rac1 and Nck. *Nature.* (2002) 418:790-3.

Egile C, Loisel TP, Laurent V, Li R, Pantaloni D, Sansonetti PJ, Carrier MF. Activation of the CDC42 effector N-WASP by the *Shigella flexneri* IcsA protein promotes actin

nucleation by Arp2/3 complex and bacterial actin-based motility. *J Cell Biol.* (1999) Sep 20;146(6):1319-32.

Ellis, S, Mellor, H. The novel Rho-family GTPase Rif regulates coordinated actin-based membrane rearrangements. *Current Biology* (2005) 10:1387–1390.

Ellis RW, Defeo D, Shih TY, Gonda MA, Young HA, Tsuchida N, Lowy DR, Scolnick EM. The p21 src genes of Harvey and Kirsten sarcoma viruses originate from divergent members of a family of normal vertebrate genes. *Nature.* (1981) 292:506-11.

Erickson HP, O'Brien ET. Microtubule dynamic instability and GTP hydrolysis. *Annu. Rev. Biophys. Biomol. Struct.* (1992) 21:145-66.

Ermeikova KS, Zambrano N, Linn H, Minopoli G, Gertler F, Russo T, Sudol M. The WW domain of neural protein FE65 interacts with proline-rich motifs in Mena, the mammalian homolog of *Drosophila* enabled. *J Biol Chem.* (1997) 272:32869-77.

Etienne-Manneville S, Hall A. Rho GTPases in cell biology. *Nature.* (2002) 420:629-35.

Eva A, Aaronson SA. Isolation of a new human oncogene from a diffuse B-cell lymphoma. *Nature.* (1985) 316:273-5.



Fedorov AA, Fedorov E, Gertler F, Almo SC. Structure of EVH1, a novel proline-rich ligand-binding module involved in cytoskeletal dynamics and neural function. *Nat Struct Biol.* (1999) 6:661-5.

Feig LA. Tools of the trade: use of dominant-inhibitory mutants of Ras-family GTPases. *Nat Cell Biol.* (1999) 1:E25-7. Review.

Feig LA, Cooper GM. Relationship among guanine nucleotide exchange, GTP hydrolysis, and transforming potential of mutated ras proteins. *Mol Cell Biol.* (1988) 8:2472-8.

Flanagan LA, Chou J, Falet H, Neujahr R, Hartwig JH, Stossel TP. Filamin A, the Arp2/3 complex, and the morphology and function of cortical actin filaments in human melanoma cells. *J Cell Biol.* (2001) 155:511-7.

Franke TF, Yang SI, Chan TO, Datta K, Kazlauskas A, Morrison DK, Kaplan DR, Tschlis PN. The protein kinase encoded by the Akt proto-oncogene is a target of the PDGF-activated phosphatidylinositol 3-kinase. *Cell.* (1995) 81:727-36.

Friedl HP, Karrer K, Kuhbock J. The relation of tumour size to the results of chemotherapy in malignant tumours. *Rev Eur Etud Clin Biol.* (1971) 16:268-72.

Frischknecht F, Way M. Surfing pathogens and the lessons learned for actin polymerization. *Trends Cell Biol.* (2001) 11:30-38. Review.

Fujiwara T, Mammoto A, Kim Y, Takai Y. Rho small G-protein-dependent binding of mDia to an Src homology 3 domain-containing IRSp53/BAIAP2. *Biochem Biophys Res Commun.* (2000) 271:626-9.

Fukuoka M, Suetsugu S, Miki H, Fukami K, Endo T, Takenawa T. A novel neural Wiskott-Aldrich syndrome protein (N-WASP) binding protein, WISH, induces Arp2/3 complex activation independent of Cdc42. *J Cell Biol.* (2001) 152:471-82.

Fuchs E, Cleveland DW. A structural scaffolding of intermediate filaments in health and disease. *Science.* (1998) 279:514-9. Review.

Fujisawa K, Fujita A, Ishizaki T, Saito Y, Narumiya S. Identification of the Rho-binding domain of p160ROCK, a Rho-associated coiled-coil containing protein kinase. *J Biol Chem.* (1996) 271:23022-8.

Fukamoto Y, Kaibuchi K, Hori Y, Fujioka H, Araki S, Ueda T, Kikuchi A, Takai Y. Molecular cloning and characterization of a novel type of regulatory protein (GDI) for the rho proteins, ras p21-like small GTP-binding proteins. *Oncogene* (1990) 5:1321-28.

Fukuoka M, Miki H, Takenawa T. Identification of N-WASP homologs in human and rat brain. *Gene*. (1997) 196:43-8.

Funato Y, Terabayashi T, Suenaga N, Seiki M, Takenawa T, Miki H. IRSp53/Eps8 complex is important for positive regulation of Rac and cancer cell motility/invasiveness. *Cancer Res*. (2004) 64:5237-44.

Galler AB, Garcia Arguinzonis MI, Baumgartner W, Kuhn M, Smolenski A, Simm A, Reinhard M. VASP-dependent regulation of actin cytoskeleton rigidity, cell adhesion, and detachment. *Histochem Cell Biol*. (2006) 125:457-74.

Gallop, JL. Mechanism of endophilin N-Bar domain-mediated membranes curvature. *EMBO J*. (2006) 25:2898-910.

Garrett MD, Self AJ, van Oers C, Hall A. Identification of distinct cytoplasmic targets for ras/R-ras and rho regulatory proteins. *J Biol Chem*. (1989) 264:10-3.

Gautreau, A., Ho, H. Y., Li, J., Steen, H., Gygi, S. P., Kirschner, M. W. Purification and architecture of the ubiquitous Wave complex. *Proc Natl Acad Sci U S A*. (2004) 101:4379-83.

Geese M, Loureiro J, Bear J, Wehland J, Gertler FB, Sechi AS. Contribution of Ena/VASP Proteins to Intracellular Motility of *Listeria* Requires Phosphorylation and Proline-rich Core but Not F-Actin Binding or Multimerization. *Mol. Biol. Cell.* (2002) 13:2383-2396.

Gertler FB, Niebuhr K, Reinhard M, Wehland J, Soriano P. Mena, a relative of VASP and *Drosophila* Enabled, is implicated in the control of microfilament dynamics. *Cell.* (1996) 87:227-39.

Gertler FB, Comer AR, Juang JL, Ahern SM, Clark MJ, Liebl EC, Hoffmann FM. enabled, a dosage-sensitive suppressor of mutations in the *Drosophila* Abl tyrosine kinase, encodes an Abl substrate with SH3 domain-binding properties. *Genes Dev.* (1995) 9:521-33.

Gertler FB, Doctor JS, Hoffmann FM. Genetic suppression of mutations in the *Drosophila* abl proto-oncogene homolog. *Science.* (1990) 248:857-60.

Glaven JA, Whitehead IP, Normanbhoy T, Kay R, Cerione RA. Lfc and Lsc oncoproteins represent two new guanine nucleotide exchange factors for the Rho GTP-binding protein. *J. Biol. Chem.* (1996) 271:27374-81.

Goldschmidt-Clermont PJ, Machesky LM, Baldassare JJ, Pollard TD. The actin-binding protein profilin binds to PIP2 and inhibits its hydrolysis by phospholipase C. *Science* (1990) 247:1575-78.

Golovanov AP, Chuang TH, DerMardirossian C, Barsukov I, Hawkins D, Badii R, Bokoch GM, Lian LY, Roberts GC. Structure-activity relationships in flexible protein domains: regulation of rho GTPases by RhoGDI and D4 GDI. *J Mol Biol.* (2001) 305:121-35.

Gomez J, Martinez C, Fernandez B, Garcia A, Rebollo A. Ras activation leads to cell proliferation or apoptotic cell death upon interleukin-2 stimulation or lymphokine deprivation, respectively. *Eur J Immunol.* (1997) 27:1610-8.

Gomez TM, Letourneau PC. Filopodia initiate choices made by sensory neuron growth cones at laminin/fibronectin borders in vitro. *J Neurosci.* (1994) 4:5959-72.

Ghosh M, Song X, Mouneimne G, Sidani M, Lawrence DS, Condeelis JS. Cofilin promotes actin polymerization and defines the direction of cell motility. *Science.* (2004) 304:743-6.

Govind S, Kozma R, Monfries C, Lim L, Ahmed S. Cdc42Hs facilitates cytoskeletal reorganization and neurite outgrowth by localizing the 58-kD insulin receptor substrate to filamentous actin. *J Cell Biol.* (2001) 152, 579-94.

Habats GG, van der Kammen RA, Stam JC, Michiels F, Collard JG. Sequence of human invasion-inducing TiAM1 gene, its conservation in evolution and its expression in tumor cell lines of different tissue origin. *Oncogene* (1995) 10:1371-76.

Hahne P, Sechi A, Benesch S, Small JV. Scar/WAVE is localised at the tips of protruding lamellipodia in living cells. *FEBS Lett.* (2001) 492:215-20.

Hall A. Rho GTPases and the actin cytoskeleton. *Science.* (1998) 279:509-14.

Hall A. ras and GAP--who's controlling whom? *Cell.* (1990) 61:921-3. Review.

Hall C, Monfries C, Smith P, Lim HH, Kozma R, Ahmed S, Vanniasingham V, Leung, T, Lim L. Novel human cDNA encoding a 34,000 Mr protein n-chimaerin, related to both the regulatory domain of protein kinase C and BCR, the product of the breakpoint cluster region gene. *J Mol. Biol.* (1990) 211:11-16.

Han J, Luby-Phelps K, Das B, Shu X, Xia Y, Mosteller RD, Krishna UM, Falck JR, White MA, Broek D. Role of substrates and products of PI 3-kinase in regulating activation of Rac-related guanosine triphosphatase by Vav. *Science* (1997) 279:559-60.

Harden N, Lee J, Loh HY, Ong YM, Tan I, Leung T, Manser E, Lim L. A *Drosophila* homolog of the Rac- and Cdc42-activated serine/threonine kinase PAK is a potential

focal adhesion and focal complex protein that colocalizes with dynamic actin structures. *Mol Cell Biol.* (1996) 16:1896-908.

Hartwig JH, Bokoch GM, Carpenter CL, Janmey PA, Taylor LA, Toker A, Stossel TP. Thrombin receptor ligation and activated Rac uncap actin filament barbed ends through phosphoinositide synthesis in permeabilized human platelets. *Cell.* (1995) 82:643-53.

Hauser W, Knobloch KP, Eigenthaler M, Gambaryan S, Krenn V, Geiger J, Glazova M, Rohde E, Horak I, Walter U, Zimmer M. Megakaryocyte hyperplasia and enhanced agonist-induced platelet activation in vasodilator-stimulated phosphoprotein knockout mice. *Proc Natl Acad Sci U S A.* (1999) 96:8120-5.

Hawkins PT, Eguinoa A, Qiu RG, Stokoe D, Cooke FT, Walters R, Wennstrom S, Claesson-Welsh L, Evans T, Symons M, et. al. PDGF stimulates an increase in GTP-Rac via activation of phosphoinositide 3-kinase. *Curr Biol.* (1995) 5:393-403.

Herrmann C, Nassar N. Ras and its effectors. *Prog Biophys Mol Biol.* (1996) 66(1):1-41.

Heyworth PG, Knaus UG, Settleman J, Curnutte JT, Bokoch GM. Regulation of NADPH oxidase activity by Rac GTPase activating protein(s). *Mol Biol Cell.* (1993) 4:1217-23.

Higgs HN, Pollard T. Regulation of actin filament network formation through ARP2/3 complex: activation by a diverse array of proteins. *Annu Rev Biochem.* (2001)70:649-76.

Higgs HN, Pollard TD. Activation by Cdc42 and PIP(2) of Wiskott-Aldrich syndrome protein (WASp) stimulates actin nucleation by Arp2/3 complex. *J Cell Biol.* (2000) 150:1311-20.

Higgs HN, Pollard TD. Regulation of actin polymerization by Arp2/3 complex and WASp/Scar proteins. *J Biol Chem.* (1999) 274:32531-4. Review.

Hirokawa N, Funakoshi T, Sato-Harada R, Kanai Y. Selective stabilization of tau in axons and microtubule-associated protein 2C in cell bodies and dendrites contributes to polarized localization of cytoskeletal proteins in mature neurons. *J Cell Biol.* (1996) 132:667-79.

Ho HY, Rohatgi R, Lebensohn AM, Le Ma, Li J, Gygi SP, Kirschner MW. Toca-1 mediates Cdc42-dependent actin nucleation by activating the N-WASP-WIP complex. *Cell.* (2004) 118:203-16.

Ho HY, Rohatgi R, Ma L, Kirschner MW. CR16 forms a complex with N-WASP in brain and is a novel member of a conserved proline-rich actin-binding protein family. *Proc Natl Acad Sci U S A.* (2001) 98:11306-11.

Hoffman GR, Nassar N, Cerione RA. Structure of the Rho family GTP-binding protein Cdc42 in complex with the multifunctional regulator RhoGDI. *Cell.* (2000) 100:345-56.



Hori K, Yasuda H, Konno D, Maruoka H, Tsumoto T, Sobue K. NMDA receptor-dependent synaptic translocation of insulin receptor substrate p53 via protein kinase C Signaling. *J Neurosci.* (2005) 25:2670-81.

Hori K, Konno D, Maruoka H, Sobue K. MALS is a binding partner of IRSp53 at cell-cell contacts. *FEBS Lett.* (2003) 554:30-4.

Howard TH, Watts RG. Actin polymerization and leukocyte function. *Curr. Opin. Hematol.* (1994)1:61-8.

Hu KQ, Settleman J. Tandem SH2 binding sites mediate the RasGAP-RhoGAP interaction: a conformational mechanism for SH3 domain regulation. *EMBO J.* (1997) 16:473-83.

Herbrand U, Ahmadian MR. p190-RhoGAP as an integral component of the Tiam1/Rac1-induced downregulation of Rho. *Biol Chem.* (2006) 387:311-7.

Hussain NK, Jenna S, Glogauer M, Quinn CC, Wasiake S, Guipponi M, Antonarakis SE, Kay BK, Stossel TP, Lamarche-Vane N, McPherson PS. Endocytic protein intersectin-1 regulates actin assembly via Cdc42 and N-WASP. *Nat Cell Biol.* (2001) 3:927-32.

Innocenti M, Gerboth S, Rottner K, Lai FP, Hertzog M, Stradal TE, Frittoli E, Didry D, Polo S, Disanza A, Benesch S, Di Fiore PP, Carlier MF, Scita G. Abi1 regulates the activity of N-WASP and WAVE in distinct actin-based processes. *Nat Cell Biol.* (2005) 7:969-76.

Innocenti M, Zucconi A, Disanza A, Frittoli E, Areces LB, Steffen A, Stradal TE, Di Fiore PP, Carlier MF, Scita G. Abi1 is essential for the formation and activation of a WAVE2 signaling complex. *Nat Cell Biol.* (2004) 6:319-27.

Insall RH, Machesky LM. Regulation of WASP: PIP2 Pipped by Toca-1? *Cell.* (2004) 118:140-1. Review.

Insall R, Muller-Taubenberger A, Machesky L, Kohler J, Simmeth E, Atkinson SJ, Weber I, Gerisch G. Dynamics of the Dictyostelium Arp2/3 complex in endocytosis, cytokinesis, and chemotaxis. *Cell Motil Cytoskeleton.* (2001) 50:115-28.

Ishizaki T, Morishima Y, Okamoto M, Furuyashiki T, Kato T, Narumiya S. Coordination of microtubules and the actin cytoskeleton by the Rho effector mDia1. *Nat Cell Biol.* (2001) 3:8-14.

Itoh K, Yoshioka K, Akedo H, Uehata M, Ishizaki T, Narumiya S. An essential part for Rho-associated kinase in the transcellular invasion of tumor cells. *Nat Med.* (1999) 5:221-5.

Itoh, T. Dyanmin and the actin cytoskeleton cooperatively regulate plasma membrane invagination by BAR and F-BAR proteins. *Dev. Cell* (2005) 9:791-804.

Jaffe AB, Hall A. Rho GTPases: biochemistry and biology. *Annu Rev Cell Dev Biol.* (2005) 21:247-69. Review.

Jenzora A, Behrendt B, Small JV, Wehland J, Stradal TE. PREL1 provides a link from Ras signaling to the actin cytoskeleton via Ena/VASP proteins. *FEBS Lett.* (2006) 580:455-63.

Joberty G, Perlungher RR, Macara IG. The Borgs, a new family of Cdc42 and TC10 GTPase-interacting proteins. *Mol Cell Biol.* (1999) 19:6585-97.

Johnson DI. Cdc42: An essential Rho-type GTPase controlling eukaryotic cell polarity. *Microbiol Mol Biol Rev.* (1999) 63:54-105. Review.

Katz ME, McCormick F. Signal transduction from multiple Ras effectors. *Curr Opin Genet Dev.* (1997) 7:75-9. Review.

Kim AS, Kakalis LT, Abdul-Manan N, Liu GA, Rosen MK. Autoinhibition and activation mechanisms of the Wiskott-Aldrich syndrome protein. *Nature.* (2000) 404:151-8.

Kaverina I, Stradal TE, Gimona M. Podosome formation in cultured A7r5 vascular smooth muscle cells requires Arp2/3-dependent *de novo* actin polymerization at discrete microdomains. *J Cell Sci.* (2003) 116:4915-24.

Kawamura K, Takano K, Suetsugu S, Kurisu S, Yamazaki D, Miki H, Takenawa T, Endo T. N-WASP and WAVE2 acting downstream of phosphatidylinositol 3-kinase are required for myogenic cell migration induced by hepatocyte growth factor. *J Biol Chem.* (2004) 279:54862-71.

Kenny AJ. Regulatory peptide metabolism at cell surfaces: the key role of endopeptidase-24.11. *Biomed Biochim Acta.* (1986) 45:1503-13.

Kidd T, Brose K, Mitchell KJ, Fetter RD, Tessier-Lavigne M, Goodman CS, Tear G. Roundabout controls axon crossing of the CNS midline and defines a novel subfamily of evolutionarily conserved guidance receptors. *Cell.* (1998) 92:205-15.

Kolluri R, Toliaas KF, Carpenter CL, Rosen FS, Kirchhausen T. Direct interaction of the Wiskott-Aldrich syndrome protein with the GTPase Cdc42. *Proc Natl Acad Sci U S A.* (1996) 93:5615-8.

Knaus UG, Morris S, Dong HJ, Chernoff J, Bokoch GM. Regulation of human leukocyte p21-activated kinases through G protein—coupled receptors. *Science.* (1995) 269:221-3.

Knaus UG, Heyworth PG, Evans T, Curnutte JT, Bokoch GM. Regulation of phagocyte oxygen radical production by the GTP-binding protein Rac 2. *Science*. (1991) 254:1512-5.

Kobayashi K, Kuroda S, Fukata M, Nakamura T, Nagase T, Nomura N, Matsuura Y, Yoshida-Kubomura N, Iwamatsu A, Kaibuchi K. p140Sra-1 (specifically Rac1-associated protein) is a novel specific target for Rac1 small GTPase. *J Biol Chem*. (1998) 273:291-5.

Koh CG, Tan EJ, Manser E, Lim L. The p21-activated kinase PAK is negatively regulated by POPX1 and POPX2, a pair of serine/threonine phosphatases of the PP2C family. *Curr Biol*. (2002) 12:317-21.

Koh CG, Manser E, Zhao ZS, Ng CP, Lim L. Beta1PIX, the PAK-interacting exchange factor, requires localization via a coiled-coil region to promote microvillus-like structures and membrane ruffles. *J Cell Sci*. (2001) 114:4239-51.

Kozma R, Ahmed S, Best A, Lim L. The GTPase-activating protein n-chimaerin cooperates with Rac1 and Cdc42Hs to induce the formation of lamellipodia and filopodia. *Mol Cell Biol*. (1996) 16:5069-80.

Kozma R, Ahmed S, Best A, Lim L. The Ras-related protein Cdc42Hs and bradykinin promote formation of peripheral actin microspikes and filopodia in Swiss 3T3 fibroblasts. *Mol Cell Biol.* (1995) 15:1942-52.

Krause M, Sechi AS, Konradt M, Monner D, Gertler FB, Wehland J. Fyn-binding protein (Fyb)/SLP-76-associated protein (SLAP), Ena/vasodilator-stimulated phosphoprotein (VASP) proteins and the Arp2/3 complex link T cell receptor (TCR) Signaling to the actin cytoskeleton. *J Cell Biol.* (2000) 149:181-94.

Krugmann S, Jordens I, Gevaert K, Driessens M, Vandekerckhove J, Hall A. Cdc42 induces filopodia by promoting the formation of an IRSp53:Mena complex. *Curr Biol.* (2001) 11:1645-55.

Kunda P, Craig G, Dominguez V, Baum B. Abi, SRA1, and Kette control the stability and localization of SCAR/WAVE to regulate the formation of actin-based protrusions. *Curr Biol.* (2003) 13:1867-75.

Kuroda S, Fukata M, Nakagawa M, Fujii K, Nakamura T, Ookubo T, Izawa I, Nagase T, Nomura N, Tani H, Shoji I, Matsuura Y, Yonehara S, Kaibuchi K. Role of IQGAP1, a target of the small GTPases Cdc42 and Rac1, in regulation of E-cadherin-mediated cell-cell adhesion. *Science.* (1998) 281:832-5.

Kwiatkowski DJ. Functions of Gelsolin: Motility, signaling, apoptosis, cancer. *Curr. Opin. Cell Biol.* (1999) 11:103-08.

Laudanna C, Campbell JJ, Butcher EC. Role of Rho in chemoattractant-activated leukocyte adhesion through integrins. *Science.* (1996) 271:981-83.

Lambrechts A, Kwiatkowski AV, Lanier LM, Bear JE, Vandekerckhove J, Ampe C, Gertler FB. cAMP-dependent protein kinase phosphorylation of EVL, a Mena/VASP relative, regulates its interaction with actin and SH3 domains. *J Biol Chem.* (2000) 275:36143-51.

Lancaster A, Taylor-Harris, PM, Self AJ, Brill S, van Erp HE, Hall A. Characterization of rhoGAP. A GTPase-activating protein for rho-related small GTPases. *J Biol. Chem.* (1994) 269:1137-42.

Lanier LM, Gertler FB. From Abl to actin: Abl tyrosine kinase and associated proteins in growth cone motility. *Curr Opin Neurobiol.* (2000) 10:80-7. Review.

Lanier LM, Gates MA, Witke W, Menzies AS, Wehman AM, Macklis JD, Kwiatkowski D, Soriano P, Gertler FB. Mena is required for neurulation and commissure formation. *Neuron.* (1999) 22:313-25.

Laurent V, Loisel TP, Harbeck B, Wehman A, Grobe L, Jockusch BM, Wehland J, Gertler FB, Carrier MF. Role of proteins of the Ena/VASP family in actin-based motility of *Listeria monocytogenes*. *J Cell Biol.* (1999) 144:1245-58.

Lelias JM, Adra CN, Wulf GM, Guillemot JC, Khagad M, Caput D, Lim B. cDNA cloning of a human mRNA preferentially expressed in hematopoietic cells and with homology to a GDP-dissociation inhibitor for the rho GTP-binding proteins. *Proc Natl Acad Sci U S A.* (1993) 90:1479-83.

Les Erickson F, Corsa AC, Dose AC, Burnside B. Localization of a class III myosin to filopodia tips in transfected HeLa cells requires an actin-binding site in its tail domain. *Mol Biol Cell.* (2003) 14:4173-80.

Letourneau PC, Shattuck TA. Distribution and possible interactions of actin-associated proteins and cell adhesion molecules of nerve growth cones. *Development.* (1989) 105:505-19

Leung T, Chen XQ, Tan I, Manser E, Lim L. Myotonic dystrophy kinase-related Cdc42-binding kinase acts as a Cdc42 effector in promoting cytoskeletal reorganization. *Mol Cell Biol.* (1998) 18:130-40.



Leung T, Chen XQ, Manser E, Lim L. The p160 RhoA-binding kinase ROK alpha is a member of a kinase family and is involved in the reorganization of the cytoskeleton. *Mol Cell Biol.* (1996) 16:5313-27.

Leung T, Manser E, Tan L, Lim L. A novel serine/threonine kinase binding the Ras-related RhoA GTPase which translocates the kinase to peripheral membranes. *J Biol Chem.* (1995) 270:29051-4.

Lewis AK, Bridgman PC. Nerve growth cone lamellipodia contain two populations of actin filaments that differ in organization and polarity. *J Cell Biol.* (1992) 119:1219-43.

Li HY, Cao K, Zheng Y. Ran in the spindle checkpoint: a new function for a versatile GTPase. *Trends Cell Biol.* (2003) 13:553-7.

Li Z, Hannigan M, Mo Z, Liu B, Lu W, Wu Y, Smrcka AV, Wu G, Li L, Liu M, Huang CK, Wu D. Directional sensing requires G beta gamma-mediated PAK1 and PIX alpha-dependent activation of Cdc42. *Cell.* (2003) 114:215-27.

Lim L, Manser E, Leung T, Hall C. Regulation of phosphorylation pathways by p21 GTPases. The p21 Ras-related Rho subfamily and its role in phosphorylation signaling pathways. *Eur J Biochem.* (1996) 242:171-85. Review.

Linder S, Aepefelbacher M. Podosomes: adhesion hot-spots of invasive cells. *Trends Cell Biol.* (2003) 13:376-385.

Lommel S, Benesch S, Rottner K, Franz T, Wehland J, Kuhn R. Actin pedestal formation by enteropathogenic *Escherichia coli* and intracellular motility of *Shigella flexneri* are abolished in N-WASP-defective cells. *EMBO Rep.* (2001) 2:850-7.

Loo TH, Ng YW, Lim L, Manser E. GIT1 activates p21-activated kinase through a mechanism independent of p21 binding. *Mol Cell Biol.* (2004) 24:3849-59.

Lauffenburger DA, Horwitz AF. Cell migration: a physically integrated molecular process. *Cell.* (1996)84:359-69.

Lockyer PJ, Kupzig S, Cullen PJ. CAPRI regulates Ca<sup>2+</sup>-dependent inactivation of the Ras-MAPK pathway. *Curr. Biol.* (2001)11:981-6.

Lockyer PJ, Bottonley JR, Reynolds JS, McNulty TJ, Venkateswarlu K, Potter BV, Dempsey CE, Cullen PJ. Distinct subcellular localizations of the putative inositol 1,3,4,5-tetrakisphosphate receptors GAP1IP4BP and GAP1m result from the GAP1IP4BP PH domain directing plasma membrane targeting. *Curr. Biol.* (1997) 7:1007-10.

Ma AD, metjian A, Bagrodia S, Taylor S, Abrams CS. Cytoskeletal reorganization by G protein-coupled receptors is dependent on phosphoinositide 3-kinase gamma, a Rac guanosine exchange factor, and Rac. *Mol. Cell Biol.* (1998)18:4744-51.

Machesky LM, Mullins RD, Higgs HN, Kaiser DA, Blanchoin L, May RC, Hall ME, Pollard TD. Scar, a WASp-related protein, activates nucleation of actin filaments by the Arp2/3 complex. *Proc Natl Acad Sci U S A.* (1999) 96:3739-44.

Machesky LM, Insall RH. Scar1 and the related Wiskott-Aldrich syndrome protein, WASP, regulate the actin cytoskeleton through the Arp2/3 complex. *Curr Biol.* (1998) 8:1347-56.

Machesky LM, Reeves E, Wientjes F, Mattheyse FJ, Grogan A, Totty NF, Burlingame AL, Hsuan JJ, Segal AW. Mammalian actin-related protein 2/3 complex localizes to regions of lamellipodial protrusion and is composed of evolutionarily conserved proteins. *Biochem J.* (1997) 328:105-12.

Machesky LM, Hall A. Role of actin polymerization and adhesion to extracellular matrix in Rac- and Rho-induced cytoskeletal reorganization. *J Cell Biol.* (1997) 138:913-26.

Machesky LM, Hall A. Rho: a connection between membrane receptor signaling and the cytoskeleton. *Trends Cell Biol.* (1996) 6:304-10.

Machesky LM, Atkinson SJ, Ampe C, Vandekerckhove J, Pollard TD. Purification of a cortical complex containing two unconventional actins from *Acanthamoeba* by affinity chromatography on profilin-agarose. *J Cell Biol.* (1994) 127:107-15.

Machesky LM, Poland TD. Profilin as a potential mediator of membrane-cytoskeleton communication. *Trends Cell Biol.* (1993) 3:381-5.

Madaule P, Eda M, Watanabe N, Fujisawa K, Matsuoka T, Bito H, Ishizaki T, Narumiya S. Role of citron kinase as a target of the small GTPase Rho in cytokinesis. *Nature.* (1998) 394:491-4.

Mallavarapu A, Mitchison T. Regulated actin cytoskeleton assembly at filopodium tips controls their extension and retraction. *J Cell Biol.* (1999) 146:1097-106.

Manabe R, Kovalenko M, Webb DJ, Horwitz AR. GIT1 functions in a motile, multi-molecular Signaling complex that regulates protrusive activity and cell migration. *J Cell Sci.* (2002) 115:1497-510.

Manser E, Loo TH, Koh CG, Zhao ZS, Chen XQ, Tan L, Tan I, Leung T, Lim L. PAK kinases are directly coupled to the PIX family of nucleotide exchange factors. *Mol Cell.* (1998) 1:183-92.

Manser E, Huang HY, Loo TH, Chen XQ, Dong JM, Leung T, Lim L. Expression of constitutively active alpha-PAK reveals effects of the kinase on actin and focal complexes. *Mol Cell Biol.* (1997) 17:1129-43.

Manser E, Chong C, Zhao ZS, Leung T, Michael G, Hall C, Lim L. Molecular cloning of a new member of the p21-Cdc42/Rac-activated kinase (PAK) family. *J Biol Chem.* (1995) 270:25070-8.

Manser E, Leung T, Salihuddin H, Zhao ZS, Lim L. A brain serine/threonine protein kinase activated by Cdc42 and Rac1. *Nature.* (1994) 367:40-6.

Manser E, Leung T, Salihuddin H, Tan L, Lim L. A non-receptor tyrosine kinase that inhibits the GTPase activity of p21cdc42. *Nature.* (1993) 363 :364-7.

Manser E, Leung T, Monfries C, Teo M, Hall C, Lim L. Diversity and versatility of GTPase activating proteins for the p21rho subfamily of ras G proteins detected by a novel overlay assay. *J Biol Chem.* (1992) 267:16025-8.

Marler KJ, Kozma R, Ahmed S, Dong JM, Hall C, Lim L. Outgrowth of neurites from NIE-115 neuroblastoma cells is prevented on repulsive substrates through the action of PAK. *Mol Cell Biol.* (2005) 25:5226-41.

Masuda, M. Endophilin BAR domain drives membrane curvature by two newly identified structure-based mechanisms. *EMBO J.* (2006)25:2889-97.

Martinez-Quiles N, Rohatgi R, Anton IM, Medina M, Saville SP, Miki H, Yamaguchi H, Takenawa T, Hartwig JH, Geha RS, Ramesh N. WIP regulates N-WASP-mediated actin polymerization and filopodium formation. *Nat Cell Biol.* (2001) 3:484-91.

Matsui T, Amano M, Yamamoto T, Chihara K, Nakafuku M, Ito M, Nakano T, Okawa K, Iwamatsu A, Kaibuchi K. Rho-associated kinase, a novel serine/threonine kinase, as a putative target for small GTP binding protein Rho. *EMBO J.* (1996) 15:2208-16.

Matsudaria P. Modular organization of actin crosslinking proteins. *Trends. Biochem. Sci.* (1991) 16:87-92.

McHuge B, Krause SA, Yu B, Deans AM, Heasman S, McLaughlin P, Heck MM. Invadolysin: a novel, conserved metalloprotease links mitotic structural rearrangements with cell migration. *J Cell Biology*, 167:673-686.

Memon AR. The role of ADP-ribosylation factor and SAR1 in vesicular trafficking in plants. *Biochim Biophys Acta.* (2004) Jul 1;1664(1):9-30. Review. Erratum in: *Biochim Biophys Acta.* (2004) 1665:201.

Michiels F, Habets GG, Stam JC, van der Kammen RA, collard JG. A role of Rac in Tiam1-induced membrane ruffling invasion. *Nature* (1995)375:338-40.

Miki H, Yamaguchi H, Suetsugu S, Takenawa T. IRSp53 is an essential intermediate between Rac and WAVE in the regulation of membrane ruffling. *Nature*. (2000) 408:732-5.

Miki H, Takenawa T. WAVE2 serves a functional partner of IRSp53 by regulating its interaction with Rac. *Biochem Biophys Res Commun*. (2002) 293:93-9.

Miki H, Yamaguchi H, Suetsugu S, Takenawa T. IRSp53 is an essential intermediate between Rac and WAVE in the regulation of membrane ruffling. *Nature*. (2000) 408:732-5.

Miki H, Suetsugu S, Takenawa T. WAVE, a novel WASP-family protein involved in actin reorganization induced by Rac. *EMBO J*. (1998)17:6932-41.

Miki H, Takenawa T. Direct binding of the verprolin-homology domain in N-WASP to actin is essential for cytoskeletal reorganization. *Biochem Biophys Res Commun*. (1998) 243:73-8.

Miki H, Sasaki T, Takai Y, Takenawa T. Induction of filopodium formation by a WASP-related actin-depolymerizing protein N-WASP. *Nature*. (1998) 391:93-6.

Miki H, Miura K, Takenawa T. N-WASP, a novel actin-depolymerizing protein, regulates the cortical cytoskeletal rearrangement in a PIP2-dependent manner downstream of tyrosine kinases. *EMBO J.* (1996) 15:5326-35.

Millard TH, Bompard G, Heung MY, Dafforn TR, Scott DJ, Machesky LM, Futterer K. Structural basis of filopodia formation induced by the IRSp53/MIM homology domain of human IRSp53. *EMBO J.* (2005) 24:240-50.

Minden A, Lin A, Claret FX, Abo A, Karin M. Selective activation of the JNK Signaling cascade and c-Jun transcriptional activity by the small GTPases Rac and Cdc42Hs. *Cell.* (1995) 81:1147-57.

Mira JP, Benard V, Groffen J, Sanders LC, Knaus UG. Endogenous, hyperactive Rac3 controls proliferation of breast cancer cells by a p21-activated kinase-dependent pathway. *Proc Natl Acad Sci U S A.* (2000) 97:185-9.

Mitchison TJ, Cramer LP. Actin-based cell motility and cell locomotion. *Cell.* (1996) 84:371-79.

Miura K, Miki H, Shimazaki K, Kawai N, Takenawa T. Interaction of Ash/Grb-2 via its SH3 domains with neuron-specific p150 and p65. *Biochem J.* (1996) 316 :639-45.



Molina IJ, Sancho J, Terhorst C, Rosen FS, Remold-O'Donnell E. T cells of patients with the Wiskott-Aldrich syndrome have a restricted defect in proliferative responses. *J Immunol.* (1993) 151:4383-90.

Molina IJ, Kenney DM, Rosen FS, Remold-O'Donnell E. T cell lines characterize events in the pathogenesis of the Wiskott-Aldrich syndrome. *J Exp Med.* (1992) 176:867-74.

Moncrieff CL, Bailey ME, Morrison N, Johnson KJ. Cloning and chromosomal localization of human Cdc42-binding protein kinase beta. *Genomics.* (1999) 57:297-300.

Mouneimne G, Soon L, DesMarais V, Sidani M, Song X, Yip SC, Ghosh M, Eddy R, Backer JM, Condeelis J. Phospholipase C and cofilin are required for carcinoma cell directionality in response to EGF stimulation. *J Cell Biol.* (2004) 166:697-708.

Moreau V, Tatin F, Varon C, Genot E. Actin can reorganize into podosomes in aortic endothelial cells, a process controlled by Cdc42 and RhoA. *Mol Cell Biol.* (2003) 23:6809-22.

Moreau V, Frischknecht F, Reckmann I, Vincentelli R, Rabut G, Stewart D, Way M. A complex of N-WASP and WIP integrates signaling cascades that lead to actin polymerization. *Nat Cell Biol.* (2000) 2:441-8.

Musacchio A, Gibson T, Rice P, Thompson J, Saraste M. The PH domain: a common piece in the structural pathwork of signalling proteins. *Trends. Biochem. Sci.* (1993)18:343-48.

Mullins RD, Heuser JA, Pollard TD. The interaction of Arp2/3 complex with actin: nucleation, high affinity pointed end capping, and formation of branching networks of filaments. *Proc Natl Acad Sci U S A.* (1998) 95:6181-6.

Murphy AM, Montell DJ. Cell type-specific roles for Cdc42, Rac, and RhoL in *Drosophila* oogenesis. *J Cell Biol.* (1996)133:617-30.

Nagata K, Driessens M, Lamarche N, Gorski JL, Hall A. Activation of G1 progression, JNK mitogen-activated protein kinase, and actin filament assembly by the exchange factor FGD1. *J Biol. Chem.* (1998) 273:15453-57.

Nakagawa H, Miki H, Nozumi M, Takenawa T, Miyamoto S, Wehland J, Small JV. IRSp53 is colocalised with WAVE2 at the tips of protruding lamellipodia and filopodia independently of Mena. *J Cell Sci.* (2003) 116:2577-83.

Nakagawa H, Miki H, Ito M, Ohashi K, Takenawa T, Miyamoto S. N-WASP, WAVE and Mena play different roles in the organization of actin cytoskeleton in lamellipodia. *J Cell Sci.* (2001) 114:1555-65.

Nakagawa O, Fujisawa K, Ishizaki T, Saito Y, Nakao K, Narumiya S. ROCK-I and ROCK-II, two isoforms of Rho-associated coiled-coil forming protein serine/threonine kinase in mice. *FEBS Lett.* (1996) 392:189-93.

Nakahara H, Otani T, Sasaki T, Miura Y, Takai Y, Kogo M. Involvement of Cdc42 and Rac small G proteins in invadopodia formation of RPMI7951 cells. *Genes Cells.* (2003) 8:1019-27.

Nie Z, Boehm M, Boja ES, Vass WC, Bonifacino JS, Fales HM, Randazzo PA. Specific regulation of the adaptor protein complex AP-3 by the Arf GAP AGAP1. *Dev Cell.* (2003) 5:513-21.

Niebuhr K, Ebel F, Frank R, Reinhard M, Domann E, Carl UD, Walter U, Gertler FB, Wehland J, Chakraborty T. A novel proline-rich motif present in ActA of *Listeria monocytogenes* and cytoskeletal proteins is the ligand for the EVH1 domain, a protein module present in the Ena/VASP family. *EMBO J.* (1997) 16:5433-44.

Nikolic M, Chou MM, Lu W, Mayer BJ, Tsai LH. The p35/Cdk5 kinase is a neuron-specific Rac effector that inhibits Pak1 activity. *Nature.* (1998) 395:194-8.

Nishimura T, Yamaguchi T, Kato K, Yoshizawa M, Nabeshima Y, Ohno S, Hoshino M, Kaibuchi K. PAR-6-PAR-3 mediates Cdc42-induced Rac activation through the Rac GEFs STEF/Tiam1. *Nat Cell Biol.* (2005) 7:270-7.

Nobes CD, Hall A. Rho GTPases control polarity, protrusion, and adhesion during cell movement. *J Cell Biol.* (1999) 144:1235-44.

Nobes CD, Hall A. Rho, rac and cdc42 GTPases: regulators of actin structures, cell adhesion and motility. *Biochem Soc Trans.* (1995) 23:456-9. Review.

Nomanbhoy TK, Erickson JW, Cerione RA. Kinetics of Cdc42 membrane extraction by RhoGDI monitored by real-time fluorescence resonance energy transfer. *Biochemistry.* (1999) 38(6):1744-50.

Nurse PM. Nobel Lecture. Cyclin dependent kinases and cell cycle control. *Biosci Rep.* (2002) 22:487-99.

O'Connor TP, Duerr JS, Bentley D. Pioneer growth cone steering decisions mediated by single filopodial contacts in situ. *J Neurosci.* (1990) 10:3935-46.

Obermeier A, Ahmed S, Manser E, Yen SC, Hall C, Lim L. PAK promotes morphological changes by acting upstream of Rac. *EMBO J.* (1998) 17:4328-39.

Ochs HD. The Wiskott-Aldrich syndrome. *Semin Hematol.* (1998) 35:332-45.

Oda A, Miki H, Wada I, Yamaguchi H, Yamazaki D, Suetsugu S, Nakajima M, Nakayama A, Okawa K, Miyazaki H, Matsuno K, Ochs HD, Machesky LM, Fujita H, Takenawa T. WAVE/Scars in platelets. *Blood*. (2005) ;105:3141-8.

Oda K, Shiratsuchi T, Nishimori H, Inazawa J, Yoshikawa H, Taketani Y, Nakamura Y, Tokino T. Identification of BAIAP2 (BAI-associated protein 2), a novel human homologue of hamster IRSp53, whose SH3 domain interacts with the cytoplasmic domain of BAI1. *Cytogenet Cell Genet*. (1999) 84:75-82.

Okamura-Oho Y, Miyashita T, Yamada M. Distinctive tissue distribution and phosphorylation of IRSp53 isoforms. *Biochem Biophys Res Commun*. (2001) 289:957-60.

Olofsson B. Rho guanine dissociation inhibitors: pivotal molecules in cellular signaling. *Cell Signal*. (1999) 11:545-54. Review.

Olson MF, Sterpetti P, Nagata K, Toksoz D, Hall A. Distinct roles for DH and PH domains in the Lbc oncogene. *Oncogene* (1997) 15 2827-31.

Olson MF, Ashworth A, Hall A. An essential role for Rho, Rac and Cdc42 GTPases on cell cycle progression through G1. *Science* (1996) 269:1270-72.

Paglini G, Caceres A. The role of the Cdk5--p35 kinase in neuronal development. *Eur J Biochem.* (2001) 268:1528-33.

Pantaloni D, Boujemaa R, Didry D, Gounon P, Carlier MF. The Arp2/3 complex branches filament barbed ends: functional antagonism with capping proteins. *Nat Cell Biol.* (2000) 2:385-91.

Park SJ, Suetsugu S, Takenawa T. Interaction of HSP90 to N-WASP leads to activation and protection from proteasome-dependent degradation. *EMBO J.* (2005) 24:1557-70.

Parrini MC, Lei M, Harrison SC, Mayer BJ. Pak1 kinase homodimers are autoinhibited in trans and dissociated upon activation by Cdc42 and Rac1. *Mol Cell.* (2002) 9:73-83.

Pasqualato S, Renault L, Cherfils J. Arf, Arl, Arp and Sar proteins: a family of GTP-binding proteins with a structural device for 'front-back' communication. *EMBO Rep.* (2002) 3:1035-41.

Pasteris NG, Cadle A, Logie LJ, Porteous ME, Schwartz CE, Stevenson RE, Glover TW, Wilroy RS, Gorski JL. Isolation and characterization of the faciogenital dysplasia (Aarskog- Scott syndrome) gene: a putative Rho/Rac guanine nucleotide exchange factor. (1994) *Cell* 79:669-78.

Paterson HF, Self AJ, Garrett MD, Just I, Aktories K, Hall A. Microinjection of recombinant p21rho induces rapid changes in cell morphology. *J Cell Biol.* (1990) 111:1001-7.

Pendergast AM. The Abl family kinases: mechanisms of regulation and Signaling. *Adv. Cancer Res.* (2002) 85:51-100.

Pellegrin S, Mellor H. The Rho family GTPase Rif induces filopodia through mDia2. *Curr Biol.* (2005) 15:129-33.

Peng J, Wallar BJ, Flanders A, Swiatek PJ, Alberts AS. Disruption of the Diaphanous-related formin Drf1 gene encoding mDia1 reveals a role for Drf3 as an effector for Cdc42. *Curr Biol.* (2003) 13:534-45.

Pereira-Leal JB, Seabra MC. Evolution of the Rab family of small GTP-binding proteins. *J Mol Biol.* (2001) 313:889-901.

Perry SV. Vertebrate tropomyosin: distribution, properties and function. *J Muscle Res Cell Motil.* (2001) 22:5-49. Review.

Peter, BJ. BAR domains as sensors of membrane curvature: the amphophysin BAR structures. *Science* (2004) 303:495-99.

Pirone DM, Carter DE, Burbelo PD. Evolutionary expansion of CRIB-containing Cdc42 effector proteins. *Trends Genet.* (2001) 17:370-3.

Pollard TD, Blanchoin L, Mullins RD. Molecular mechanisms controlling actin filament dynamics in nonmuscle cells. *Annu Rev Biophys Biomol Struct.* (2000) 29:545-76. Review.

Pollard TD, Almo S, Quirk S, Vinson V, Lattman EE. Structure of actin binding proteins: insights about function at atomic resolution. *Annu Rev Cell Biol.* (1994) 10:207-49. Review.

Pollard TD, Borisy GG. Cellular motility driven by assembly and disassembly of actin filaments. *Cell.* (2003) Feb 21;112(4):453-65. Review. Erratum in: *Cell.* (2003) 113(4):549.

Prehoda KE, Scott JA, Mullins RD, Lim WA. Integration of multiple signals through cooperative regulation of the N-WASP-Arp2/3 complex. *Science.* (2000) 290:801-6.

Prehoda KE, Lee DJ, Lim WA. Structure of the enabled/VASP homology 1 domain-peptide complex: a key component in the spatial control of actin assembly. *Cell.* (1999) May 14;97(4):471-80.



Prendergast GC, Khosravi-Far R, Solski PA, Kurzawa H, Lebowitz PF, Der CJ. Critical role of Rho in cell transformation by oncogenic Ras. *Oncogene*. (1995) 10:2289-96.

Prigmore E, Ahmed S, Best A, Kozma R, Manser E, Segal AW, Lim L. A 68-kDa kinase and NADPH oxidase component p67phox are targets for Cdc42Hs and Rac1 in neutrophils. *J Biol Chem*. (1995) 270:10717-22.

Pruitt K, Der CJ. Ras and Rho regulation of the cell cycle and oncogenesis. *Cancer Lett*. (2001)171:1-10. Review.

Qualmann B, Kelly RB. Syndapin isoforms participate in receptor-mediated endocytosis and actin organization. *J Cell Biol*. (2000) 148:1047-62.

Qualmann B, Roos J, DiGregorio PJ, Kelly RB. Syndapin I, a synaptic dynamin-binding protein that associates with the neural Wiskott-Aldrich syndrome protein. *Mol Biol Cell*. (1999) 10:501-13.

Ramesh N, Anton IM, Hartwig JH, Geha RS. WIP, a protein associated with wiskott-aldrich syndrome protein, induces actin polymerization and redistribution in lymphoid cells. *Proc Natl Acad Sci U S A*. (1997) 94:14671-6.

Reinhard M, Giehl K, Abel K, Haffner C, Jarchau T, Hoppe V, Jockusch BM, Walter U. The proline-rich focal adhesion and microfilament protein VASP is a ligand for profilins. *EMBO J.* (1995)14:1583-9.

Reinhard M, Halbrugge M, Scheer U, Wiegand C, Jockusch BM, Walter U. The 46/50 kDa phosphoprotein VASP purified from human platelets is a novel protein associated with actin filaments and focal contacts. *EMBO J.* (1992) 11:2063-70.

Remold-O'Donnell E, Van Brocklyn J, Kenney DM. Effect of platelet calpain on normal T-lymphocyte CD43: hypothesis of events in the Wiskott-Aldrich syndrome. *Blood.* (1992) 79:1754-62.

Repasky GA, Chenette EJ, Der CJ. Renewing the conspiracy theory debate: does Raf function alone to mediate Ras oncogenesis? *Trends Cell Biol.* (2004) 14:639-47.

Remold-O'Donnell E, Rosen FS, Kenney DM. Defects in Wiskott-Aldrich syndrome blood cells. *Blood* (1996) 87:2621-31.

Ridley AJ. Rho proteins: linking Signaling with membrane trafficking. *Traffic.* (2001) 2:303-10. Review.

Ridley AJ, Self AJ, Kasmi F, Paterson HF, Hall A, Marshall CJ, Ellis C. rho family GTPase activating proteins p190, bcr and rhoGAP show distinct specificities *in vitro* and *in vivo*. EMBO J. (1993)12:5150-60.

Ridley AJ, Paterson HF, Johnston CL, Diekmann D, Hall A. The small GTP-binding protein rac regulates growth factor-induced membrane ruffling. Cell. (1992) 70:401-10.

Robinson RC, Turbedsky K, Kaiser DA, Marchand JB, Higgs HN, Choe S, Pollard TD. Crystal structure of Arp2/3 complex. Science. (2001) 294:1679-84.

Robinson RC, Mejillano M, Le VP, Burtnick LD, Yin HL, Choe S. Domain movement in gelsolin: a calcium-activated switch. Science. (1999) 286:1939-42.

Rohatgi R, Nollau P, Ho HY, Kirschner MW, Mayer BJ. Nck and phosphatidylinositol 4,5-bisphosphate synergistically activate actin polymerization through the N-WASP-Arp2/3 pathway. J Biol Chem. (2001) 276:26448-52.

Rohatgi R, Ma L, Miki H, Lopez M, Kirchhausen T, Takenawa T, Kirschner MW. The interaction between N-WASP and the Arp2/3 complex links Cdc42-dependent signals to actin assembly. Cell. (1999) 97:221-31.

Ron D, Zannini M, Lewis M, Wickner RB, Hunt LT, Graziani G, Tronick SR, Aaronson SA, Eva A. A region of proto-dbl essential for its transforming activity shows sequence similarity to a yeast cell cycle gene, CDC24 and the human breakpoint cluster gene, bcr, *New Biol.* (1991) 3:372-79.

Rossman KL, Der CJ, Sondek J. GEF means go: turning on RHO GTPases with guanine nucleotide-exchange factors. *Nat. Rev. Mol. Cell Biol.* (2005) 6:167-80.

Rottner K, Behrendt B, Small JV, Wehland J. VASP dynamics during lamellipodia protrusion. *Nat Cell Biol.* (1999) 1:321-2.

Sakamuro D, Elliott KJ, Wechsler-Reya R, Prendergast GC. BIN1 is a novel MYC-interacting protein with features of a tumour suppressor. *Nat Genet.* (1996) 14:69-77.

Sarner S, Kozma R, Ahmed S, Lim L. Phosphatidylinositol 3-kinase, Cdc42, and Rac1 act downstream of Ras in integrin-dependent neurite outgrowth in N1E-115 neuroblastoma cells. *Mol Cell Biol.* (2000) 20:158-72.

Schafer DA, Welch MD, Machesky LM, Bridgman PC, Meyer SM, Cooper JA. Visualization and molecular analysis of actin assembly in living cells. *J Cell Biol.* (1998) 143:1919-30.

Sekerko G, Loomis PA, Changyaleket B, Zheng L, Eytan R, Chen B, Mugnaini E, Bartles JR. Novel espin actin-bundling proteins are localized to Purkinje cell dendritic spines and bind the Src homology 3 adapter protein insulin receptor substrate p53. *J Neurosci.* (2003) 23:1310-9.

Self AJ, Paterson HF, Hall A. Different structural organization of Ras and Rho effector domains. *Oncogene.* (1993) 8:655-61.

Settleman J, Albright CF, Foster LC, Weinberg RA. Association between GTPase activators for Rho and Ras families. *Nature* (1992) 359:153-54.

Sheetz MP, Wayne DB, Pearlman AL. Extension of filopodia by motor-dependent actin assembly. *Cell Motil Cytoskeleton.* (1992) 22:160-9. Review.

Shi Y, Alin K, Goff SP. Abl-interactor-1, a novel SH3 protein binding to the carboxy-terminal portion of the Abl protein, suppresses v-abl transforming activity. *Genes Dev.* (1995) 21:2583-97.

Shou C, Farnsworth CL, Neel BG, Feig LA. Molecular cloning of cDNAs encoding a quinine-nucleotide-releasing factor for Ras p21. *Nature.* (1992) 358:351-54.

Small JV, Stradal T, Vignal E, Rottner K. The lamellipodium: where motility begins. *Trends Cell Biol.* (2002) 2:112-20. Review.

Small JV, Rottner K, Kaverina I, Anderson KI. Assembling an actin cytoskeleton for cell attachment and movement. *Biochim Biophys Acta.* (1998) 1404:271-81.

Small JV. Lamellipodia architecture: actin filament turnover and the lateral flow of actin filaments during motility. *Semin Cell Biol.* (1994) 5:157-63.

Snapper SB, Rosen FS. The Wiskott-Aldrich syndrome protein (WASP): roles in signaling and cytoskeletal organization. *Annu Rev Immunol.* (1999)17:905-29. Review.

Soltau M, Berhorster K, Kindler S, Buck F, Richter D, Kreienkamp HJ. Insulin receptor substrate of 53 kDa links postsynaptic shank to PSD-95. *J Neurochem.* (2004) 90:659-65.

Soltau M, Richter D, Kreienkamp HJ. The insulin receptor substrate IRSp53 links postsynaptic shank1 to the small G-protein cdc42. *Mol Cell Neurosci.* (2002) 21:575-83.

Spinardi L, Rietdorf J, Nitsch K, Bono M, Tacchetti C, Way M, Marchisio PC. A dynamic podosome-like structure epithelial cells. *Exp Cell Res.* (2004) 295:360-74.

Steketee MB, Tosney KW. Three functionally distinct adhesions in filopodia: shaft adhesions control lamellar extension. *J Neurosci.* 2002 Sep 15;22(18):8071-83.

Stevens B, Tanner S, Fields RD. Control of myelination by specific patterns of neural impulses. *J Neurosci.* (1998) 18:9303-11.

Stewart M. Intermediate filament structure and assembly. *Curr. Opin. Cell Biol.* (1993) 5:3-11.

Stewart DM, Treiber-Held S, Kurman CC, Facchetti F, Notarangelo LD, Nelson DL. Studies of the expression of the Wiskott-Aldrich syndrome protein. *J Clin Invest.* (1996) 97:2627-34.

Stossel TP. On the crawl of animal cells. *Science.* (1996) 260:1086-96.

Stovold CF, Millard TH, Machesky LM. Inclusion of Scar/WAVE3 in a similar complex to Scar/WAVE1 and 2. *BMC Cell Biol.* (2005) 6:11.

Suetsugu S, Murayama K, Sakamoto A, Hanawa-Suetsugu K, Seto A, Oikawa T, Mishima C, Shirouzu M, Takenawa T, Yokoyama S. The RAC binding domain/IRSp53-MIM homology domain of IRSp53 induces RAC-dependent membrane deformation. *J Biol Chem.* (2006) 281:35347-58.

Suetsugu S, Kurisu S, Oikawa T, Yamazaki D, Oda A, Takenawa T. Optimization of WAVE2 complex-induced actin polymerization by membrane-bound IRSp53, PIP(3), and Rac. *J Cell Biol.* (2006) 173:571-85.

Suetsugu S, Hattori M, Miki H, Tezuka T, Yamamoto T, Mikoshiba K, Takenawa T. Sustained activation of N-WASP through phosphorylation is essential for neurite extension. *Dev Cell.* (2002) 3:645-58.

Suetsugu S, Miki H, Takenawa T. Spatial and temporal regulation of actin polymerization for cytoskeleton formation through Arp2/3 complex and WASP/WAVE proteins. *Cell Motil Cytoskeleton.* (2002) 51:113-22. Review.

Suetsugu S, Miki H, Yamaguchi H, Obinata T, Takenawa T. Enhancement of branching efficiency by the actin filament-binding activity of N-WASP/WAVE2. *J Cell Sci.* (2001) 114:4533-42.

Suetsugu S, Miki H, Takenawa T. Identification of another actin-related protein (Arp) 2/3 complex binding site in neural Wiskott-Aldrich syndrome protein (N-WASP) that complements actin polymerization induced by the Arp2/3 complex activating (VCA) domain of N-WASP. *J Biol Chem.* (2001) 276:33175-80..

Suetsugu S, Miki H, Yamaguchi H, Takenawa T. Requirement of the basic region of N-WASP/WAVE2 for actin-based motility. *Biochem Biophys Res Commun.* (2001) 282:739-44.



Suetsugu S, Miki H, Takenawa T. Distinct roles of profilin in cell morphological changes: microspikes, membrane ruffles, stress fibers, and cytokinesis. *FEBS Lett.* (1999) 457:470-4.

Suetsugu S, Miki H, Takenawa T. Identification of two human WAVE/SCAR homologues as general actin regulatory molecules which associate with the Arp2/3 complex. *Biochem Biophys Res Commun.* (1999) 260:296-302.

Suetsugu S, Miki H, Takenawa T. The essential role of profilin in the assembly of actin for microspike formation. *EMBO J.* (1998) 17:6516-26.

Symons M, Derry JM, Karlak B, Jiang S, Lemahieu V, McCormick F, Francke U, Abo A. Wiskott-Aldrich syndrome protein, a novel effector for the GTPase CDC42Hs, is implicated in actin polymerization. *Cell.* (1996) 84:723-34.

Sullivan KE, Mullen CA, Blaese RM, Winkelstein JA. A multiinstitutional survey of the Wiskott-Aldrich syndrome. *J Pediatr.* (1994) 125:876-85.

Suzuki T, Mimuro H, Miki H, Takenawa T, Sasaki T, Nakanishi H, Takai Y, Sasakawa C. Rho family GTPase Cdc42 is essential for the actin-based motility of *Shigella* in mammalian cells. *J Exp Med.* (2000)191:1905-20.

Suzuki T, Miki H, Takenawa T, Sasakawa C. Neural Wiskott-Aldrich syndrome protein is implicated in the actin-based motility of *Shigella flexneri*. *EMBO J.* (1998) 17:2767-76.

Svitkina TM, Bulanova EA, Chaga OY, Vignjevic DM, Kojima S, Vasiliev JM, Borisy GG. Mechanism of filopodia initiation by reorganization of a dendritic network. *J Cell Biol.* (2003) 160:409-21.

Svitkina TM, Borisy GG. Arp2/3 complex and actin depolymerizing factor/cofilin in dendritic organization and treadmilling of actin filament array in lamellipodia. *J Cell Biol.* (1999) 145:1009-26.

Svitkina TM, Verkhovsky AB, McQuade KM, Borisy GG. Analysis of the actin-myosin II system in fish epidermal keratocytes: mechanism of cell body translocation. *J Cell Biol.* (1997) 139:397-415.

Svitkina TM, Verkhovsky AB, Borisy GG. Plectin sidearms mediate interaction of intermediate filaments with microtubules and other components of the cytoskeleton. *J Cell Biol.* (1996) 135:991-1007.

Takenawa T, Miki H. WASP and WAVE family proteins: key molecules for rapid rearrangement of cortical actin filaments and cell movement. *J Cell Sci.* (2001) 114:1801-9. Review.

Tan I, Seow KT, Lim L, Leung T. Intermolecular and intramolecular interactions regulate catalytic activity of myotonic dystrophy kinase-related Cdc42-binding kinase alpha. *Mol Cell Biol.* (2001) 21:2767-78.

Taylor JM, Macklem MM, Parsons JT. Cytoskeletal changes induced by GRAF, the GTPase regulator associated with focal adhesion kinase, are mediated by Rho. *J Cell Sci.* (1999) 112:231-42.

Teddler TF, Steeber DA, Chen A, Engel P. The selectins:vascular adhesion molecules. *FASEB J.* (1995) 9:866-73.

Theriot JA. Accelerating on a treadmill: ADF/cofilin promotes rapid actin filament turnover in the dynamic cytoskeleton. *J Cell Biol.* (1997)136:1165-68.

Tominaga T, Sahai E, Chardin P, McCormick F, Courtneidge SA, Alberts AS. Diaphanous-related formins bridge Rho GTPase and Src tyrosine kinase Signaling. *Mol Cell.* (2000) 5:13-25.

Trinczek B, Biernat J, Baumann K, Mandelkow EM, Mandelkow E. Domains of tau protein, differential phosphorylation, and dynamic instability of microtubules. *Mol Biol Cell.* (1995) 6:1887-1902.

Turner CE, Brown MC, Perrotta JA, Riedy MC, Nikolopoulos SN, McDonald AR, Bagrodia S, Thomas S, Leventhal PS. Paxillin LD4 motif binds PAK and PIX through a novel 95-kD ankyrin repeat, ARF-GAP protein: A role in cytoskeletal remodeling. *J Cell Biol.* (1999) 145:851-63.

Van Aelst L, Joneson T, Bar-Sagi D. Identification of a novel Rac1-interacting protein involved in membrane ruffling. *EMBO J.* (1996)15:3778-86.

Vale RD, Fletterick RJ. The design plan of kinesin motors. *Annu Rev Cell Dev Biol.* (1997) 13:745-77. Review.

Van der Flier A, Sonnenberg A. Structural and functional aspects of filamins. *Biochim Biophys Acta.* (2001) 1538:99-117. Review.

Vasioukhin V, Bauer C, Yin M, Fuchs E. Directed actin polymerization is the driving force for epithelial cell-cell adhesion. *Cell.* (2000) 100:209-19.

Vetter IR, Wittinghofer A. The guanine nucleotide-binding switch in three dimensions. *Science.* (2001) 294:1299-304. Review.

Vignjevic D, Kojima S, Aratyn Y, Danciu O, Svitkina T, Borisy GG. Role of fascin in filopodial protrusion. *J Cell Biol.* (2006) 174:863-75.

Wang B, Mysliwiec T, Krainc D, Jensen RA, Sonoda G, Testa JR, Golemis EA, Kruh GD. Identification of ArgBP1, an Arg protein tyrosine kinase binding protein that is the human homologue of a CNS-specific *Xenopus* gene. *Oncogene* (1996) 12:1921-29.

Wang W, Goswami S, Sagai E, Wyckoff, JE Condeelis. Tumor cells caught in the act of invading: their strategy for emotional cell motility. *Trend Cell Biol.* (2005). 15:138-145.

Wang W, Goswami S, Lapidus K, Wells AL, Wycokoff JB, Sahai E, Singer RH, Segall JE, Condeelis JS. Identification and testing of a gene expression signature of invasive carcinoma cells within primary mammary tumors. *Cancer Res.* (2004) 64:8585-94.

Wang W, Wyckoff JB, Frolich VC, Olenikov Y, Huttlermaier S, Zavadil J, Cermak L, Bottinger EP, Singer SH, White JG. Single cell behaviour in metastatic primary mammary tumors correlated with gene expression patterns revealed by molecular profiling. *Cancer Res.* (2002) 62:6278-88.

Watanabe N, Madaule P, Reid T, Ishizaki T, Watanabe G, Kakizuka A, Saito Y, Nakao K, Jockusch BM, Narumiya S. p140mDia, a mammalian homolog of *Drosophila* diaphanous, is a target protein for Rho small GTPase and is a ligand for profilin. *EMBO J.* (1997) 16:3044-56.

Watanabe G, Saito Y, Madaule P, Ishizaki T, Fujisawa K, Morii N, Mukai H, Ono Y, Kakizuka A, Narumiya S. Protein kinase N (PKN) and PKN-related protein rhophilin as targets of small GTPase Rho. *Science*. (1996) 271:645-8.

Weaver AM, Karginov AV, Kinley AW, Weed SA, Li Y, Parsons JT, Cooper JA. Cortactin promotes and stabilizes Arp2/3-induced actin filament network formation. *Curr Biol*. (2001) 11:370-4.

Weis K. Regulating access to the genome: nucleocytoplasmic transport throughout the cell cycle. *Cell*. (2003) 112:441-51. Review.

Weissenhorn, W. Crystal structure of the endophilin-A1 BAR domain. *J. Mol. Biol.* (2005) 351:653-61.

Wenger A. Heat to tail polymerization of actin. *J Mol. Biol.* (1976) 385:265-69.

Wennerberg K, Der CJ. Rho-family GTPases: it's not only Rac and Rho (and I like it). *J. Cell Sci.* (2004) 117:1301-12.

White MA, Nicolette C, Minden A, Polverino A, Van Aelst L, Karin M, Wigler MH. Multiple Ras functions can contribute to mammalian cell transformation. *Cell* (1995) 80:533-41.

Wills Z, Bateman J, Korey CA, Comer A, Van Vactor D. The tyrosine kinase Abl and its substrate enabled collaborate with the receptor phosphatase Dlar to control motor axon guidance. *Neuron*. (1999) 2:301-12.

Wills Z, Marr L, Zinn K, Goodman CS, Van Vactor D. Profilin and the Abl tyrosine kinase are required for motor axon outgrowth in the *Drosophila* embryo. *Neuron*. (1999) 2:291-9.

Winter D, Lechler T, Li R. Activation of the yeast Arp2/3 complex by Bee1p, a WASP-family protein. *Curr Biol*. (1999) 9:501-4.

Woodings JA, Sharp SJ, Machesky LM. MIM-B, a putative metastasis suppressor protein, binds to actin and to protein tyrosine phosphatase delta. *Biochem J*. (2003) 371:463-71.

Yamagishi A, Masuda M, Ohki T, Onishi H, Mochizuki N. A novel actin bundling/filopodium-forming domain conserved in insulin receptor tyrosine kinase substrate p53 and missing in metastasis protein. *J Biol Chem*. ((2004)) 279:14929-36.

Yamaguchi H, Lorenz M, Kempiak S, Sarmiento C, Coniglio S, Symons M, Segall J, Eddy R, Miki H, Takenawa T, Condeelis J. Molecular mechanisms of invadopodium formation: the role of the N-WASP-Arp2/3 complex pathway and cofilin. *J Cell Biol*. (2005) 168:441-52.

Yamaguchi H, Miki H, Suetsugu S, Ma L, Kirschner MW, Takenawa T. Two tandem verprolin homology domains are necessary for a strong activation of Arp2/3 complex-induced actin polymerization and induction of microspike formation by N-WASP. *Proc Natl Acad Sci U S A.* (2000) 97:12631-6.

Yamazaki D, Suetsugu S, Miki H, Kataoka Y, Nishikawa S, Fujiwara T, Yoshida N, Takenawa T. WAVE2 is required for directed cell migration and cardiovascular development. *Nature.* (2003) 424:452-6.

Yang C, Huang M, DeBiasio J, Pring M, Joyce M, Miki H, Takenawa T, Zigmond SH. Profilin enhances Cdc42-induced nucleation of actin polymerization. *J Cell Biol.* (2000)150:1001-12.

Yang W, Cerione RA. Cloning and characterization of a novel Cdc42-associated tyrosine kinase, ACK-2, from bovine brain. *J Biol Chem.* (1997) 272:24819-24.

Yeh TC, Ogawa W, Danielsen AG, Roth RA. Characterization and cloning of a 58/53-kDa substrate of the insulin receptor tyrosine kinase. *J Biol Chem.* (1996) 271:2921-8.

Yu W, Datta A, Leroy P, O'Brien LE, Mak G, Jou TS, Matlin KS, Mostov KE, Zegers MM. Beta1-integrin orients epithelial polarity via Rac1 and laminin. *Mol Biol Cell* (2005) 16:433-45.



Zalcman G, Closson V, Camonis J, Honore N, Rousseau-Merck MF, Tavitian A, Olofsson B. RhoGDI-3 is a new GDP dissociation inhibitor (GDI). Identification of a non-cytosolic GDI protein interacting with the small GTP-binding proteins RhoB and RhoG. *J Biol Chem.* (1996) 271:30366-74.

Zegers MM, Forget MA, Chernoff J, Mostov KE, ter Beest MB, Hansen SH. Pak1 and PIX regulate contact inhibition during epithelial wound healing. *EMBO J.* (2003) 22(16):4155-65.

Zerial M, McBride H. Rab proteins as membrane organizers. *Nat Rev Mol Cell Biol.* (2001) 2:107-17. Review. Erratum in: *Nat Rev Mol Cell Biol* (2001) 3:216.

Zhao ZS, Manser E. PAK and other Rho-associated kinases--effectors with surprisingly diverse mechanisms of regulation. *Biochem J.* (2005) 386:201-14. Review.

Zhao ZS, Manser E, Loo TH, Lim L. Coupling of PAK-interacting exchange factor PIX to GIT1 promotes focal complex disassembly. *Mol Cell Biol.* (2000) 20:6354-63.

Zhao ZS, Manser E, Lim L. Interaction between PAK and nck: a template for Nck targets and role of PAK autophosphorylation. *Mol Cell Biol.* (2000) 20:3906-17.

Zhao ZS, Leung T, Manser E, Lim L. Pheromone signaling in *Saccharomyces cerevisiae* requires the small GTP-binding protein Cdc42p and its activator CDC24. *Mol Cell Biol.* (1995) 15:5246-57.

Zheng Y, Fischer DJ, Santos MF, Tigyi G, Pasteris NG, Gorski JL, Xu Y. The faciogenital dysplasia gene product FDG1 functions as a Cdc42Hs-specific guanine-nucleotide exchange factor. *J. Biol. Chem.* (1996) 271:33169-72.

Zheng Y, Olson MF, Hall A, Cerione RA, Toksoz D. Direct involvement of the small GTP-binding protein Rho in lbc oncogene function. *J. Biol. Chem.* (1995) 270:9031-34.

Zigmond SH. Beginning and ending an actin filament: control at the barbed end. *Curr Top Dev Biol.* (2004) 63:145-88.

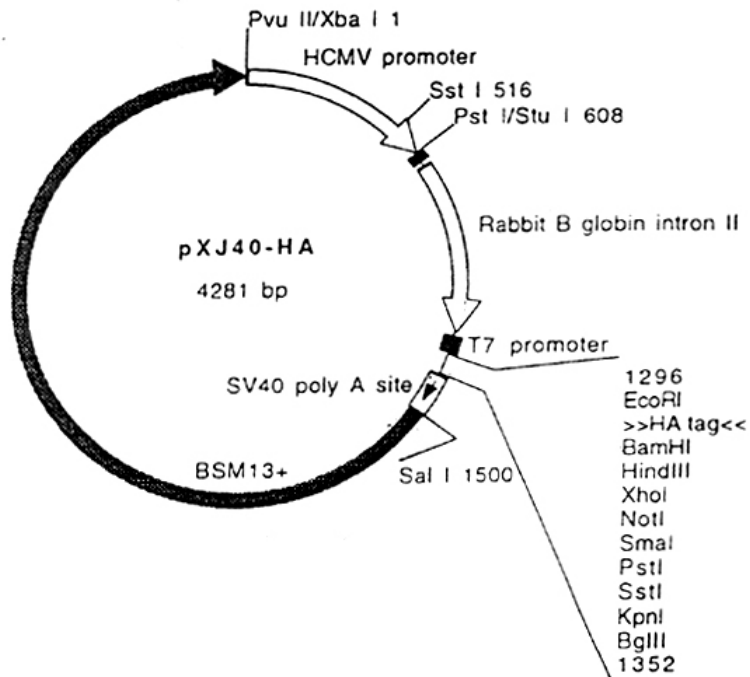
Zigmond SH. Formin-induced nucleation of actin filaments. *Curr Opin Cell Biol.* (2004) 16:99-105.

# **APPENDICES**

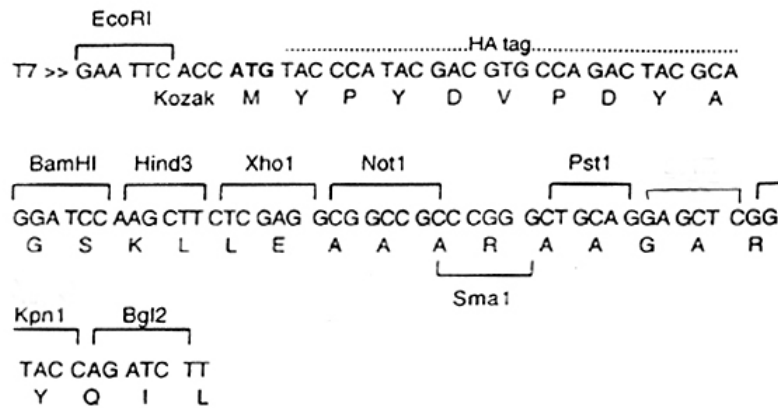
# APPENDICES

## Appendix I Vectors

### 1. pXJ40-HA eukaryotic expression vector



#### pXJ40-HA MCS



## 2. pSUPER Basic Vector Map

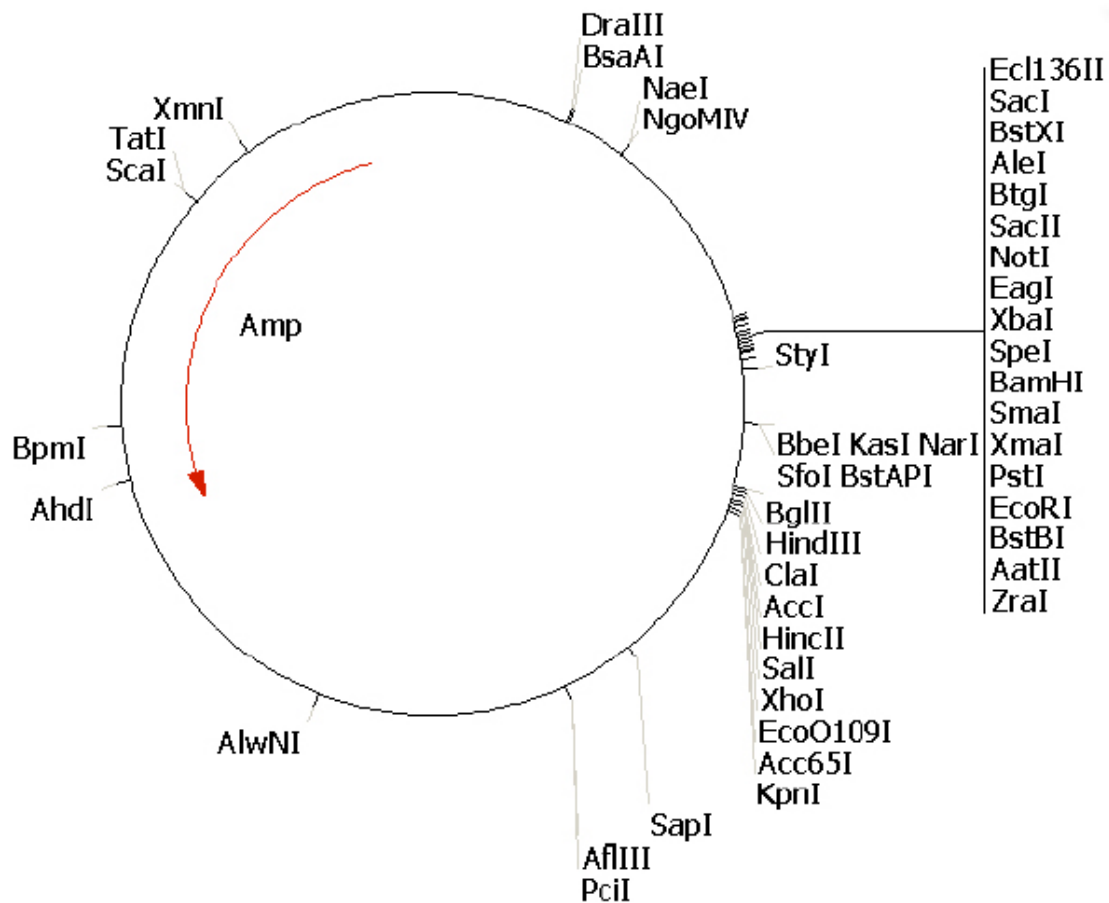
### Key Sites

BglII: 928  
 HindIII: 934  
 EcoRI: 707  
 Sall: 949  
 XhoI: 955

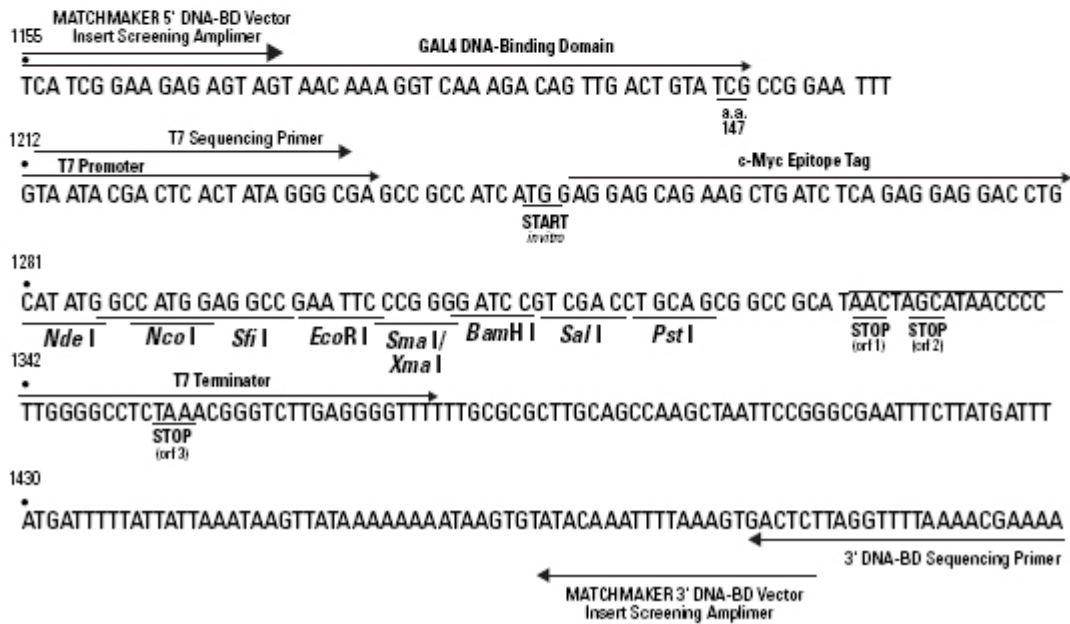
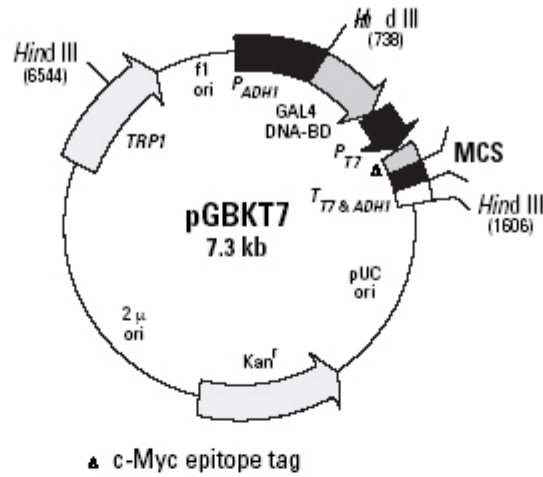
### Vector Features

f1(+) origin: 441-135  
 H1 promoter: 708 - 934  
 pUC origin: 1373-2040  
 Ampicillin resistance ORF: 3048-2191

T7 primer binding site (AATACGACTCACTATAG): 627-643  
 T3 primer binding site (CTTTAGTGAGGGTTAAT): 989-1005  
 M13(-20) primer binding site (GTAAAACGACGGCCAGT): 600-616  
 M13 reverse primer binding site (CATGGTCATAGCTGTT): 1023-1038



### 3. pGBKT7 Vector Map



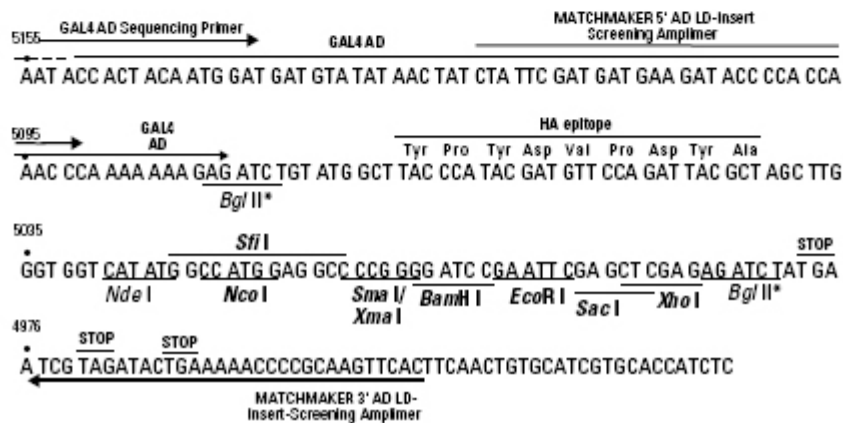
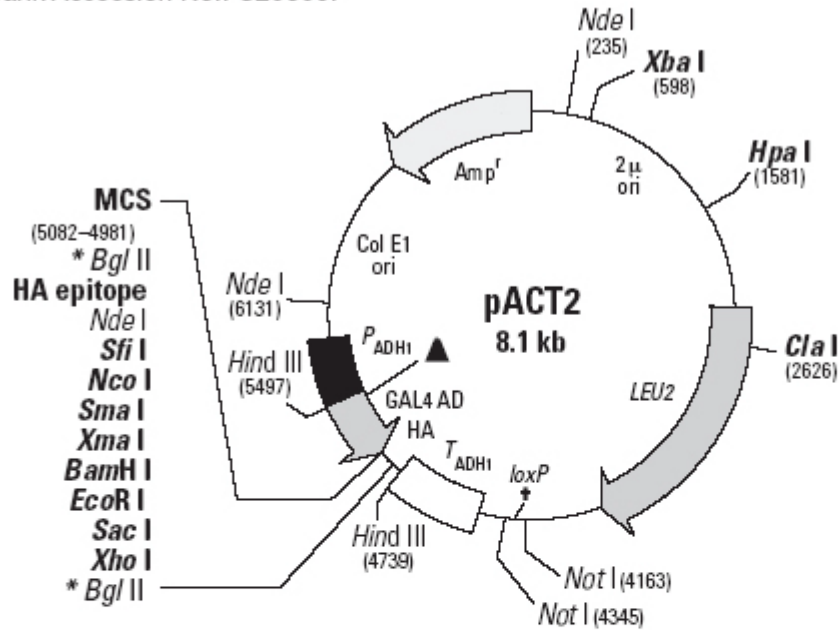
## 4. pACT2 Vector Map

### pACT2 AD Vector Information

GenBank Accession No.: U29899.

PT3022-5

Catalog 638822



## Apendix II. IRSp53 Variants

### IRSp53 GenBank Resource

IRSp53 (BAIAP2)		
Organism	Accession #	g.l
<i>Bos taurus</i>	BT020639	59857642
	BC111352	83405333
<i>Cricetinae gen. sp.</i>	U41899	1203819
<i>Homo sapiens</i>	AB015019	4126474
	AB015020	4126476
	AB017119	4239981
	AB017120	4239983
	AB104726	28804792
	AK222670	62896898
	BC014020	33878456
	BC032559	21619131
	<i>Macaca fascicularis</i>	AB169737
<i>Mus musculus</i>	AB105196	28971723
<i>Mus musculus</i>	AF390178	14573640
	AF390179	15029333
	AK004918	26338407
	AK049469	26340201
	AK143783	74150867
	AK145924	74219242
	AK160401	74137430
	BC006620	13879291
	BC048937	29124482
	BC015459	15930030
	BC016411	16741114
	<i>Rattus norvegicus</i>	AY037934
BC074009		49258139
BC089216		58402628
BC105815		BC105815
<i>Danio rerio</i>	AY398378	37681866
	BC050238	29571120
	BC068330	46249678
	BC092786	62204322
	BX571946	53748640
	BX571961	42517007



### Appendix III. Filopodia Characterization

Characteristics	Cdc42 V12/Rac1N17	IRSp53	N-WASP	TOCA -1
Contains F-actin	Yes	Yes	Yes	Yes
average length (mm)	8.37 $\pm$ 1.5	6.83 $\pm$ 1.97	7.35 + 0.97	8.12 + 1.3
minimum length (mm)	6.57	4.43	6.34	6.3
maximum length (mm)	10.24	10.22	9.14	10.21
average thickness (mm)	1.27 $\pm$ 0.28	1.26 $\pm$ 0.12	1.27 $\pm$ 0.19	1.19 $\pm$ 0.14
average life time (s)	157 $\pm$ 30	187 $\pm$ 38	154 $\pm$ 20.7	163 $\pm$ 21.4
minimum life time (s)	130	130	130	130
maximum life time (s)	210	240	180	190

#### Characterization of Filopodia dynamics

Cdc42V12/Rac1N17, IRSp53, N-WASP and Toca-1 induced filopodia were characterized for dynamics, as per described in Table 6.1. All measurements are presented as average  $\pm$  SD.